PHYSICOCHEMICAL AND STRUCTURAL STUDIES

ON TWO TRIDENTATE ANTITUMOUR LIGAND SYSTEMS

A thesis presented in partial fulfilment of the requirements for the degree of

Doctor of Philosophy in Chemistry at Massey University.

JOHN DAVID RANFORD

1988

Massey University Library

Thesis Copyright Form

Title of thesis: Physicochemical and Structural Studies on two Tridentate Antitumour Ligand Systems

(1) (a) I give permission for my thesis to be made available to readers in the Massey University Library under condition determined by the Librarian.

~~(b)~~ I do not wish my thesis to be made available to readers without my written consent for _____ months.

(2) (a) I agree that my thesis, or a copy, may be sent to another institution under conditions determined by the Librarian.

~~(b)~~ I do not wish my thesis, or a copy, to be sent to another institution without my written consent for _____ months.

(3) (a) I agree that my thesis may be copied for Library use.

~~(b)~~ I do not wish my thesis to be copied for Library use for _____ months.

Signed J.D. Ranford

Date 18/10/88

The copyright of this thesis belongs to the author. Readers must sign their name in the space below to show that they recognise this. They are asked to add their permanent address.

NAME AND ADDRESS	DATE
27 Epsom Road Palmerston North	18/10/88

DEDICATION

To all the people, especially Mona and Alan Wong, who constantly remind me how silly I must be to have to stay at school for **SO** long.

ABSTRACT

This work is an investigation into the physicochemical and structural properties of two tridentate, antitumour ligand systems and is divided into two sections. In the first (Chapters 1 to 4), the ligand 2-formylpyridine thiosemicarbazone (LH - containing an NNS donor set), several of its congeners and a range of complexes (predominantly Cu(II)) were prepared. The second section (Chapters 5 and 6) deals with a range of ligands based on salicylaldehyde benzoylhydrazone (sbH_2 - containing an ONO donor set), their complexes (predominantly Cu(II)) and the cytotoxicity data for all of this work.

In Chapter 1, complexes of the general formulation $[CuLX]_2$ for the deprotonated and $[Cu(LH)X]_2X_2$ for the neutral, protonated ligand were prepared (where X = e.g. halide, pseudohalide, NO_3^-, ClO_4^-, CH_3COO^-, CF_3COO^-). The complexes formed are very stable in strong, non-oxidising acid solutions and with mildly reducing anions, but are susceptible to oxidising acids and anions. The crystal structures of the neutral ligand, dimeric, one-atom anion bridged complex $[Cu(LH)(CF_3COO)]_2(CF_3COO)_2$ and the monomeric complex $[Cu(LH)(ClO_4)_2H_2O]\cdot 2H_2O$ with axially coordinated perchlorato groups were determined.

In Chapter 2, the possibility that *in vivo* S and N donor atom adducts of CuL^+ may form was investigated *in vitro*. Stable complexes containing a copper(II)-thiolato bond were isolated at ambient temperatures, under aerobic conditions. The e.s.r. parameters for these were very similar to a species formed from the interaction of CuL^+ with human blood components. Ternary, Lewis-base adducts of nitrogen donor atoms were also isolated, and the crystal structures for two of these, $[CuL(2,2'\text{-bipyridyl})]ClO_4$ and $[CuL(saccharinato)H_2O]\cdot \frac{1}{2}H_2O$, were solved.

The possibility of CuL^+ interacting with O donor groups (in particular phosphates) *in vivo* was investigated *in vitro* in Chapter 3. The ternary complexes isolated contain the anions mono-

and dihydrogenphosphate, pyrophosphate, phenolate and molybdate. The crystal structure of $[Cu(LH)(H_2PO_4)]_2(H_2PO_4)_2(H_3PO_4)_2{\cdot}2H_2O$ showed the complex is dimeric, having a unique one-atom dihydrogenphosphate bridge, three inequivalent phosphates and a very strong interphosphate hydrogen-bond. In contrast, the ternary, pyrophosphato complex $[(CuL)_4P_2O_7]{\cdot}12H_2O$ is a tetramer, with each Cu(II) centre having a one-atom S, a three-atom pyrophosphato and two five-atom pyrophosphato bridges.

The low temperature magnetic properties of $[CuL(CH_3COO)]_2$ fit the Bleany-Bowers expression well, whereas for $[(CuL)_4P_2O_7]{\cdot}12H_2O$ a very weak interaction through the five-atom pyrophosphato bridge may account for the non-dimeric behaviour observed. Both complexes are weakly antiferromagnetic ($-2J \sim 6$ cm^{-1}).

In Chapter 4, four variations on the ligand LH and a representative series of their Cu(II) complexes were synthesised. Reduction potentials for a Cu(II) complex of each ligand, as well as for two thiolato and a Lewis-base adduct of CuL^+, were measured. N.m.r. spectroscopy was used to characterise the ligands and pKa values for both the ligands and their Cu(II) complexes were determined. No correlation between any of these values and the cytotoxicities was found.

In Chapter 5, Section 2, a range of ligands based on sbH_2 (salicylaldehyde benzoylhydrazone) and their transition metal complexes (predominantly Cu(II)) were synthesised for cytotoxicity trials (on the cell line HCT-8). A number of the Cu(II) complexes had depressed room temperature magnetic moments and displayed e.s.r. spectral features which were attributed to magnetic interactions in the solid state. The crystal structure of $[Cu(sbH)ClO_4(EtOH)]_2$ revealed it to be a planar, side-by-side dimer with $Cu(sbH)^+$ moieties bridged via the phenolato-oxygens.

Depending upon the pH, sbH_2 can coordinate as either a neutral, monoanionic or dianionic moiety to transition metals. The interaction of $CuF_2.2H_2O$ in HF with sbH_2 resulted in the *in*

situ formation of H_2SiF_6. The crystal structure of the resulting complex, $[(Cu(sbH)H_2O)_2SiF_6]\cdot 2H_2O$, showed it to be a dimer, with the Cu(II) centres linked by the coordinated SiF_6^{2-} anion. The crystal structure of a cytotoxically inactive $Cu(sbH)^+$ analogue, $[Cu(saH)Cl(H_2O)]H_2O$ was also solved.

In the final chapter, the cytotoxicity data for all compounds tested are presented. The copper(II) complexes generally showed activities different to the metal free ligands. For LH congeners the complexes were no better than the ligands; in contrast to the sbH_2 analogues where the Cu(II) chelates were statistically more cytotoxic. Transition metals other than Cu(II) either did not improve the activity or resulted in a reduction or loss of cytotoxicity.

For LH congeners, changes in cytotoxicity could be related to altered electronic and steric properties, whereas for the sbH_2 series of compounds, statistical analysis showed the lipophilicity conferred by a substituent to be the dominant factor. Comparisons with proven anticancer drugs are made and possible future studies to maximise the biological activity are suggested. All of the compounds tested for their antiviral activity were either cytotoxic or inactive at the concentrations used.

ACKNOWLEDGEMENTS

Much of this work would not have been possible without the gratefully acknowledged contributions from the following people:

Drs E W Ainscough and A M Brodie for their supervision and contagious enthusiasm.

Dr J M Waters for her guidance and expertise with the X-ray crystallography.

Drs W A Denny and G J Finlay, Cancer Research Laboratory, Auckland Medical School, for very generously determining the cytotoxicity data.

Dr G E Norris for solving one of the X-ray crystallographic structures and for proof reading this work.

Dr K W Jolley and Mr M H Smith for running n.m.r. spectra.

Professor R Hodges, Massey University, and Dr G J Shaw and Mr J M Allen, DSIR, Palmerston North, for running mass spectra.

Dr W T Robinson, Canterbury University, for collecting three X-ray diffraction data sets.

Dr K S Murray and Mr C Delfs, Monash University, for low temperature magnetic data.

Dr J W Blunt, Canterbury University, for kindly carrying out the antiviral assays.

Dr G A Bowmaker, Auckland University, for guidance and the use of electrochemical apparatus.

Professor A D Campbell, Otago University, for microanalytical data.

Diane Reay for typing this tome.

I would also like to sincerely thank everyone else who contributed with helpful discussions and I am also indebted to Massey University for the position of Graduate Assistant during my studies.

TABLE OF CONTENTS

ABBREVIATIONS

a.a.	atomic absorption
a.m.u.	atomic mass units
bipy[a]	2, 2′-bipyridyl
cisplatin[b]	*cis*-diamminedichloroplatinum(II)
c.t.	charge transfer
dips	diisopropylsalicylic acid
dmap	4-N,N-dimethylaminopyridine
dmf	dimethylformamide
dmso	dimethylsulphoxide
DNA	deoxyribonucleic acid
edta	ethylenediaminetetraacetic acid
en	ethylenediamine
e.s.d.	estimated standard deviation
e.s.r.	electron spin resonance
H	in a ligand or complex refers to an ionisable proton
Hb	haemoglobin
IC_{50}	inhibitory concentration to 50%; the concentration required to inhibit cell growth to 50% compared with that of a control
ir	infrared
LD_{50}	lethal dose to 50%; the single injected dose that kills 50% of the animals
LH[a,c]	2-formylpyridine thiosemicarbazone
2′L[c]	2-formylpyridine 2′-methylthiosemicarbazone
4′LH[c]	2-formylpyridine 4′-methylthiosemicarbazone
6LH[c]	6-methyl-2-formylpyridine thiosemicarbazone
mbtH[a]	2-mercaptobenzothiazole
miH[a]	2-mercaptoimidazole
mmiH[a]	2-mercapto-1-methylimidazole

mpH_2[a]	2-mercapto-3-pyridinol
m.t.	mull transmittance
mttH[a]	4-methyl4H-1,2,4-triazole-3-thiol
n.m.r.	nuclear magnetic resonance
ntpH	4-nitrothiophenol
pbH[a]	2-formylpyridine benzoylhydrazone
pctpH	pentachlorothiophenol
pftpH	pentafluorothiophenol
phen[a]	1,10-phenanthroline
ptpH[a]	paratritylphenol
py	pyridine
rdr[e]	ribonucleoside diphosphate reductase (ribonucleotide reductase)
RNA	ribonucleic acid
saH_2[a,d]	salicylaldehyde acetylhydrazone
sbH_2[a,d]	salicylaldehyde benzoylhydrazone
spy	square-pyramidal
tipH	2,4,6-triiodophenol
tby	trigonal-bipyramidal
TMS	tetramethylsilane
uv/vis	ultraviolet/visible

a structure abbreviated on following page

b see Figure 1.1

c see Figure 4.1 in Chapter 4 introduction

d see Figure 2.5.11 for this and all other structurally related ligands for Section 2

e see Figure 1.4

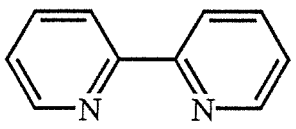

bipy

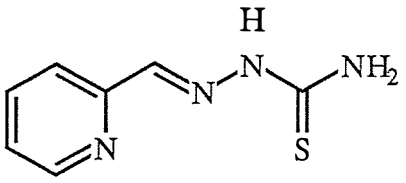

LH

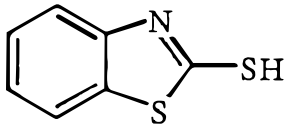

mbtH

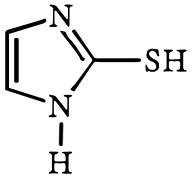

miH

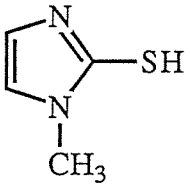

mmiH

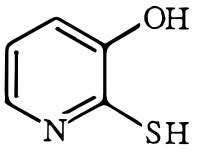

mpH_2

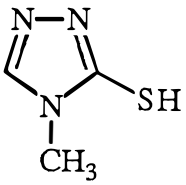

mttH

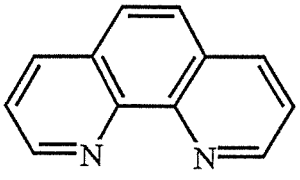

phen

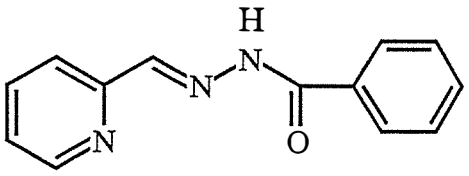

pbH

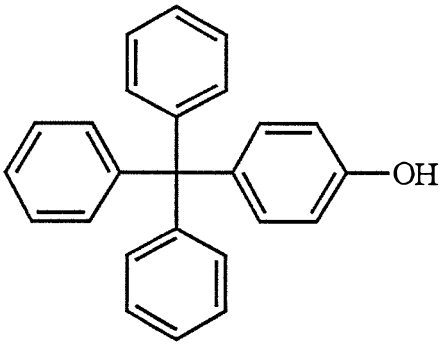

ptpH

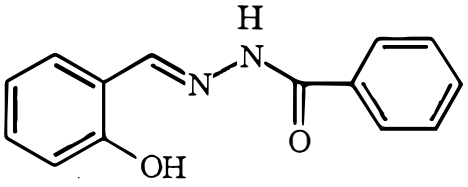

sbH_2

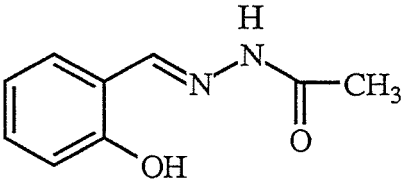

saH_2

Figures for the abbreviations.

INDEX OF FIGURES

Chapter 1

Chapter 2

Chapter 3

Chapter 4

Section 2

Introduction to Section 2

Chapter 5

Chapter 6

INDEX OF TABLES

Chapter 2

Chapter 3

Chapter 4

Section 2

Chapter 5

Chapter 6

GENERAL INTRODUCTION

1.1 Platinum Complexes as Anticancer Agents

The serendipitous discovery by Rosenberg [1] in 1969 of the anticancer properties of *cis*-diamminedichloroplatinum(II) (cisplatin - see Figure 1.1(a)) has opened a new and potentially very beneficial area in cancer research. This has stimulated research in the area of the so-called 'second generation' platinum compounds and other metal-based antitumour agents such as titanium, vanadium, germanium, gold and copper complexes.

Cisplatin is now one of the most widely used anticancer drugs in the United States, Europe and Japan (both by itself and in combination chemotherapy) and is listed as one of the fourteen 'essential drugs' for cancer chemotherapy by the World Health Organisation [2]. It has been successfully used in the treatment of bladder, lung, head and neck, cervical and especially testicular and ovarian cancers [3].

Some details of the mechanism of action for this anticancer drug are currently understood. A large body of evidence indicates that cisplatin exhibits its biological activity by binding to DNA and inhibiting replication, but the mechanism by which DNA replication is inhibited in tumour cells is only beginning to emerge now.

In plasma, where the chloride ion concentration is high (103 mM), the predominant species is the neutral, dichloro complex, which can passively diffuse across cell membranes. Once inside the cell, the chloride concentration drops to about 4 mM and the labile chloride ions are displaced by water in a stepwise manner as shown by the following equations:

$$cis - [Pt(NH_3)_2Cl_2] \rightleftarrows cis - [Pt(NH_3)_2Cl(H_2O)]^+ + Cl^-$$

$$cis - [Pt(NH_3)_2Cl(H_2O)]^+ \rightleftarrows cis - [Pt(NH_3)_2(H_2O)_2]^{2+} + Cl^-$$

The diaqua species may also lose protons to form the mono- and dihydroxy species, but at least one aqua group is present in 42% of the platinum complexes at 4 mM chloride ion concentration [4,5].

The cellular target appears to be the negatively charged DNA helix which can electrostatically attract the positively charged platinum complexes. The complex binds covalently under neutral conditions to the N7 atom of guanine, the N7 and N1 atoms of adenine and the N3 atom of cytosine, with the preferred site being the N7 atom of guanine [5]. Coordination to phosphato, purine or pyrimidine oxygens and intercalation of the platinum complexes with the DNA helix have been shown to be insignificant [5].

Bifunctional, intrastrand cross-linking of cisplatin appears to be the active binding mode of the drug, as monofunctional adducts formed from transplatin and platinum complexes such as $[Pt(dien)Cl]^+$ (dien = diethylenetriamine) are inactive as antitumour agents.

Both the *cis* and *trans* isomers of this platinum complex bind to DNA and there is no preferential cellular uptake of either compound. The difference in activity can be explained from the kinetic results. Whereas cisplatin continues to bind steadily to cellular DNA over a 48 hour period, the *trans* isomer binds rapidly for the first six hours of incubation and then equally as rapidly is removed. This suggests that transplatin adducts are preferentially repaired from DNA. Little more of these mechanisms is presently known.

Although cisplatin is widely used, it displays a number of toxic side effects such as kidney toxicity, nausea and vomiting and neurotoxicity. Because of these drawbacks, a second-generation of platinum drugs was sought which were be selected on a number of criteria.

These were (1) high solubility (for potential oral administration), (2) less kidney toxicity, (3) less nausea and vomiting, (4) a better penetration of the blood-brain barrier, (5) an improved therapeutic index, (6) potentially different mechanisms of action, (7) drugs which can act synergistically in combination chemotherapy [1,4].

Of over 1000 complexes screened by 1978, approximately 80 were highly active, and of these, seven were tested in a comparison with cisplatin [4,6].

Three of these, carboplatin (JM-8), iproplatin (JM-9) and spiroplatin (TNO-6) (see Figure 1.1) have reached clinical trials. The most promising of these, carboplatin, is an agent of equivalent activity to cisplatin in the treatment of ovarian cancer, and has the advantage of minimal toxicity to the kidneys, hearing and nervous systems as well as causing less severe gastrointestinal disturbance.

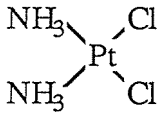

(a) Cisplatin

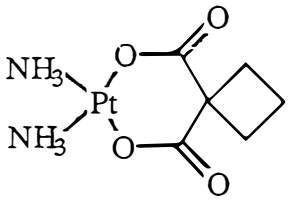

(b) Carboplatin (JM-8)

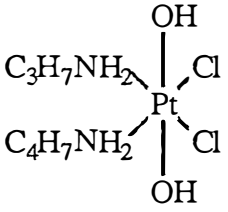

(c) Iproplatin (JM-9)

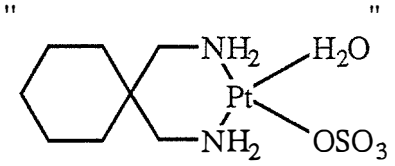

(d) Spiroplatin (TNO-6)

Figure 1.1 The structures of some platinum anticancer drugs (after [6]).

Once sufficient controlled testing (e.g. experimental models, treatment schedules) of analogues had been carried out, structure-activity relationships in terms of the 'leaving group', 'non-leaving group' and oxidation state of the platinum (chloro, amine and Pt(II) in cisplatin

respectively) were determined leading to third generation platinum compounds. Criteria for these include higher activity per dose compared with carboplatin (and ideally cisplatin) but interest is now focusing on other metal complexes as antitumour agents which show promise.

1.2 Categories of Metal Containing Antitumour Agents

Synthesis of metal containing compounds as antitumour agents broadly fall into several categories at present and a brief summary of these systems will be included here. The first are complexes with one or more labile ligands which can be displaced. It has been proposed that the coordinatively unsaturated complex can then complex to DNA, viruses, enzymes or proteins and hinder replication or the disease-causing properties [4]. An example of this class of compounds is the previously discussed cisplatin. Another category is complexes of known organic anticancer compounds. The rational for this is; if the ligand is active as an antitumour agent itself, then the complex will have acted as a carrier for the biologically active ligand to the site where it can most effectively exert its activity [4]. The complex may thus act as a integral unit, or the ligand may be separated, so that it or the metal acts as the antitumour agent. Examples of such systems are 6-mercaptopurine (6-mp) and its platinum complex, *trans*-$[Pt(Cl)_4(6\text{-mp})_2]^{2-}$ [4] and the antineoplastic antibiotic bleomycin and its copper and iron complexes [7-10].

Radioactive ligands or metal ions in complexes located in regions of significant biological activity have also been proposed as anti tumour agents. If such a the complex or ligand binds to DNA (or viruses) of tumour systems, then the radiation from incorporated low energy isotopes could help to destroy such systems (and serve to find locations of relatively high concentration of the radioisotope). For example it has been proposed that ^{35}S might be incorporated into 6-mercaptopurine before complex synthesis [4].

Where they exist, through sufficient dissymmetry, optically active ligands or complexes may be resolved into their optical enantiomers and screened separately, as the individual enantiomers will most likely not exhibit the same biological activity. Examples of this are the potential ligands levo-epinephine and dextro-penicillamine [4].

The final major category has no mechanistic rational for antitumour activity. This involves the testing of inorganic salts and complexes on the off chance activity will be found. Once activity has been found, further experiments are conducted to try and elucidate the mechanism of action and/or the cellular target. Initial interest focused on the platinum group metals such as ruthenium, rhodium and palladium, with a number of these complexes exhibiting antitumour properties, e.g. binuclear rhodium(II) carboxylates [9,10]. More recently, non-platinum main-group and transition metals have been investigated.

1.3 Biologically Active Non-Platinum Group Metal Compounds

Three groups of antitumour main-group metal complexes have been detected so far [10]. The first of these are gallium salts such as gallium(III) nitrate. The second group has two main representatives, which are organometallic germanium compounds and appear to have activity based on host-mediated, immunopotentiating mechanisms. Therefore these are undergoing clinical studies as biological response modifiers. The third of these groups are tin(IV) complexes which structurally resemble the cytostatic platinum metal complexes with respect to the presence of a cis-dihalometal moiety [10].

Köpf-Maier in a recent review [10] divided the transition metal (t.m.) complexes, other than the platinum group metals, into three groups: early, medium or late.

The carcinostatic early-t.m. complexes are mainly metallocene complexes of the general formulation $M(cp)_2X_2$ (where M = Ti, V, Nb, Mo; cp = cyclopentadiene and e.g., $X=Cl^-$).

The medium-t.m. compounds are again metallocenium complexes (but are saltlike rather than neutral as the early-t.m. complexes are) with the general formulation $M(cp)_2X$ (where M = Fe, Co and e.g. $X^- = FeCl_4^-$). Although the early-t.m. cyclopentadienyl complexes have a *cis*-configuration of the two X groups similar to cisplatin, both the early and medium cp complexes have diminished tumour inhibition when substitutions are made into the cp ring, with the titanocene complexes containing pentamethylated cp ring ligands being cytostatically inactive. The implication of this is the cp rings play an active part in the antitumour properties of these complexes [10,11].

1.4 Biologically Active Gold Complexes

Recently gold(I) bischelated diphosphine complexes such as $[Au(dppe)_2]Cl$ (where dppe = (diphenylphosphino)ethane) have shown promise as antitumour agents [12-14]. Gold compounds though remain relatively unexplored as antineoplastic agents. As such, little is known about their biological activities, but the mechanism/s for Au(I) complexes are clearly different from that of cisplatin. The gold(I) complexes are lipophilic in nature and readily enter human red blood cells and bind to cellular components such as glutathione. Au(I) is a very 'soft' ion compared to Pt(II) and Au(III) and forms weak bonds to nitrogen ligands (Au(III) is isoelectronic with Pt(II), forming square planar complexes and strong bonds to nitrogen ligands but is highly polarising and often a strong oxidant so its complexes are not generally studied as antitumour agents - although some Au(III) alkyls have activity [12]). In the case of the tetrahedral $[Au(dppe)_2]^+$ complex ion, the mechanism is though to involve the delivery of the toxic phosphine to the cellular target rather than direct binding to DNA bases [12].

1.5 Biologically Active Copper Complexes

In contrast to gold, there has been considerable interest in the biological activity of copper complexes. There are a number of reasons for this. The platinum group metals and gold etc. are classed as heavy-metal toxins, in contrast to copper (Mn, Fe, and Zn also) which is an essential metalloelement and as such has mechanisms for its metabolisation [9]. Copper is found in all human cells and is primarily associated with copper-dependent enzymes, some of which are listed in Table 1.1 [7,15].

TABLE 1.1

Recognized copper-dependent enzymes and their biochemical function[a]

Cu-dependent enzyme	*Function*
Cytochrome C oxidase	Cellular utilization of oxygen
Superoxide dismutase	Disproportionation of superoxide
Tyrosinase	Synthesis of dopa from tyrosine
Dopamine-β-hydroxylase	Synthesis of norepinephrine from dopamine
Lysyl oxidase	Synthesis of collagen and elastin from procollagen and proelastin
Soluble pyridoxal dependent monoamine oxidase and perhaps the insoluble membrane-bound flavin-dependent monoamine oxidase	Catecholamine oxidations to aldehydes

a after [7]

With the onset of a neoplastic disease there is a characteristic rise in serum copper levels which return to normal upon spontaneous or therapy induced remission [7] (see Figure 1.2).

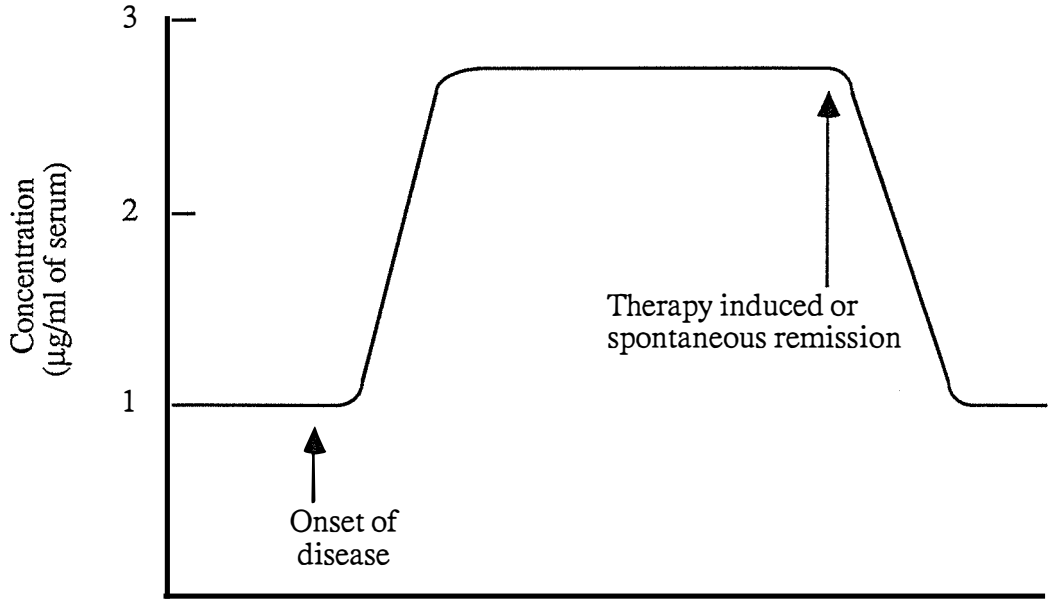

Figure 1.2 Profile of copper level at onset of neoplasis through therapy induced or spontaneous remission (after [7]).

This rise in serum copper levels was thought to be pathological but this idea has been questioned because of the proven biological activities of copper complexes. The mobilisation of copper (via suggested transport systems such as albumin, transcuprein, ceruloplasmin and small amounts of low molecular weight amino acid complexes) may be a physiological response in an attempt to activate copper-dependent enzymes to remedy the disease state [7].

There are a number of cases where copper is needed for, or enhances the biological activity of potential ligand systems. For kethoxal-bis(thiosemicarbazone) ($KTSH_2$), dithizone and N-methylisatin β-thiosemicarbazone [9] (see Figure 1.3) the preformed copper complexes are much more active than the free ligand. Addition of edta can prevent the inhibitory activity of the free ligands. This suggests the possibility that the ligands complex copper or other metals present in the virion or in the solutions and it is this complex which is therefore active.

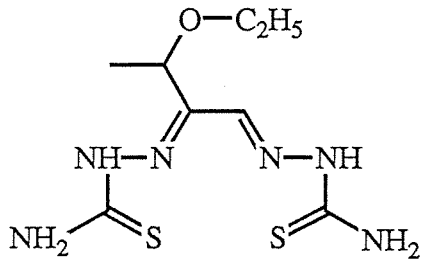

Kethoxal-bis(thiosemicarbazone)
($KTSH_2$)

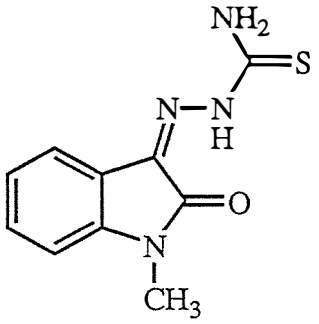

N-methylisatin ß-thiosemicarbazone

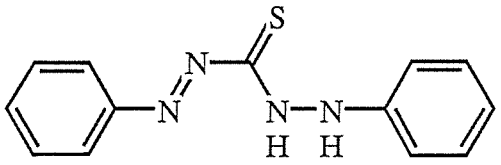

Diphenylthiocarbazide (dithizone)

Figure 1.3 Examples of three ligands which require copper for biological activity.

Other systems where copper has been shown to be necessary for, or to enhance, biological activities include:

(i) a range of Cu(I) (and Au(I)) diphosphine complexes which are at least 20 times more potent as antitumour agents than the ligands alone [14].

(ii) the cytotoxic α-N-heterocyclic carboxaldehyde thiosemicarbazones and salicylaldehyde benzoylhydrazones [7] are markedly more active as their copper complexes (see Sections 1 and 2 respectively of this work).

(iii) the active form of the fungicide dimethyldithiocarbamic acid is the copper complex [16].

(iv) for the naturally occurring and synthetic tripeptide GHL (Glycyl-L-Histyl-L-Lysyl) exhibits a range of activities including antitumour and wound healing, copper must be present [7,17-19].

(v) the antibiotic bleomycin (Blm) has been reported to have the following order for both antitumour activity and cytotoxicity: Cu(II)Blm > Blm > Zn(II)Blm > Fe(III)Blm >> Co(II)Blm = nontreated control [7,20].

(vi) the copper complexes of non-steroidal, antiinflammatory and analgesic agents (e.g. $Cu(II)_2(acetylsalicylate)_4$ (aspirin) and $Cu(II)(3,5\text{-diisopropylsalicylate})_2$) have been shown to be more effective than the parent compounds [21].

(vii) it has been observed that by increasing the dietary copper of rats, tumour induction time can be lengthened [7,22].

As well, numerous other examples of systems containing copper which possess biological activity are known.

Other reasons for the use of copper include the relative thermodynamic stability of copper complexes as compared to other first row transition elements, as well as their general ease of preparation.

The extensive range of biological activities exhibited by copper complexes including antiinflammatory, antiulcer, anticonvulsant, anticancer, anticarcinogenic, antidiabetic, antiarthritic, antimutagenic and radiation protection [15,23] may therefore be due in part to some of the previously mentioned properties of copper complexes.

1.6 Possible Antitumour Mechanisms

The exact mechanisms by which these copper complexes exert their activities is not clear, due in main to the large number of potential sites of action in the cell (and the difficulties associated with monitoring and unequivocally assigning a reaction to a particular step).

Possible mechanisms include:

(i) binding of the drug to DNA.

There are at least three possible modes for a drug to bind to DNA -

(a) intercalation

(b) interactions with the base groups or

(c) interactions with the phosphate groups.

Once a complex has coordinated to DNA, replication may be inhibited by the integral unit. Also, the metal may be removed from the complex if the ligand is labile enough; the released ligand may then intercalate or react with other cellular components. The metal may also play an active role in DNA destruction as it is known that both free copper or iron in oxygen atmospheres produce reactive free radicals [24].

(ii) deactivation of ribonucleoside diphosphate reductase (rdr).

This is a key enzyme in the synthesis of precursors of DNA (see Figure 1.4) and can be deactivated by either complexation of the free ligand by iron at the active site, or coordination of the copper complex to free thiols in the enzyme. The subsequent reduction of the coordinated complex results in the release of the ligand which can then complex the iron. Interruption of the cell cycle at the G_1/S interphase is

consistent with deactivation of rdr so this mechanism is favoured for cupric-thiosemicarbazones [25].

(iii) inhibition of the RNA dependent DNA polymerase (rddp).

Several thiosemicarbazones can inactivate RNA tumour viruses to cause malignant transformations as a result of the inhibition of rddp in the virion. It has been proposed that this is due to binding of the copper complex to the viral RNA since it has been found that N-methylisatin ß-thiosemicarbazone copper complexes bind to RNA and DNA [26,27].

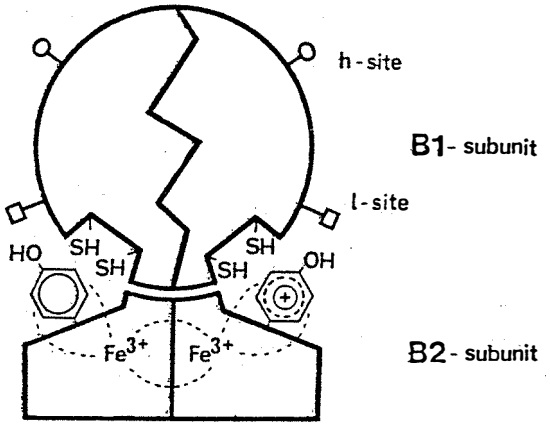

Figure 1.4 Schematic diagram of ribonucleoside diphosphate reductase (rdr) (after [25a]).

(iv) superoxide dismutase (sod) mimetic activity.

Sod is a copper/zinc containing enzyme which catalyses the dismutation of the superoxide radical as follows:

$$E\text{–}Cu^{2+} + O_2^{\cdot-} \rightarrow E\text{–}Cu^{+} + O_2 \quad \text{and}$$

$$E\text{–}Cu^{+} + O_2^{\cdot-} + 2H^{+} \rightarrow E\text{–}Cu^{2+} + H_2O_2$$

A deficiency of intracellular sod in malignant cells can result in an accumulation of superoxide which may attack cellular structures and initiate neoplasia. Other cellular pro-oxidant states (increased concentrations of active oxygen compounds including organic peroxides and oxy-radicals) could also promote initiated cells to neoplastic states [28]. It has been shown that some Cu(II) salicylates scavenge superoxide and may act as antineoplastic agents. For these complexes to disproportionate superoxide, they must be coordinatively unsaturated or have an easily displaced ligand so superoxide can complex. For this reason [7,29,30] the *in vivo* structure and/or thermodynamic stability of these complexes must be important.

(v) DNA-scission and protein-cleavage.

Ascorbate ions in the presence of oxygen and Cu(GHL) or Cu(o-phenanthrolines)$_2$ (which have antitumour activity in their own right) produce reactive oxygen species. These are capable of producing DNA-scissions and protein-cleavage because of the previously mentioned lower levels of oxygen-scavenging enzymes in malignant cells and hence act as anti-neoplastic agents [7,31].

(vi) The inhibition of DNA synthesis and oxidative phosphorylation by cuprous thiolates.

A possible mechanism for copper complexes of thiosemicarbazones is as follows for Cu(II)KTS (see equation):

$$Cu(II)KTS + 2RSH \rightarrow Cu(I)SR + H_2KTS + \tfrac{1}{2}RSSR$$

where RSH is an intracellular thiol. Once the cuprous thiolate has formed it can react with other thiols in an exchange reaction and it is these cuprous complexes which are thought to inhibit DNA synthesis and oxidative phosphorylation [7].

(vii) the facilitation of absorption and distribution of copper.

It has been generally assumed that copper complexes exhibited antineoplastic activities because of their cytotoxicity, but an attractive alternative is the ability of copper complexes to facilitate copper-dependent processes. In a disease state, as previously shown, plasma copper levels are increased. This mobilisation of low molecular weight copper complexes may be in an attempt to distribute copper for the synthesis of copper-dependent enzymes. Addition of copper drugs may therefore help in this absorption and distribution for the bodies defence mechanisms to operate more efficiently.

Because the field of inorganic antitumour drugs is in its infancy there are many more questions than answers at present. The mechanism of activity for cisplatin is emerging now after 10 years of research but little definite is known about copper complexes as yet. There appear to be a number of compelling reasons why copper complexes should be studied for their biological activities but only by extending the chemistry, (exploring new avenues and synthesising new compounds) and obtaining a better understanding of the mechanisms involved, can we hope to answer some of these questions.

1.7 Tridentate Ligands: Past and Present

As the present study involves the synthesis of a range of complexes based on the two tridentate ligand systems 2-formylpyridine thiosemicarbazone and salicylaldehyde benzoylhydrazone (see Figure 1.5) a brief review of tridentate ligand systems and their chemistry seems appropriate.

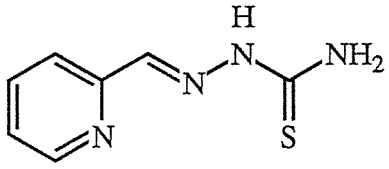

2-Formylpyridine thiosemicarbazone (LH)

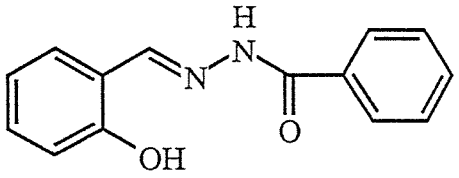

Salicylaldehyde benzoylhydrazone (sbH_2)

Figure 1.5 The two basic ligand systems used in this study.

Research on multidentate chelating agents has been stimulated by a number of factors, viz.

(a) their often unique stereochemical properties

(b) their widespread occurrence in nature and

(c) the many practical applications found for sequestering metal ions.

Interest in tridentate ligands initially focused on those containing nitrogen and mixed nitrogen/oxygen donor atoms - often Schiff-bases [32]. In the early 1960's a number of tridentate arsines and phosphines were also investigated (see Figure 1.6 for some structural examples). In these systems, the emphasis was on the synthesis and stereochemical properties of the complexes with limited reactivity studies and few solid state structure determinations being carried out.

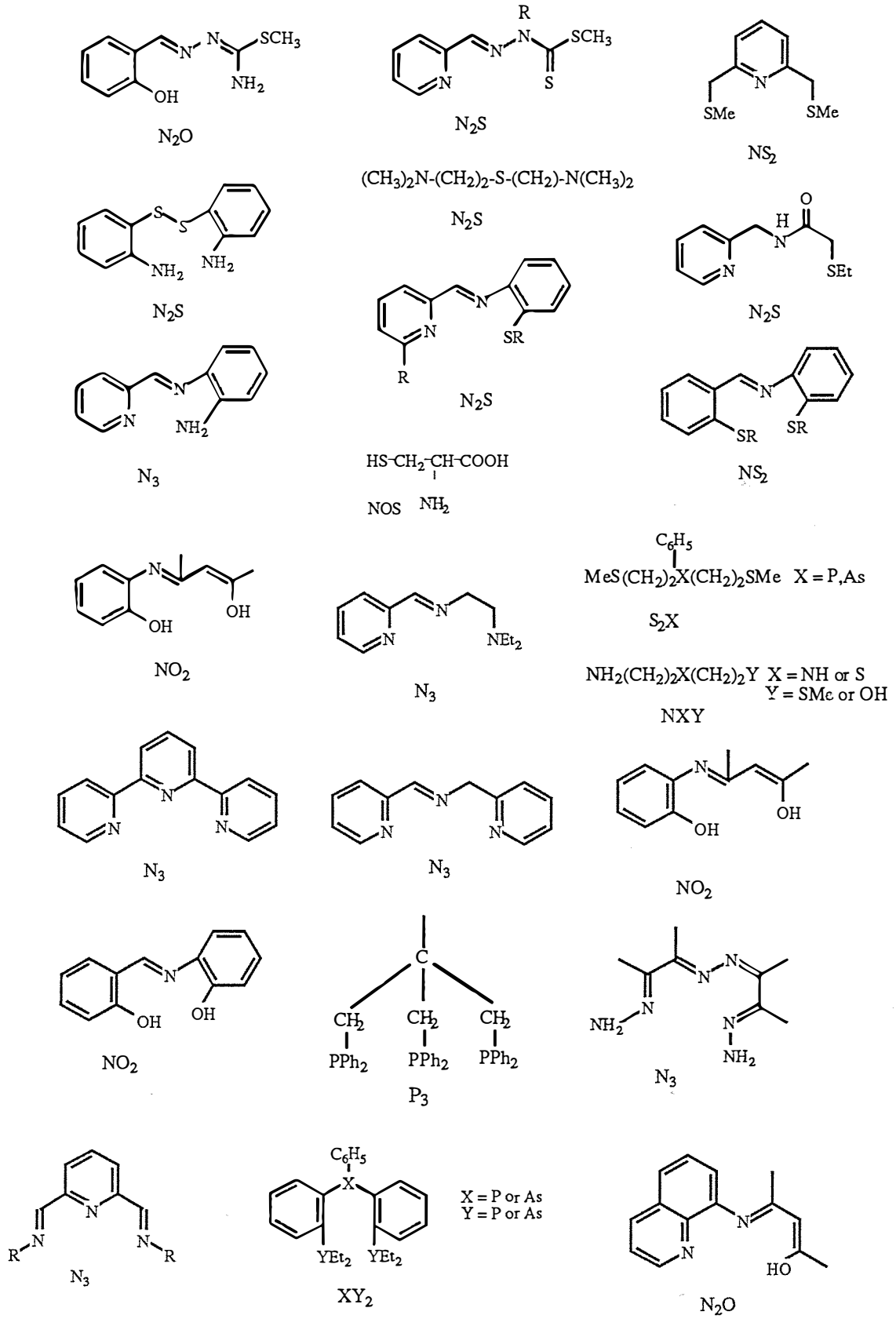

Figure 1.6 Some structural examples of tridentate ligands (after [33-43])

Interest in copper complexes of sulphur containing ligands was stimulated originally by their intense colour and more recently because of the presence of cysteine thiolate and methionine thioether sulphur coordination to copper in three copper proteins [44] and tetrahydrothiophene coordination in vitamin H (d-biotin) [43].

Livingstone *et al.* (see Figure 1.6 for some refs.) in the 1960's and 70's studied the transition metal coordination chemistry of mixed S and N containing tridentate ligands (see Figure 1.6). The physicochemical behaviour of these complexes was studied, and attempts were made (albeit crudely) to determine the coordination behaviour of the ligands as well as the stereochemistry of the complexes. As X-ray analyses were not generally available until the middle of the 60's, educated guesses were made about the structures of these complexes.

With the advent of high-speed computers for X-ray crystal structure analysis, easier access to more advanced spectroscopic and synthetic organic and inorganic techniques, complete characterisations of compounds are now possible.

1.8 The Present Study

The aims of the present study were to investigate and extend the solid state and solution chemistry on the potential tridentate antitumour ligand systems 2-formylpyridine thiosemicarbazone (LH - Section 1) and salicylaldehyde benzoylhydrazone (sbH_2 - Section 2: see Figure 1.5 for the ligand structures) and their metal complexes. The hope also was that solution studies would provide *in vitro* models to help confirm or deny various proposed mechanisms of antitumour behaviour which have been postulated for these systems. As well, the inorganic chemistry of these systems has not been overly studied so that there exists good potential for further investigations.

To obtain a full physicochemical study, single-crystal X-ray structural analyses, chemical reactivities, physical methods and spectroscopic techniques were applied and cytotoxic activities measured.

This thesis is divided into two: Section 1 dealing with LH (and its analogues) and their metal complexes and Section 2 with sbH_2 (and its analogues) and their metal complexes.

In Chapter 1, a series of copper complexes based on the halides and some pseudohalides were prepared for both the deprotonated and neutral ligand species. The single-crystal X-ray structures of $[Cu(LH)(CF_3COO)]_2(CF_3COO)_2$ and$[Cu(LH)(ClO_4)_2H_2O]\cdot 2H_2O$ are presented as well as the spectroscopic properties of the complexes prepared.

In Chapter 2, ternary copper complexes of the deprotonated ligand (L^-) with sulphur and nitrogen donor ligands were prepared and the single crystal X-ray structures of $[CuL(bipy)]ClO_4$ and $[CuL(saccharinato)H_2O]\cdot\frac{1}{2}H_2O$ are presented. Reactivity studies on CuL^+ species with thiolates gave e.s.r. and uv/vis spectra consistent with sulphur coordination and in some cases it was possible to isolate stable Cu(II) thiolato complexes.

In Chapter 3, copper complexes of LH and L^- with oxygen donors were prepared and the single-crystal X-ray structures of the tetrameric $[(CuL)_4P_2O_7]\cdot 12H_2O$ and the dimeric $[Cu(LH)(H_2PO_4)]_2(H_2PO_4)_2(H_3PO_4)_2\cdot 2H_2O$ are presented. As well, spectroscopic and magnetic properties of the complexes prepared are given.

In Chapter 4, three methylated versions of LH, a new ligand pbH, and their copper complexes as well as Zn, Cd, Hg, Ag, Au and Pb complexes of LH were prepared. Spectroscopic and n.m.r. data are used to characterise the compounds and pKa's determined and compared with the original and substituted ligands and their copper complexes.

In Chapter 5 (Section 2), a large range of ligands, based on sbH_2, and their Cu(II), Ni(II), Co(II), Cr(III) and Fe(III) complexes were prepared.

The single crystal X-ray structures of the dimeric $[Cu(sbH)ClO_4(EtOH)]_2$, the dimeric $[(Cu(sbH)H_2O)_2SiF_6]\cdot 2H_2O$ and the monomeric $[Cu(saH)Cl(H_2O)]H_2O$ are presented. The ligand sbH_2 was shown to be able to coordinate to copper in the neutral, anionic and dianionic forms, but little adduct chemistry was possible. Spectroscopic and n.m.r. data are presented and e.s.r. spectra and room temperature magnetic moments are used to show that magnetic coupling occurs in a number of copper complexes in the solid state.

Finally, in Chapter 6, the cytotoxicity results for all compounds tested are presented. Correlations between the Hansch lipophilicity parameter (π) and the Hammett electronic parameter (σ) and the activity of compounds as well as the significance of the transition metals in the complexes is discussed.

SECTION 1

STUDIES ON THE 2-FORMYLPYRIDINE THIOSEMICARBAZONE (LH) LIGAND SYSTEM

INTRODUCTION TO SECTION 1

1.9 Background

Thiosemicarbazide ($NH_2CSNHNH_2$–tsc) and thiosemicarbazones ($NH_2CSNHNR_1R_2$–tscone) have received considerable attention as chelating agents since Domagta's original report of anti-tubercular activity of thiosemicarbazones in 1946 [45]. Activities for tscones which now include anti:- tumour, viral, malarial, leprosy, influenza, protozoa and smallpox [46 and refs.therein] have been related to their metal-complexing ability, but few of these coordination compounds have been extensively studied.

Reported complexes generally involve the latter half of the transition metal ions, which is a reflection on sulphur's coordination preference for a "soft acid-soft base" type interaction. The importance of the tscones ability to coordinate metals for biological activity may be borne out by the observation that selenosemicarbazones are more active than the corresponding thiosemicarbazones as antifungal agents, which are in turn more active than the semicarbazones [47]. This may be attributed to the softer donor (Se→S→O) more readily complexing transition metals.

1.10 Complexes of Thiosemicarbazide

In all known complexes (except for Ag(I)) the tsc moiety coordinates as a bidentate chelator through sulphur and the hydrazinic nitrogen in the cis configuration [46] (see Figure 1.7).

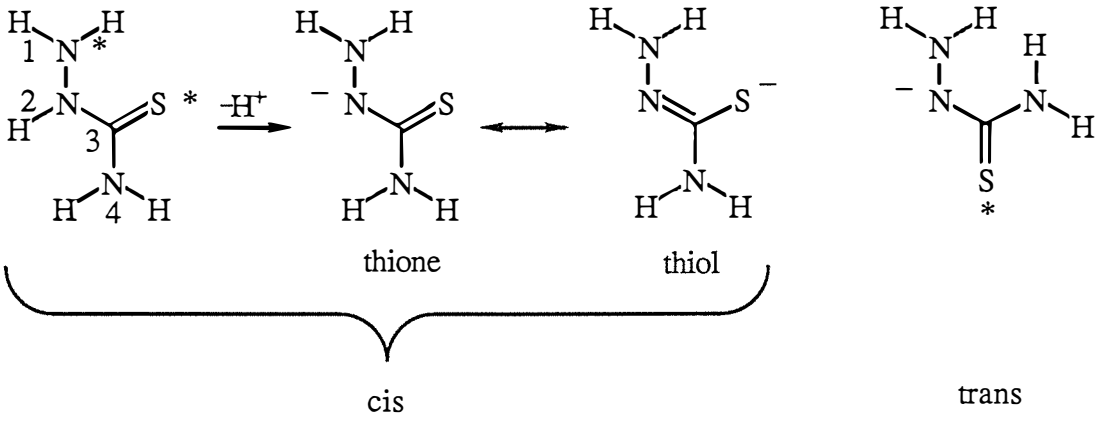

Figure 1.7 Conformations of thiosemicarbazide: bidentate(cis) and monodentate(trans). Coordination sites are indicated by *.

Although complexes of the general formulation $M(tsc)_2X_2$ have been isolated for divalent transition metals[46,48,49] (where for example M = Cu,Ni,Fe,Zn, and X = Cl^-, Br^-, NO_3^-, ClO_4^-, SO_4^{2-}) in one case it was shown to be possible to remove the proton from the central N(2) to form the complex $Ni(tsc–H)_2$ [46 and refs. therein]. The Ni–N and Ni–S bond distances in this complex are similar to those in $Ni(tsc)_2SO_4$ and $Ni(tsc)_2SO_4 \cdot 3H_2O$ but the bond angles about the Ni and the C–N(2) bond are markedly changed. In $Ni(tsc–H)_2$ the C–N(2) bond distance is shorter than in the protonated $Ni(tsc)_2X_2$ complexes (1.247 vs 1.333Å (av)) showing this to be essentially a localised double bond. The implication is that the ligand is binding in the thiolato form (see Figure 1.7). The ability to coordinate in either the neutral thione or deprotonated thiol form plays an important part in the transition metal chemistry of these ligands.

Silver(I), unlike the divalent metals, forms the only known complexes of tsc which are monodentate, coordinating through the sulphur[50,51]. All the structures involving Ag(I) and tsc carried out so far have in common a long Ag-S bond (2.99–3.10 Å) bridging another molecule as part of the coordination polyhedron. A number of copper(II) complexes of tscones have also been shown to have long Cu–S interactions and, as will be shown, these are important in the solid state magnetic behaviour of these complexes.

1.11 Complexes of Thiosemicarbazones

Thiosemicarbazone ligands are generally derived by condensing aliphatic, aromatic, or heterocyclic aldehydes or ketones with thiosemicarbazide (see Figure 1.8):

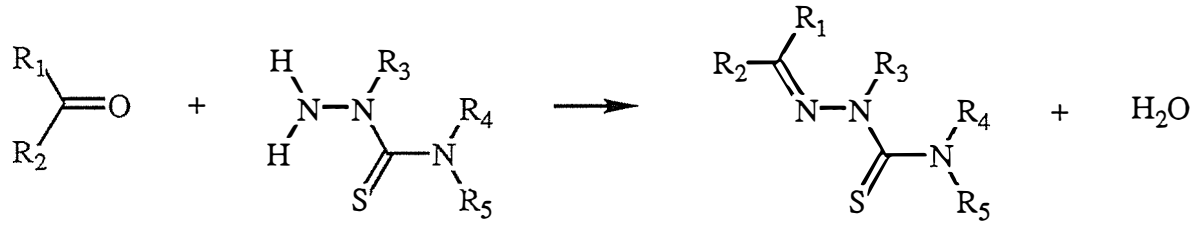

Figure 1.8 Reaction scheme for the formation of thiosemicarbazones.

In the solid state the tscone usually exists in the thione form but, in solution, if R_2 = H, it is in equilibrium with its tautomeric thiol form [46,52].

Where the R groups do not possess suitable coordinating groups, the tscone usually acts as a bidentate moiety, coordinating through the now imine nitrogen and the thione/thiol (if R_3 = H) sulphur (see Figure 1.9(a)).

(a) (b)

Figure 1.9 Coordination modes of bidentate thiosemicarbazones. Coordination sites are indicated by *.

If the sulphur centre has been substituted, it has been shown [53] that bidentate bonding may still occur, but now through the hydrazine nitrogen and the amide nitrogen (see Figure 1.9(b)).

When an additional suitable coordinating functionality is present, the ligands can complex in a tridentate manner (e.g. see Figure 1.10):

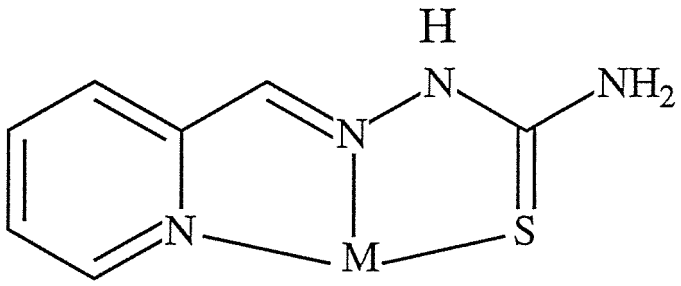

Figure 1.10 An example of a tridentate thiosemicarbazone: 2-formylpyridine thiosemicarbazone (LH).

It has been shown recently [54] that alkylation of the sulphur of thiosemicarbazone derivatives, not only results in coordination through the terminal amino group, but confers sufficient acidic character to the coordinated ligands that they can condense with a second aldehyde or ketone to give tetradentate ligands (see Figure 1.11).

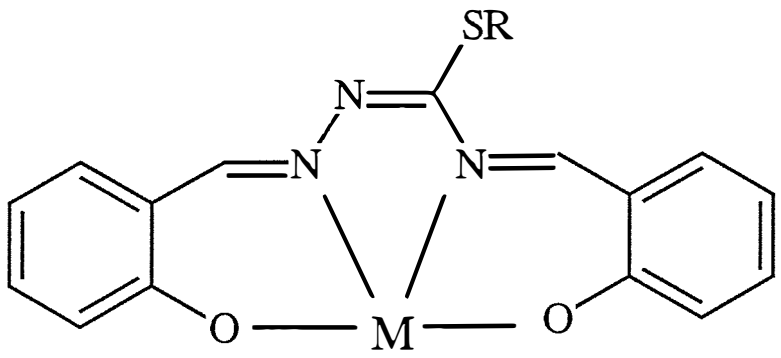

Figure 1.11 An example of a tetradentate thiosemicabazone.

It has been claimed that complexes isolated from such template reactions have no sulphur coordination [55].

Reaction of a dialdehyde or diketone with two moles of a thiosemicarbazide can yield tetradentate and pentadentate ligands e.g. kethoxal-bis(thiosemicarbazone) [56] ($KTSH_2$ -see Figure 1.3).

The complex stability in going from bidentate to tridentate to a tetradentate tscone, as expected, greatly increases, as exemplified and shown by the log stability constants for the copper complexes of tsc, LH and $KTSH_2$: 6.1 [46] < 16.9 [57] < 22.2 [56] (see Figures 1.7, 1.10 and 1.3 respectively for the structures of these ligands). Although a large number of transition metal complexes with a wide range of tscones (see Table 1.2) have now been synthesised, few of these investigations have been concerned with the synthetic aspects of these complexation reactions. Instead many rely upon spectral studies and tend to be tentative in nature.

Large amounts of ir data have been tabulated on tscone compounds, but because of the complex nature of the spectra, only a limited number of single or group modes can be

assigned with any certainty. In their review of tscones in 1985, Kauffman and Padhye [52] stated that the stereochemistries adapted by tscone complexes of transition metals are most commonly octahedral and square planar but on rare occasions, five-coordinate structures have been obtained. This generalisation is based mainly on spectroscopic and magnetic data, as well as a limited number of X-ray crystal structures. Unfortunately, for copper complexes, few crystallographic studies have been carried out, and the interpretation of spectroscopic data tends to lead to ambiguous results.

A large number of these tscones synthesised were for structure/activity relationship studies and have apparently not had any transition metal complexes investigated [58,59].

The precise mechanism by which tscones exert their biological activity is still unclear. A number of possibilities have been put forward, some of which are included in the general introduction (see page 11), but the main ones will briefly be expanded upon here.

The deactivation of ribonucleoside diphosphate reductase (rdr) and the inhibition of DNA synthesis and oxidative phosphorylation by cuprous thiolates (mechanisms (ii) and (vi) from the General Introduction respectively), have the same basic first step in their mechanisms: namely, the reduction of the cupric complex by thiolates to a cuprous species. There is no spectral evidence for significant adduct formation between CuKTS and Lewis bases whereas for CuL^+ such species have been shown to be present *in vivo* and isolated *in vitro* [present study, 72,73 and refs. therein]. Both mechanisms have the copper complex as the active species, therefore the redox potentials of these complexes are important. With one exception, the relative rates of thiol oxidation can be correlated with the *in vitro* cytotoxicity for a range of CuKTS analogues [71 and refs. therein].

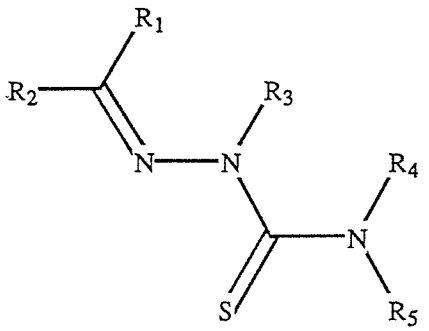

R_1	R_2	R_3	R_4	R_5	ref.
CH_3	CH_3	H	H	H	[46]
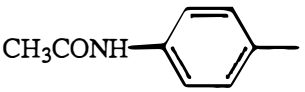		H	H	H	[16]
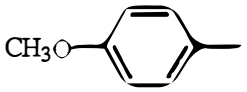		H	H	H	[60,61]
C_2H_5O-CO-CH_2-		CH_3	H	H	[62]
isoquinoline 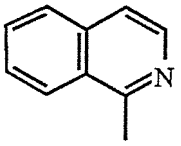		H	H	H	[63]
pyridine 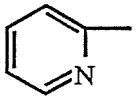		H	H	H	[64-66]
pyridoxal 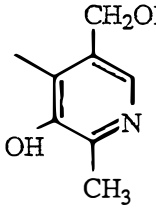		H	H	H	[67,68]
isatin 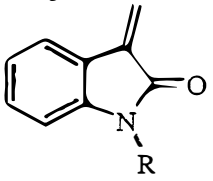		H	H	H	[69]
pyridine-N-oxide 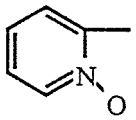		CH_3	H		[70]
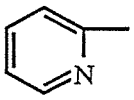		CH_3	H	CH_3	CH_3	[71]

Table 1.2 Some examples of thiosemicarbazones.

In a study on the combined modality of CuL^+ and radiation [74], either inhibition of rdr by binding to a form of the antitumour agent or interacting by means of a redox couple was considered consistent with the generally observed blockage at the G_1/S interphase. Although cells are most sensitive at the G_1/S interphase, some whole cycle killing is caused which suggests an alternative or secondary mechanism. This may be similar to radical formation as the presence of thiols and O_2/CuL^+ is known to generate $O_2^{\cdot-}$ and ·OH [75] and encompasses the theme of radicals for mechanism (iv) (see the General Introduction).

Very little consideration has been given to the possibility of DNA binding for Cu tscones (mechanism (i) in the General Introduction) most probably due to the observed blockage of the cell cycle at the G_1/S interphase. For the tridentate copper(II) metallodrug 1–(α–pyridylmethylene)–2–(α–pyridyl)hydrazine (see Section 2, Figure 2.2(b)), intercalation was found to be insignificant and of the other two broad classes of binding, outside binding to phosphato groups rather than base binding was most consistent with the data obtained [76].

The underlying themes for all the mechanisms proposed to date show the exact nature of the cytotoxic species is uncertain but copper appears to be necessary. Because of the difficulties in studying metallodrugs *in vivo*, the exact mechanism/s or site/s of action are uncertain.

1.12 2-Formylpyridine Thiosemicarbazide (LH)

LH behaves as a tridentate monoanionic or neutral ligand depending upon the pH (see Figure 1.12). In acid conditions (pH < 2.4) the ligand coordinates through the pyridine N, the imine N and the predominantly thione S whereas in the anionic form coordination is through thiolate S as well as the two Ns.

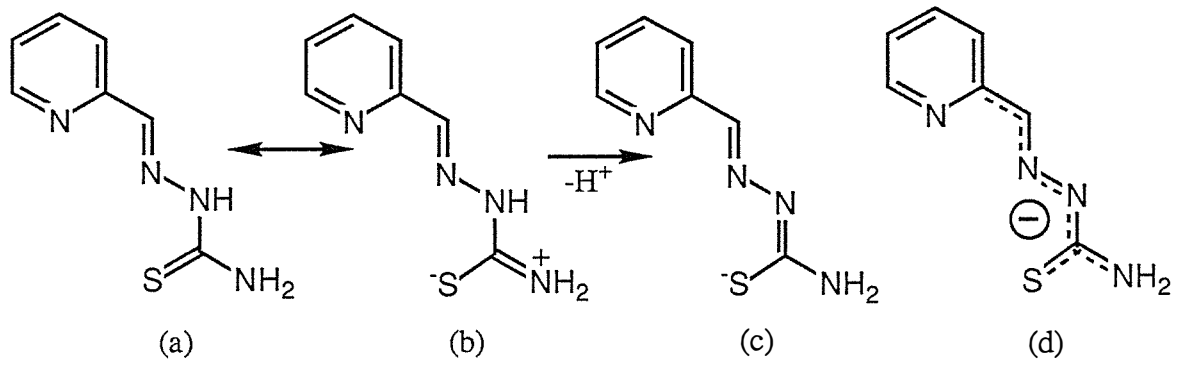

Figure 1.12 Resonance forms for 2-formylpyridine thiosemicarbazone.

In the solid state and acid conditions form (a) predominates whereas for the deprotonated species it is (c). Resonance stabilisation of canonical forms means the bonding can not truly be represented by structures (a) → (c) and is best represented by some intermediate conjugated system such as (d).

When LH is complexed to transition metal ions, two general stereochemistries of the ligand are adopted, depending on the metal: an octahedral configuration of two orthogonal ligands or a 'square planar' structure (see Figure 1.13). Addition of a second mole of L^- to CuL^+ to form the complex CuL_2, similar to (a) has not proven possible.

Until recently, little of the chemistry of LH with transition metals had been investigated, possibly due in part to the difficulty in obtaining 2-formylpyridine (pyridine-2-aldehyde) and to the fact that the majority of researchers interested in the system were pharmacologically orientated.

5–OH LH was used in clinical trials but was dropped due to severe gastro-intestinal toxicity and large-scale mobilisation of iron by complexation, forming a blue Fe/L^- complex which was excreted in the urine [77].

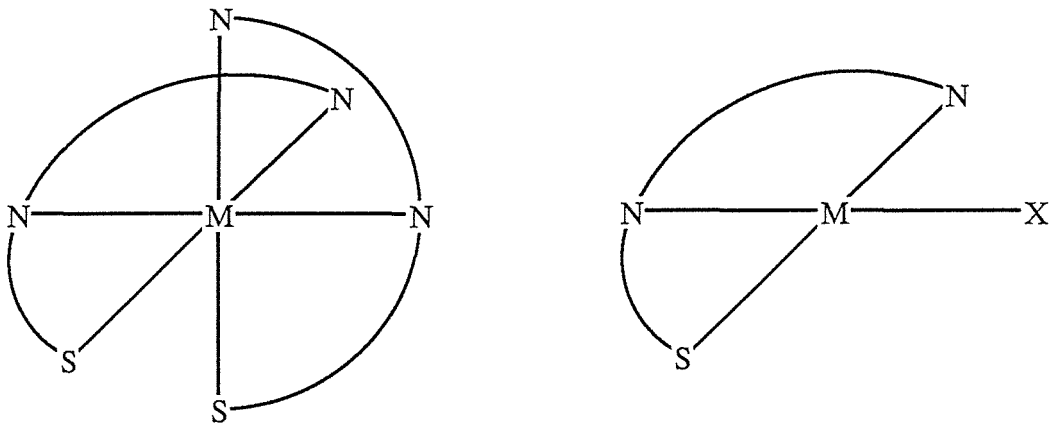

(a) octahedral (M = e.g. Fe(III),Ni(II))

(b) square planar (M = e.g. Cu(II))

Figure 1.13 Schematic diagrams for the coordination modes of NNS tridentate thiosemicarbazones.

The original complexes prepared for antitumour work appear to have been $CuL(CH_3COO)$, $(CuL)_2SO_4$ [26] and FeL_2/FeL_2^+ [78]. Little was done to characterise these complexes in the solid state as the research was predominantly centered around their interactions with biological systems. Ir data on LH and its complexes, as with the tscones, proved to be difficult and ambiguous in interpretation and a limited number of bands could be assigned with certainty. More recently, the resonance raman spectra of Fe(II) and Fe(III) and the pre-resonance raman spectra of Cu(II) and Zn(II) complexes of L^- and LH itself have been studied [78,79]. These were carried out over a range of pHs and assignments of vibrations have been made.

As stated, the majority of the research on LH and its Cu and Fe complexes, until recently, was biologically orientated. A large number of compounds based on LH and the closely related 1-formylisoquinoline thiosemicarbazone were prepared by French *et al.* in the late 1960s [59,80]. Later these were reanalysed by Dunn and Hodnett in 1977 [81] and tested for their

carcinostatic activity [58] and for the inhibition of tumour-derived rdr [59]. A number of trends were observed within these LH series of compounds, the major ones being:

(a) 2-formylpyridine thiosemicarbazone was active but its 3 and 4 isomers were not,

(b) lipophilic and electronic effects are important in determining the level of potency,

(c) highly ionic or readily metabolizable groups (e.g. –OH) are to be avoided,

(d) substitution of Me, Et or Ph into any position on the side chain results in reduced or lost activity,

(e) electron withdrawing groups in the pyridine ring are less active,

(f) bulky substituents may sterically inhibit binding at the active site in rdr.

The finding that the 3 and 4 isomers were inactive confirms earlier findings [82] and it was postulated that the N-N-S tridentate constellation was necessary for binding to divalent transition metals [83]. Electron withdrawing groups within the pyridine ring would destabilise this chelate formation and hence reduce potency.

Findings on the stabilities of the Fe(II) complexes (2:1) tend to rule out the hypothesis that this is the active form of the drug [59]. Unfortunately trials with Cu(II) were not conducted in conjunction with the Fe(II) so a comparison could not be made, but there is a large body of evidence from other researchers which suggests the Cu(II) adduct is the active form of these drugs [74,84].

Physical measurements on a series of 5-substituted versions of LH and their copper complexes were carried out by Petering *et al.* in 1979 [57]. Protonation constants for the

ligands and complexes, formation constants for the copper complexes and half-wave reduction potentials of the Fe(III) and Cu(II) were measured. The complex formation constants were determined by using ethylenediamine (en) as a competing ligand with L^-. E.s.r. spectra of the species involved showed the formation of an en adduct; $CuL(en)^+$. In Petering's work, it was found that there was a trend in antitumour activity with respect to the substituent in certain cell lines (if only the active compounds were considered) and that there may be other reasons, such as differences in drug solubility, which render compounds inactive. Only small changes in the binding constants and pKa's were observed for the substituents tested, even with the variation in $E_{½}$ recorded. From these findings, all complexes were expected to be sufficiently stable in biological systems so that they can reach and then react with thiols the proposed cellular target.

To further investigate the interaction of CuL^+ with biological systems, studies utilising human plasma and red cell components, human and cat haemoglobins (Hb), ferritin and ascites fluid were carried out by Antholine *et al.* [85-87]. Findings of this work have proven interesting. When $Fe(III)L_2^+$, $Fe(II)L_2$ under anaerobic conditions, or CuL^+ were incubated in human plasma and mouse ascites fluid, no change in the visible spectra was observed after 30-60 minutes. This implies the metal complexes are stable in typical biological media, in agreement with the physical results previously reported.

When CuL^+ interacts with cat Hb, adducts with S and N donor atoms were formed whereas for human Hb, only N adducts were detected, using e.s.r. spectroscopy. The adducts formed resulted in increased oxygen affinity for the Hbs and it was suggested that allosteric enzyme inhibition may be a mechanism for this drug [86].

CuL^+ adducts of glutathione (HSG) and Hb have been proposed as the initial species formed upon addition of CuL^+ to human red cells as determined by e.s.r. spectroscopy. The CuL-SG adduct once formed probably catalyses the oxidation of excess HSG to the disulphide (GSSG) using molecular oxygen.

In spite of these solution studies showing Lewis-base adduct formation for CuL^+, no *in vitro* adducts had been isolated. Instead they were only detected by spectroscopic means and the possibility of such interactions were inferred.

Three papers simultaneously published in 1987 by Ainscough *et al.* [64] and Bell *et al.* [65,66] reported the first systematic studies *in vitro* of LH with Cu(II) and single crystal X-ray crystallographic structures.

The complexes CuLX, where X = Cl^-, Br^-, I^-, CH_3COO^-, NO_3^-, ClO_4^-, SCN^- and Cu(LH)Y where Y = SO_4^{2-} and $2Cl^-$ were isolated and characterised by spectroscopic means. The single-crystal X-ray crystallographic structures of the compounds formulated as $CuL(CH_3COO)$ and $Cu(LH)SO_4$ showed them to be in fact centrosymmetric dimers, viz. $[CuL(CH_3COO)]_2$ and $[Cu(LH)SO_4]_2$, with bridging anions. The ligand coordinates in a planar tridentate N-N-S constellation in both the neutral $[Cu(LH)SO_4]_2$ and deprotonated $[CuL(CH_3COO)]_2$ structures. An anion oxygen occupies the fourth in-plane position and the distorted square-pyrimadal geometry is completed by a longer axial bond to the bridging anion from the other centrosymmetrically related half of the dimer.

Although these complexes are dimers, and three of the other copper compounds reported had low room temperature magnetic moments viz. ($CuL(ClO_4)$, $CuL(NO_3)$ and $Cu(LH)Cl_2$), no low temperature magnetic data was reported.

The reactivity of the CuL^+ species towards model cellular components such as thiolates, phosphates and nitrogen bases is not known because no adduct chemistry has been carried out on the CuLX system to test *in vitro* the proposed *in vivo* mechanisms.

The aqueous solubility and stability of CuL^+, the ease of metathetical replacement of CH_3COO^- from $[CuL(CH_3COO)]_2$, the possibility of both deprotonated and neutral forms of

the coordinated ligand and the proven dimeric nature of the copper complexes affords an excellent opportunity to study a wide range of anions in a variety of coordination modes.

From a consideration of all of these aspects and the paucity of physicochemical and structural data on the Cu/LH system, an extensive range of mainly copper(II) complexes of 2-formylpyridine thiosemicarbazone (LH) was undertaken using a number of physicochemical and spectroscopic techniques. The results of this study are presented in Section 1, Chapters 1 to 4 of this thesis.

CHAPTER 1

HALIDE AND PSEUDOHALIDE COPPER COMPLEXES OF LH/L$^-$

1.1.1 INTRODUCTION

Few systems exist where a ligand can coordinate to a transition metal either as a neutral or anionic species. One such system is provided by 2-formylpyridine thiosemicarbazone (LH) bound to copper(II). Earlier work from this laboratory identified the deprotonated ligand in the complex $[CuL(CH_3COO)]_2$ whereas the protonated form was found in $[Cu(LH)SO_4]_2$. The remarkable stability of the copper(II)/2-formylpyridine thiosemicarbazone system, over a wide pH range, allows it to be used as a probe for the coordination modes of a variety of anions.

In this, the first chapter, complexes of the general formulation $[CuLX]_2$ for the deprotonated and $[Cu(LH)X]_2X_2$ for the protonated ligand have been synthesised (where X = halide, pseudohalide, CF_3COO^-, NO_3^-, ClO_4^- and $\frac{1}{2}(SO_4^{2-})$). Two stable copper(I) complexes were also prepared.

During the course of this study, Bingham *et al.* [64] and Bell *et al.* [65,66] simultaneously published between them the syntheses and characterisation of the complexes $[CuLX]_2$ (where X = CH_3COO^-, Cl^-, Br^-, I^-, NO_3^-, ClO_4^- and SCN^-), $[Cu(LH)X]_2X_2$ (where X = Cl^- and $\frac{1}{2}(SO_4^{2-})$) and the copper(I) complex [Cu(LH)Cl]. The complexes presented in this chapter include further study on those mentioned above (except [Cu(LH)Cl]) and extends the series of halides and pseudohalides. Characterisation of the compounds was performed using electronic, infrared and electron spin resonance spectroscopies. The single-crystal X-ray crystallographic structures of the neutral ligand complexes $[Cu(LH)(ClO_4)_2H_2O]\cdot 2H_2O$ and $[Cu(LH)(CF_3COO)]_2(CF_3COO)_2$ were solved.

Synthesis of the Complexes

Two general methods of preparation for the copper(II) complexes were employed in this section. In the first, the ligand 2-formylpyridine thiosemicarbazone (LH) was added to the appropriate copper(II) salt to yield anionic ligand complexes;

$$CuX_2 + LH \rightarrow CuLX + HX \quad (X = \text{e.g. } CH_3COO^- \text{ or } ClO_4^-).$$

The second method used involved the metathetical displacement of the acetato anion from an aqueous solution of $[CuL(CH_3COO)]_2$ using either an acid to give neutral ligand complexes;

$$CuL(CH_3COO) \xrightarrow{H_2O} CuL^+ \xrightarrow{HX} Cu(LH)X_2 \quad (X = \text{e.g. } CF_3COO^- \text{ or } ClO_4^-)$$

or a simple salt to retain the anionic ligand;

$$CuL^+ \xrightarrow{X^-} CuLX \quad (X = \text{e.g. } I^- \text{ or } NCS^-).$$

The last reaction type illustrates the ability of the ligand to stabilise the copper(II) oxidation state when the counter ion is a reducing species for the copper(II) aqua ion. The formation of Cu(I) complexes e.g. Cu(I)(LH)I and $Cu(I)(LH)ClO_4$ with this ligand can however be achieved in some cases by using a Cu(I) salt in the presence of excess reducing agent.

The complexes prepared in this chapter are given in Table 1.1.1 along with their analytical and room temperature magnetic moment data.

TABLE 1.1.1

Analytical and Magnetic Data for Chapter 1

Complex	Colour	Analyses (%)[a]				μ_{eff}[b]
		C	H	N	Other	
$[CuL(CH_3COO)]_2$	Dark Green	36.1 (35.8)	3.8 (3.4)	18.5(18.6)		1.82
$[Cu(LH)(CF_3COO)]_2(CF_3COO)_2$	Green Black	28.2 (28.1)	1.7 (1.7)		24.3 (24.5)[c]	1.83
$[CuLF]_2 \cdot 5{\cdot}4H_2O$[d]	Dark Green	27.1 (27.1)	3.3 (4.0)	17.4 (18.1)	6.4 (6.1)[c]	1.71
$[Cu(LH)F]_2F_2$	Dark Green	29.4 (29.8)	2.9 (2.9)	19.5 (19.9)	13.4 (13.4)[c]	1.45
$[CuLCl]_2H_2O$	Dark Green	29.4 (29.4)	2.6 (2.8)	19.8 (19.6)		1.88
$[Cu(LH)Cl]_2Cl_2 \cdot 2H_2O$	Pale Green	25.1 (25.3)	3.0 (3.0)	16.5 (16.8)		1.86
$[CuLBr]_2$	Dark Green	26.0 (25.8)	2.2 (2.1)	17.4 (17.2)		1.83
$[Cu(LH)Br]_2Br_2 \cdot 2H_2O$	Green	19.9 (19.9)	2.3 (2.4)	13.5 (13.3)		1.78
[CuLI]	Brown	23.0 (22.7)	1.9 (1.9)	15.5 (15.2)		1.78
$[Cu(LH)I]_2I_2$	Red Orange	16.8 (16.9)	1.8 (1.6)	11.2 (11.3)	50.9 (51.0)[e]	0.43_{av}
$[Cu(LH)I] \cdot \frac{3}{2} H_2O$	Brown	21.0 (21.1)	2.1 (2.8)	13.6 (14.1)	34.5 (32.4)[e]	Diamagnetic
$[CuL(NO_3)]_2$	Green Black	27.5 (27.6)	2.8 (2.3)	22.3 (23.0)		1.42
$[CuLH(NO_3)_2H_2O]$	Green	21.7 (21.8)	2.6 (2.6)	21.6 (21.8)		1.82
$[CuL(ClO_4)]_2$	Green	24.6 (24.6)	2.6 (2.1)	15.7 (16.4)		1.34
$[Cu(LH)(ClO_4)_2H_2O] \cdot 2H_2O$	Emerald	17.6 (17.6)	2.3 (3.0)	11.6 (11.8)		1.87
$[Cu(LH)(ClO_4)]$	Red Orange	25.6 (24.5)	2.5(2.4)	16.3 (16.3)	12.1 (10.3)[f]	Diamagnetic
$[(CuL)_2SO_4(H_2O)_2]H_2O$	Green	26.2 (26.5)	2.5 (3.2)	17.6 (17.6)		1.76
$[Cu(LH)(SO_4)]_2$	Blue Green	24.7 (24.7)	2.6 (2.4)	16.5 (16.5)		1.86
$[CuL(NCS)]_2$	Green	31.8 (31.9)	2.3 (2.4)	23.1 (23.3)		1.81
$[CuLN_3]_2H_2O$	Dark Green	28.6 (28.6)	2.4 (2.4)	34.2 (33.4)		1.83
$[CuL(CN)]_2 \cdot 2H_2O$	Brown	34.0 (33.5)	2.9 (3.2)	24.6 (24.4)		2.04

a calculated values given in parentheses
b measured at 293 K and quoted in B.M. per copper(II) ion
c % F
d hygroscopic complex
e % I
f % Cl

1.1.2 CRYSTAL STRUCTURE OF Di-μ-trifluoroacetato-bis[(2-formylpyridine thiosemicarbazone) copper(II)] Bistrifluoroacetate

A thermal ellipsoid diagram for the title compound (abbreviated as $[Cu(LH)(CF_3COO)]_2(CF_3COO)_2$) showing the numbering scheme used is depicted in Figure 1.1.1. Bond length and angle data are given in Tables 1.1.2 and 1.1.3 respectively.

The complex $[Cu(LH)(CF_3COO)]_2(CF_3COO)_2$ crystallises as a discrete centrosymmetric dimer, bridged by two trifluoroacetato ligands; the remaining trifluoroacetates are not coordinated. The copper adopts a distorted square-pyramidal geometry with an approximately planar base to this pyramid. The base is comprised of the tridentate 2-formylpyridine thiosemicarbazone NNS moiety, with the fourth position occupied by a CF_3COO^- oxygen atom. The coordination geometry is completed by a fifth axial oxygen from a more weakly bound bridging CF_3COO^-.

The plane of best-fit* through the donor atoms S, N(1), N(2) and 0(11) shows the copper atom to be displaced out of the mean-plane (by 0.102 Å) toward the bridging axial oxygen 0(11'). A very similar situation exists for the complex $[CuL(CH_3COO)]_2$ despite the fact that here the ligand is in the deprotonated form [64]. Again, the copper lies out of the mean-plane of the four donor atoms (0.086 Å) towards 0(11').

The in-plane bonding distances for the copper complexes of 2-formylpyridine thiosemicarbazone are given in Table 1.1.4. The remarkable feature demonstrated here, is that there are no differences between the average bond lengths in going from the neutral, protonated

* Plane (i) S, N(1), N(2), 0(11)
-0.1165X -0.4575Y -0.8815Z + 4.3498 = 0
[S 0.006, N(1) 0.007, N(2) -0.008, 0(11) -0.006, Cu 0.102]
Distances of atoms from the plane (Å) are given in square brackets.

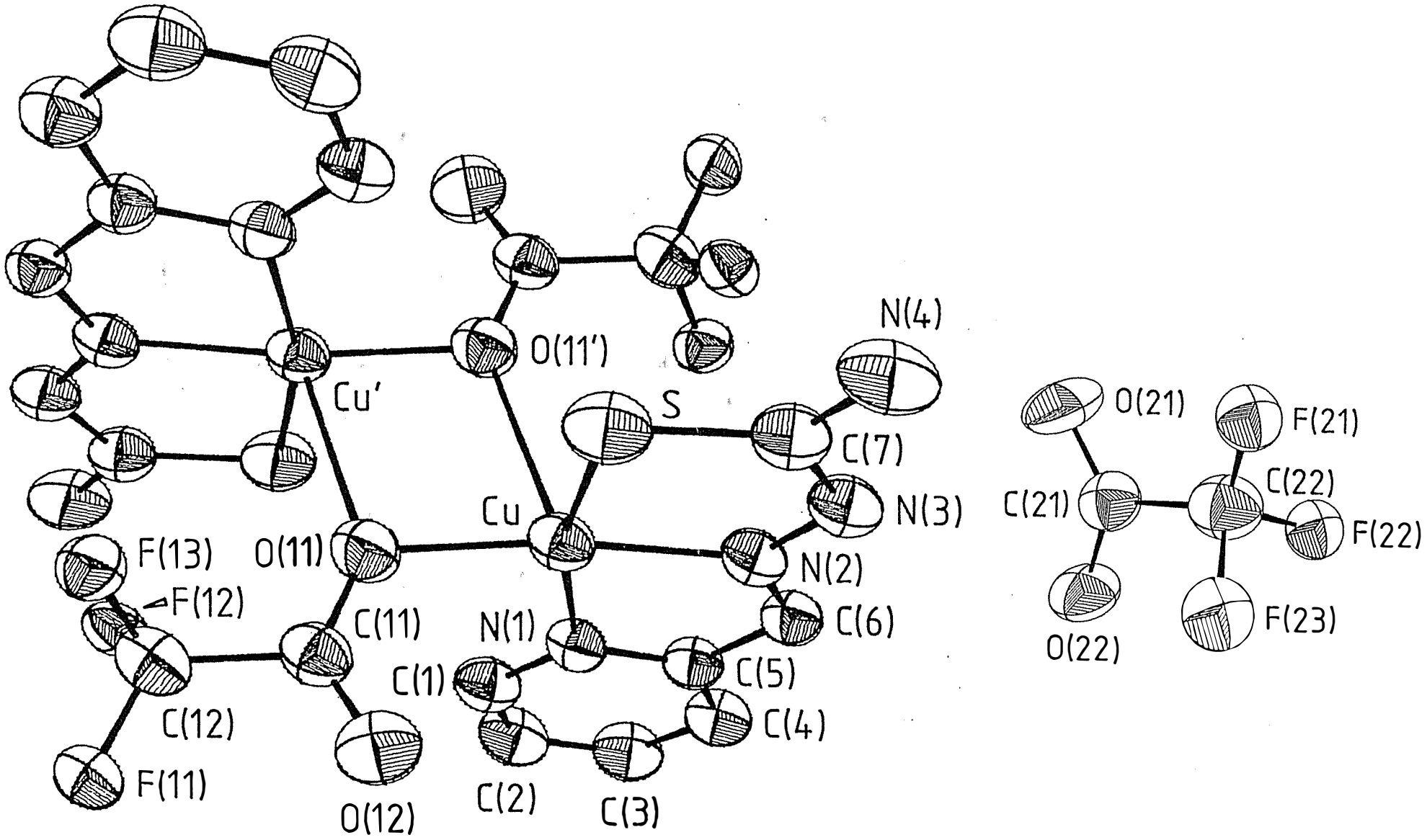

Figure 1.1.1: The dimeric cation for $[Cu(LH)(CF_3COO)]_2(CF_3COO)_2$ and a non-coordinated CF_3COO^- anion (arbitrary positioning) showing the atom numbering scheme. Hydrogen atoms have been omitted for clarity.

TABLE 1.1.2
Bond Lengths (Å) with Estimated Standard Deviations in Parentheses for the Complexes $[Cu(LH)(ClO_4)_2H_2O]\cdot 2H_2O$ and $[Cu(LH)(CF_3COO)]_2(CF_3COO)_2$*

	$[Cu(LH)(ClO_4)_2\ H_2O]\cdot 2H_2O$		$[Cu(LH)(CF_3COO)_2]_2$ $(CF_3COO)_2$
Cu–N(1)	2.018(2)		2.034(3)
Cu–N(2)	1.932(2)		1.959(3)
Cu–S	2.278(1)		2.275(1)
S–C(7)	1.707(3)		1.715(4)
N(1)–C(1)	1.324(4)		1.336(4)
N(1)–C(5)	1.364(4)		1.348(5)
N(2)–N(3)	1.363(3)		1.348(3)
N(2)–C(6)	1.287(4)		1.287(5)
N(3)–C(7)	1.348(4)		1.356(5)
N(4)–C(7)	1.313(4)		1.305(4)
C(1)–C(2)	1.402(5)		1.386(5)
C(2)–C(3)	1.368(6)		1.399(6)
C(3)–C(4)	1.380(5)		1.388(4)
C(4)–C(5)	1.383(5)		1.378(5)
C(5)–C(6)	1.461(4)		1.460(4)
Cu–O(1)	1.931(2)	Cu–O(11)	1.948(3)
Cu–O(11)	2.595(4)	Cu–O(11′)	2.516(4)
Cu–O(21)	2.712(5)	Cu···Cu′	3.557(4)

Perchlorate and Trifluoroacetate Bond Lengths (Å)

		O(11)–C(11)	1.273(3)
Cl(1)–O(11)	1.434(3)	O(12)–C(11)	1.202(4)
Cl(1)–O(12)	1.425(4)	C(11)–C(12)	1.549(5)
Cl(1)–O(13)	1.436(3)	O(21)–C(21)	1.228(5)
Cl(1)–O(14)	1.459(4)	O(22)–C(21)	1.252(4)
Cl(2)–O(21)	1.405(4)	C(21)–C(22)	1.527(6)
Cl(2)–O(22)	1.446(8)		
Cl(2)–O(23)	1.460(6)		
Cl(2)–O(24)	1.402(9)		
Cl(2)–O(25)	1.540(16)		
Cl(2)–O(26)	1.453(21)		
Cl(2)–O(27)	1.425(19)		

* C–F bond lengths 1.10–1.55 Å, mean 1.35 Å
N(4)–H bond lengths 0.92–1.00 Å, mean 0.97 Å
O–H bond lengths 0.87–1.14 Å, mean 1.01 Å
C–H and N(3)–H(31) bond lengths fixed at 1.08 Å

TABLE 1.1.3
Bond Angles (°) with Estimated Standard Deviations in Parentheses for the Complexes $[Cu(LH)(ClO_4)_2H_2O]\cdot 2H_2O$ and $[Cu(LH)(CF_3COO)]_2(CF_3COO)_2$*

	$[Cu(LH)(ClO_4)_2H_2O]\cdot 2H_2O$		$[Cu(LH)(CF_3COO)_2]_2(CF_3COO)_2$
N(1)–Cu–N(2)	80.5(1)		80.3(1)
N(1)–Cu–S	165.7(1)		163.9(1)
N(1)–Cu–O(1)	96.3(1)	N(1)–Cu–O(11)	96.7(1)
N(1)–Cu–O(11)	76.8(1)	N(1)–Cu–O(11′)	91.9(1)
N(1)–Cu–O(21)	79.5(1)		
N(2)–Cu–S	85.1(1)		84.2(1)
N(2)–Cu–O(1)	176.0(1)	N(2)–Cu–O(11)	173.1(1)
N(2)–Cu–O(11)	88.7(1)	N(2)–Cu–O(11′)	111.1(1)
N(2)–Cu–O(21)	82.9(2)		
S–Cu–O(1)	98.0(1)	S–Cu–O(11)	98.3(1)
S–Cu–O(11)	103.1(1)	S–Cu–O(11′)	97.7(1)
S–Cu–O(21)	98.8(1)		
O(1)–Cu–O(11)	92.9(1)	O(11)–Cu–O(11′)	75.1(1)
O(1)–Cu–O(21)	94.2(2)	Cu–O(11)–Cu′	104.9(1)
O(11)–Cu–O(21)	155.9(2)		
Cu–N(1)–C(1)	129.0(2)		128.6(3)
Cu–N(1)–C(5)	112.2(2)		112.7(2)
C(1)–N(1)–C(5)	118.9(3)		118.7(3)
N(1)–C(1)–C(2)	122.3(3)		122.2(4)
C(1)–C(2)–C(3)	118.8(3)		118.8(3)
C(2)–C(3)–C(4)	119.2(3)		118.8(3)
C(3)–C(4)–C(5)	119.8(3)		118.7(4)
C(4)–C(5)–C(6)	124.3(3)		122.9(3)
N(1)–C(5)–N(1)	121.1(3)		122.7(3)
N(1)–C(5)–C(6)	114.7(2)		114.3(3)
C(5)–C(6)–N(2)	114.0(3)		115.6(3)
C(6)–N(2)–Cu	118.7(2)		117.0(2)
N(3)–N(2)–Cu	120.7(2)		121.8(2)
N(2)–N(3)–C(7)	116.5(2)		115.8(3)
C(6)–N(2)–N(3)	120.6(2)		121.1(3)
N(3)–C(7)–S	121.6(2)		121.4(2)
N(3)–C(7)–N(4)	117.1(3)		116.6(4)
S–C(7)–N(4)	121.3(2)		121.9(3)
C(7)–S–Cu	96.0(1)		96.7(1)

Perchlorate and Trifluoroacetate Bond Angles (°)

O(11)–Cl(1)–O(12)	109.4(2)	Cu–O(11)–C(11)	113.6(2)
O(11)–Cl(1)–O(13)	109.3(2)	Cu′–O(11)–C(11)	141.4(4)
O(11)–Cl(1)–O(14)	107.7(2)	O(11)–C(11)–O(12)	128.2(4)
O(12)–Cl(1)–O(14)	109.0(2)	O(11)–C(11)–C(12)	112.9(3)
O(12)–Cl(1)–O(13)	110.6(3)	O(12)–C(11)–C(12)	118.9(3)
O(13)–Cl(1)–O(14)	110.7(2)	O(21)–C(21)–O(22)	127.7(4)
O(21)–Cl(2)–O(22)	106.5(3)	O(21)–C(21)–C(22)	116.8(3)
O(21)–Cl(2)–O(23)	101.0(4)	O(22)–C(21)–C(22)	115.5(4)
O(21)–Cl(2)–O(24)	118.8(4)		
O(22)–Cl(2)–O(23)	103.9(4)		
O(22)–Cl(2)–O(24)	118.9(4)		
O(23)–Cl(2)–O(24)	105.1(4)		
Cu–O(11)–Cl(1)	130.3(2)		
Cu–O(21)–Cl(2)	139.3(3)		

* C(11)–C(12)–F and C(21)–C(22)–F bond angles 103.8-121.1°, mean 111°
F–C(12)–F and F–C(22)–F bond angles 93.8-121.1°, mean 108°

ligand (LH) to the anionic deprotonated ligand (L^-) for these copper complexes. This unexpected result shows the combined electronic flexibility of the ligand and the copper's ability to accommodate either the neutral or anionic tridentate ligand without significantly altering its ligating properties. The difference observed between the Cu-N(1) and Cu-N(2) bond lengths for the trifluoroacetato and acetato complexes (Table 1.1.4) may therefore be a reflection of the anion binding strength rather than the changed ligand form. The weaker axial bonding in the CF_3COO^- complex would result in slightly stronger in-plane bonding, and hence shorter bond lengths, as observed.

The 2-formylpyridine thiosemicarbazone ligand (LH) coordinates as a neutral, tridentate moiety via the N(1), N(2) and S atoms. In doing so it creates two five-membered chelate rings with the copper.

A comparison of bond lengths and bond angles within the pyridine ring of LH (average C-N 1.344 Å, C-C 1.383 Å) with those of unsubstituted pyridines coordinated to copper (average C-N 1.351 Å, C-C 1.377 Å, [89]) shows no significant deviations. Examination of the bond length data presented in Table 1.1.5 shows that all the distances within the thiosemicarbazone side chain are intermediate between formal single and double bonds which is consistent with electron delocalisation over this ligand. A necessary condition for electron delocalisation through both the thiosemicarbazone chain and the pyridine ring is planarity. The plane of best-fit* for the whole ligand shows this condition to be met, with the biggest deviation from the plane being 0.037 Å for N(2). A better representation of the bonding therefore is (d) in Figure 1.12.

---

* Plane (ii) S, N(1), N(2), N(3), N(4), C(1), C(2), C(3), C(4), C(5), C(6), C(7)
-0.1252X -0.4794Y -0.8686Z +4.4710 = 0
[S 0.011, N(1) 0.002, N(2) 0.037, N(3) -0.007, N(4) -0.028, C(1) -0.020, C(2) -0.006, C(3) 0.011, C(4) -0.006, C(5) 0.004, C(6) -0.010, C(7) 0.010]
Distances of atoms from the plane (Å) are given in square brackets.

TABLE 1.1.4
Bond Distances (Å) for In-Plane Coordinating Atoms of Cu and LH/L⁻ [a]

Complex	Cu–N(1)	Cu–N(2)	Cu–S	Cu–X[b]
$[Cu(LH)(SO_4)]_2$	2.024(2)	1.953(2)	2.279(1)	1.922(2)
$[Cu(LH)(H_2PO_4)]_2(H_2PO_4)_2(H_3PO_4)_2 \cdot 2H_2O$	2.016(3)	1.966(3)	2.283(1)	1.923(2)
$[Cu(LH)(ClO_4)_2H_2O] \cdot 2H_2O$	2.018(2)	1.932(2)	2.278(1)	1.931(2)
$[Cu(LH)(CF_3COO)]_2(CF_3COO)_2$	2.034(3)	1.959(3)	2.275(1)	1.948(3)
Average	2.023(3)	1.953(3)	2.279(1)	1.931(3)
$[CuL(CH_3COO)]_2$	2.059(2)	1.970(2)	2.274(1)	1.951(1)
$[(CuL)_4P_2O_7] \cdot 12H_2O$[c]	2.005(6)	1.947(7)	2.279(3)	1.906(7)
$[CuL(saccharinato)H_2O] \cdot \frac{1}{2}H_2O$	2.020(8)	1.956(7)	2.264(3)	1.974(7)
$[CuL(bipyridyl)]ClO_4$	2.049(4)	1.949(4)	2.275(1)	1.987(4)
Average	2.021(5)	1.952(6)	2.276(2)	1.933(5)

a LH = 2-formylpyridine thiosemicarbazone

b X is the fourth in-plane coordinating atom

c average values

TABLE 1.1.5
Comparison of Thiosemicarbazone Bond Lengths (Å)

bond	CF_3COO[a]	CH_3COO[b]	Experimentally determined bond lengths (Å)[c]		
C(5)–C(6)	1.460(4)	1.451(4)	C–C	1.541	
			C=C	1.337	simple double
C(6)–N(2)	1.287(5)	1.290(3)	C–N	1.472	
C(7)–N(3)	1.356(5)	1.335(3)	C⋯N	1.322	partial double
C(7)–N(4)	1.305(4)	1.333(4)	C–S	1.81	
C(7)–S	1.715(4)	1.725(2)	C⋯S	1.73	partial double
N(2)–N(3)	1.348(3)	1.359(3)	N–N	1.44	
			N=N	1.24	

a $[Cu(LH)(CF_3COO)]_2(CF_3COO)_2$

b $[CuL(CH_3COO)]_2$

c after [88]

Tables 1.1.5 and 1.1.6 also highlight the difference in bonding between the neutral protonated (LH) and the anionic deprotonated (L^-) forms of the ligand. Delocalisation of the negative charge over the side chain in the deprotonated ligand is expected to lengthen the 'formal' double bonds and shorten the single bonds, relative to the protonated form. This difference should manifest itself throughout the side chain, becoming less significant the further the atoms are from the sulphur. The ligand in the protonated form should have a greater contribution from the thione rather than the thiolate structure (see Figure 1.12). Hence, the C(7)-S bond length is expected to be shorter in the former than in the deprotonated ligand. From Table 1.1.6 the average S-C(7) bond lengths for the LH and L^- complexes are 1.710(4) Å and 1.733(7) Å. This difference in bond lengths is also shown for (i) the N(3)-C(7) distance which is expected to be longer in the LH structures. The average value of 1.354(4) Å for LH compared with that of 1.331(8) Å for the L^- complexes bears this out and (ii) the N(4)-C(7) distance which, due to the importance of resonance structure (b) in Figure 1.12 for LH is expected to be shorter than for L^-. Again, the significant difference between the average LH and L^- values of 1.310(4) and 1.338(8) respectively shows the importance of the bonding around C(7) on the form of the ligand. These differences are accompanied by a similar change in the bond angles around C(7) as exemplified in Table 1.1.6.

The major differences between the structures of $[Cu(LH)(CF_3COO)_2](CF_3COO)_2$ and $[CuL(CH_3COO)]_2$ (i.e. in addition to the intraligand changes between LH and L^-) are in the bond lengths associated with the trifluoroacetato (CF_3COO^-) and acetato (CH_3COO^-) moieties. In the trifluoroacetato structure, the bridging bond length of 2.516(4) Å from O(11) to Cu′ is significantly longer than the comparable distance of 2.427(2) Å observed in the acetato complex [64]. The differences in the angles Cu-O(11)-Cu′ (104.9(1)° in CF_3COO^- and 103.5(1)° in CH_3COO^-), and O(11)-Cu-O(11′) (75.1(1)° in CF_3COO^- and 76.5(1)° in CH_3COO^-) between the two acetato complexes are probably much less significant. This increase of the long,

TABLE 1.1.6
Bond Lengths (Å) and Angles (°) About C(7) in Thiosemicarbazide and Thiosemicarbazone Compounds

Compound	S–C(7)	N(3)–C(7)	N(4)–C(7)	N(3)–C(7)–S	N(4)–C(7)–S	Ref.
Thiosemicarbazide HCl	1.692(3)	1.363(4)	1.314(3)	121.0(2)	124.5(2)	90
5-hydroxy LH	1.706(6)	1.336(7)	1.307(7)	a	a	91
2-formylthiophene thiosemicarbazone	1.695(3)	1.345(4)	1.315(4)	118.0	123.0	92
acetone thiosemicarbazone	1.690(5)	1.342(6)	1.344(6)	a	a	91
Cu (thiosemicarbazide)$_2$(NO_3)$_2$	1.713(5)	1.330(5)	1.315(5)	121.2(3)	120.2(3)	93
[Cu(LH)(SO_4)]$_2$	1.703(3)	1.362(3)	1.309(3)	121.5(2)	122.7(2)	64
[Cu(LH)(H_2PO_4)]$_2$(H_2PO_4)$_2$(H_3PO_4)$_2$.2H_2O	1.714(3)	1.350(4)	1.313(4)	121.1(2)	120.6(2)	This work
[Cu(LH)(ClO_4)$_2$$H_2O$]·2$H_2O$	1.707(3)	1.348(4)	1.313(4)	121.6(2)	121.3(2)	This work
[Cu(LH)(CF_3COO)]$_2$(CF_3COO)$_2$	1.715(4)	1.356(6)	1.305(4)	121.4(2)	121.9(3)	This work
Average	1.710(4)	1.354(4)	1.310(4)	121.4(2)	121.6(3)	
[Ni L_2][b]	1.732(8)	1.317(10)	1.344(10)	126.8(6)	117.2(6)	94
[CuL(CH_3COO)]$_2$	1.725(2)	1.335(3)	1.333(4)	124.8(2)	118.7(2)	64
[CuL(bipyridyl)]ClO_4	1.742(4)	1.326(6)	1.339(6)	125.2(4)	117.5(3)	This work
[CuL(saccharinato)H_2O]·½H_2O	1.721(9)	1.340(12)	1.327(12)	124.6(7)	118.2(7)	This work
[(CuL)$_4$$P_2O_7$]·12$H_2O$[b]	1.747(9)	1.323(11)	1.352(11)	124.9(7)	117.8(7)	This work
Average	1.733(7)	1.331(8)	1.338(8)	124.9(6)	118.1(6)	

LH = 2-formylpyridine thiosemicarbazone

a values not given

b average value for complex

bridging acetato bond arises from the reduced coordinating ability expected for the CF_3COO^- anion (c.f. acetato) due to its weaker basicity (pKa CF_3COOH = -0.26 [95], pKa CH_3COOH = 4.75 [96]).

The bond angle of 141.4(4)° for Cu'-O(11)-C(11) in the CF_3COO^- complex shows an increase of 3.5° over that found in the CH_3COO^- [64] complex but the O(11)-C(11)-C(12) angle decreases 3.0° from 115.9(3)° to 112.9(3)° in going from the CH_3COO^- to the CF_3COO^- structure. The overall effect of these changes is to leave C(12) equidistant from N(2), the atom of closest approach for C(12) (3.833 Å for CH_3COO^- and 3.824 Å for CF_3COO^-). This brings F(13) to within 3.02 Å from N(2). From a consideration of the disorder present in the F positions and taking into account that the sum of the van Der Waals radii for N and F is 2.85 Å [97], it is unlikely that this approach represents an interaction necessary for stability.

The inductive effect of the three fluorines can best be seen by examining the C(11)-C(12) bond lengths in the acetato and trifluoroacetato complexes. Reduction in electron density on C(12) (and C(22)) is expected to increase this bond length. This is observed with a distance of 1.506(4) Å in the CH_3COO^- molecule and 1.549(5) and 1.527(6) Å for C(11)-C(12) and C(21)-C(22) respectively of the CF_3COO^- ions. This inductive effect does not appear to significantly alter the C-O bond lengths in the bridging CF_3COO^- and CH_3COO^- moieties (C(11)-O(11) 1.273(3)Å and C(11)-O(12) 1.202(4) Å in CF_3COO^-; C(11)-O(11) 1.279(3) Å and C(11)-O(12) 1.224(4) Å in CH_3COO^- [64])

The difference in the C-O bond lengths between the coordinated, bridging oxygen, O(11), and the non-coordinated O(12) suggests the C(11)-O(11) distance of 1.273(3) Å has greater single-bond character than the value of 1.202(4) Å for C(11)-O(12). The latter bond may best be represented as a formal double-bond although C(11)-O(11) has appreciably doubled-bond character as well (C-O 1.43±1 Å, C=O 1.23±1 Å [88]). In the non-coordinated CF_3COO^- this difference in the C-O bond lengths has been reduced (C(21)-O(21) 1.228(5) Å, C(21)-O(22)

TABLE 1.1.7
Hydrogen-Bonding Distances (Å) and Angles (°) for $[Cu(LH)(CF_3COO)]_2(CF_3COO)_2$

Atoms[a]	Distance (Å)	Symm[b]	T_x, T_y, T_z
N(3)···O(22)	2.582	2	1 0 1
N(4)···O(21)	2.811	2	1 0 1
N(4)···O(21)	2.817	1	1 0 0

a the first atom is at symmetry position 1

b symmetry positions
1 (x, y, z)
2 ($\bar{x}$, $\bar{y}$, $\bar{z}$)

Atoms	Angle (°)	Atoms	Angle (°)
N(2)–N(3)···O(22)	117.2	C(7)–N(3)···O(22)	126.1
C(7)–N(4)···O(21)	115.7	C(7)–N(4)···O(21)	145.6
O(21)···N(4)···O(21)	92.2		

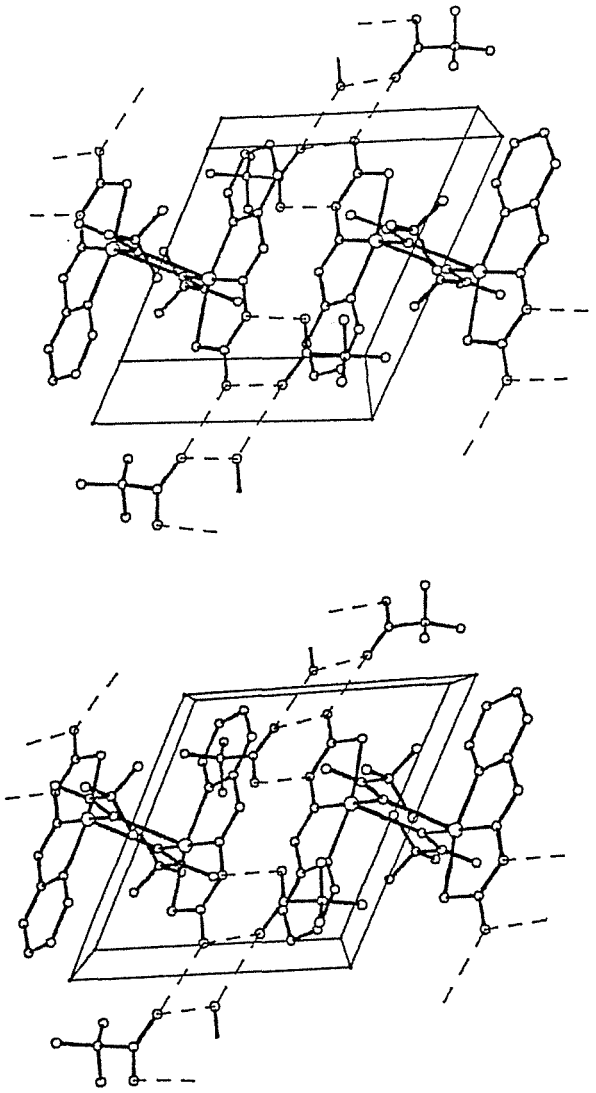

Figure 1.1.2: Stereo-view of the unit-cell packing diagram for $[Cu(LH)(CF_3COO)]_2(CF_3COO)_2$ showing the hydrogen-bonding scheme.

1.252(4) Å) due to the delocalisation of the negative charge. However the difference between these C-O bonds is significant and the lengthened C(21)-O(22) bond may be attributed to the strong hydrogen-bonding contact of 2.582 Å between N(3) and O(22) (see Table 1.1.7).

The average bond lengths and bond angles in the trifluoroacetate molecules agree well with those reported in literature and are assumed to be normal [98].

In the structures of $[CuL(CH_3COO)]_2$ and $[Cu(LH)(SO_4)]_2$ [64,65] respectively, weak sixth contacts of 2.925(2) Å and 3.128(2) Å were reported between Cu and O(12) and Cu and a sulphato oxygen. The value of 2.921(2) Å for $[Cu(LH)(CF_3COO)]_2(CF_3COO)_2$ is in close agreement with the former acetate value, as are the O(11)-Cu-O(12) angles (49.7(2)° in CF_3COO^-, 49.0(2)° in CH_3COO^- and 50.3(2)° in SO_4^{2-}). Whereas long, off-axis interactions of this type have tentatively been classed as bonds [99,100], their effect on the electronic properties of the central copper atom may be negligible. Of greater consequence is that the long interaction effectively blocks the sixth coordination site from approach by other potential ligands, e.g. solvent.

The formation of a dimeric, anion bridging structure seems to be preferred even though a second, potentially coordinating trifluoroacetate anion (to give a monomer) is present. This non-coordinating anion is however stabilised by the formation of hydrogen-bonds to the protonated nitrogens of the thiosemicarbazone side chain (see Table 1.1.7).

The hydrogen-bonding scheme is depicted in the stereo-view of the unit-cell (see Figure 1.1.2). In the non-coordinated CF_3COO^-, O(21) and O(22) form hydrogen-bonds to the hydrogens H(41) and H(31) on N(4) (2.817 Å) and N(3) (2.582 Å) respectively. An additional contact between O(21) and the remaining hydrogen on N(4) (2.811 Å), H(42), completes the hydrogen-bonding to the free CF_3COO^-. No significant interactions involving the fluorines were detected. This may account for the disorder observed in the fluorine atom sites, with the $-CF_3$ groups showing almost free rotation about the C(11)-C(12) and C(21)-C(22) bonds.

1.1.3 CRYSTAL STRUCTURE OF Aqua(2-formylpyridine thiosemicarbazone diperchlorato) copper(II) Dihydrate.

A thermal ellipsoid diagram for the title compound (abbreviated as $[Cu(LH)(ClO_4)_2H_2O]\cdot 2H_2O$) showing the numbering scheme used is depicted in Figure 1.1.3. Bond length and angle data are given in Tables 1.1.2 and 1.1.3 respectively.

The complex $[Cu(LH)(ClO_4)_2H_2O]\cdot 2H_2O$ crystallises as a discrete monomer. The 2-formylpyridine thiosemicarbazone ligand (LH) coordinates as a neutral, tridentate moiety via the N(1), N(2) and S atoms. Bond lengths and bond angles are considered to be normal for this neutral ligand as they are similar to those found for the same ligand in other crystal structures (see Table 1.1.6) [This work, 64].

The copper adopts a pseudoctahedral geometry comprised of the tridentate NNS constellation from LH and a water oxygen in the plane. Two long bonds to perchlorato oxygens complete the coordination sphere.

The plane of best-fit* through the donor atoms S, N(1), N(2) and O(1) shows the copper to lie slightly out of the mean-plane (by 0.024 Å), being displaced towards the shorter of the two perchlorato bonds (O(11)).

The complex Cu(2-formylpyridine S-methyl-2-amino thiophenol)$(ClO_4)_2$ $[Cu(pap')(ClO_2)_2H_2O]H_2O$ [44], shows a number of similar features to $[Cu(LH)(ClO_4)_2H_2O]\cdot 2H_2O$ worthy of note, namely:

* Plane (i) S, N(1), N(2), O(1)
O.9934X – 0.0298Y – 0.1105Z – 1.2336 = 0
[S 0.015, N(1) 0.018, N(2) -0.019, O(1) -0.014, Cu 0.024]
Distances of atoms from the plane (Å) are given in square brackets.

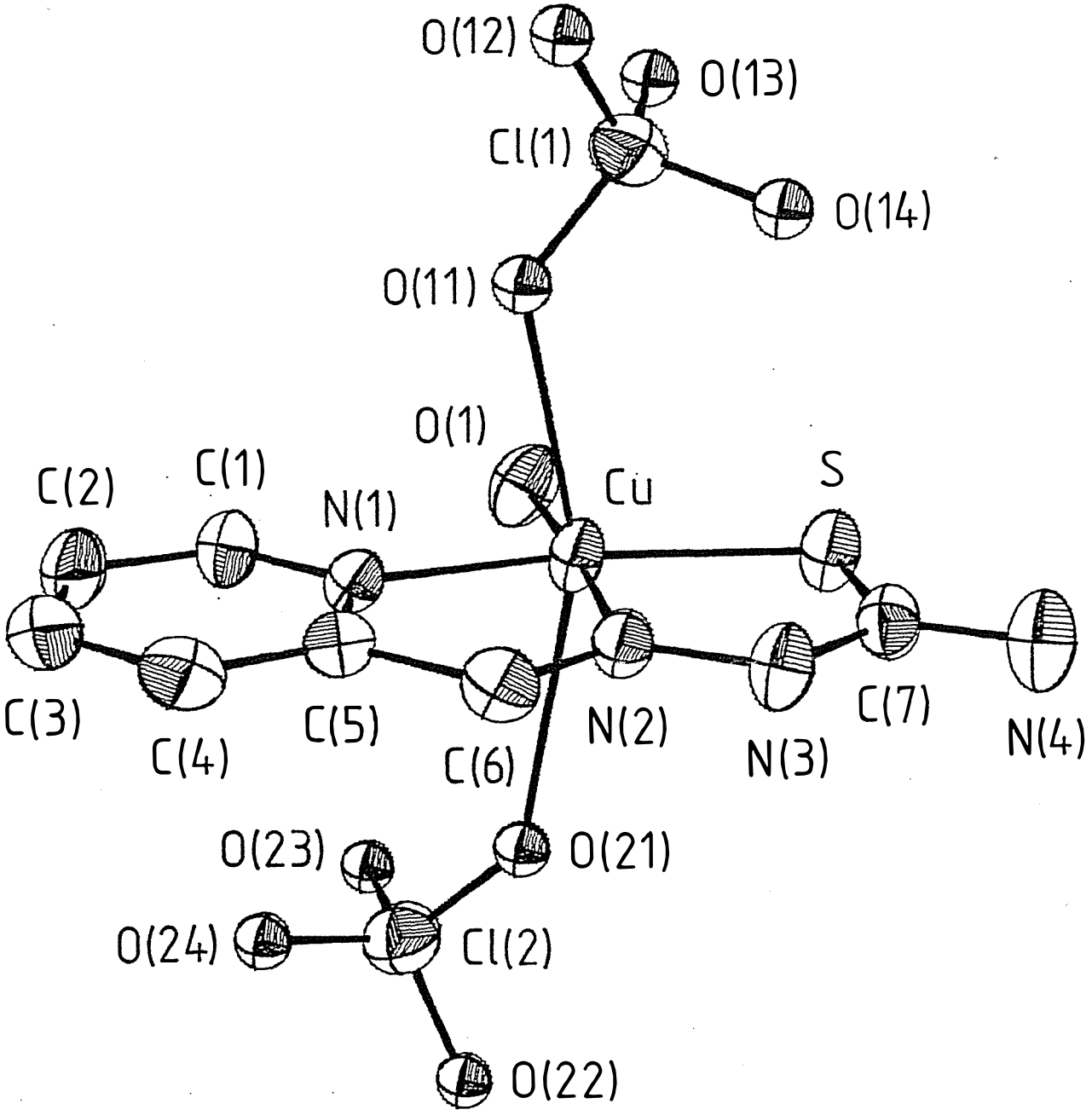

Figure 1.1.3: The monomer $[Cu(LH)(ClO_4)_2H_2O]\cdot 2H_2O$ showing the atom numbering scheme. The two non-coordinated water molecules and hydrogen atoms have been omitted for clarity.

(i) both have tridentate NNS ligands, although in LH the sulphur is from a thioamide (Cu-S of 2.278 Å) and in pap⁻ it is from a thioether (Cu-S of 2.320(1) Å)

(ii) the fourth in-plane position is occupied by a water molecule, and

(iii) there are trans, axial, perchlorato groups coordinated to the tetragonally distorted copper centre.

A comparison of the bond length and angle data for a selection of diperchlorato copper complexes, including the previous example is given in Table 1.1.8.

From Table 1.1.8, the increase of 0.614 Å in the average Cu-O axial bond lengths (2.654(5) Å) over the mean in-plane bonding distance (2.040(2) Å) observed for the title complex is typical of Jahn-Teller distortions observed for copper (II) species [105]. This long bond length agrees well with those of the tetracycles (NNNN and SSSS in Table 1.1.8) but is 0.129 Å longer than for $[Cu(pap')(ClO_4)_2H_2O]H_2O$. This may be a reflection of (i) the in-plane bonding strength of LH to copper-being comparable to the tetracycles but stronger than the thioether containing (pap⁻) and/or (ii) decreased orbital overlap between the copper and the two axial perchlorato groups due to the significant off-axis deviation (O(11)-Cu-O(21) 155.9(4)°) from the expected value of 180° for such weakly coordinated trans groups. This deviation is not thought to arise from a static distortion of the pseudo-octahedral coordination sphere in an attempt to lift the ground state degeneracy, as previously cited examples do not show such a trend. Instead it seems more plausible that it arises from crystal packing forces.

The formation of a monomeric structure, as opposed to the previously found dimeric complexes for this ligand with copper may be a reflection on the coordinating ability of the perchlorato group. This anion is a weaker base than water (pKa H_2O = 7.0, pKa $HClO_4$ =

-10.0 [106]) and is normally classified as 'non-coordinating' [107]. The formation of a perchlorato one-atom bridging structure seems highly unfavourable for a weak base.

The remaining two water molecules (O(2) and O(3)) are not coordinated but are involved in a hydrogen-bonding scheme which link the monomers via the coordinated water, perchlorato anions and protonated nitrogen atoms. This hydrogen-bonding scheme is depicted in the stereo-view of the unit-cell, Figure 1.1.4. The associated distances and angles are given in Table 1.1.9.

The coordinated water molecule, O(1), forms two strong O-H···O hydrogen-bonds, one to a perchlorate oxygen, O(22) (2.725 Å), and another to a second water molecule, O(2) (2.672 Å). This latter water molecule (O(2)) is then involved in two more hydrogen-bonds, again one to a perchlorate oxygen, O(14) (2.830 Å), and another to a third water molecule, O(3) (2.830 Å). Atom O(3) is involved in a total of four hydrogen-bonding contacts. One of these is to N(3) (2.681 Å) of the ligand. Another the O(3)···O(12) interaction, at a distance of 3.117 Å must be considered very weak (sum of the relevant van Der Waals radii = 3.04 Å [97]). The stabilisation of the Cl(1) perchlorato group is aided by two final weak contacts between the terminal N(4) nitrogen of the ligand with both O(11) and O(14) (3.192 Å and 3.002 Å respectively).

TABLE 1.1.8
Selected Data for some Copper(II) Diperchlorato Complexes

	In-plane donor set	$Cu-OClO_3$ distances (Å)		$O-Cu-O$ angle (°)	Ref.
1	NNSO	2.595(4)	2.712(5)	155.9(2)	this work
2	NNSO	2.490(3)	2.560(4)	175.7(1)	[44]
3	SSSS	2.652(4)[a]		180	[101]
4	NNNN	2.64(4)	2.70(4)	164.3(11)	[102]
5	NNNN	2.57(4)[a]		180	[103]
6	NNNN	2.59(1)[a]		180	[104]

a Copper atom at a centre of symmetry
1 2-formylpyridine thiosemicarbazone
2 2-formylpyridine S-methyl-2-aminothiophenol
3 1, 4, 8, 11 - tetrathiacyclotetradecane
4 1, 4, 7, 10 - tetraazacyclotetradecane
5 1, 4, 8, 11 - tetraazacyclotetradecane
6 6,13-dimethyl-1,4,8,11-tetraazacyclotetradecane-6,13-diamine

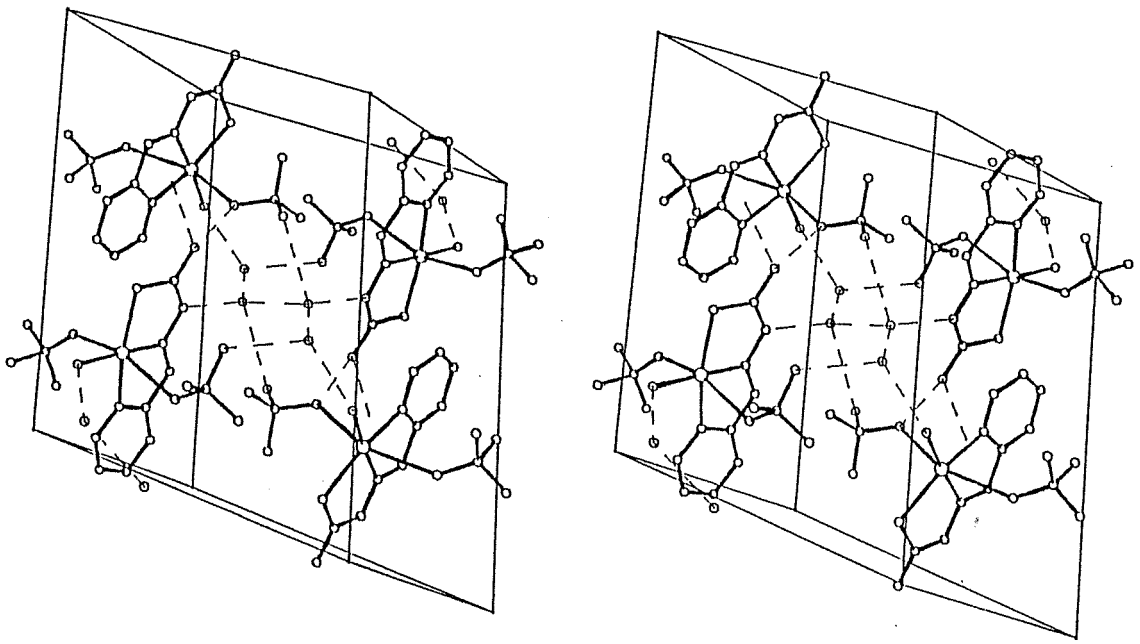

Figure 1.1.4: Stereo-view of the unit-cell packing diagram for $[Cu(LH)(ClO_4)_2H_2O]\cdot 2H_2O$ showing the hydrogen-bonding scheme.

TABLE 1.1.9
Hydrogen-Bonding Distances (Å) and Angles (°) for $[Cu(LH)(ClO_4)_2H_2O]\cdot 2H_2O$

Atoms[a]	Distance (Å)	Symm[b]	T_x,	T_y,	T_z
O(1)···O(22)	2.725	4	0	$\bar{1}$	0
O(1)···O(2)	2.672	4	0	$\bar{1}$	$\bar{1}$
O(2)···O(14)	2.830	1	$\bar{1}$	0	$\bar{1}$
O(2)···O(3)	2.830	3	$\bar{1}$	0	$\bar{1}$
O(2)···O(24)	2.969	3	0	0	$\bar{1}$
O(3)···O(3)	2.870	2	1	0	0
O(3)···N(3)	2.681	4	1	$\bar{1}$	0
O(3)···O(12)	3.117	1	0	0	0
N(4)···O(11)	3.192	3	0	0	0
N(4)···O(14)	3.002	2	1	0	1

a the first atom is at symmetry position 1

b symmetry positions

1 (x, y, z)

2 ($\bar{x}$, $\bar{y}$, $\bar{z}$)

3 ($\bar{x}$, 0.5 + y, 0.5 − z)

4 (x, 0.5 − y, 0.5 + z)

Atoms	Angle (°)	Atoms	Angle (°)
Cu–O(1)···O(22)	124.3	N(3)···O(3)···O(12)	97.8
Cu–O(1)···O(2)	123.2	N(3)···O(3)···O(3)	97.8
O(2)···O(1)···O(22)	100.9	O(12)···O(3)···O(3)	77.5
O(1)···O(2)···O(14)	113.6	C(7)–N(3)···O(3)	124.1
O(1)···O(2)···O(3)	116.5	N(2)–N(3)···O(3)	119.1
O(3)···O(2)···O(14)	107.1	O(11)···N(4)–C(7)	130.8
O(2)···O(3)···N(3)	132.5	O(14)···N(4)–C(7)	117.4
O(2)···O(3)···O(12)	111.8	O(11)···N(4)···O(14)	105.8
O(2)···O(3)···O(3)	123.7		

1.1.4 RESULTS AND DISCUSSION

1.1.4(a) Electronic Spectra

Introduction to ligand field (d-d) transitions

The d^9 configuration of the copper(II) ion can in theory give rise to a maximum of four d-d transitions but these are generally only resolved by use of Gaussian analysis or single crystal polarisation studies. Instead, one or maybe two absorption bonds are often observed. The single unpaired electron of the e_g ground state is in the vast majority of Cu(II) complexes in the non-degenerate d_{x2-y2} orbital, resulting from a static form of tetragonal distortion. A large number of complexes have a d_{z2} ground state, normally from a trigonal bipyramidal stereochemistry, whereas the few having a d_{xy} ground state are confined to square-coplanar complexes [105].

The majority of complexes, as stated, are in a tetragonal environment and for this stereochemistry three principal absorption bands are expected. In order of increasing energy these transitions are $^2B_{1g} \rightarrow {}^2A_{1g}$; $^2B_{1g} \rightarrow {}^2B_{2g}$ and $^2B_{1g} \rightarrow {}^2E_g$. Because of the low intensity of $^2B_{1g} \rightarrow {}^2B_{2g}$, this band is usually not resolved [108] and because the bands tend to be broad, often only one asymmetric envelope is observed. In most cases however, it is possible to distinguish unambiguously between the d_{x2-y2} (or d_{xy}) and the d_{z2} ground states from powder e.s.r. spectra.

The Present Study

Analytical and magnetic data are presented in Table 1.1.1 whereas the absorption maxima and conductance data appear in Table 1.1.10.

TABLE 1.1.10

Absorption Maxima and Conductance Data for Chapter 1

Complex	Absorption Maxima (nm)[a] Charge Transfer		d-d	Molar Conductance[b] ($s\ mol^{-1}\ l$)	Solvent[c]
$[CuL(CH_3COO)]_2$	433		630 (b		m.t.
	413	(11700)	608 (190;br)	0	dmso
	382	(10 000)	628 (160)	63	H_2O
$[Cu(LH)(CF_3COO)]_2(CF_3COO)_2$	420		597 (br)		m.t.
	415	(12 400)	630 (210;br)	52	dmso
	383	(11 300)	630 (180)	385	H_2O
$[CuLF]_2 \cdot 5 \cdot 4H_2O$	429		650 (br)		m.t.
	412	(3 700)	600	13	dmso
	382		626		H_2O
$[Cu(LH)F]_2F_2$	390	(sh)	(sh)		m.t.
	384	(10 300)	628 (180;br)	4	dmso
	383	(9 600)	629 (160)	210	H_2O
$[CuLCl]_2H_2O$	428		646 (br)		m.t.
	415	(12 400)	634 (220)	1	dmso
	384	(10 300)	631 (170)	99	H_2O
$[Cu(LH)Cl]_2Cl_2 \cdot 2H_2O$	382		705 (br)		m.t.
	418	(12 300)	640 (200)	37	dmso
	412		702		EtOH
$[CuLBr]_2$	426		652 (br)		m.t.
	413	(12 100)	629 (210)	13	dmso
	384		629		H_2O
$[Cu(LH)Br]_2Br_2 2H_2O$	386		705 (br)		m.t.
	414	(12 300)	632 (220)	60	dmso
	421		(sh)		acetone
$[CuLI]_2$	431		650		m.t.
	415	(13 200)	628 (200)	35	dmso
	384		624		H_2O
$[Cu(LH)I]_2I_2$	428	(br)	d		m.t.
	414	(12 800)	629 (200	60	dmso
	374		d		acetone
$[Cu^{I}(LH)I]\frac{3}{2}H_2O$	430				m.t.
$[CuL(NO_3)]_2$	406		(sh)		m.t.
	414	(12 300)	634 (180)	33	dmso
	383	(11 300)	634 (170)	97	H_2O
$[Cu(LH)(NO_3)_2H_2O]$	400		670 (br)		m.t.
	410	(13 100)	628 (210;br)	67	dmso
	383	(10 100)	629 (170)	475	H_2O
$[CuL(ClO_4)]_2$	392		(sh)		m.t.
	413	(11 800)	634 (170)	28	dmso
	383	(9 500)	629 (160)	89	H_2O
$[Cu(LH)(ClO_4)_2H_2O] \cdot 2H_2O$	386		621		m.t.
	416	(11 800)	628 (210)	65	dmso
	383	(10 200)	633 (160)	476	H_2O
$[Cu^{II}(LH)(ClO_4)]$	492				m.t.
$[(CuL)_2SO_4(H_2O)_2]H_2O$	429		630 (sh)		m.t.
	415		625		dmso
	383		628		H_2O
$[Cu(LH)(SO_4)]_2$	403		708		m.t.
	415	(12 700)	630 (180;br)	20	dmso
	383	(9 900)	630 (170)	430	H_2O

TABLE 1.1.10 continued

Complex	Absorption Maxima (nm)[a] Charge Transfer	d-d	Molar Conductance[b] (s mol^{-1} l)	Solvent[c]
$[CuL(NCS)]_2$	440 (sh)	635 (br)		m.t.
	417 (12 300)	630 (250;br)	18	dmso
	415	587		acetone
$[CuLN_3]_2H_2O$	425	600 (br)		m.t.
	415 (12 000)	585 (430)	0	dmso
	411	540 (br)		acetone
$[CuL(CN)]_2 \cdot 2H_2O$	430 (br)	(sh)		m.t.
	414 (12 600)	573 (220)	8	dmso
	413	(sh)		EtOH

a extinction coefficients given in parentheses (1 mol^{-1} cm^{-1})
br = broad
sh = shoulder
b for typical molar conductivity ranges see Appendix 3
c m.t. = mull transmittance
d tail into near ir

The single-crystal X-ray crystallographic structures for $[CuL(CH_3COO)]_2$, $[Cu(LH)(CF_3COO)]_2(CF_3COO)_2$ and $[Cu(LH)(SO_4)]_2$ show the copper(II) ion to be in a square pyramidal geometry whereas in $[Cu(LH)(ClO_4)_2H_2O]\cdot 2H_2O$ the copper stereochemistry is distorted elongated octahedral. However, similar d-d spectra are often observed in such cases, with one band usually being observed in the range of 550-670 nm [109 and refs. therein]. The mull transmittance spectra in Table 1.1.10 have d-d absorptions ranging from 597 to 708 nm therefore the stereochemistry of these complexes is accordingly assigned as square-pyramidal or, more unusual, elongated octahedral. These findings are in agreement with Bingham *et al.* [64], Bell *et al.* [66] and for related systems [52,110].

For the three pairs of complexes with equivalent anions of neutral and anionic ligands (e.g. $[CuLCl]_2$ and $[Cu(LH)Cl]_2Cl_2\cdot 2H_2O$]) for which both d-d absorption maxima could be resolved in the solid state, the deprotonated ligand complexes, L^-, have bands at shorter wavelength (higher energy) compared with the appropriate neutral ligand, LH, case. This is to be expected from the ordering of the coordinating ability of the more thiolato sulphur in L^- compared with the predominantly thione sulphur in LH ($RS^- > R_2S > RC{=}S$; [38]) assuming the coordination geometry about the copper centre is the same between pairs. This difference observed above is, expectedly, not reflected in the Cu-S bond lengths for the two types of complexes (see Table 1.1.4), where both are the same.

The analogous d-d maxima for the pair $[CuL(CH_3COO)]_2$ and $[Cu(LH)(CF_3COO)]_2(CF_3COO)_2$ of 630 and 597 nm respectively are different to the above observed trend due to the different anions involved in coordination. The X-ray structures of both complexes have been carried out ([64] and this work for the previous ordering) and reveal that the donor sets are equivalent. The in-plane Cu-donor distances between these two complexes do not appear to be sufficiently different to account for this observation (see Table 1.1.4). The difference may however result from the more weakly coordinated apical oxygen of

the trifluoroacetato anion (Cu-O = 2.516(4) Å), compared with the corresponding acetato complex (Cu-O = 2.427(2) Å) as increased axial coordination leads to band shifts to lower energy for d-d transitions [111].

The mull transmittance charge transfer (c.t) maxima in Table 1.1.10 for the deprotonated ligand complexes (thiolato sulphur) are in all cases at lower energy than the analogous anion, neutral ligand complexes (thiono sulphur) with an average difference of 23 nm between the eight pairs of complexes tabulated.

The c.t. maxima for the anionic ligand copper(II) complexes, on going from dmso to water shifts on average 20 nm to shorter wavelength (higher energy), in accord with the greater polarity of water.

The molar conductance values in dmso for the deprotonated ligand complexes indicate that these compounds are basically non-electrolytes, the anion remaining coordinated in solution. It is feasible therefore that a six coordinate species with dmso coordination exists, the long bridging anion bonds in the dimeric units having been broken to give solvated monomers.

For the neutral ligand complexes in dmso, 1-1 electrolytes are generally observed. Whether this is consistent with ionisation (a) or (b) (see below) may be open to question. However, the d-d band position for

$$\tfrac{1}{2}([Cu(LH)X]_2X_2) \xrightarrow{dmso} CuLX_2^- + H^+ \qquad (a)$$

$$\tfrac{1}{2}([Cu(LH)X]_2X_2) \xrightarrow{dmso} Cu(LH)X^+ + X^- \qquad (b)$$

neutral and deprotonated ligand complexes of the equivalent anion are approximately the same (within ± 6 nm), indicating (a) may be favoured. Even though the complex formulated as

$[Cu(LH)F]_2F_2$, is only weakly ionised, process (a) may still hold because the solution product formed is a weaker acid.

In aqueous solution the positions of both the c.t. and d-d bands at 383 and 629 nm respectively are essentially constant for all relevant complexes. This suggests the complexes decompose in water to give a common mononuclear species of the type $[CuL(H_2O)]^+$ e.g.

$$\tfrac{1}{2}[CuLX]_2 \xrightarrow{H_2O} [CuL(H_2O)]^+ + X^-$$

This is also supported by the electrolytic nature of the aqueous solutions of these complexes. Anionic ligand complexes have molar conductance values consistent with 2 charges per copper (i.e. 1-1 electrolytes) whereas the protonated ligand complexes range from approximately 4 for $[Cu(LH)F]_2F_2$ to 8 for $[Cu(LH)(NO_3)_2H_2O]$. Complete dissociation of the anions and deprotonation of the still coordinated ligand is expected to give 4 charges in aqueous solution e.g.

$$Cu(LH)X_2 \xrightarrow{H_2O} CuL^+ + H^+ + 2X^-$$

The molar conductance values in excess of 4 charges may arise from trace amounts of acid, from which the complexes were prepared, adhering to the crystalline compounds. As these complexes decompose in water and often have some solubility in organic solvents, rigorous attempts to remove this acid were not undertaken.

The higher energy d-d transitions observed for $[CuL(CN)]_2$ and $[CuL(NCS)]_2$ of 573 nm (dmso) and 630 nm (dmso) respectively corresponds to their position in the spectrochemical series [112]. The azido analogue $[CuL(N_3)]_2$ has absorption maxima of 585 nm (dmso) and 540 nm (acetone) although it is below NCS^- in this series [112].

The charge transfer maxima at ~400 nm has been assigned to S → Cu [64,113] although an anion → Cu component may be present also [64]. The latter may be seen in the red-orange complex $[Cu(LH)I]_2I_2$where a tail into the near ir is observed (which does not allow resolution of d-d absorptions) and is assigned to I → Cu. On changing from dmso to a more polar solvent such as water, the c.t. maxima shifts to higher energy.

1.1.4(b) Infrared Spectra

The ir spectra for LH (and related ligands) and its compounds are complicated and very difficult to assign with certainty. The bands tend to be combination modes so changes in these resulting from coordination, deprotonation or differing anions are difficult to interpret [52,67,68,70,78,79,114-116] . Table 1.1.11 lists several of the combination modes which have tentatively been assigned (after [66]) for the ligand and four representative complexes. A definitive difference between neutral and anionic ligand complexes with copper(II) could not be established so analytical figures (Table 1.1.1) and analogous compounds in the literature were used to formulate complexes.

The mainstay of the ir spectra was in anion identification and analysis of the coordination mode. Unfortunately anion bands often coincided with those in the complex and appeared as shoulders or were completely obscured, therefore rendering accurate assignments impossible. The anion bands presented in Table 1.1.12 are those which could be identified with some certainty. All are consistent with coordination, with the acetato, perchlorato and sulphato anions indicating one atom coordination [107,117]. The azido band at 2 060 cm^{-1} can not be used to distinguish between terminal or bridging coordination. For the cyano complex, the absorption at 2 150 cm^{-1} is consistent with coordination through the carbon atom whereas the thiocyanato bands at 2 110 and 2 080 cm^{-1} can not safely distinguish between nitrogen, sulphur or bridging (M-NCS-M) modes of attachment [107,118].

TABLE 1.1.11

Selected Ir Spectral Bands (cm^{-1}) for Representative Chapter 1 Compounds

Assignment[a]	Compound				
	LH	$[CuL(CH_3COO)]_2$	$[Cu(LH)(CF_3COO)]_2(CF_3COO)_2$	$[CuL(ClO_4)]_2$	$[Cu(LH)(ClO_4)_2H_2O]\cdot 2H_2O$
$\nu(NH) + \nu(NH_2)$	3 440 (s)	3 400 (s)	3 330 (s)	3 440 (m)	3 480 (w;br)
	3 280 (s;br)	3 295 (s)		3 270 (s)	3 350 (m;br)
	3 165 (s;br)	3 100 (m;br)		3 120 (w;br)	3 250 (w;br)
			3 040 (w;br)		
$\nu(CS) + \nu(CN) + \delta(NH_2)$	1 300 (s)	1 302 (s)	1 310 (m)	1 300 (w)	1 318 (m)
	1 150 (m)	1 170 (s)	1 180 (s)	1 175 (w)	1 175 (s)
	1 112 (s)	1 150 (m)	1 150 (w)	–	1 160 (w;sh)
$\nu(CS)$	812 (s)	760 (m)	–	780 (m)	775 (w)

a Assignments according to [66]

TABLE 1.1.12

Anion Infrared Bands for Chapter 1

Complex	bands (cm^{-1})[a]			
$[CuL(CH_3COO)]_2$	1 635 (s)			
$[Cu(LH)(CF_3COO)]_2(CF_3COO)_2$	1 693 (s)			
$[CuL(ClO_4)]_2$	1 146 (s)	1 122 (s)	1 100 (s)	1 088 (s)
$[Cu(LH)(ClO_4)_2H_2O{\cdot}2H_2O$	1 145 (s)	1 115 (s)		1 087 (s)
$[Cu(LH)(ClO_4)]$		1 120 (s)	1 095 (s)	1 075 (s)
$[(CuL)_2SO_4(H_2O)_2]H_2O$	1 132 (vs)		960 (s)	
$[Cu(LH)(SO_4)]_2$	1 100 (s)	1 025 (vs)	945 (s)	
$[CuL(NCS)]_2$	2 110 (s)	2 080 (s)		
$[CuLN_3]_2$	2 060 (vs)			
$[CuL(CN)]_2$	2 150 (m)			

a Only identifiable bands are tabulated.

1.1.4(c) Magnetic Properties

The room temperature magnetic moments observed for the complexes in this section are presented in Table 1.1.1. Monomeric copper(II) complexes generally exhibit moments close to the spin-only value of 1.73 B.M. although due to mixing-in of some orbital angular momentum from excited states via spin-orbit coupling they can lie appreciably above this [105]. The moments for Chapter 1 complexes generally lie above the spin-only value of 1.73 B.M. However the complexes formulated as $[CuLX]_2$ where $X = NO_3^-$ and ClO_4^- and $[Cu(LH)X]_2X_2$ where $X = F^-$ and I^- with the respective magnetic moments of 1.42, 1.34, 1.45 and 0.43_{av} B.M. are appreciably reduced. The low room temperature moments for these four complexes indicate antiferromagnetic coupling exists between the two copper(II) ions. Unfortunately none of these compounds could be crystallised to determine the stereochemistry around the copper centre and hence the nature of the metal ion interaction. In their review of transition metal complexes of semicarbazones and thiosemicarbazones in 1984, Padhyé and Kauffman [52] noted that some thiosemicarbazone complexes have room temperature moments much lower than expected on the basis of the spin-only formula but have not been investigated in detail. Due to the dimeric structure of $[CuL(CH_3COO)]_2$ [64,65] (Cu···Cu′ separation of 3.450 Å) and the novel tetrameric structure in the complex $[(CuL)_4P_2O_7]\cdot 12H_2O$ (Cu···Cu′ separations of 3.282 and 3.233 Å; this will be discussed in Chapter 3), low temperature magnetic investigations were carried out on the above complexes and will be presented in Chapter 3.

The crystallographically determined dimeric nature of the acetato, trifluoroacetato and sulphato complexes, the low magnetic moments of the four previously mentioned complexes and the monomeric $[Cu(LH)(ClO_4)_2H_2O]\cdot 2H_2O$ species were used in the formulation of mono- or dimeric formula for the copper complexes listed in Table 1.1.1.

1.1.4(d) Electron Spin Resonance Spectra

The e.s.r. results for this chapter, presented in Table 1.1.13 show, for the powder spectra, typical axial (e.g. $[Cu(LH)F)_2F_2$ - see Figure 1.2.7(c)) and rhombic (e.g. $[CuL(CH_3COO)]_2$ - see Figure 1.2.7(d)) spectral parameters. The 'G' values calculated for the non-isotropic spectra in this table give some indication of the alignment of the tetragonal axes and/or exchange coupling. The interpretation placed on this parameter by Hathaway [105] is; if G > 4.0, then the local tetragonal axes are aligned parallel or only slightly misaligned; if G < 4.0, significant exchange coupling is present and the misalignment is appreciable (assuming the in-plane and axial bond lengths and the electronic transitions involved are comparable). Inspection of the data in Table 1.1.13 shows that a number of the G parameters are approximately equal to or greater than 4.0 showing slight exchange coupling or tetragonal axis misalignment. For the four complexes in this table for which the crystal structures have been determined the tetragonal axes are all aligned parallel indicating any lowering of this value is due to exchange coupling.

All of the complexes in Table 1.1.13, except $[Cu(LH)(ClO_4)_2H_2O]\cdot 2H_2O$, are formulated as dimers. In spite of this, no signal in the 1 500 G region where Cu···Cu dimeric interactions give rise to additional absorbances was detected, even when the room temperature magnetic moments were depressed. It was therefore very surprising to find indications of magnetic exchange in the e.s.r. spectrum of the monomeric complex $[Cu(LH)(ClO_4)_2H_2O]\cdot 2H_2O$. A signal corresponding to a $\Delta Ms = 2$ transition was detected in the powder spectrum giving a g value of 4.144, but no hyperfine structure was able to be resolved (see Figure 1.1.5). The appearance of a signal indicating copper-copper magnetic interaction is unexpected as the coordination geometry is a distorted octahedron where the closest Cu···Cu distance is 7.758 Å. In the stereo-view unit-cell diagram, Figure 1.1.4, for this compound it can be seen that the copper centres are linked via the coordinated ligand, bound water and perchlorato groups

Table 1.1.13

E.s.r. Results for Selected Chapter 1 Complexes[a]

Complex	g_1	$g_\perp$	g_2	$g_{/\!/}(g_3)$	$A_{/\!/}(A_3)$[b]	G[c]	Solvent
$[CuL(CH_3COO)]_2$	2.035		2.057	2.202		4.4	powder
		2.054		2.206	183		dmso
		2.059		2.199	187		EtOH[e,f]
$[Cu(LH)(CF_3COO)]_2(CF_3COO)_2$	2.035		2.052	2.185		4.1	powder
$[CuLF]_2 \cdot 5 \cdot 4H_2O$			2.074[h]				powder
$[Cu(LH)F]_2F_2$		2.038		2.174		4.5	powder
$[CuLCl]_2H_2O$	2.042		2.088	2.182		2.8	powder
$[Cu(LH)Cl]_2Cl_2 \cdot 2H_2O$		2.045		2.201		4.5	powder
$[CuLBr]_2$	2.030		2.055	2.160		3.8	powder
$[Cu(LH)Br]_2Br_2 \cdot 2H_2O$		2.045		2.176		3.9	powder
$[CuLI]_2$			2.073[h]				powder
$[Cu(LH)I]_2I_2$	2.035		2.061	d			powder
		2.0611		2.227	174		dmso
$[CuL(NO_3)]_2$			2.040				powder
$[Cu(LH)(NO_3)_2H_2O]$		2.055		2.218			powder
$[CuL(ClO_4)]_2$		2.047		2.208		3.7	powder
$[Cu(LH)(ClO_4)_2H_2O] \cdot 2H_2O$[i]	2.036		2.062	2.202		4.1	powder
$[Cu(LH)(SO_4)]_2$	2.055		2.076	2.234		3.5	powder
		2.061		2.200	188		dmso
$[CuL(NCS)]_2$	2.041		2.053	2.182		3.9	powder
		2.055		2.190	184		EtOH[e,g]
$[CuLN_3]_2$		2.053		2.178	181		dmso
$[CuL(CN)]_2$		2.030		2.147		4.9	powder
		2.045		2.151	183		EtOH[e,g]

a via simple first-order spectral analysis
b h.f. coupling constants in 10^{-4} cm^{-1}
c $G = (g_{11} - 2)/(g_\perp - 2)$
d not resolved
e containing 10% dmso
f $A_N \approx 13 \times 10^{-4}$ cm^{-1} from 5 superhyperfine lines on lowest field peak
g $A_N \approx 11 \times 10^{-4}$ cm^{-1} from 7 superhyperfine lines on lowest field peak
h g_{iso} value
i $g_{\Delta Ms} = 2$ of 4.144

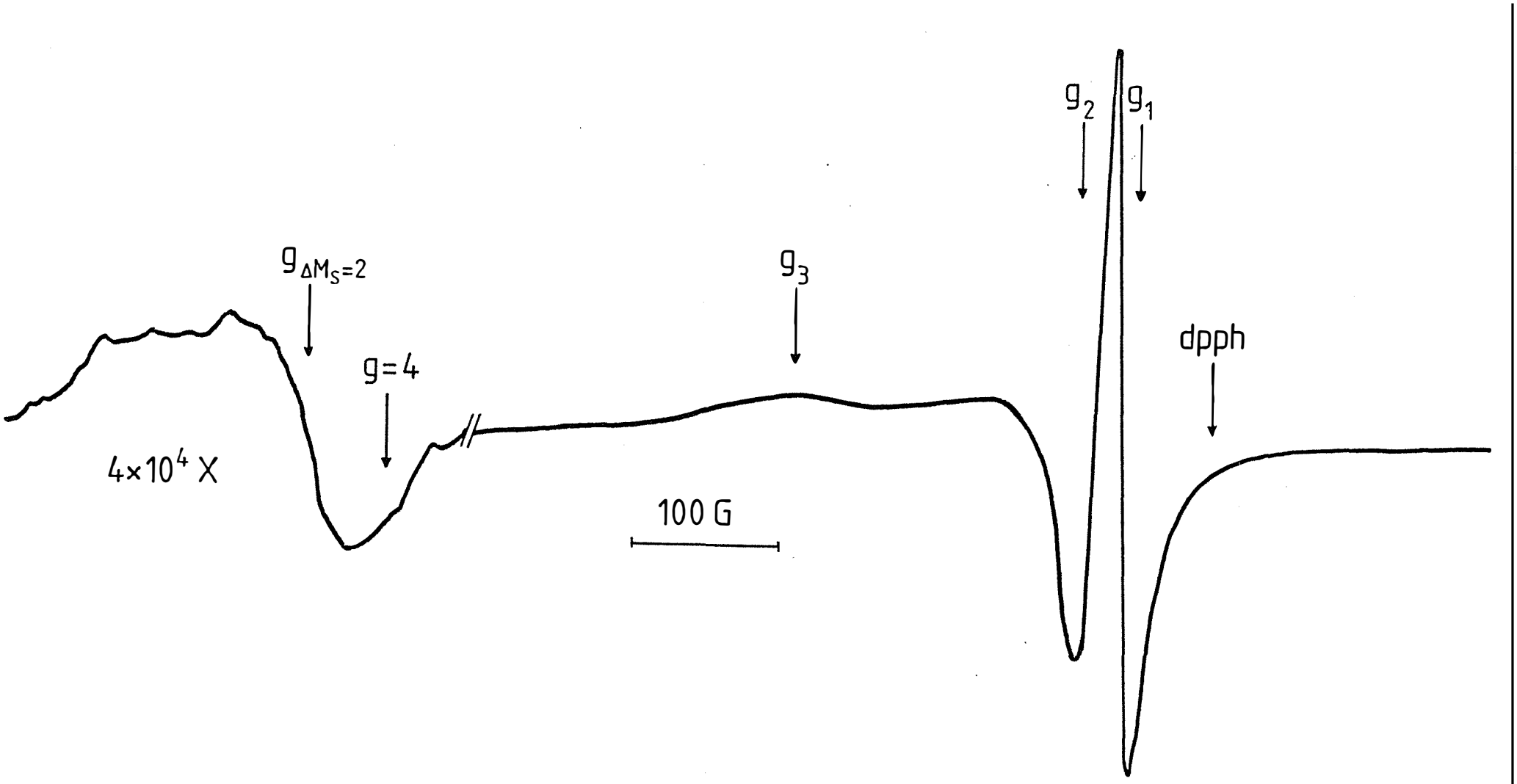

Figure 1.1.5: Powder e.s.r. spectra for $[Cu(LH)(ClO_4)_2H_2O]\cdot 2H_2O$ at 110 K showing the g = 2 (ΔMs = 1) and g = 4 (ΔMs = 2) regions.

through the hydrogen-bonding network. This gives a minimum of seven bonds (chemical and hydrogen) to link any two copper atoms. Although an interaction through such a system seems unlikely, a rough upper limit for the distance over which identifiable electronic effects may be transmitted has been estimated to be about 10 Å [119]. The solid-state spectra for both $[Cu(BBES)(acac)]PF_6$ and $[Cu(Me_2BBEO)_2](ClO_4)_2 \cdot H_2O$ [120] (where BBES is 1,5-bis(benzimidazol-2-yl)-3-thiapentane; Me_2BBEO is 1,5-bis(N-methylbenzimidazol-2-yl)-3-oxopentane; and acac is pentane-2,4-dionate anion) shows them to be magnetically dilute with the shortest Cu···Cu distance of 7.346 Å. However, the spacings between the hyperfine lines in the powder spectra are only about half the solution $A_{||}$ value, and a very weak transition associated with the $\Delta M_2 = 2$ resonance was detected. This indicates the molecules are interacting pairwise in the solid state which has been attributed to a dipolar spin-spin interaction in the absence of evidence for another coupling pathway. Magnetic exchange has also been observed in the solid state e.s.r. spectra for copper(II) tetraphenylporphyrin [121] and $[Cu_2(dien)_2(DHNQ)](BPh_4)_2$ [122] (where dien is diethylenetriamine and DHNQ is 5,8-dihydroxy-1,4-napthoquinone dianion) where the Cu···Cu separations are 8.3 and 8.075 Å respectively and was attributed to dipolar effects.

The magnetic exchange observed at liquid nitrogen temperature for $[Cu(LH)(ClO_4)_2H_2O] \cdot 2H_2O$ may therefore be due to a dipolar spin-spin interaction. Further investigation of the magnetic properties of this complex over a temperature range seem warranted. The occurrence of large, broad isotropic spectra for $[CuLF]_2 \cdot 5.4H_2O$, $[CuLI]_2$ and $[CuL(NO_3)]_2$ are also indicative of extensive exchange coupling in the non-magnetically dilute solids.

In the ethanolic solutions of $[CuL(CH_3COO)]_2$, $[CuL(NCS)]_2$ and $[CuL(CN)]_2$ nitrogen superhyperfine splittings are observed on the lowest field copper(II) hyperfine peak and in the $g_\perp$ region of the spectra. In the first example, 5 superhyperfine lines are apparent, indicating 2

nitrogen spins coupled to the copper centre*, both of which are assumed to be from the coordinated NNS ligand (see Figure 1.2.7(a)). For the latter two cases, 7 lines indicating 3 nitrogens coupled to copper are discernable showing the anions to be coordinated to the copper via the nitrogen in solution.

1.1.4(e) Complex Stability

Remarkably, the neutral ligand copper(II) complexes formed from 2.0 - 3.8 M non-oxidising acid solutions are stable and are often isolated as crystalline solids. The integrity of the $Cu(LH)^{2+}$ species can be visually verified in solution by its emerald green colour. Appreciable acid hydrolysis of the complexed ligand is not apparent even after the solutions have been standing for months.

With the oxidising acids HNO_3 and $HClO_4$ however, ⅓ M solutions were used to isolate stable complexes. If the acid concentration used was above 1M, then the dark green aqueous solution of CuL^+ immediately went pale blue, indicating decomposition of the solution species, possibly by ligand oxidation to give a $Cu(II)O_6$ type solution species. For the CuL^+/(⅓ M)HNO_3 reaction mixture (after crystallisation and removal of some $[Cu(LH)(NO_3)_2H_2O]$) pale blue crystals were isolated upon the solution going to dryness, the ir spectrum of which is consistent with a hydrated copper(II) nitrate species [107] and very little organic matter.

When excess $S_2O_8^{-2}$ was added with warming to aqueous CuL^+, the green colour faded over ~¼ hour to give a clear solution (which turned brown after a few weeks). From this and the preceding results it would appear the CuL^+ species is susceptible to attack and decomposition by strong oxidising acids and anions.

---

* Number of superhyperfine lines = 2nI + 1 where n is the number of equivalent nuclear spins coupled to the copper and I is the nuclear spin quantum number; $I_N = 1$.

The 2-formylpyridine thiosemicarbazono ligand, L^-, stabilises the copper(II) state sufficiently so that complexes of reducing anions (towards $Cu(H_2O)_6^{2+}$) such as I^-, CN^- and NCS^- can be isolated with no sign of decomposition to Cu(I) species.

The three stable Cu(I) complexes isolated to date have been made from copper(I) salts reacting with the ligand. Bell *et al.* [66] isolated the black complex formulated as Cu(I)(LH)Cl. The analogous I^- and ClO_4^- complexes prepared in this work are diamagnetic and have better analytical figures, adding credence to their formulations. It is interesting to note that the complex formulated as $[Cu(I)(LH)(ClO_4)]$ was synthesised by adding a suspension of Cu(I)(thiolate) (formed from the addition of excess thiol to $Cu(II)(ClO_4)_2 \cdot 6H_2O$ in solution) to a solution of LH. The expected product was [Cu(I)(LH)(thiolate)]. Why this did not form is unclear, as is the fate of the thiolate. More will be discussed on this in Chapter 2 where surprisingly stable copper(II) thiolato complexes (Cu(II)LSR) were isolated.

1.1.4(f) Summary

Copper(II) complexes of the ligand 2-formylpyridine thiosemicarbazone, LH, were prepared either from the appropriate copper salt or via metathetical displacement of the acetate ion from aqueous solution (see Experimental section).

The complexes formed are very stable in non-oxidising acidic solution and with mildly reducing anions but are susceptible to oxidising acids and anions.

X-ray crystallographic structures on $[Cu(LH)(ClO_4)_2H_2O] \cdot 2H_2O$ and $[Cu(LH)(CF_3COO)]_2(CF_3COO)_2$ show the copper coordination spheres to be distorted elongated octahedral and distorted square-planar respectively which is in accord with the electronic and e.s.r. spectroscopic results.

1.1.5 EXPERIMENTAL

1.1.5(a) Instrumentation

The general instrumentation and reagents used in this and succeeding chapters is described in Appendices 1 and 2 respectively.

1.1.5(b) Preparation of Compounds

2-formylpyridine thiosemicarbazone (LH)

To a hot solution of thiosemicarbazide (10.2 g, 0.112 mols) in 95% ethanol (100 cm^3) was added water (40 cm^3). To the resulting filtered solution, 2-formylpyridine (pyridine-2-aldehyde, pyridine-2-carboxaldehyde) was added dropwise (11.0 cm^3, 0.116 mols) and the mixture refluxed for 2 hours. Upon cooling, yellow crystals of the title compound separated. These were filtered off and washed with water then cold ethanol and vacuum dried. Yield 17.63 g (87%) m.p. 209-212° C (c.f. Lit. = 210° C [123]).

Preparation of copper complexes

$[CuL(CH_3COO)]_2$

This complex was synthesised following a published procedure [64]. To a solution of LH (3.60 g, 20.0 mmols) in N,N-dimethylformamide (140 cm^3) was added dropwise a solution of $Cu(CH_3COO)_2H_2O$ (4.03 g, 20.2 mmols) in water (150 cm^3). The dark green compound which separated was filtered and washed with ethanol then diethyl ether and vacuum dried. Yield 5.02 g (83 %); m.p. 226-8° C.

$[CuLF]_2$

$CuF_2{\cdot}2H_2O$ powder (282 mg, 2.05 mmols) was added slowly with constant stirring to a hot filtered solution containing LH (400 mg, 2.22 mmols) and sodium metal (60 mg, 2.61 mmols) in methanol (40 cm^3). The resulting solution was boiled for 5 minutes then filtered to remove any solid NaF or unreacted CuF_2. The volume was reduced on a rotary evaporator to 20 cm^3 and the solution cooled in a fridge for 3 hours. The title complex separated as a dark green hydroscopic sludge and was filtered off and washed with diethyl ether then vacuum dried. Yield 264 mg (41%).

$[CuLX]_2$ (X = Cl^- or Br^-)

These complexes were synthesised according to a slightly modified procedure for $[CuLCl]_2$ (after [64]). To a solution of LH (1.00 g, 4.99 mmols) in N, N-dimethyformamide (40 cm^3) was added dropwise a solution of $CuCl_2{\cdot}2H_2O$ (0.958 g, 5.62 mmols) or $CuBr_2$ (1.256 g, 5.62 mmols) in water (40 cm^3). The dark green products were heated for 5 minutes, filtered and washed with ethanol and vacuum dried. Yields $[CuLCl]_2H_2O$ 1.393 g (88%); $[CuLBr]_2$ 1.641 g (92%).

$[CuLI]_2$

This complex was synthesised following a published method [64]. To a solution of LH (0.90 g, 4.99 mmols) in N, N-dimethylformamide (35 cm^3), was added KI (16.6 g, 100 mmols) in water (50 cm^3). This solution was filtered and to it was added $Cu(CH_3COO)_2H_2O$ (1.00 g, 5.01 mmols) in water (40 cm^3). The dark green compound which formed was heated for 5 minutes then filtered and washed successively with water, ethanol and diethyl ether before beging vacuum dried. Yield 1.747 g (95%).

[CuLX] (X = NO_3^- or ClO_4^-)

A slightly modified procedure (after [64]) was used for these complexes. To a hot solution of LH (1.00 g, 5.55 mmols) in ethanol (70 cm^3) and water (30 cm^3) was added $Cu(NO_3)_2 \cdot \frac{5}{2} H_2O$ (1.309 g, 5.63 mmols) or $Cu(ClO_4)_2 \cdot 6H_2O$ (2.071 g, 5.59 mmols) in water (30 cm^3). The resulting dark green solution was heated for 5 minutes then left in a fridge overnight. The dark green crystalline products were filtered and given a cursory wash with cold water then vacuum dried. Yields $[CuL(NO_3)]_2$ 0.422 g (25%); $[CuL(ClO_4)]_2$ 1.104 g (58%).

$[(CuL)_2SO_4(H_2O)_2]H_2O$

To a hot solution containing LH (301 mg, 1.67 mmols) and sodium metal (47 mg, 2.04 mmols) in ethanol (40 cm^3) was added $CuSO_4 \cdot 5H_2O$ (417 mg, 1.67 mmols) in water (10 cm^3). The green precipitated was filtered and washed with water, ethanol then diethyl ether. Yield 288 mg (54%).

$[CuLX]_2$ (X = NCS^- or N_3^-)

Upon addition of KSCN (165 mg, 1.70 mmols) or NaN_3 (140 mg, 2.15 mmols) in water (10 cm^3) to $Cu(CH_3COO)_2H_2O$ (322 mg, 1.66 mmols) in methanol (30 cm^3) a milky green solution formed. To this was added a solution of LH (296 mg, 1.64 mmols) in methanol (30 cm^3). The resulting dark green solution was refluxed gently for one hour then the green solids were filtered off and washed successively with water, methanol and diethyl ether then vacuum dried. Yields $[CuL(SCN)]_2$ 384 mg (77%) m.p. 212-4° C; $[CuLN_3]_2H_2O$ 386 mg (79%).

$[CuL(CN)]_2$

A solution of $[CuL(CH_3COO)]_2$ (302 mg, 1.00 mmols) was briefly boiled in water (100 cm^3) then filtered. While this was still hot a solution of NaCN (53 mg, 1.08 mmols) in water (10

cm^3) was added dropwise. The brown precipitate which formed immediately was filtered and washed with boiling water then vacuum dried. Yield 94 mg (33%).

$[Cu(LH)F]_2F_2$

To a solution of 3 M HF (7 cm^3) (in a plastic beaker) was added $[CuL(CH_3COO)]_2$ (260 mg, 0.86 mmols) with heating to form a saturated solution. This was then filtered to remove any undissolved matter and put aside for 6 weeks until the solution had gone to dryness. The dark green/black compound was put on a vacuum line for 1 day to remove any acetic acid present. Yield 175 mg (72%).

$[Cu(LH)(CF_3COO)]_2(CF_3COO)_2$ and $[Cu(LH)(SO_4)]_2$

Following the general procedure used by Bingham *et al.* [64] $[CuL(CH_3COO)]_2$ (302 mg, 1.00 mmols) was added to a 2.6 M CF_3COOH solution (25 cm^3) or a 2.0 M H_2SO_4 solution (30 cm^3) with heat. The resulting emerald green solutions were filtered immediately then left for 1 day. The dark green crystals which separated were removed from solution and given a cursory wash with diethyl ether. Yields $[Cu(LH)(CF_3COO)]_2(CF_3COO)_2$ 182 mg (39%); $[Cu(LH)(SO_4)]_2$ 184 mg (54%).

$[Cu(LH)X]_2X_2$ (X = Cl^-, Br^- or I^-)

To $[CuL(CH_3COO)]_2$ (320 mg, 1.06 mmols) in water (20 cm^3) was added the appropriate concentrated acid (10 cm^3) and the mixture heated for 5 minutes. The emerald green (X = Cl^- and Br^-) or red/orange (X = I^-) precipitates were filtered and washed with acetone. Yields $[Cu(LH)Cl]_2Cl_2{\cdot}2H_2O$ 315 mg (89%); $[Cu(LH)Br]_2Br_2{\cdot}2H_2O$ 407 mg (91%); $[Cu(LH)I]_2I_2$ 483 mg (92%).

$[Cu(LH)X_2]$ (X = NO_3^- or ClO_4^-)

To a ⅓ M solution of the appropriate acid, HX (10 cm^3), solid $[CuL(CH_3COO)]_2$ (155 mg, 0.51 mmols) was added to give a green solution. After a very cold night 10 weeks later both solutions deposited green/blue crystals which were given a cursory wash with the appropriate ⅓ M acid. The perchlorato complex was found to be unstable when heated and may explode. Yields $[Cu(LH)(ClO_4)_2H_2O]\cdot 2H_2O$ 66 mg (28%); $[Cu(LH)(NO_3)_2H_2O]$ 127 mg (65%).

$[Cu(I)(LH)I]\cdot\frac{3}{2}H_2O$

To CuI (400 mg, 2.10 mmols) was added LiI (2.0 g, 14.94 mmols) in the minimum volume of hot ethanol (15 cm^3) required to dissolve most of the CuI. This was decanted into a flask and LH (384 mg, 1.27 mmols) in ethanol (50 cm^3) was added dropwise. The mixture was then refluxed under nitrogen for 2 hours. The resulting brown product was washed successively with an ethanolic LiI solution (10 cm^3), hot ethanol and diethyl ether then vacuum dried. Yield 489 mg (96%).

$[Cu(I)(LH)(ClO_4)]$

An attempt was made to isolate a copper(I) thiolato complex with LH. To $Cu(ClO_4)_2\cdot 6H_2O$ (373 mg, 1.00 mmols) in ethanol (10 cm^3) was added a solution containing pentafluorothiophenol (0.27 cm^3, 2.00 mmols) in ethanol (5 cm^3). The resulting yellow gel was heated briefly and was then added slowly with heat to a solution of LH (216 mg, 1.20 mmols) in ethanol (20 cm^3). A deep red/brown solution containing a red precipitate formed which was then refluxed overnight. An orange/red powder which analysed as the title complex was filtered off and washed with hot ethanol, hot chloroform then diethyl ether and vacuum dried. Yield 323 mg (94%).

1.1.5(c) X-ray Crystallography

Nine single-crystal X-ray crystallographic structures were determined in this work. Six of these were collected on an Enraf-Nonius CAD-4 diffractometer at Massey University and the remaining three were collected at Canterbury University by Dr Ward Robinson on a Nicolet R3M diffractometer.

As the general procedure for the data collection on the CAD-4 was similar in all six cases, a more detailed description of the collection parameters is given only for the first structure. Tables summarising the crystal and data collection parameters for all structures are given in their corresponding experimental sections.

1.1.5(d) Data collection procedure for Di-μ-trifluoroacetato-bis [(2-formylpyridine thiosemicarbazone)copper (II)] Bistrifluoroacetate.

The title compound was synthesised as described in section 1.1.5(a). A crystal of approximate dimensions 0.060 x 0.015 x 0.004 cm was mounted on a glass fibre using 'Araldite' adhesive.

Twenty-five initial reflections were located using the routine 'search' and an approximate cell was calculated. A thin-shell of data was collected (θ 30-40°) and from this, twenty-five strong reflections with the following additional criteria were chosen to calculate the cell dimensions.

1 Phi values to cover ±180°.

2 Chi values distributed within the range ±40°.

3 Largest possible values for h, k and l

The refined cell dimensions are: a = 9.6015(7), b = 10.8374(10), c = 8.8105(16)Å; α = 100.706(11), β = 117.064(10) and γ = 80.877(7)°. For a cell volume of 799.3 $Å^3$ and a molecular weight of 939.6 a.m.u. ($C_{22}H_{16}Cu_2F_{12}N_8O_8S_2$) the density was calculated to be 1.952 g cm^{-3} for one formula weight in the unit cell. Diffraction symmetry was consistent with the triclinic crystal class (space group P1 or P$\bar{1}$). Final analysis proved P$\bar{1}$ to be the correct space group.

The intensity data were collected on an Enraf-Nonius CAD-4 diffractometer with Cu-K_α radiation (μ (Cu-K_α) = 38.36 cm^{-1}) using the $\omega/2\theta$ scan technique (θ_{max} = 75°). The ω scan is given by $\omega = A + B\tan\theta$, where A is a constant dependent on the crystal mosaic spread and the divergence of the primary beam, and the $B\tan\theta$ term allows for reflection widening due to α_1 - α_2 splitting at high theta angles. Values used in this case were A = 0.80 and B = 0.142. The scans were automatically extended by 25% at each side of the peak to afford background measurements.

The width of the variable aperture of the detector is given by $Apt = A + B\tan\theta$. For this structure A = 1.70 and B = 1.20 were used. The vertical size of the aperture is fixed and consists of a manually insertable slot of height 4 mm.

The initial intensity measurements were made by a fixed speed 'prescan'. If the relative $\sigma(F^2)^*/F^2$ of the prescan measurement is not equal to or less than a specified acceptance parameter, then the reflection is considered unobserved and a final, slower scan is not undertaken. The speed of the final scan is calculated on the basic prescan and a second $\sigma(F^2)/F^2$ which is required for the final measurement, the maximum time on the final scan being set by the operator. For this structure initial intensity measurements were made by a fixed speed prescan of (20/3)°/min with the relative $\sigma(F^2)/F^2$ for the prescan acceptance parameter set at 0.80. The final scan $\sigma(F^2)/F^2$ was set at 0.018 with a maximum scan time of 100 s.

* $\sigma(I) = (INT + 4\ (BGL + BGR))^{½}$, where INT represents the total count and BGL and BGR are the left and right background counts respectively.

Three standard reflections were monitored at hourly intervals so that scaling of the final data could be carried out should crystal decomposition occur. For this data set, the total loss of intensity was 12.5%; minimum and maximum corrections for anisotropic decay were later determined as 0.9974 and 1.1902 respectively.

The same three reflections were used to check that the scattering vectors did not deviate more than 0.08° from their calculated positions. No such deviation occurred for this structure.

A total of 3504 reflections were collected for the $\underline{h}\,\underline{k}\,\underline{l}$ range: -12→10, -13→13, 0→11. After averaging equivalent measurements, the data set consisted of 2974 reflections for which $F^2 > 3\sigma(F^2)$. The raw intensity was calculated from the expression:

$$I_{raw} = \frac{20.1166 \times ATN}{NPI}(C - R \times B)$$

where ATN = attenuation factor (= 12.34 - automatically inserted if the count rate exceeded 10 000 counts per second during the scan)

NPI = ratio of fastest possible scan rate to scan rate for the actual measurement

C = total count

B = total background count

R = ratio of scan time to background counting time (2.0 for CAD-4)

The standard deviations in the observed intensities are given by;

$$\sigma(I) = \frac{20.1166 \times ATN}{NPI}(C + R^2 \times B)^{1/2}$$

For all nine structures Lorentz and polarisation corrections were made to the data. Corrections were also made for absorption.

For numerical (analytical) absorption corrections [124,125] a precise description of the crystal in terms of its size and the identification of the crystal faces is needed. The maximum dimensions of the crystal along each of the crystallographic axes are used to determine a relative grid density which in turn is used in a Gaussian integration. The path length travelled within the crystal by the beam reflected from each infinitesimal element of volume is calculated and then these results are integrated over the entire volume of the crystal. In this way the absorption correction for each reflection is obtained. Individual numerical corrections are then applied to the intensity data.

For empirical absorption corrections [126] a set of four reflections with Chi near 90° is chosen. An accurate scan in Phi over the range 0 to 360° is then carried out on the diffractometer for each reflection. Interpolation of the data for each curve enables intensities at 10° intervals to be calculated and then averaged about phi of 0°. The maximum intensity for each curve is found and this is considered to be 100% transmission. Transmission factors for other points on the curve are calculated relative to the maximum transmission and then averaged for all curves. Absorption corrections can thus be applied when crystal faces can not readily be indexed or crystals are mounted in capillaries.

For this data set numerical absorption corrections were applied using the displayed faces {0 $\bar{1}$ 0}, {$\bar{1}$ 0 0}, {0 1 0}, {1 0 0}, {0 0 $\bar{1}$} and {0 0 1} with a grid size of 4 x 4 x 8. Minimum and maximum transmission coefficients were 0.2328 and 0.7841 respectively.

Tables 1.1.14 and 1.1.15 summarise the relevant crystal and data collection parameters respectively.

1.1.5(e) Structure solution and refinement

The copper position was located from a Patterson map and a structure factor calculation based on this site with a fixed isotropic temperature factor (U = 0.04) for copper returned a residual of 0.60. The remaining non-hydrogen atoms were located on the heavy atom electron-density map. Three cycles of least-squares with all parameters allowed to refine assuming isotropic thermal motion returned an R-factor of 0.17. Inspection of a difference map revealed sites for all hydrogen atoms as well as showing disordered sites for fluorine atoms of both trifluoroacetate groups. Four major positions for each fluorine (with the indicated occupancy given in the appropriate table on the microfiche) were included after fixing the isotropic thermal parameters at 0.04 and refining the occupancy. This resulted in an R-factor of 0.14. Hydrogen atoms were included at calculated positions in these computations. A further least-squares cycle with the copper and sulphur refined assuming anisotropic thermal motion gave an R-factor of 0.10.

For the final least-squares cycle, the six highest occupancy fluorine positions and all other non-hydrogen atoms were refined assuming anisotropic thermal motion and converged to values of 0.0707 and 0.0816 for R and R_w respectively. The function minimised was $\Sigma w(|F_o| - |F_c|)^2$ for the 319 parameters and 2974 data for which $F^2 > 3\sigma(F^2)$ with the weight, w, being defined as $1.000/(\sigma^2(F) + 0.017134\ F^2)$. The largest parameter shift per estimated standard deviation, (esd) was 0.46.The atomic scattering factors and anomalous dispersion coefficients for copper for this and all other structures in this thesis were taken from [127]. The four highest peaks in the final difference electron density map were in the range 1.11 - 0.57 ē $Å^{-3}$, and these were associated with the residual electron density around the copper and sulphur atoms.

Final atomic parameters and the observed and calculated structure factors are on the microfiche in the pocket inside the back cover of this thesis. The bond length and bond angle data are in Tables 1.1.2 and 1.1.3 respectively.

TABLE 1.1.14
($[Cu(LH)(CF_3COO)]_2(CF_3COO)_2$)

CRYSTAL DATA

Compound:	Di-μ-trifluoroacetato-bis[(2-formylpyridine thiosemicarbazone) copper(II)] Bistrifluoroacetate
Colour:	Green
Formula:	$C_{22}H_{16}Cu_2F_{12}N_8O_8S_2$
Formula weight:	939.6 a.m.u.
Space group:	$P\bar{1}$
a:	9.6015(7) Å
b:	10.8374(10) Å
c:	8.8105(16) Å
α:	100.706(11)°
β:	117.064(10)°
γ:	80.877(7)°
V:	799.3 $Å^3$
Z:	1
ρ_c:	1.952 g cm^{-3}
Crystal faces:	{0 $\bar{1}$ 0}, {$\bar{1}$ 0 0}, {0 1 0}, {1 0 0}, {0 0 $\bar{1}$}, {0 0 1}
Crystal dimensions:	0.060 x 0.015 x 0.004 cm
μ (Cu-$K_{\bar{\alpha}}$):	38.36 cm^{-1}
F(OOO):	462

TABLE 1.1.15
($[Cu(LH)(CF_3COO)]_2(CF_3COO)_2$)

Parameters Associated with Data Collection

Radiation used:	Cu-K_α (λ = 1.5418 Å)
Graphite monochromator used:	no
Incident beam collimator (diameter):	1.3 mm
ω scan angle:	$(0.80 + 0.142 \tan \theta)^\circ$
Horizontal aperture width:	$(1.70 + 1.20 \tan \theta)$ mm
Vertical aperture height:	4 mm
Scan type:	$\omega/2\theta$
Prescan speed:	$(20/3)^\circ$/min
Prescan acceptance; relative $\sigma(F^2)/F^2$ required:	0.8
Final scan acceptance $\sigma(F^2)/F^2$:	0.018
Maximum time limit for final scan:	100 s
Intensity control frequency:	3 600 s
Orientation acceptance; maximum deviation of any scattering vector from its calculated position:	0.08°
θ Range:	1–75°
Total number of reflections in data set:	3 504
Observed data criterion:	2 974 unique reflections with $F^2 > 3\sigma(F^2)$
Collection temperature:	293 K

1.1.5(f) Data collection procedure for Aqua(2-formylpyridine thiosemicarbazone diperchloraro)copper(II) Dihydrate.

The title compound was synthesised as described in section 1.1.5(a). A crystal of approximate dimensions 0.045 x 0.025 x 0.020 cm displayed faces of the forms {1 1 0}, {$\bar{1}$ 1 0}, {$\bar{1}$ $\bar{1}$ 0},{1 $\bar{1}$ 0}, {0 1 1}, {$\bar{1}$ 0 1}, {0 $\bar{1}$ 1}, {1 0 1} and {0 1 $\bar{1}$}. Cell dimensions determined from a least-squares refinement of the setting angles of 25 reflections are: $\underline{a}$ = 12.9601(6), $\underline{b}$ = 9.7623(4), $\underline{c}$ = 14.9950(10) Å and β = 111.580(5)°. For a cell volume of 1764.2 Å^3 and a molecular weight of 496.8 a.m.u. ($C_7H_{14}Cl_2CuN_4O_{11}S$) the density was calculated to be 1.870 g cm^{-3} for four formula weights in the cell. Systematic absences ($\underline{h}$ 0 $\underline{l}$, $\underline{l}$ = 2n + 1; and 0 $\underline{k}$ 0, $\underline{k}$ = 2n + 1) established the space group as $P2_1/c$. A total of 4032 reflections were collected on an Enraf-Nonius CAD-4 diffractometer with Cu–K_α radiation (μ (Cu-$K_{\bar{\alpha}}$) = 59.81 cm^{-1}) using the $\omega/2\theta$ scan technique (θ_{max} = 75.0°). The $\underline{h}$ $\underline{k}$ $\underline{l}$ limits were: -16 → 15, 0 → 12, 0 → 18.

The intensities of three standard reflections were monitored at 2 hourly intervals during the data collection. The total loss of intensity was 4.8% so corrections for anisotropic decay were applied, minimum and maximum corrections being 0.9836 and 1.0586 respectively.

Analytical absorption corrections were applied [125,125], minimum and maximum transmission coefficients being 0.0666 and 0.3775 respectively.

Tables 1.1.16 and 1.1.17 summarise the relevant crystal and data collection parameters.

1.1.5(g) Structure solution and refinement

The copper atom located from the Patterson synthesis, yielded a residual of 0.57 after two cycles of refinement over one quarter of the unit cell. The subsequent electron density map, based on the calculated phase of this copper site revealed the positions of the two Cls the S and four peaks designated as N. A least-squares refinement returned an R factor of 0.36. All non-hydrogen atoms were located from a series of electron density and least-squares calculations to give R = 0.10. A difference electron density map revealed peaks within bonding distance of Cl(2). These were included as one quarter weighted oxygens. All hydrogen atoms were located, those in the pyridine and on C(6) being fixed at 1.08 Å.

The final least-squares refinement cycle converged to values of 0.0586 and 0.0725 for R and R_w respectively for the 250 parameters and 3 247 data for which $F^2 > 3\sigma(F_2)$. The function minimised was $\Sigma w(|F_o| - |F_c|)^2$ with the weight, w, being defined as $1.000/(\sigma^2(F) + 0.1146\ F^2)$. The largest parameter shift per esd of 0.4 was associated with a disordered perchlorate oxygen. The three one quarter weighted perchlorato oxygen atoms and the hydrogen atoms were refined with isotropic thermal parameters. All other atoms were refined assuming anisotropic thermal motion.

The highest peak of 0.60 $\bar{e}$ $Å^{-3}$ in the final difference electron density map was associated with the residual electron density around the copper atom.

Final atomic parameters and the observed and calculated structure factors are on the microfiche in the pocket inside the back cover of this thesis. The bond length and bond angle data are in Tables 1.1.2 and 1.1.3 respectively.

TABLE 1.1.16
([Cu(LH)(ClO$_4$)$_2$H$_2$O]·2H$_2$O

CRYSTAL DATA

Compound:	Aqua(2-formylpyridine thiosemicarbazone diperchlorato)copper(II) Dihydrate
Colour:	Green
Formula:	$C_7H_{14}Cl_2CuN_4O_{11}S$
Formula weight:	496.8 a.m.u.
Space group:	$P2_1/c$
a:	12.9601(6) Å
b:	9.7623(4) Å
c:	14.9950(10) Å
β:	111.580(5)°
V:	1764.2 Å^3
Z:	4
ρ_c:	1.870 g cm^{-3}
Crystal faces:	{1 1 0}, {$\bar{1}$ 1 0}, {$\bar{1}$ $\bar{1}$ 0}, {1 $\bar{1}$ 0}, {0 1 1}, {$\bar{1}$ 0 1}, {0 $\bar{1}$ 1}, {1 0 1}, {0 1 $\bar{1}$}
Crystal dimensions:	0.045 x 0.025 x 0.020 cm
μ (Cu-K$_{\bar{\alpha}}$):	59.81 cm^{-1}
F(OOO):	1004

TABLE 1.1.17
($[Cu(LH)(ClO_4)_2H_2O]\cdot 2H_2O$

Parameters Associated with Data Collection

Radiation used:	Cu-K_α (λ = 1.5418 Å)
Graphite monochromator used:	no
Incident beam collimator (diameter):	0.8 mm
ω scan angle:	$(0.80 + 0.14 \tan\theta)^\circ$
Horizontal aperture width:	$(1.70 + 1.20 \tan\theta)$ mm
Vertical aperture height:	4 mm
Scan type:	$\omega/2\theta$
Prescan speed:	(20/3)°/min
Prescan acceptance; relative $\sigma(F^2)/F^2$ required:	0.8
Final scan acceptance $\sigma(F^2)/F^2$:	0.018
Maximum time limit for final scan:	100 s
Intensity control frequency:	7 200 s
Orientation acceptance; maximum deviation of any scattering vector from its calculated position:	0.08°
θ Range:	1–75°
Total number of reflections in data set:	4 032
Observed data criterion:	3 247 unique reflections with $F^2 > 3\sigma(F^2)$
Collection temperature:	293 K

CHAPTER 2

TERNARY S AND N DONOR ATOM COPPER COMPLEXES OF L$^-$

1.2.1 INTRODUCTION

One of the proposed antitumour mechanisms outlined in the general introduction was the interaction of a copper(II) drug with the thiol containing enzyme, ribonucleoside diphosphate reductase (rdr). Briefly recapping, CuL^+ or LH (released by reduction of CuL^+ with thiols) may displace the iron from the metal binding site in rdr and/or the CuL^+ species may bind to a thiol group of the enzyme. Also it appears that the drug can bind to intracellular thiols such as glutathione giving a thiolato complex [9,87]. This in turn is able to promote redox reactions with other thiols and oxygen to produce a disulphide along with $O_2^{\cdot-}$ and $OH^{\cdot}$ radicals (which could be partly responsible for the cytotoxicity).

A second possible mechanism outlined involves the binding of the copper(II) drug species to the nitrogen bases of DNA or RNA, hindering or blocking base replication. Antholine *et al.* [128] have studied the interactions of CuL^+ with ethylenediamine (en) using e.s.r. spectroscopy and deduced significant adduct formation. Generally however, there has been little work published on the Lewis-base interactions with complexes containing tridentate monoanionic ligands.

The aims of the present study were therefore twofold. Firstly, it was hoped that stable, isolable adducts of both model thiolates and nitrogen bases could be synthesised and characterised to show the possibility that *in vitro* such mechanisms may occur *in vivo*. The second aim was for intrinsic reasons; very few stable copper(II) thiolato adducts have been isolated and studied due to the following reaction predominating:

$$Cu(II) + RS^- \rightarrow Cu(I) + \tfrac{1}{2}\ RSSR$$

In this study thiolato adducts were synthesised by metathetical displacement of the acetate ion from an aqueous solution of $[CuL(CH_3COO)]_2$ e.g.

$$CuL^+ + RS^- \rightarrow CuL(SR) \text{ (where RSH = e.g. pentafluorothiophenol).}$$

Sterically bulky, electron withdrawing thiols were chosen to help in the immediate precipitation and stabilisation of the adducts.

As stated above, only limited Lewis-base interactions have been studied with copper and LH, so such reactions were carried out to isolate and characterise these ternary adducts. The single-crystal X-ray crystallographic structures of two anionic ligand, ternary complexes, [CuL(2,2'-bipyridyl)]ClO_4 and [CuL(saccharrinato)H_2O]·½H_2O, were determined.

Complexes of the general formulation [CuL(Lewis-base)]X (where Lewis-base = e.g. 2, 2'-bipyridyl or 2(dimethylaminopyridine) and X = e.g. PF_6^-) were prepared by the addition of stoicheometric amounts, or an excess, of the Lewis-base to an aqueous solution of $[CuL(CH_3COO)]_2$, and generally precipitated upon the addition of aqueous NH_4PF_6. The complexes prepared in this chapter, along with their analytical and room temperature magnetic moment data, are presented in Table 1.2.1.

TABLE 1.2.1

Analytical and Magnetic Data for Chapter 2

Complex[a]	Colour	Analyses (%)[b]				μ_{eff}[c]
		C	H	N	Other	
$[CuL(pftp)]_2 \cdot 4H_2O$	Brown	32.9 (32.7)	1.7 (2.3)	12.1(11.7)	19.5 (19.9)[d]	2.26
$[CuL(pctp)]_2$	Brown	29.9 (29.7)	1.2 (1.4)	10.7 (10.7)	33.4 (33.8)[e]	1.87
$[CuL(ntp)]_2 \cdot 6H_2O$	Dark Brown	34.5 (34.6)	2.3 (3.8)	15.8 (15.5)		1.59
[Cu(I)(ntp)]	Orange	33.1 (33.2)	1.9 (1.9)	6.4 (6.6)		Diamag.
$[Cu(mpH)_2]$	Brown Green	37.7 (38.0)	2.6 (2.6)	9.1 (8.9)		2.03
$[CuL(mbt)] \cdot \frac{1}{2}H_2O$	Green	40.5 (40.2)	2.7 (2.9)	16.8 (16.8)		1.87
$[CuL(mmiH)_2]PF_6 \cdot H_2O$	Green	28.3 (28.4)	3.4 (3.4)	17.2 (17.7)		2.30
$[CuL(miH)_2]PF_6 \cdot \frac{1}{2}H_2O$	Green	26.5 (26.2)	3.0 (2.7)	17.4 (18.8)		2.45
$[CuL(mi)] \cdot 2H_2O \cdot EtOH$	Green	33.6 (34.0)	3.1 (4.7)	19.7 (19.8)		2.11
[CuL(mtt)]	Dark Green	32.8 (32.8)	3.2 (3.3)	26.9 (26.8)		1.98
$[CuL(bipy)]ClO_4$	Dark Green	40.8 (41.0)	2.9 (3.0)	17.1 (16.9)	7.9 (7.1)[e]	1.78
$[CuL(bipy)]PF_6$	Dark Green	37.7 (37.5)	3.0 (2.8)	15.7 (15.5)		1.82
$[CuL(bipy)]_2SO_4 \cdot 8H_2O$	Dark Green	39.3 (39.3)	3.0 (4.4)	16.1 (16.2)		1.74
$[CuL(phen)]PF_6$	Dark Green	40.8 (40.2)	2.6 (2.7)	14.5 (14.8)		1.78
$[CuL(dmap)_2]PF_6$	Green	39.6 (39.9)	4.2 (4.3)	17.7 (17.7)	18.0 (18.0)[d]	2.19
$[CuL(sacc)H_2O] \cdot \frac{1}{2}H_2O$	Dark Green	36.5 (37.2)	3.1 (3.1)	15.1 (15.5)		1.80

a see page x for abbreviations
b calculated values are given in parentheses
c measured at 293 K and quoted in B.M. per copper(II) ion
d %F
e %Cl

1.2.2 CRYSTAL STRUCTURE OF Aqua(2-formylpyridine thiosemicarbazonato)(saccharinato-N)copper(II) Hemihydrate

A thermal ellipsoid diagram for the title compound (abbreviated as [CuL(sacc)H_2O]·½H_2O) showing the numbering scheme used is depicted in Figure 1.2.1. Bond length and angle data are given in Tables 1.2.2 and 1.2.3 respectively.

The complex [CuL(sacc)H_2O]·½H_2O crystallises as a discrete monomer. The copper atom adopts a distorted square-pyramidal geometry comprising the tridentate 2-formylpyridine thiosemicarbazonato ligand (pyridine nitrogen N(1), imine nitrogen N(2) and thioamide sulphur S(1)) the saccharinato anion, N(11), and a water molecule, O(10). This latter occupies the fifth, apical position and, as is typical of the Jahn-Teller distortions observed for such five coordinate copper complexes, is weakly bound [105].

The plane of best-fit* through the in-plane donor atoms S(1), N(1), N(2) and N(11) shows the copper to be displaced out of this mean-plane by 0.176 Å, towards the apical oxygen, O(10). The closest sixth contact to the copper atom is that to O(3) (of the coordinated saccharin) at 3.241 Å. The positioning of this oxygen (the angle O(10)-Cu-O(3) is 133.3°) may well sterically hinder the approach of any possible sixth coordinating ligand but is not considered to interact significantly with the copper.

Within the accuracy of this structure which, due to poor crystal quality, is not high, the bond distances and angles observed within the 2-formylpyridine thiosemicarbazonato ligand present are considered to be normal (see Table 1.1.5).

---

* Plane (i) S(1), N(1), N(2), N(11)
0.8932X – 0.2066Y – 0.3994Z – 0.6464 = 0
[S -0.014, N(1) -0.016, N(2) 0.017, N(11) 0.013, Cu -0.176]
Distances of atoms from the plane (Å) are given in square brackets.

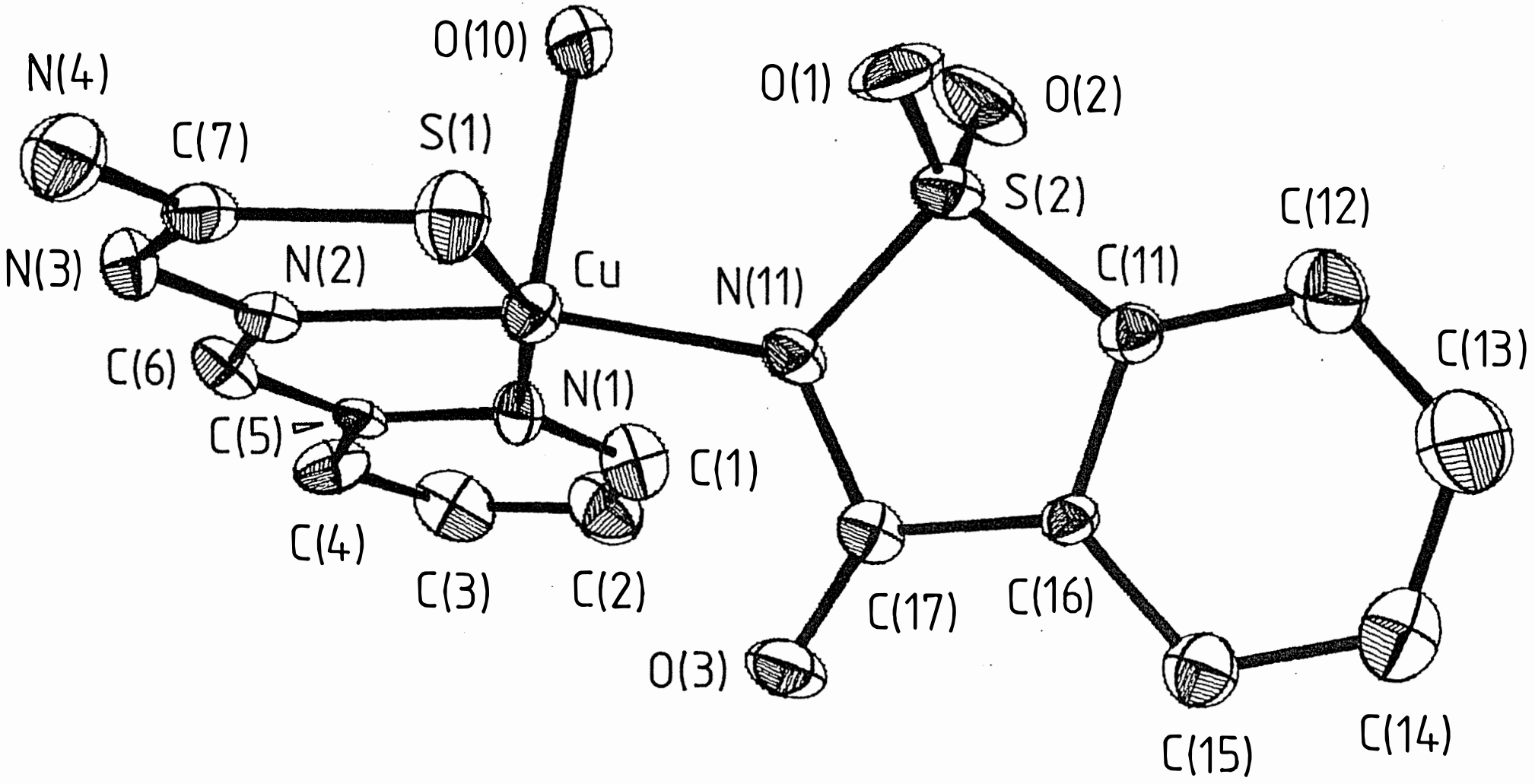

Figure 1.2.1: The monomer $[CuL(sacc)H_2O]\cdot\frac{1}{2}H_2O$ showing the atom numbering scheme. The non-coordinated water molecule and hydrogen atoms have been omitted for clarity.

TABLE 1.2.2
Bond Lengths (Å) with Estimated Standard Deviations in Parentheses for the Complexes [CuL(saccharinato)H_2O]·½H_2O and [CuL(bipyridyl)]ClO_4*

	[CuL(sacc)H_2O]·½H_2O		[CuL(bipy)]ClO_4
Cu–N(1)	2.020(8)		2.049(4)
Cu–N(2)	1.956(7)		1.949(4)
Cu–S(1)	2.264(3)		2.275(1)
S–C(7)	1.721(9)		1.742(4)
N(1)–C(1)	1.314(12)		1.339(6)
N(1)–C(5)	1.362(12)		1.356(5)
N(2)–N(3)	1.358(10)		1.372(6)
N(2)–C(6)	1.285(13)		1.281(6)
N(3)–C(7)	1.340(12)		1.326(6)
N(4)–C(7)	1.327(12)		1.339(6)
C(1)–C(2)	1.408(17)		1.377(7)
C(2)–C(3)	1.397(17)		1.372(6)
C(3)–C(4)	1.358(15)		1.392(8)
C(4)–C(5)	1.411(15)		1.383(7)
C(5)–C(6)	1.451(13)		1.459(7)
Cu–N(11)	1.974(7)	Cu–N(11)	2.180(4)
Cu–O(10)	2.393(7)	Cu–N(12)	1.987(4)

Saccharinato and Bipyridyl Bond Lengths (Å)

S(1)–O(1)	1.420(7)	N(11)–C(10)	1.337(6)
S(2)–O(2)	1.444(9)	C(11)–C(10)	1.376(8)
S(2)–N(11)	1.648(8)	C(12)–C(11)	1.366(8)
S(2)–C(11)	1.700(5)	C(13)–C(12)	1.397(7)
N(11)–C(17)	1.408(12)	C(14)–C(13)	1.377(8)
C(17)–O(3)	1.195(12)	N(11)–C(14)	1.345(6)
C(11)–C(12)	1.395	C(15)–C(14)	1.481(6)
C(12)–C(13)	1.395	C(16)-C(15)	1.392(6)
C(13)–C(14)	1.395	C(17)–C(16)	1.378(7)
C(14)–C(15)	1.395	C(18)–C(17)	1.371(9)
C(15)–C(16)	1.395	C(19)–C(18)	1.387(7)
C(11)–C(16)	1.395	N(12)–C(19)	1.346(6)
C(16)–C(17)	1.465(11)		N(12)–C(15)
	1.346(7)		

Fixed Ring

* N(4)–H bond lengths 0.93 – 1.04 Å, mean 0.97 Å
O–H bond lengths 0.81 – 1.01 Å, mean 0.96 Å
Cl–O bond lengths 1.408 – 1.448 Å, mean 1.426 Å
C–H bond lengths fixed at 1.08 Å

TABLE 1.2.3

Bond Angles (°) with Estimated Standard Deviations in Parentheses for the Complexes $[CuL(sacc)H_2O]\cdot\frac{1}{2}H_2O$ and $[CuLbipy]ClO_4$*

	$[CuL(sacc)H_2O]\cdot\frac{1}{2}H_2O$		[CuL(bipy)]ClO_4
N(1)–Cu–N(2)	81.2(3)		80.4(2)
N(1)–Cu–S(1)	162.3(2)		157.0(1)
N(1)–Cu–N(11)	97.5(3)	N(1)–Cu–N(12)	95.2(1)
N(1)–Cu–O(10)	87.0(3)	N(1)–Cu–N(11)	90.7(2)
N(2)–Cu–S(1)	82.6(2)		84.0(1)
N(2)–Cu–N(11)	168.9(3)	N(2)–Cu–N(12)	175.0(2)
N(2)–Cu–O(10)	96.3(3)	N(2)–Cu–N(11)	104.0(2)
S(1)–Cu–N(11)	97.1(2)	S(1)–Cu–N(12)	99.5(1)
S(1)–Cu–O(10)	101.8(2)	S(1)–Cu–N(11)	109.6(1)
N(11)–Cu–O(10)	94.7(3)	N(12)–Cu–N(11)	78.3(1)
Cu–N(1)–C(1)	130.7(7)		130.0(3)
Cu–N(1)–C(5)	112.4(6)		111.0(3)
C(1)–N(1)–C(5)	116.9(9)		118.2(4)
N(1)–C(1)–C(2)	124.5(10)		122.4(4)
C(1)–C(2)–C(3)	117.4(10)		119.4(5)
C(2)–C(3)–C(4)	119.6(11)		119.3(5)
C(3)–C(4)–C(5)	118.9(10)		118.2(4)
C(4)–C(5)–N(1)	122.6(8)		122.4(4)
C(4)–C(5)–C(6)	124.1(9)		123.3(4)
N(1)–C(5)–C(6)	113.4(9)		114.3(4)
C(5)–C(6)–N(2)	117.5(8)		116.1(4)
C(6)–N(2)–Cu	115.4(6)		116.5(3)
C(6)–N(2)–N(3)	118.8(7)		119.7(4)
Cu–N(2)–N(3)	125.9(6)		123.7(3)
N(2)–N(3)–C(7)	110.4(7)		111.6(4)
N(3)–C(7)–N(4)	117.2(8)		117.3(4)
N(3)–C(7)–S(1)	124.6(7)		125.2(4)
N(4)–C(7)–S(1)	118.2(7)		117.5(3)
Cu–S–C(7)	96.3(3)		94.6(2)

Saccharinato and Bipyridyl Bond Angles

	$[CuL(sacc)H_2O]\cdot\frac{1}{2}H_2O$			[CuL(bipy)]ClO_4
Cu–N(11)–S(2)	123.0(4)		Cu–N(11)–C(10)	129.3(3)
Cu–N(11)–C(17)	124.0(6)		Cu–N(11)–C(14)	112.0(3)
S(2)–N(11)–C(17)	111.5(6)		C(10)–N(11)–C(14)	118.2(5)
N(11)–C(17)–O(3)	123.0(8)		N(11)–C(10)–C(11)	118.9(5)
N(11)–C(17)–C(16)	110.5(8)		C(10)–C(11)–C(12)	118.9(5)
O(3)–C(17)–C(16)	126.5(8)		C(11)–C(12)–C(13)	118.8(6)
N(11)–S(2)–O(1)	109.6(4)		C(12)–C(13)–C(14)	119.0(5)
N(11)–S(2)–O(2)	111.2(5)		C(13)–C(14)–N(11)	122.0(4)
N(11)–S(2)–C(11)	96.2(3)		C(13)–C(14)–C(15)	123.2(4)
O(1)–S(2)–O(2)	116.8(4)		N(11)–C(14)–C(15)	114.8(5)
O(1)–S(2)–C(11)	111.7(4)		C(14)–C(15)–C(16)	122.7(5)
O(2)–S(2)–C(11)	109.3(4)		C(14)–C(15)–N(12)	115.9(4)
S(2)–C(11)–C(16)	108.3(4)		N(12)–C(15)–C(16)	121.4(4)
S(2)–C(11)–C(12)	130.7(4)		C(15)–C(16)–C(17)	118.8(5)
C(12)–C(11)–C(16)	120.0		C(16)–C(17)–C(18)	120.1(5)
C(11)–C(12)–C(13)	120.0		C(17)–C(18)–C(19)	118.6(5)
C(12)–C(13)–C(14)	120.0	Fixed	C(18)–C(19)–N(12)	122.1(5)
C(13)–C(14)–C(15)	120.0		Cu–N(12)–C(19)	122.7(4)
C(14)–C(15)–C(16)	120.0		Cu–N(12)–C(15)	118.0(3)
C(15)–C(16)–C(11)	120.0		C(19)–N(12)–C(15)	119.1(4)
C(15)–C(16)–C(17)	127.5(6)			
C(11)–C(16)–C(17)	112.5(5)			

* O-Cl-O bond angles 107.3 – 111.4°, mean 109.4°

That the saccharinato moiety is planar is indicated by the largest deviation from the plane of best-fit* (excluding O(1) and O(2)) being 0.02 Å. This plane makes an angle of 71.9° with the plane through the 2-formylpyridine thiosemicarbazonato ligand§. The deviation from 90° is such that O(2) moves closer to O(10) (O(2)···O(10) 3.139 Å; O(1)···O(10) 3.577 Å). The mode of coordination via N(11) displayed by sacc has been shown in all transition metal complexes to date with one exception [129-133]. Usually compounds of the general formulation $[M(sacc)_2(H_2O)_4]\cdot 2H_2O$ (where M(II) = V, Cr, Fe, Co, Ni, Cu, Zn, Cd,Hg) are formed in which the two sacc anions bind in a *trans* configuration to the divalent metal with four coordinated water molecules completing an 'octohedral' geometry about the metal. With Cr(II) and Cu(II), two water molecules are bound in the more weakly coordinated axial positions arising from the Jahn-Teller distortion.

The exceptions to these complexes are a pair of isomorphous compounds which are the only ternary complexes of saccharin to date. In $[V(sacc)_2(py)_4]\cdot 2solv$ (solv = pyridine or tetrahydrofuran [132]) the sacc coordinates via the carbonyl oxygen, probably due to steric effects although other factors were not ruled out. Interestingly, there were no significant variations detected in the sacc bonds lengths between the nitrogen and oxygen coordinated vanadium(II) compounds.

In the title complex, $[CuL(sacc)H_2O]\cdot \frac{1}{2}H_2O$, some significant variations in the bonding parameters were observed. The Cu-N(11) bond length of 1.974(7) Å in $[CuL(sacc)H_2O]\cdot \frac{1}{2}H_2O$ is significantly shorter than the value of 2.061(2) Å observed in the

---

* Plane (ii), S(2), O(3), N(11), C(11), C(12), C(13), C(14), C(15), C(16), C(17)
-0.1108X – 0.7732Y – 0.6243Z + 4.1247 = 0
[S(2) 0.01, O(3) -0.01, N(11) -0.01, C(11) 0.01, C(12) -0.01, C(13) -0.02, C(14) -0.00, C(15) 0.01, C(16) 0.02, C(17) 0.00, O(1) 1.22, O(2) -1.22, Cu 0.346]

§ Plane (iii) S(1), N(1), N(2), N(3), N(4), C(1), C(2), C(3), C(4), C(5), C(6), C(7)
0.9017X – 0.2185Y – 0.3732Z – 0.6851 = 0
[S(1) -0.04, N(1) -0.04, N(2) -0.05, N(3) -0.02, N(4) 0.10, C(1) 0.03, C(2) 0.05, C(3) 0.01, C(4) 0.01, C(5) -0.02, C(6) -0.02, C(7) -0.00, Cu -0.19, N(11) 0.06]
Distances of the atoms from the plane (Å) are given in square brackets.

bis(saccharinato) complex, $[Cu(sacc)_2(H_2O)_4]\cdot 2H_2O$ [129], presumably because of the different copper coordination geometry and environment. Differences within the sacc moiety were also observed. A comparison of selected bond lengths and bond angles for saccharin species is given in Table 1.2.4.

The larger Cu-N(11)-S(2) angle, in combination with the shorter Cu-N(11) distance, in $[CuL(sacc)H_2O]\cdot \frac{1}{2}H_2O$ has the effect of bringing O(3) closer to the copper. This effect can be seen by comparing the Cu···O(3) separations of 3.241 and 3.379 Å found in the mono- and bis-saccharinato complexes respectively. The opening of this angle may be due to steric interactions between O(2) and O(10) (3.139 Å). A stronger σ bond between N(11) and copper in $[CuL(sacc)H_2O]\cdot \frac{1}{2}H_2O$ may account for the changed bonding distances and angles observed in the sacc anion (see Table 1.2.4). Another factor which may also contribute to these differences is the different hydrogen-bonding network involving the sacc moiety.

In the structure of $[Cu(sacc)_2(H_2O)_4]\cdot 2H_2O$ [129] there are two hydrogen-bonds from water molecules to the carbonyl oxygen, O(3) (2.604 A and 2.810 Å) whereas the title compound has only one weak interaction (O(3)···O(1) 2.986 Å - see Table 1.2.5). These interactions may well lengthen the C(17)-O(3) bond length in the former case.

The hydrogen-bonding scheme for $[CuL(sacc)H_2O]\cdot \frac{1}{2}H_2O$ is depicted in the stereo-view of the unit-cell, Figure 1.2.2, with the hydrogen-bonding distances and angles being tabulated in Table 1.2.5.

The coordinated water, O(10), has two more contacts in addition to the aforementioned hydrogen-bond to O(3). One is a weak contact with the water molecule, O(11), at 2.931 Å, and the other is with the deprotonated, sp^2 hybridised nitrogen, N(3), on the ligand at 2.816 Å. As previously found for other structures of copper with this ligand [64,65,this work], the terminal nitrogen N(4), has two hydrogen-bonds. One is a weak contact with O(11) (2.976 Å) whereas the other is a relatively uncommon N-H···S interaction. This hydrogen-bond of 3.481

Å, as observed for the majority of those present in this structure, lies at the upper limit of the regularly found values (observed range for N-H···S is 3.39 ± 0.12 Å [135]).

TABLE 1.2.4
Selected Bond Lengths (Å) and Angles (°) for Saccharin Compounds

	Compound			
Bond lengths (Å)	Saccharin[a]	$[CuL(sacc)H_2O]\cdot\frac{1}{2}H_2O$	$[Cu(sacc)_2(H_2O)_4]\cdot 2H_2O$[b]	$[M(sacc)_2H_2O)_4\cdot 2H_2O$[c]
S(2)–N(1 1)	1.663(4)	1.648(8)	1.655(3)	1.637(3)
S(2)–C(1 1)	1.758(4)	1.700(5)	1.753(3)	1.753(3)
N(1 1)–C(17)	1.369(5)	1.408(12)	1.362(4)	1.362(4)
C(17)–O(3)	1.214(5)	1.195(12)	1.238(4)	1.240(4)
Bond Angles (°)				
S(2)–N(1 1)–M	d	123.0(4)	120.6(1)	119.5(1)
C(17)–N(1 1)–M	d	124.0(6)	128.3(1)	129.4(1)
S(2)–N(11)–C(17)	115.1[e]	111.5(6)	110.9(1)	110.5(1)
N(11)–C(17)–C(16)	109.6[e]	110.5(8)	113.4(2)	113.2(3)
O(3)–C(17)–C(16)	112.9[e]	126.5(8)	122.9(3)	122.9(3)
O(3)–C(17)–N(11)	123.9[e]	123.0(8)	123.6(3)	123.9(3)

a Ref. [134]

b Ref. [129]

c Average value for the complexes where M = Fe(II), Co(II) NI(II) - Ref.[129] and M = Zn(II), Cd(II) - Ref. [130]

d not applicable

e std value not quoted

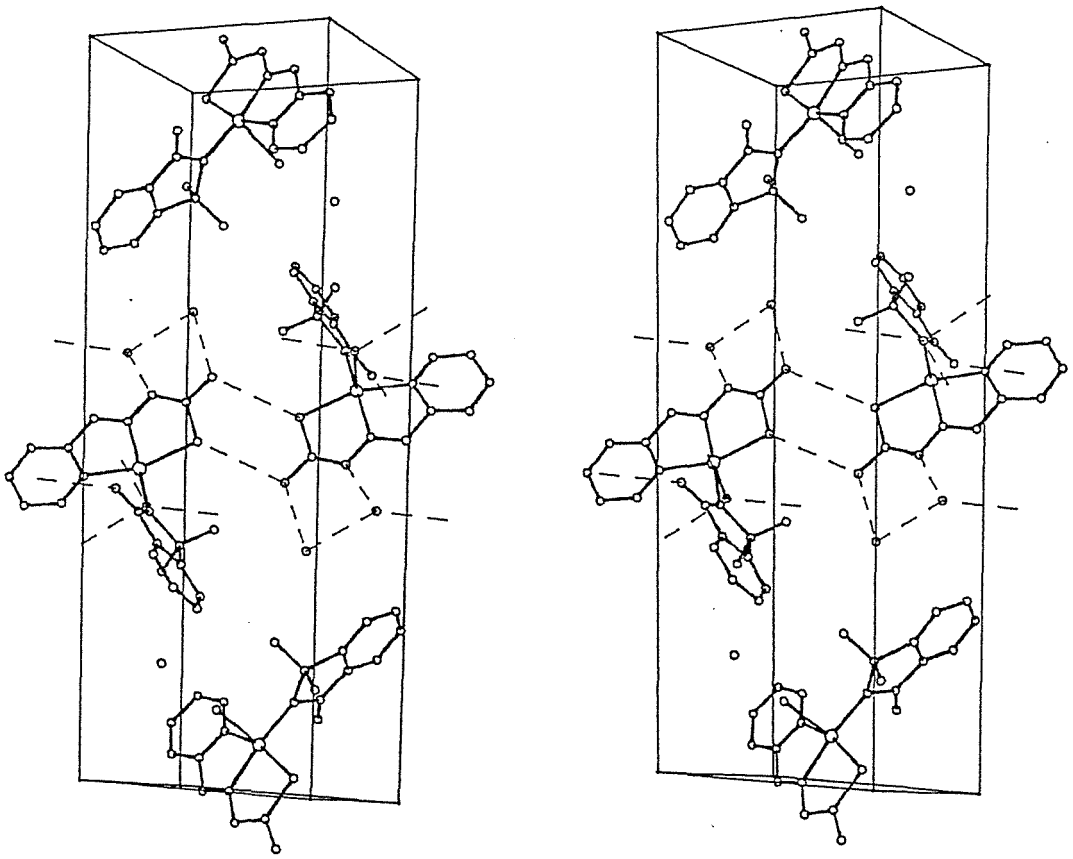

Figure 1.2.2: Stereo-view of the unit-cell packing diagram for $[CuL(sacc)H_2O]\cdot\frac{1}{2}H_2O$ showing the hydrogen-bonding scheme.

TABLE 1.2.5
Hydrogen-Bonding Distances (Å) and Angles (°) for $[CuL(sacc)H_2O]\cdot\frac{1}{2}H_2O$

Atoms[a]	Distance (Å)	Symm[b]	T_x, T_y, T_z
O(10)···N(3)	2.816	2	0 1 0
O(10)···O(3)	2.986	1	$\bar{1}$ 1 1
O(10)···O(11)	2.931	4	1 1 1
O(11)···N(4)	2.976	3	1 1 1
S(1)···N(4)	3.481	2	1 1 1

a the first atom is at symmetry position 1

b symmetry positions

1 (x, y, z)

2 ($\bar{x}$, $\bar{y}$, $\bar{z}$)

3 0.5 + x, 0.5 – y, 0.5 + z

4 0.5 – x, 0.5 + y, 0.5 – z

Atoms	Angle (°)	Atoms	Angle (°)
Cu–O(10)···O(3)	122.7	Cu–O(10)···O(11)	116.1
Cu–O(10)···N(3)	106.0	O(11)···O(10)···O(3)	121.1
O(11)···O(10)···N(3)	121.1	O(3)···O(10)···N(3)	89.7
C(7)–N(4)···O(11)	117.9	C(7)–N(4)···S(1)	111.3
O(11)···N(4)···S(1)	122.6	O(10)···O(11)···N(4)	86.4
N(2)–N(3)···O(10)	112.2	C(7)–N(3)···O(10)	133.5

1.2.3 CRYSTAL STRUCTURE OF 2, 2'-Bipyridyl(2-formylpyridine thiosemicarbazonato)copper(II) Perchlorate

The numbering scheme used for the title complex (abbreviated as $[CuL(bipy)]ClO_4$) is given in the thermal ellipsoid diagram, Figure 1.2.3. Bond length and bond angle data are given in Tables 1.2.2 and 1.2.3 respectively.

The complex $[CuL(bipy)]ClO_4$ crystallises as a discrete monomer; it has the ligand L^- in the deprotonated form and is five coordinate. In this ternary structure, the 2-formylpyridine thiosemicarbazonato ligand coordinates in the plane as previously found, via S, N(1) of the pyridine and the imine nitrogen, N(2). The bipy coordinates via the two nitrogens with N(12) completing the in-plane coordination. The donor N(11) occupies a distorted apical position. There is no sixth approach to the copper within 4.0 Å. No unusual features in either the bond lengths or bond angles for the ligand, L^- [64], the bipy [136-139] or the perchlorate ion are observed.

The stereochemistry of the copper(II) atom is intermediate between square-pyramidal (spy) and trigonal-bipyramidal (tbp) geometry. In Figure 1.2.4 the copper coordination environment is depicted for (a) tbp and (b) spy geometries. For convenience, the distortions from tbp geometry will be discussed first as the angles in this case are more easily defined. In an idealised tbp structure the axial ligands make an angle of 180° to each other and 90° to the three in-plane donor atoms. The three equatorial donor atoms are then at an angle of 120° to each other.

In the structure of $[CuL(bipy)]ClO_4$ the 'axial' donor atoms N(2) and N(12) subtend an angle at the copper atom of 175.0(2)°, approaching the theoretical value of 180°. The angles between the two 'axial' donor atoms and the three 'equatorial' donors, comprised of S, N(1) and N(11),

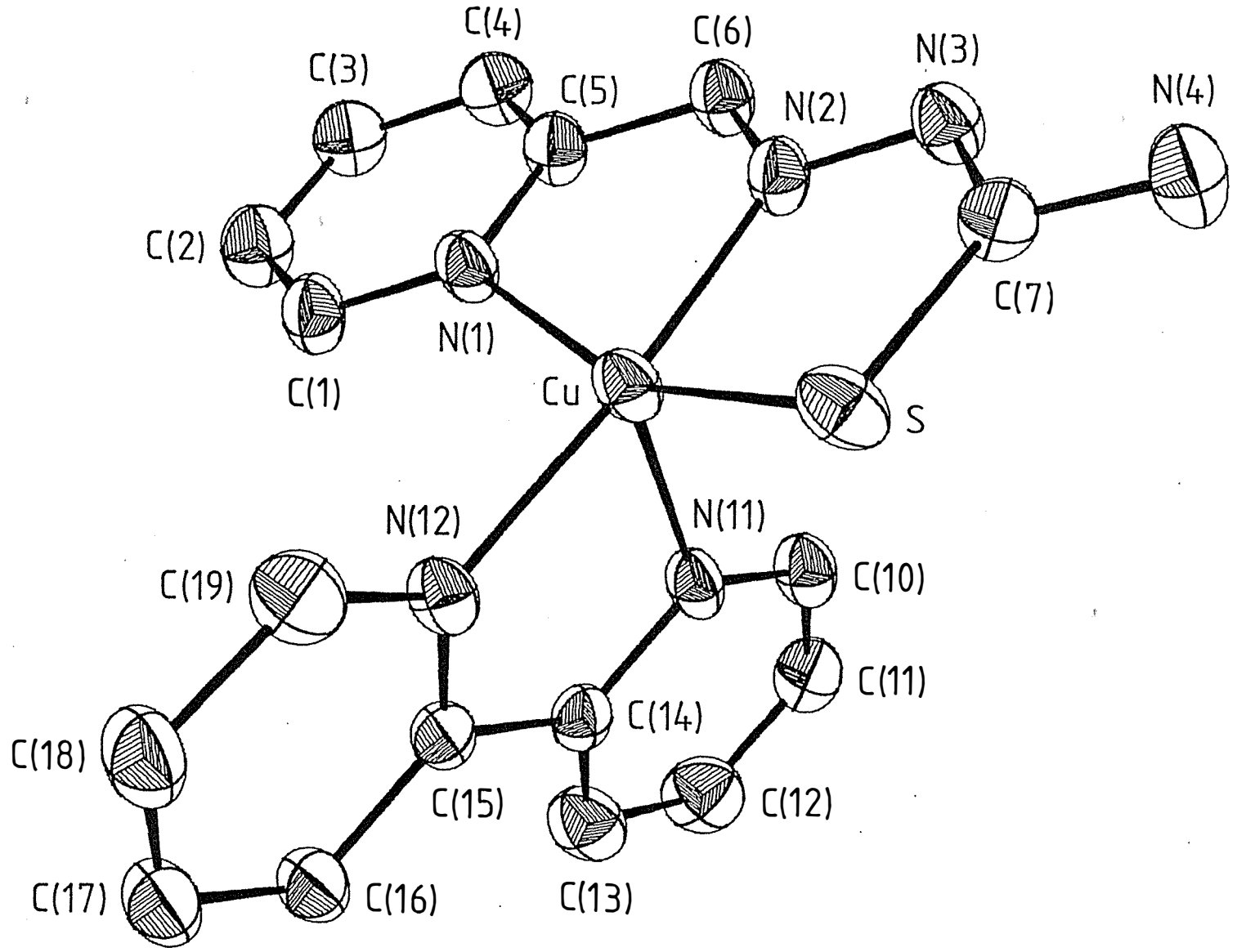

Figure 1.2.3: The monomeric cation for $[CuL(bipy)]ClO_4$ showing the atom numbering scheme. The non-coordinated ClO_4^- anion and hydrogen atoms have been omitted for clarity.

range from 78.3(1)° for N(11)-Cu-N(12) to 104.0(2)° for N(11)-Cu-N(2). The three 'equatorial' angles of N(1)-Cu-S, 157.0(1)°; N(11)-Cu-S, 109.6(1)° and N(11)-Cu-N(1), 90.7(2)° show the most marked difference from their ideal value of 120°.

The stereochemistry of square-pyramidal copper(II) complexes usually involves four basal donor atoms coordinated to the copper centre. The copper does not lie in the basal plane but is usually displaced towards a more weakly coordinated apical ligand. The angles from the apical ligand to the four basal donors are then greater than 90° (often within the range 95-100°). The angles between the four basal atoms may also be reduced from 90° and 180°, typically being within the ranges of 80-85° and 160-170° respectively; the former occur particularly when ligand constraints are imposed.

Figure 1.2.4(b) depicts the 'spy' geometry for the title complex. The 'apical' donor, N(11), a bipy nitrogen, is more weakly coordinated compared with the 'basal' bipy nitrogen, N(12) (2.180(4) and 1.987(4) Å respectively). The angles N(11) makes to the 'basal' donors are rather distorted from the expected values and range from 78.3(1)° for N(11)-Cu-N(12) to 109.6(1)° for N(11)-Cu-S. The two angles for the *trans* basal donors, N(12)–Cu-N(2) and N(1)-Cu-S, are 175.0(2) and 157.0(1)° respectively; the former being greater and the latter lesser than the expected range of 160-170°. The four angles between adjacent basal donor atoms range from 84.0(1)° for N(2)-Cu-S to 99.5(1)° for N(12)-Cu-S with an average value of 89.6° and are more indicative of a spy stereochemistry.

One of the reasons for the deviations observed from the idealised stereochemistries is the restricted bite angles imposed by both the ligand, L^-, and the bipy moiety.

In all complexes involving LH and L^- with copper, the bite angles around copper from the tridentate ligand, namely N(1)-Cu-N(2) and N(2)-Cu-S, and the required degree of planarity from the π-delocalised ligand system, limit these angles to within a small range (80.2-81.2° and

TABLE 1.2.6
Hydrogen-Bonding Distances (Å) and Angles (°) for [CuL(bipy)]ClO_4

Atoms[a]	Distance (Å)	Symm[b]	T_x, T_y, T_z
N(4)···N(3)	3.082	2	1 1 2
N(4)···O(3)	3.208	1	0 0 0

a the first atom is at symmetry position 1

b symmetry positions
1 (x, y, z)
2 (,$\bar{x}$ $\bar{y}$, $\bar{z}$)

Atoms	Angle (°)	Atoms	Angle (°)
C(7)–N(4)···N(3)	116.9	C(7)–N(4)···O(3)	123.2
C(7)–N(3)···N(4)	125.5	N(2)–N(3)···N(4)	122.4

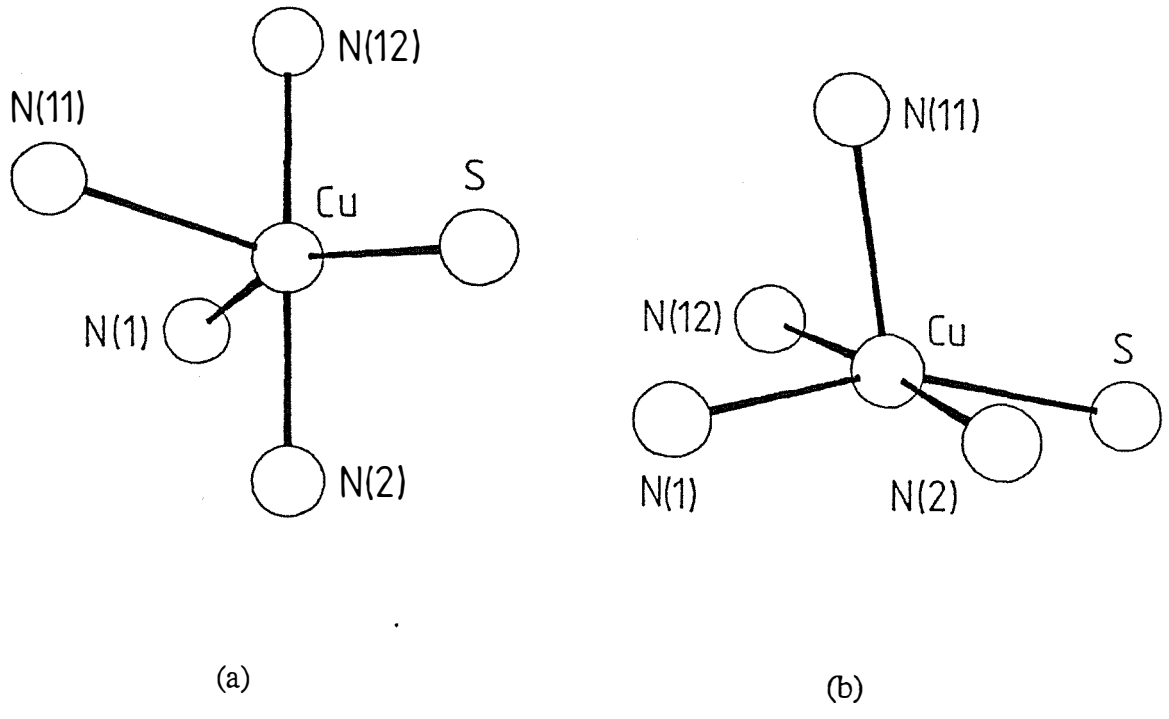

Figure 1.2.4: The copper coordination environment for [CuL(bipy)]ClO_4 viewed from (a) trigonal-bipyramidal and (b) square-pyramidal geometries.

82.6-85.4° respectively; [64,this work]. The bite angle of 78.3(1)° for the bipy about the copper atom is very limited in its flexibility and may be considered normal when compared with the average value of 77° cited in the literature for this moiety [136-138].

A comparison between the more 'regular' spy geometry observed in the previously discussed complex $[CuL(sacc)H_2O]\cdot\frac{1}{2}H_2O$ and the title complex $[CuL(bipy)]ClO_4$ may help to clarify the distortions from spy to tby in the latter. The most obvious and the biggest difference between the sacc and bipy complexes is the angle between the 'apical' donor atom and the fourth (non-ligand) in-plane donor atom. In $[CuL(bipy)]ClO_4$ this is the restricted bipy bite angle, N(11)-Cu-N(12), of 78.3(1)° whereas in $[CuL(sacc)H_2O]\cdot\frac{1}{2}H_2O$ the equivalent angle is between the coordinated sacc nitrogen, N(11), and the complexed water molecule, O(10), which subtends an angle of 94.7(3)° at the copper atom. This significant difference may be the overriding force which governs the eventual stereochemistry of the bipy complex.

The N(2)-Cu-N(12) angle of 175.0(2)° in the bipy complex has widened significantly towards 180° as expected for a tbp stereochemistry compared with the equivalent bond angle of 168.9(3)° for sacc. The three angles S-Cu-N(11) (109.6(1)°), S-Cu-N(1) (157.0(1)°) and N(1)-Cu-N(11) (90.7(2)°) have all shifted towards the tbp equatorial angle of 120° compared with the equivalent sacc angles (101.8(2)°, 162.3(2)° and 87.0(3)°). The change in the S-Cu-N(1) angle of 5.3° is unexpected since this angle is constrained within the tridentate ligand.

In $[CuL(sacc)H_2O]\cdot\frac{1}{2}H_2O$ the copper atom lies out of the plane of the four donor atoms by 0.176 Å with the biggest deviation from the plane being shown by N(2) (0.017 Å - see previous discussion). Calculation of the plane of best-fit* through the four donor atoms S, N(1), N(2) and N(12) for [CuL(bipy)]ClO shows the copper to lie out of the plane by 0.187 Å, only 0.011 Å more than in the sacc structure (a distance which is not significant). However,

* Plane (i) S, N(1), N(2), N(12)
0.4086X + 0.8592Y – 0.3079Z + 2.0058 = 0
[S -0.122, N(1) -0.145, N(2) 0.154, N(12) 0.113, Cu 0.187]
Distances of atoms from the plane (Å) are given in square brackets.

the four donor atoms in the bipy complex are far from being planar. The biggest deviation from the plane for $[CuL(bipy)]ClO_4$ is for N(2) which at 0.154 Å is nine times as large as that found in $[CuL(sacc)H_2O]\cdot\frac{1}{2}H_2O$ (chi-squared values calculated for these planes being 11352 and 41 respectively). This suggests that the sacc complex involves a more regular square-base pyramidal stereochemistry than the title complex. A similar effect can be found elsewhere in other complexes [138].

The difference in the coordinated bipyridyl bond lengths (Cu-N(12) 1.987(4), Cu-N(11) 2.180(4) Å) has been observed in several other cases where chelation between an equatorial and an axial position occurs (mean equatorial value 2.034 Å, mean axial value 2.179 Å [136-138]). The two pyridine rings of the bipyridyl are approximately planar with the biggest deviation from their respective planes being only -0.015 Å* . The two rings are inclined at an angle of 4.8° to one another via a twist in the C(14)-C(15) bond. This observation is in agreement with previously observed values [136-138]. The bipyridyl chelate as a whole§, makes an angle of 73.1° to the plane of best-fit through the ligand L^-, which is in accord with the value found for the saccharinato anion (71.9°) with this ligand. This figure is a little reduced from the value found for the complex, bis(2-aminoethyl)amine(2,2′-bipyridyl)copper(II) nitrate [137] in which a comparable angle of 83.7° has been observed. Physical and electronic differences in the equatorial ligand and packing forces may account for this.

A comparison of the distances of atoms from the planes of best-fit for the 2-formylpyridine

---

* Plane (ii) N(11), C(10), C(11), C(12), C(13), C(14)
0.7132X – 0.2486Y – 0.6554Z + 7.2577 = 0
[N(11) -0.014, C(10) 0.002, C(11) 0.012, C(12) -0.015, C(13) 0.004, C(14) 0.011]

* Plane (iii) N(12), C(15), C(16), C(17), C(18), C(19)
0.7590X – 0.2758Y – 0.5898Z + 6.9265 = 0
[N(12) 0.006, C(15) -0.004, C(16) -0.001, C(17) 0.004, C(18) -0.002, C(19) -0.003]

§ Plane (iv) N(11), N(12), C(10) C(11), C(12), C(13), C(14), C(15), C(16), C(17), C(18), C(19)
0.7378X – 0.2613Y – 0.6224Z + 7.0681 = 0
[N(11) 0.024, N(12) -0.047, C(10) 0.059, C(11) 0.033, C(12) -0.052, C(13) -0.055, C(14) -0.010, C(15) -0.013, C(16) 0.045, C(17) 0.057, C(18) 0.007, C(19) -0.046]
Distances of atoms from plane (Å) are given in square brackets.

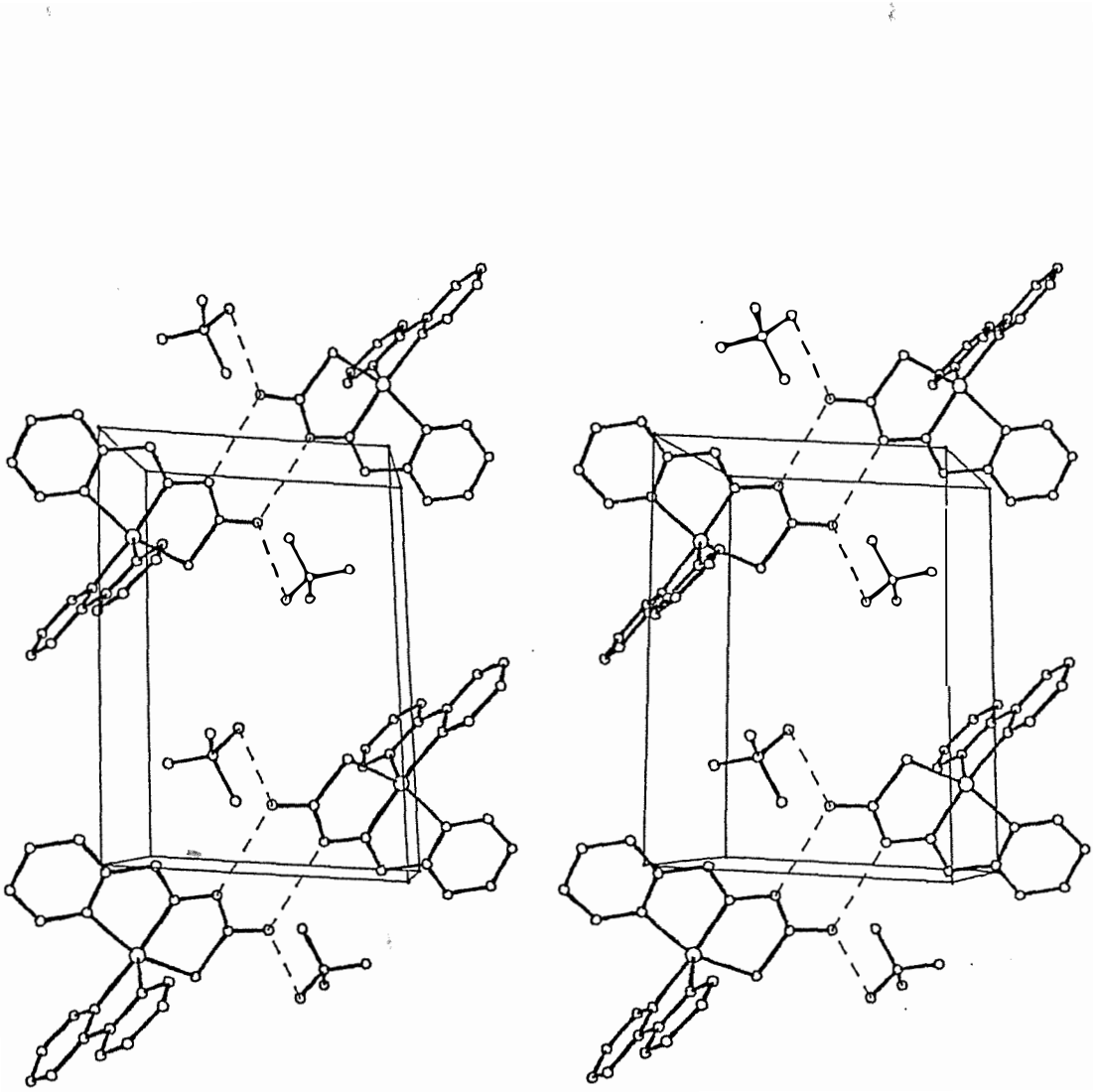

Figure 1.2.5: Stereo-view of the unit-cell packing diagram for [CuL(bipy)]ClO_4 showing the hydrogen-bonding scheme.

thiosemicarbazonato ligand (L^-) in $[CuL(bipy)]ClO_4$ and $[CuL(sacc)H_2O]\cdot\frac{1}{2}H_2O$ shows that in the former complex the ligand is relatively less planar (chi-squared values of 3472 and 490 respectively). This effect may result from the previously discussed distortion of the complex towards a trigonal bipyramidal geometry.

The hydrogen-bonding scheme for the title complex is depicted in the stereo-view of the unit-cell, Figure 1.2.5, with hydrogen-bonding distances and angles listed in Table 1.2.6. The terminal amino group of the ligand, N(4), forms two contacts. One is to N(3) (3.082(Å)) of an adjacent molecule, whereas the other may be considered a weak contact to O(3) (3.208(Å)), a perchlorate oxygen. No other contacts of any significance appear to be present.

1.2.4 RESULTS AND DISCUSSION

1.2.4(a) Electronic Spectra

Analytical and magnetic moment data are presented in Table 1.2.1 whereas the electronic absorption maxima and molar conductance data are given in Table 1.2.7.

The d-d absorption maxima in Table 1.2.7 give a good indication of the copper(II) geometry in the complexes. The crystal structure of the monomer $[CuL(sacc)H_2O]\cdot\frac{1}{2}H_2O$ shows the copper to have a distorted square-pyramidal geometry, very similar to those found in the dimeric $[CuL(CH_3COO)]_2$, $[Cu(LH)(SO_4)]_2$ [64] and $[Cu(LH)(CF_3COO)]_2(CF_3COO)_2$ [this work] species. The electronic spectra for these complexes all have a single resolved d-d transition at ~610 nm therefore the ternary complexes presented in this chapter, except those of bipy and phen, are assigned a distorted square-pyramidal (or possibly tetragonal) stereochemistry.

The ternary complexes containing the bidentate bipy and phen moieties exhibit two d-d maxima in the solid state at ~650 and ~880 nm. The crystal structure of $[CuL(bipy)]ClO_4$ shows the copper(II) to be in an environment intermediate between square-pyramidal (spy) and trigonal-bipyramidal (tby) stereochemistries. A brief review of copper(II) electronic spectra by Taylor and Coleman [109] reveals absorption bands in the range 800 - 1 000 nm have previously been assigned to tby stereochemistries. From the crystallographic evidence for a distorted tby structure and the occurrence of d-d bands in the range 850-937 nm, distorted trigonal-bipyramidal stereochemistries are assigned by analogy to the solid state structures of the four bipy and phen complexes.

Where two nitrogens are assumed to coordinate to the copper, as in $[CuL(dmap)_2]PF_6$ (dmap is

TABLE 1.2.7

Absorption Maxima and Conductance Data for Chapter 2

Complex[a]	Absorption Maxima (nm)[b] Charge Transfer	d-d	Molar Conductance[c] (s mol^{-1} l)	Solvent[d]
$[CuL(pftp)]_2 \cdot 4H_2O$	440 (br)	659 (br)		m.t.
	418 (12 500)	(sh)	14	dmso
	420	700 (sh)		EtOH
$[CuL(pctp)]_2$	426	(sh)		m.t.
	412 (12 100)	(sh)	9	dmso
	395 420 (sh)	710 (sh)		acetone
$[CuL(ntp)]_2 \cdot 6H_2O$	426 (sh)	(sh)		m.t.
	417 (15 300)	(sh)	6	dmso
	407	(sh)		EtOH
$[Cu(mpH)_2]$	420 (sh)	(sh)		m.t.
	382 (34 100)	600 (240; br)	0	dmso
	380			EtOH
$[CuL(mbt)] \cdot \frac{1}{2}H_2O$	420	(sh)		m.t.
	414 (11 800)	619 (200)	8	dmso
	409	(sh)		EtOH
$[CuL(mmiH)_2]PF_6 \cdot H_2O$	410 (sh)	680 (br)		m.t.
	415 (20 800)	(sh)	23	dmso
	410 (15 400)	(sh)	67	CH_3NO_2
$[CuL(miH)_2]PF_6 \cdot \frac{1}{2}H_2O$	420	680 (br)		m.t.
	416 (20 100)	570 (600;sh)	24	dmso
	410	570 (730;sh)		CH_3NO_2
$[CuL(mi)] \cdot 2H_2O \cdot EtOH$	420	(sh)		m.t.
	415 (13 600)	600 (270; br)	3	dmso
	410	570 (sh)		CH_3NO_2
[CuL(mtt)]	423	635 (br)		m.t.
	411	600 (sh)		dmso
	414			CH_3NO_2
$[CuL(bipy)]ClO_4$	415	650 860 (br)		m.t.
	414 (8 200)	634 (190)	21	dmso
	407 (10 700)	639 (220) 880 (70;sh)	65	CH_3NO_2
$[CuL(bipy)]PF_6$	419	647 850 (sh)		m.t.
	415 (9350)	625 (210; br)	19	dmso
	417 (16 100)	600 (150; br) 850 (sh)	145	acetone
$[CuL(bipy)]_2SO_4 \cdot 8H_2O$[e]	415	670(br) 890 (br)		m.t.
	414 (14 250)	632 (200; br)	33	dmso
	410 (10 050; sh)	644 (205) 900 (70; sh; br)		H_2O
$[CuL(phen)]PF_6$	397	590 (sh) 937		m.t.
	415 (10 800)	(sh) (sh)	30	dmso
	415 (11 700)	(sh) (sh)	153	acetone
$[CuL(dmap)_2]PF_6$	400 (sh)	635 (br)		m.t.
	415 (12 100)	590 (200; br)	22	dmso
$[CuL(sacc)H_2O] \cdot \frac{1}{2}H_2O$	413	609 (br)		m.t.
	414 (15 800)	633 (190)	23	dmso
	384 (br)	630		H_2O

a see page x for abbreviations
b extinction coefficients given in parentheses (l mol^{-1} cm^{-1})
c for typical molar conductance ranges see Appendix 3
d m.t. = mull transmittance
e extinction coefficients and molar conductance values quoted per Cu(II) ion

N, N-dimethylaminopyridine), but no longer have a constrained 'bite angle' due to both N's being in the one bipy or phen moiety, spectra consistent with a square-pyramidal copper(II) geometry result.

The thiolato complexes, $[CuLSR]_2$ where SR is $pftp^-$, $pctp^-$ and ntp^- and $[CuL(mp)_2]$ are all brown, and exhibit a broad electronic absorption band in the range 420 - 440 nm. The presence of two thiolato groups in these complexes results in two $S(\sigma) \rightarrow Cu$ charge transfer transitions which tend to overlap giving the one broad band that tails into the visible region of the spectrum, obscuring, in a number of cases, the d-d absorption maxima. However, for the complex $[CuL(pctp)]_2$ in acetone, the two maxima are sufficiently well separated to allow resolution. The main peak occurs at 395 nm with a weaker (~85%) shoulder at ~420 nm. In dmso however, only a broad peak is observed which has moved to slightly higher energy compared with the mull transmittance position. This is the general trend observed for all complexes in Section 2 when in donor solvents such as dmso.

A number of the complexes in Table 1.2.1 have the possibility that the fourth in-plane position could be occupied by either a nitrogen or a sulphur donor atom. This possibility arises for the adducts containing mbt^- (2-mercaptobenzothiazolate), mmiH (2-mercapto-1-methylimidazole), miH and mi^- (2-mercaptoimidazole and its anion respectively), and mtt^- (4-methyl4H-1,2,4-triazole-3-thiolate). These complexes are all green and have charge transfer peaks that are not so broad, indicating that the nitrogen is most likely coordinated in the solid state.

The molar conductance data presented in Table 1.2.7 show that in some cases, the dmso solutions have values up to 33 s mol^{-1} l, indicating partial dissociation of the anion. A number of the Lewis-base adducts have conductance values in non-dmso solvents consistent with 1-1 electrolytes. In these cases it is assumed the adducts remain intact in solution with only the non-coordinated counter-ion dissociating.

1.2.4(b) Infrared Spectra

The ir spectra for this chapter generally proved too complicated to assign with any degree of certainty. Their main use was in the identification of hydrated adducts through the broadening seen in the 3 500 - 3 000 cm^{-1} region [107] and to confirm the presence of anions; e.g. PF_6^- has a very strong, broad band at ~850 cm^{-1} [140].

1.2.4(c) Magnetic Properties

The room temperature magnetic moments in Table 1.2.1 are all considered to be normal except for the complexes $[CuL(miH)_2]PF_6{\cdot}\frac{1}{2}H_2O$ and $[CuL(ntp)]_2{\cdot}6H_2O$ with values of 2.45 and 1.59 B.M. respectively. Consequently, the latter complex and the other two thiolato complexes ($[CuL(pftp)]_2$ and $[CuL(pctp)]_2$) were formulated as dimers. The higher than expected value of 2.45 B.M. for the prior complex is thought to arise from impurities as the analysis figures do not give a good fit.

1.2.4(d) Electron Spin Resonance Spectra

E.s.r. spectroscopy proved to be a very useful means of showing adduct formation, usually giving clear evidence of sulphur or nitrogen coordination as the case may be. The e.s.r. parameters for the complexes isolated in this chapter are presented in Table 1.2.8.

The replacement of 'hard' or class (a) donor atoms by 'soft' or class (b) donor atoms tends to shift both $g_{/\!/}$ and $A_{/\!/}$ to smaller values. This can be seen in the values of $g_{/\!/}$ and $A_{/\!/}$ for the three thiolato complexes $[CuLSR]_2$ (SR = $pftp^-$, $pctp^-$ and ntp^-) in Table 1.2.8. This is represented diagramatically in Figure 1.2.6 where the experimentally determined 'best-fit' lines through inorganic copper(II) donor sets are shown on a plot of $g_{/\!/}$ versus $10^4|A_{/\!/}|$ [141]. The effect of replacing the in-plane oxygen donor in $[CuL(CH_3COO)]_2$ (N_2OS) with sulphur, as in the cases

TABLE 1.2.8

E.s.r. Results for Selected Chapter 2 Complexes[a]

Complex	g_1	$g_\perp$	g_2	$g_{/\!/}$ (g_3)	$A_{/\!/}$ (A_3)[b]	G[c]	α^{2}[d]	Solvent
$[CuL(pftp)]_2 \cdot 4H_2O$		2.026		2.110 (sh)		4.2		powder
		2.043		2.151	175		0.69	dmf
	Species 1	2.049	Major	2.151	174		0.69	EtOH[e]
	Species 2		Minor	2.190	~184		0.76	
$[CuL(pctp)]_2$		2.028		2.121		4.3		powder
		2.051		2.150	171		0.69	dmf
		2.038		2.149	176		0.69	EtOH[e]
$[CuL(ntp)]_2 \cdot 6H_2O$			2.077[f]					powder
	Species 1	2.053	Equal	2.151	170		0.69	dmf
	Species 2		Equal	2.187	183		0.76	
		2.063		2.196	187		0.78	dmso
$[Cu(mpH)_2]$	2.057		2.082	2.134		1.9		powder
		2.035		2.187	192		0.76	dmso
$[CuL(mbt)] \cdot \frac{1}{2}H_2O$		2.029		2.159		5.5		powder
		2.049		2.178	188		0.76	dmf
	Species 1	2.051	Major	2.157	173		0.70	EtOH[e]
	Species 2		Minor	2.187	182		0.75	
$[CuL(mmiH)_2]PF_6 \cdot H_2O$			2.078[f]					powder
	Species 1	2.054	Minor	2.154	179		0.71	H_2O[e]
	Species 2		Major	2.195	177		0.75	
$[CuL(mtt)]$		2.035		2.192		5.5		powder
	1.982		2.061	2.194				dmso
		2.055		2.176	185		0.75	dmf
$[CuL(bipy)]ClO_4$	2.026		2.068	2.168		3.6		powder
$[CuL(bipy)]PF_6$	2.032		2.058	2.177		3.9		powder
		2.061		2.181	181		0.75	dmso
$[CuL(phen)]PF_6$	2.013		2.089	2.179		3.5		powder
$[CuL(dmap)_2]PF_6$	2.063	2.195			173		0.74	H_2O[e]
$[CuL(sacc)H_2O] \cdot \frac{1}{2}H_2O$	2.048	2.190(sh)				4.0		powder

a via simple first-order spectral analysis
b h.f. coupling constants in 10^{-4} cm^{-1}
c $G = (g_{/\!/} - 2)/(g_\perp - 2)$
d $\alpha^2 = (A_{/\!/}/0.036) + (g_{/\!/} - 2) + 3/7(g_\perp - 2) + 0.04$ where α^2 gives an indication of the covalent nature of the bonding, the trend being the smaller the value of α^2 the greater the covalent nature of the bond [142]
e containing 10% dmso
f g_{iso} value

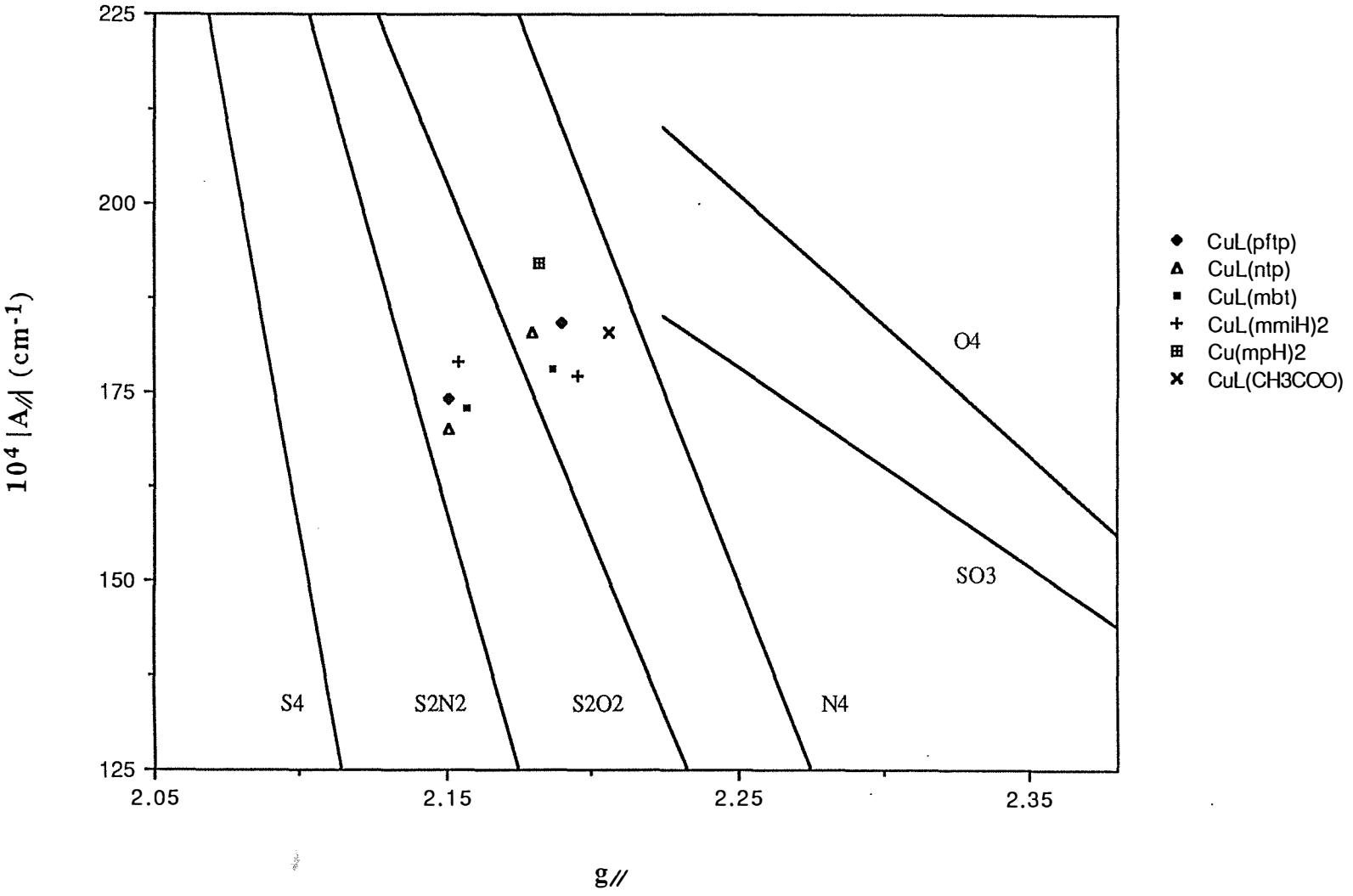

Figure 1.2.6: Plot of $10^4 |A_{//}|$ (cm^{-1}) vs. $g_{//}$ for various in-plane donor atom sets (after [141]). Selected solution species have been plotted (see the legend).

of $[CuLSR]_2$ (N_2S_2) shows the expected shifts to lower $g_{//}$ and $A_{//}$ values, indicating that in solution he thiolate remains coordinated in the plane. The spectrum of $[CuL(pftp)]_2$ in ethanol shows two species. The major one corresponds to the thiolate being coordinated whereas the minor is assumed to result from a species where the thiolate is dissociated and the solvent coordinates. A similar result is obtained for the complex $[CuL(ntp)]_2$ in dmf but two equally intense species are observed (see Table 1.2.8 and Figure 1.2.6). Similar phenomena are not seen in dmso in accordance with their non-electrolytic behaviour in this solvent.

For $[CuL(pftp)]_2$ and $[CuL(pctp)]_2$ in the solid state, typical axial type spectra were obtained (see Figure 1.2.7(c)) whereas for $[CuL(ntp)]_2$ the spectrum was isotropic.

Several of the complexes where the fourth donor atom in the plane could be either S or N (CuL(mbt), $CuL(mmiH)_2PF_6$ and CuL(mtt)) have powder, e.s.r. parameters which lie between the N_2S_2 and N_3S values for the other complexes in the table, so no definite assignment is possible from the solid state e.s.r. spectra alone. The solution spectra for two of these, (CuL(mbt) and $CuL(mmiH)_2PF_6$), have two species, one of which lies with the N_2S_2 donor sets on Figure 1.2.6. The other, from a consideration of the non-electrolytic behaviour of the compounds and the similarity of their e.s.r. spectral parameters to the nitrogen-donor complexes in Table 1.2.8, most likely results from the ternary component coordinating through its nitrogen. In solution therefore, there appears to be some sulphur adduct formation, although as discussed for the electronic spectra, this does not seem to be so in the solid state. The preference for the 'hard' N over the 'soft' S in the solid state may be a reflection upon the presence of the more polarising Cu(II) in these complexes (c.f. Cu(I)). In solution it is possible an equilibrium exists between the two coordination modes.

The powder e.s.r spectra for the bipy and phen complexes show rhombic character (see Figure 1.2.7 (d)) which is in agreement with the crystal structure of $[CuL(bipy)]ClO_4$ where the

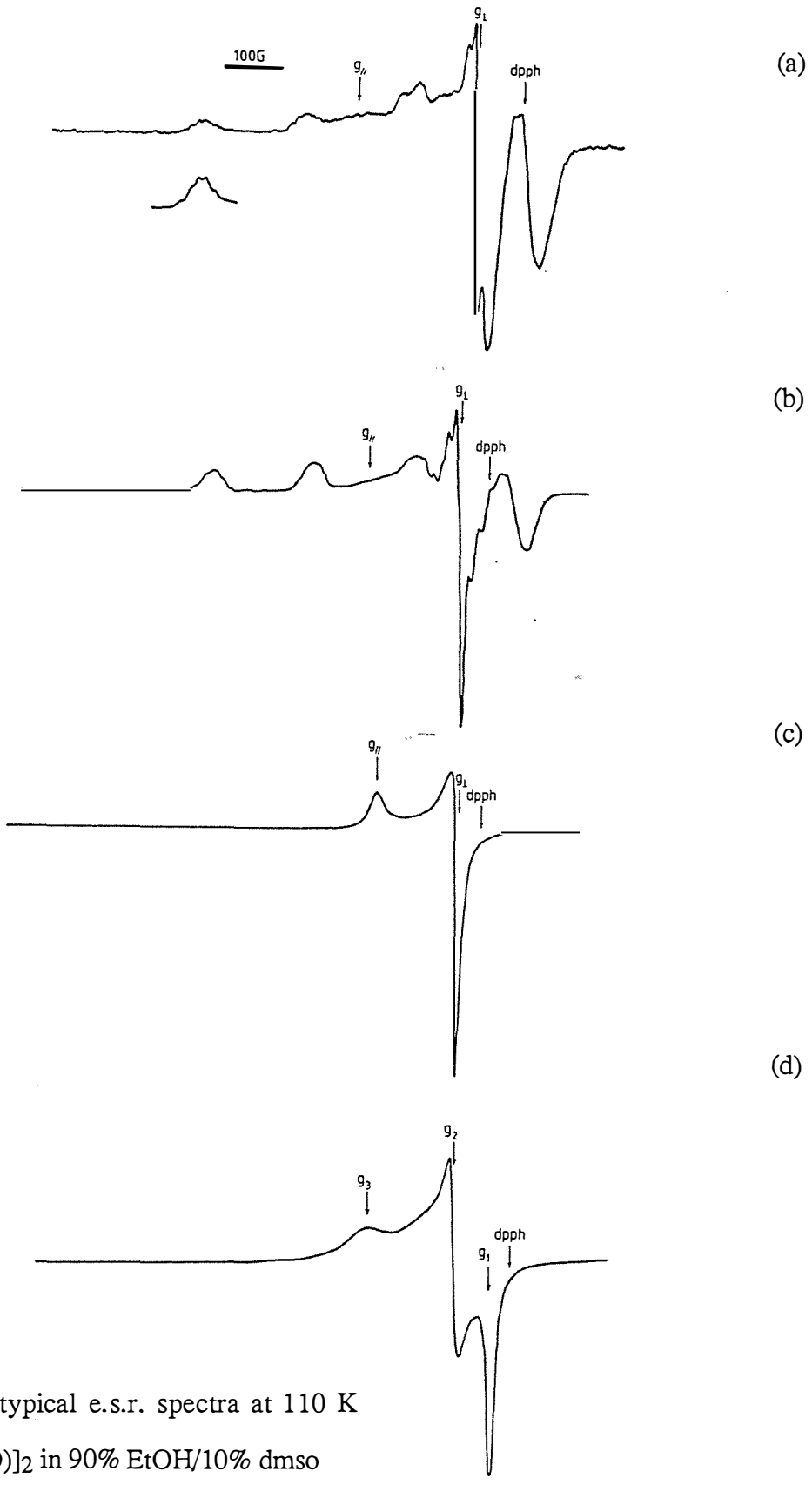

Figure 1.2.7: Some typical e.s.r. spectra at 110 K

(a) $[CuL(CH_3COO)]_2$ in 90% EtOH/10% dmso

(b) $[CuL(pctp)]_2$ in 90% EtOH/10% dmso

(c) $[CuL(pctp)]_2$ powder

(d) $[CuL(bipy)]ClO_4$ powder.

copper centre is in a geometry intermediate between square-pyramidal and trigonal-bipyramidal [this work].

The crystal structure of $[CuL(sacc)H_2O]\cdot\frac{1}{2}H_2O$ shows the copper environment to be essentially square-pyramidal, and this is displayed by the powder spectrum with $g_{/\!/}$ and $g_{\perp}$ being resolved without broadening in the $g_{\perp}$ region.

The only complex in Table 1.2.6 which does not have the ligand LH coordinated is $[Cu(mpH)_2]$. The powder spectrum was considerably broadened in the $g_{\perp}$ region (relative to the previously observed axial spectra) and was accordingly assigned as rhombic. The dmso solution spectrum displayed in Figure 1.2.8 however gave an axial spectrum with splitting on all the copper hyperfine lines and sharp splitting in the $g_{\perp}$ region. When $g_{/\!/}$ and $A_{/\!/}$ are plotted on Figure 1.2.6, a value consistent with an S_2O_2 donor set is obtained, indicating the nitrogen is not involved in bonding and that either one of the coordinated phenol or thiophenol is still protonated (unless the proton has shifted to the pyridine N).

The solution spectrum for copper(II) + 2-mercapto-3-pyridinol (Cu(II):mpH_2, 1:2) in ethanol has been reported by Ainscough *et al.* [141] but the complex $Cu(mpH)_2$ does not appear to have previously been isolated. In their spectrum, splitting of the M_I= 3/2 and ½ lines into three and two parts respectively was observed. By analogy [143] this was attributed to the two isotopes of copper, ^{63}Cu and ^{65}Cu, splitting the peak in two, with further splitting resulting from solvation of some of the molecules in the axial position. Nitrogen donor systems do not show this coupling from the two isotopes as a result of superhyperfine coupling interactions [144] which may explain why it occurs here for an S_2O_2 donor set and is not seen elsewhere in this work.

The dmso spectrum for $[Cu(mpH)_2]$ given in Figure 1.2.8 (this work) shows three definitely resolved components on the M_I = 3/2 hyperfine line with a shoulder on the low-field side of the

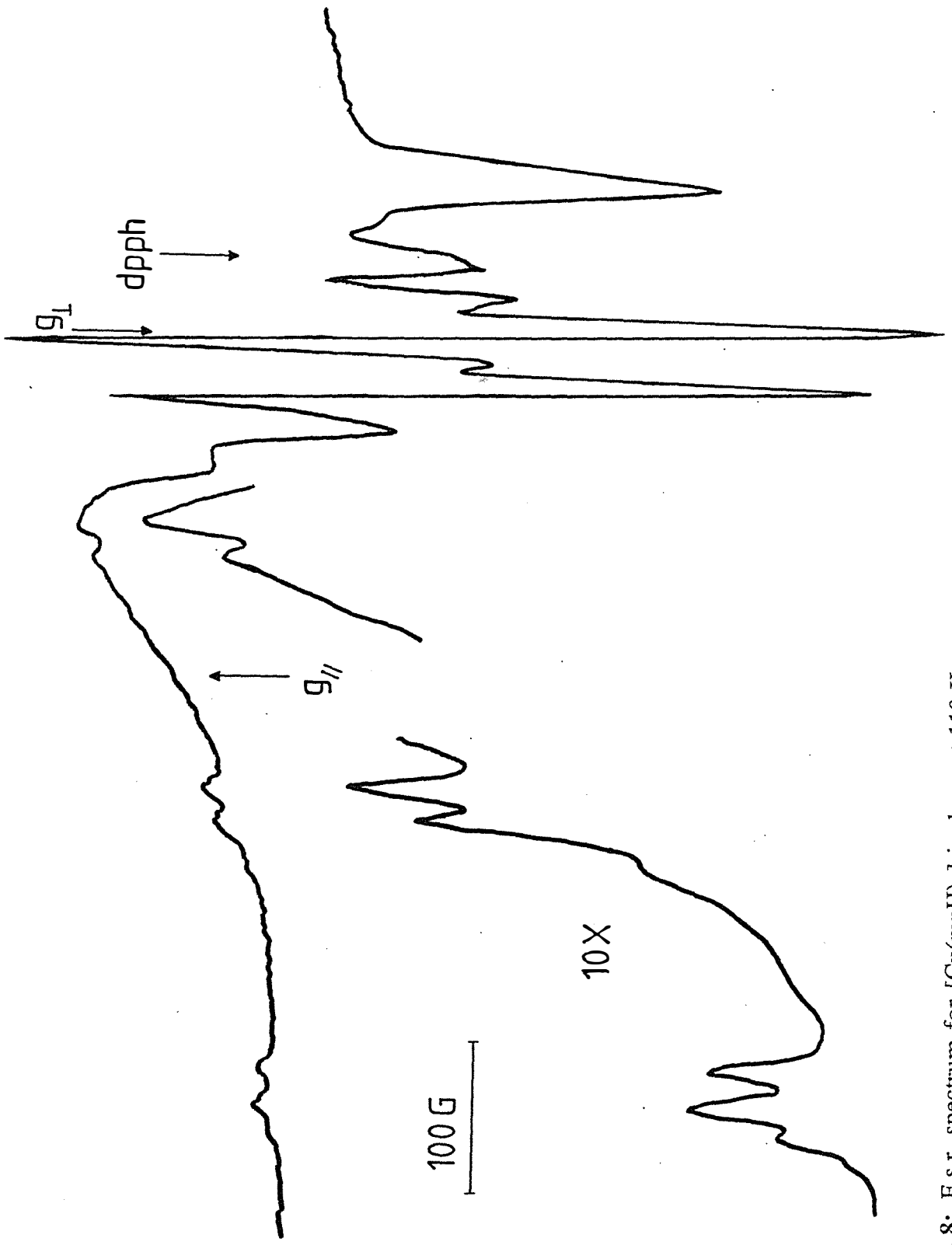

Figure 1.2.8: E.s.r. spectrum for $[Cu(mpH)_2]$ in dmso at 110 K.

peak and two resolved components on the M_I = ½ hyperfine line again with a low-field shoulder. Splitting on the M_I = -½ and -3/2 hyperfine lines is also seen but not resolved well. Raymond *et al.* [145] observed similar e.s.r. spectra for several copper(II) hydroxamate complexes in different solvents. They concluded that solvation of some of the molecules in the axial position was an unlikely source of any splitting. Instead it was proposed that significant quantities of two geometric isomers was a more plausible explanation. In combination with the isotopic coupling this may result in a maximum of four components on each copper(II) hyperfine line. The occurrence of a similar splitting pattern for the $[Cu(mpH)_2]$ spectrum from this work and ref. [141], which were run in different solvents, adds credence to Raymond's proposal. Another possibility however, which has not been discounted, is coupling of a ligand proton (I = ½) to the copper. This would have a similar effect as two geometrical isomers. By using isotopically pure copper, running the spectrum in a variety of solvents and/or using a deuterated ligand the sources of the observed splitting may be resolved.

1.2.4(e) E.s.r. spectra of CuL^+ with Blood Components

The interaction of CuL^+ with red cell components [87], Ehrlich cells [9] and cat and normal human haemoglobins (Hb) [86] have been studied previously. One of the first interactions of CuL^+ in the body is with blood components which results in extensive haemolysis [87]. It was found that the drug was readily taken up by red cells with a rapid accumulation and slow efflux and initially was bound to glutathione and haemoglobin. Glutathione was depleted within 5 hours, presumably by oxidation mediated by CuL^+ and O_2 with the concomittant generation of toxic oxygen species. It was suggested that in spite of these toxic oxygen species and the ability of CuL^+ to inhibit thiol enzymes, the cell exerted protective effects [87].

When CuL^+ was reacted with human Hb, only nitrogen donor atoms coordinated, whereas cat Hb showed spectra consistent with both sulphur and nitrogen donor atoms. The formation of a sulphur adduct with cat Hb, has been attributed to the presence of an 'extra' cysteine residue (cysteine-13α) not present in human Hb [86]. CuL^+ interacts with Hb without apparent

changes in the redox state of the hemes, in contrast to inorganic copper(II), and binds to, and interacts with, both cat and human Hb as indicated by its effect on the oxygen affinity of both proteins [86].

The interaction of CuL^+ with Ehrlich cells resulted in a new, e.s.r. detectable species which was consistent with a bound thiolato adduct. Unlike CuKTS, ($KTSH_2$ = kethoxal bis(thiosemicarbazone) see Figure 1.3), which is broken down completely and the ligand released from the cell, the CuL^+-thiolato appeared to be quite stable. There was a marked stimulation of oxygen utilisation, and at the same time, the thiol content of the cell decreased (as was found with CuKTS). These observations were considered to be consistent with the oxidation of thiols by oxygen, catalysed by the complex [71].

In the present study, the interaction of CuL^+ with human blood components (red cells and plasma) was re-examined using e.s.r. spectroscopy. The intention of this was to compare the blood adduct spectra with those of model thiolato and nitrogen base adducts of CuL^+in order to obtain reference spectra for comparison with other cupric-ligand-blood interactions as well as hopefully improving the resolution of the reported spectra.

The fresh, heparinised blood sample was centrifuged to separate the red cells from the plasma. The packed red cells were washed with, then suspended in, isotonic saline. To both the plasma and red cell samples was added CuL^+ in dmso/saline and these solutions were incubated at 37° C for ½ hour. The plasma sample was used as is, but the red cell suspension was centrifuged so spectra for both the red cells and supernatant could be recorded separately. This procedure was repeated using $CuCl_2$ as a reference with the spectra of CuL^+ in the saline being recorded also. A full procedure is given in the experimental section at the end of this chapter.

The results of the spectral analyses are given in Table 1.2.9 and are in agreement with those found by Antholine and Taketa [87]. Two equally intense species were displayed in the frozen

TABLE 1.2.9

E.s.r. Results for CuL^+ with Human Blood Components[a]

Sample		$g_\perp$	$g_\parallel$	$A_\parallel$[b]	α^2 [c]
Cu^{2+} and red cells		2.061	2.213	204	0.84
Cu^{2+} and red cells thawed then rerun		2.061	2.217	205	0.85
Cu^{2+} in red cell supernatant		2.057	2.210	211	0.86
Cu^{2+} and plasma	Major	2.055	2.187	204	0.82
	Minor	2.055	2.252	200	0.87
CuL^+ in saline solution		2.055	2.187	179	0.75
CuL^+ and red cells	Equal	2.051	2.142	176	0.69
	Equal	2.051	2.192	184	0.77
CuL^+ and red cells thawed then rerun	Minor	2.055	2.136	180	0.70
	Major	2.055	2.192	184	0.77
CuL^+ in red cell supernatant		2.054	2.187	186	0.77
CuL^+ and plasma	Minor	2.053	2.159	166	0.68
	Major	2.053	2.189	188	0.77

a via simple first-order spectral analysis

b h.f. coupling constants in 10^{-4} cm^{-1}

c $\alpha^2 = (A_\parallel/0.036) + (g_\parallel - 2) + 3/7\ (g_\perp - 2) + 0.04$

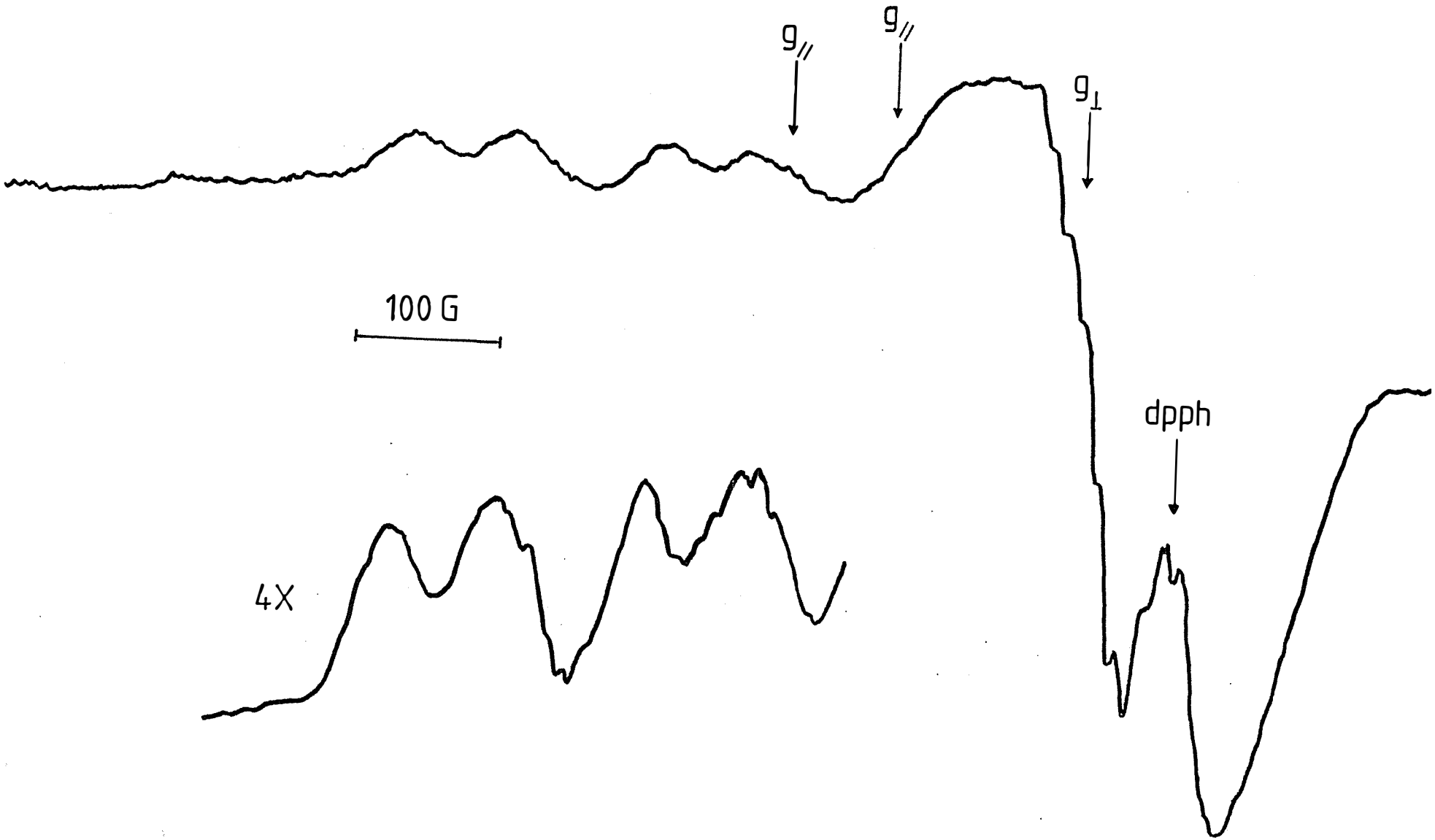

Figure 1.2.9: E.s.r. spectrum for $[CuL(CH_3COO)]_2$ in human red cells with 5% dmso at 110 K.

solution spectrum of CuL^+ with human red cells as seen in Figure 1.2.9. The resolution of this and other spectra appears to be better than that obtained by Antholine. The high-field species has $g_{//} = 2.142$ and $A_{//} = 176 \times 10^{-4}$ cm^{-1} whereas the other species displays values of $g_{//} = 2.192$ and $A_{//} = 184 \times 10^{-4}$ cm^{-1}. This decrease in both $g_{//}$ and $A_{//}$ is expected for the coordination of a 'softer' donor in the plane with the resultant smaller α^2 value and is consistent with a sulphur adduct. These parameters also agree well with the solution e.s.r. parameters of $[CuLSR]_2$ complexes presented in Table 1.2.8 and are close to the N_2S_2 line in Figure 1.2.6 (not shown).

The low-field adduct has parameters which may result from either an oxygen or a nitrogen donor but the multiple superhyperfine splitting observed in the $g_{\perp}$ region of Figure 1.2.9 and the difference between these values and those displayed by CuL^+ in saline favour a nitrogen adduct.

On thawing the now lysed red cells, exposing them to the air for some hours to allow oxidation of any cuprous species and then rerunning the spectrum at 110 K, the same two species are observed (but with the sulphur adduct now being a minor component). This results confirms the finding of Antholine [86] that the predominant species in the red cells is cupric and either its reduction is slow or its reoxidation fast.

The spectral parameters of CuL^+ in the red cell supernatant, the major species from CuL^+ in plasma and the down-field peak from CuL^+ in the red cells are all very similar and therefore are probably all nitrogen adducts. Antholine *et al.* suggested the CuL^+- nitrogen adduct from the red cell supernatant was from globin (of haemoglobin) due to a small extent (3%) of red cell haemolysis in his sample. The minor species present in the spectrum of CuL^+ with plasma is consistent with a sulphur adduct. As thiol containing enzymes and low molecular weight compounds are intracellular components, the source of this adduct is unclear but may result

from a small amount of glutathione released from cell lysis and stabilised by adduct formation with CuL^+.

Antholine *et al.* [58] recorded the e.s.r. spectrum of CuL^+ in human plasma and obtained very similar results as in the present study (minor species $g_{//} = 2.160$, $A_{//} = 170 \times 10^{-4}$ cm^{-1}; major species $g_{//} = 2.187$, $A_{//} = 184 \times 10^{-4}$ cm^{-1}). The major species observed was suggested to result from a histidine adduct as the parameters for CuL·Histidine are very similar ($g_{//} = 2.188$, $A_{//} = 183 \times 10^{-4}$ cm^{-1}).

In contrast to Antholine [87], an e.s.r. signal was detected for inorganic Cu(II) with red cells. For all species except the minor product of Cu^{2+} with plasma, the spectral parameters are approximately the same ($g_{//} = 2.207_{av}$; $A_{//} = 206 \times 10^{-4}$ cm^{-1}) as those found for Cu^{2+} and haemoglobin ($g_{//} = 2.207$; $A_{//} = 207 \times 10^{-4}$ cm^{-1} run at 77 K [146]) and accordingly may be assigned to a similar adduct. The minor product observed with Cu^{2+} and plasma has been attributed to cupric ion bound to the buffer [147].

Two further copper(II) complexes with different ligands were studied in an identical manner, the results of which will be presented in Chapter 4.

1.2.4(f) General Discussion

The ternary thiolato complexes [CuLSR] (where SR is $pftp^-$, $pctp^-$ and ntp^-) and the binary $[Cu(RSH)_2]$ (where RSH_2 is 2-mercapto-3-pyridinol (mpH_2)) are all prepared by the addition of the deprotonated thiolate to an aqueous solution of $[CuL(CH_3COO)]_2$. The formation of equatorially bound thiolato adducts is unexpected as this usually results in reduction of the copper(II) species and formation of the appropriate disulphide. Attempts to form stable Cu(II)-thiolato bonds, as models for the Type 1 blue proteins, have been limited to a few complexes containing tetradentate nitrogen macrocyclic ligands [148-152]. Besides using macrocycles which result in a more negative copper(II) redox potential to stabilise the Cu(II) state, reactions

are often carried out at low temperature under an inert atmosphere, using electron withdrawing substituents on aromatic thiophenols to give a more positive potential to the RSSR/RS^- couple. The formation of stable, thiolato adducts using a monoanionic tridentate ligand, with the reactions carried out at ambient temperature and open to the atmosphere, makes these complexes even more unusual. Unfortunately, attempts to grow crystals of these adducts were not successful.

However, when an excess of thiol is added to a cold solution of CuL^+, reduction does occur. Addition of 2 mole equivalents of ethanolic 4-nitrothiophenol (ntpH) to a dmso solution of $[CuL(CH_3COO)]_2$ immediately results in the green solution turning red. The red solution formed is mostly a Cu(I) species as there is only a weakly detectable e.s.r. signal with $g_{/\!/} = 2.155$, $g_\perp = 2.053$ and $A_{/\!/} = 174 \times 10^{-4}$ cm^{-1}. This has been assigned to an N_2S_2 thiolato adduct by comparison with species 1 in dmf for $[CuL(ntp)]_2 \cdot 6H_2O$ in Table 1.2.8.

When this red solution is left overnight, it air oxidises, turning green and a crystalline precipitate separates which was identified from its melting point as the disulphide of ntpH (found m.p. 176-9° C; lit. 182 C [153]. The e.s.r. parameters for the green solution are $g_{/\!/} = 2.188$, $g_\perp = 2.056$ and $A_{/\!/} = 183 \times 10^{-4}$ cm^{-1}, consistent with the second species observed in the e.s.r. spectrum of a dmf solution of $[CuL(ntp)]_2 \cdot 6H_2O$ (possibly being solvated CuL^+).

When the initial reaction mixture of 2:1 ntpH:CuL^+ is refluxed, an orange complex, identified as Cu(I)(ntp) is isolated (see Table 1.2.1 for analysis figures). The orange mother liquor is e.s.r. silent, indicating complete reduction of the copper(II), e.g.

$$Cu(II)L + 2(SR^-) \rightarrow Cu(I)(SR) + \tfrac{1}{2}(RSSR) + L^-$$

(where SR^- is ntp^-) and does not reoxidise to give a green Cu(II) solution as observed above.

Gingras *et al.* [47,154,155] found a similar reaction occurred when they added two mole equivalents of a range of bidentate thiosemicarbazones (e.g. benzaldehyde thiosemicarbazone) to copper(II). In this case however, the thiosemicarbazone is acting both as a chelating agent and as the thiolate e.g.

$$R\text{–}S^{-}(\text{excess}) + Cu(II) \rightarrow R\text{–}S\text{–}S\text{–}R + Cu(I)SR$$

(where R–S$^-$ is the deprotonated bidentate thiosemicarbazone). The product formed was generally the same whether Cu(I) or Cu(II) was taken, due to the prior reduction (as above) to give a Cu(I) species. Attempts to isolate stable Cu(I) complexes of the tridentate ligand LH in this work were only successful when an excess of reducing agent was present e.g. I$^-$ or SR$^-$ (see Chapter 1 discussion).

As discussed in Chapters 1 and 2, the CuL^+ species is stable in non-oxidising 4M mineral acids and when reacted with deactivating thiolates. Also, stable adducts of chelating agents have been prepared, even when excess of the chelate is added (see Table 1.2.1). However, when an attempt was made to isolate an adduct of 2-mercapto-3-pyridinol (mpH_2) from an aqueous solution of CuL^+ and mpH_2 (1:1), the product isolated was not CuL(mpH) as intended. Instead the ligand L$^-$ had been displaced and the complex $[Cu(mpH)_2]$ was isolated. This was unexpected as the binding constant of Cu^{2+} with LH has been measured to be 16.9 log units [57], (and from the above observations). Quantitative removal of the copper from an aqueous solution of CuL^+ has also been achieved by the addition of ethylenediaminetetraacetic acid (the edta binding constant for Cu^{2+} has been calculated as 18.8 log units [156]). Previous attempts by workers in this laboratory to prepare $[Cu(mpH)_2]$ from inorganic Cu(II) salts and mpH_2 had been unsuccessful.

Prior to this work, no Lewis-base adducts of CuL^+ had been isolated. Adducts formed by addition of ethylenediamine (en) and histidine (His) had been detected using e.s.r.

spectroscopy by Antholine *et al.* [85,128]. However, ternary complexes had been synthesised in other Cu(II)-thiosemicarbazone systems. Ablov *et al.* [157], using quinoline-8-aldehyde thiosemicarbazone (thqnH), a close analogue of LH, isolated the Lewis-base adduct complexes $Cu(thqn)(bipy)Cl{\cdot}2\frac{1}{2}H_2O$ and $Cu(thqn)(oxqn){\cdot}1\frac{1}{2}CH_3OH$ (where oxqn is the anionic oxime of quinoline-8-aldehyde). Another Russian group [33] prepared copper(II) complexes of salicylaldehyde S-methylthiosemicarbazone ($smtH_2$) which were formulated as $Cu(smtH)(py)NO_3{\cdot}\frac{1}{2}H_2O$, $Cu(smtH)(phen)NO_3$ and $Cu(smt)(NH_3)H_2O$. The latter compound reversibly binds the NH_3 and H_2O molecules, these being removed when heated at 120°C and reformed by adding NH_3/H_2O to Cu(smt).

The second proton which had been removed to form the neutral complex Cu(smt) appears to be from the terminal amine group ($-NH_2$), a reaction which has not been observed for CuL^+. The difference in the reactivities of the amine group undoubtedly arises from the thioether sulphur in $smtH_2$ not binding to the copper. Instead the $-NH_2$ group binds, and is polarised sufficiently to allow deprotonation to occur.

With the paucity of such adducts in the literature and the possibility of their importance for *in vivo* mechanisms, a range of Lewis-base ternary complexes were synthesised *in vitro*. The general formulation of these compounds is $[CuL(Lewis\text{-}base)]^+$ where the Lewis-bases used were bipy, phen, 2(dmap), 2(mmiH) and 2(miH). The complex formulated as $[CuL(bipy)]_2SO_4{\cdot}8H_2O$ is unusual as the source of the sulphate anion appears to have been from the hydrolysis of MoS_4^{2-}. Attempts to prepare the complex $[CuL(bipy)]_2MoS_4$ resulted in a green crystalline product which analysed as having no Mo (from a.a.) but displayed ir bands at 995 and 615 cm^{-1}, indicative of sulphate [107].

The complexes of the protonated mmiH and miH moieties were prepared by addition of three mole equivalents of the appropriate compound to CuL^+ in water, and precipitated upon the addition of a solution of PF_6^-. If however, base is added to one mole equivalent of the ternary component, the above moieties complex as anions, yielding neutral compounds which are

deposited from solution immediately. The ability to form ternary complexes with a moiety coordinating as either a neutral or anionic species warrants further investigation.

The formation of stable Lewis-base adducts with CuL^+ and their detection by e.s.r. spectroscopy in biological systems, shows such compounds may play an important role biologically.

1.2.4(g) Summary

The ability of CuL^+ to form unusually stable adducts with biologically relevant donor atoms has been demonstrated by the isolation *in vitro* of model thiolato and nitrogen-base complexes. The e.s.r. parameters of the species formed from the interaction of CuL^+ with human blood components are very similar to those of the model complexes. As the formation of such adducts appears to be the first step in the chain of biological activity for CuL^+, their importance can not be underestimated.

1.2.5 EXPERIMENTAL

1.2.5(a) Preparation of Complexes

$[CuLSR]_2$ (SR = $pftp^-$, $pctp^-$ or ntp^-)

A solution of $[CuL(CH_3COO)]_2$ (200 mg, 0.66 mmols) was boiled briefly in water (70 cm^3) then filtered. To this was added dropwise a solution of pentafluorothiophenol (pftpH) (0.075 cm^3, 0.56 mmols), pentachlorothiophenol (pctpH) (186 mg, 0.66 mmols) or 4-nitrothiophenol (ntpH) (111 mg, 0.72 mmols) in NaOH (7.5 cm^3, 0.1 N) and methanol (10 cm^3). The amorphous brown powders which separated, were filtered and washed successively with water and diethyl ether, then vacuum dried. Yields $[CuL(pftp)]_2 \cdot 4H_2O$ 177 mg (66%); $[CuL(pctp)]_2$ 193 mg (56%); $[CuL(ntp)]_2 \cdot 6H_2O$ 125 mg (42%).

[Cu(I)(ntp)]

To a filtered solution of $[CuL(CH_3COO)]_2$ (200 mg, 0.66 mmols) in dimethylsulphoxide (10 cm^3) was added a filtered ethanolic solution (20 cm^3) of 4-nitrothiophenol (204 mg, 1.31 mmols). The clear, deep red solution which resulted was refluxed under nitrogen for ½ hour during which time it had changed to orange with an orange precipitate (the title compound). This was filtered and washed with ethanol only then vacuum dried. Yield 36 mg (25%).

$[Cu(mpH)_2]$

Solid 2-mercapto-3-pyridinol (mpH_2) (86 mg, 0.68 mmols) was added slowly to a solution of $[CuL(CH_3COO)]_2$ (200 mg, 0.66 mmols) in water (60 cm^3) and methanol (230 cm^3). The fine, green powder which separated was filtered off and washed successively with water, ethanol and diethyl ether before being vacuum dried. Yield 93 mg (87%).

[CuLX] (X = mbt⁻ or mi⁻)

$[CuL(CH_3COO)]_2$ (302 mg, 1.00 mmols) was boiled in water (150 cm^3) briefly then filtered. To this solution was added a solution of 2-mercaptobenzothiazole (mbtH) (172 mg, 1.02 mmols) or 2-mercaptoimidazole (miH) (108 mg, 1.08 mmols) in ethanol (10 cm^3) which had sodium metal (30 mg, 1.30 mmols) dissolved in it. The green precipitates which formed were stirred and warmed in solution for 5 minutes then filtered and washed with water, ethanol and diethyl ether before being dried under vacuum. Yields: $[CuL(mbt)]\cdot\frac{1}{2}H_2O$ 222 mg (54%); $[CuL(mi)]\cdot 2H_2O\cdot EtOH$ 186 mg (44%). The analytical figures for the latter complex are not good (see Table 1.2.1) but it was included for completeness.

$[CuLX_2]PF_6$ (X = mmiH or miH)

To water (70 cm^3) was added $[CuL(CH_3COO)]_2$ (200 mg, 0.66 mmols) with warming. To this solution was added 2-mercapto-1-methylimidazole (mmiH) (239 mg, 2.09 mmols) or 2-mercaptoimidazole (miH) (200 mg, 2.00 mmols) slowly as the solid. The resulting clear, dark green solutions were warmed briefly and then had added to them NH_4PF_6 (114 mg, 0.70 mmols) in water (5 cm^3). The green precipitates were filtered off and washed with water then diethyl ether and vacuum dried. Yields $[CuL(mmiH)_2]PF_6\cdot H_2O$ 213 mg (51%); $[CuL(miH)_2]PF_6\cdot\frac{1}{2}H_2O$ 185 mg (47%). The latter compound, (as with the previous anionic complex $[CuL(mi)]\cdot 2H_2O\cdot EtOH$) does not have good analysis figures.

[CuL(mtt)]

The preceding procedure was repeated using solid 4-methyl4H–1,24-triazole-3-thiol (mttH) (260 mg, 2.26 mmols). However, a green precipitate formed immediately upon addition of the solid to the aqueous $[CuL(CH_3COO)]_2$ solution. This very fine powder was filtered and washed with water only. Yield 109 mg (45%).

[CuL(bipy)]ClO_4

To a solution of LH (250 mg, 1.39 mmols) in ethanol (40 cm^3) was added $Cu(ClO_4)\cdot 6H_2O$ (528 mg, 1.42 mmols) in water (10 cm^3). The dark green solution was heated and 2, 2′-bipyridyl (bipy) (240 mg, 1.54 mmols) in ethanol (5 cm^3) was stirred in. After 5 minutes the clear deep green solution was filtered. The next day dark green rod shaped crystals were removed and washed with a water/ethanol mix then dried under vacuum. Yield 539 mg (78%).

[CuL(X)]PF_6 (X = bipy or phen)

Either 2, 2′-bipyridyl (105 mg, 0.67 mmols) or 1, 10-phenathroline (phen) (133 mg, 0.67 mmols) was dissolved in boiling water (10 cm^3). This was added to a solution of $[CuL(CH_3COO)]_2$ (200 mg, 0.66 mmols) in water (40 cm^3) and refluxed for 2 hours. The resulting deep green solution was filtered while hot and had added to it NH_4PF_6 (110 mg, 0.67 mmols) in water (5 cm^3). Dark green precipitates separated immediately and were filtered and washed with hot water and diethyl ether then vacuum dried. Yields: [CuL(bipy)]PF_6 229 mg (64%); [CuL(phen)]PF_6 228 mg (61%).

$[CuL(bipy)]_2SO_4\cdot 8H_2O$

To $[CuL(CH_3COO)]_2$ (302 mg, 1.00 mmols) in water (30 cm^3) was added with heating bipy (158 mg, 1.01 mmols) in water (5 cm^3) and ethanol (5 cm^3). To this, a filtered solution containing $Na_2MoS_4\cdot 3½H_2O$ (178 mg, 0.53 mmols) in water (20 cm^3) was added. The resultant green solution was stirred for 5 minutes then filtered. Crystals of the title complex grew within hours but were unsuitable for X-ray crystallography. These were removed from solution and given a cursory wash with water and dried under vacuum. Yield 80 mg (15%).

$[CuL(dmap)_2]PF_6$

Neat 4-dimethylaminopyridine (dmap) (350 mg, 2.86 mmols) was added to an aqueous solution (30 cm^3) of $[CuL(CH_3COO)]_2$ (302 mg, 1.00 mmols) with heat. To the filtered blackish solution was added NH_4PF_6 (170 mg, 1.04 mmols) in water (5 cm^3). The green complex which resulted was filtered and washed with water and diethyl ether and dried under vacuum. Yield 135 mg (26%).

$[CuL(sacc)H_2O]\cdot \frac{1}{2}H_2O$

To $[CuL(CH_3COO)]_2$ (151 mg, 0.50 mmols) in water (75 cm^3) which had been briefly boiled then filtered, was added sodium saccharinate (sacc) (213 mg, 1.04 mmols) in water (20 cm^3). The dark green solution yielded crystals overnight which were removed and washed with water and dried on the sintered glass filter under suction only. Yield 164 mg (73%). The ratio of 2:1 sacc:CuL^+ was not important as crystalline material was obtained, under the same conditions, from 1:1 to 4.5:1 ratio mixtures also.

1.2.5(b) Preparation of Blood Samples for E.s.r. Spectroscopy

Isotonic Saline

Isotonic saline used to wash and suspend the red cells was prepared by dissolving $NaH_2PO_4\cdot 2H_2O$ (1.557 g, 0.010 moles) and NaCl (7.584 g, 0.130 mols) in water (900 cm^3). This was titrated with NaOH solution (1M) until the pH equalled 7.40. The volume was then made up to one litre.

$[CuL(CH_3COO)]_2$ solution

$[CuL(CH_3COO)]_2$ (17.5 mg, 0.058 mmols) was weighed into a 25 cm^3 volumetric flask and dissolved in dimethylsulphoxide (5 cm^3). This was then made up to the mark with isotonic saline. When 1.3 cm^3 of this stock solution was added to 4.0 cm^3 of the blood sample to be tested, the final concentration of Cu(II) was 5.8×10^{-4} mol l^{-1}. The above procedure was repeated with $CuCl_2 \cdot 2H_2O$ (9.5 mg, 0.056 mmols) to give a final Cu(II) concentration in the blood sample of 5.6×10^{-4} mol l^{-1}. With an average packed red cell concentration of 4.5 - 6.00×10^6 cells/mm^3 [158], this gives the approximate ratio of Cu:red cells of 6×10^7:1.

Blood Samples

Fresh heparinised blood from the author (~10 cm^3) was centrifuged at 5 000 rpm for 10 minutes at 4° C. The plasma (approximately one half of the total blood volume) was removed and used without modification. The packed red cells were gently washed with approximately two volumes of isotonic saline, then the sample was centrifuged at 5 000 rpm for 10 minutes The supernatant was removed and the red cells were resuspended in an equal volume of saline. Two portions of this (4 cm^3 each) were placed in two centrifuge tubes and either the $[CuL(CH_3COO)]_2$ or the $CuCl_2$ stock solution (1.3 cm^3) was added. In two test-tubes, equal volumes of plasma were placed (1.5 cm^3) and the $[CuL(CH_3COO)]_2$ or the $CuCl_2$ stock solutions (0.5 cm^3) was added. The four tubes were carefully shaken then incubated at 37° C for 30 minutes with further shaking every 5 minutes. After this time, the two plasma samples were ready for use but the red cell samples required one further step. Both tubes were centrifuged at 5 000 rpm for 10 minutes to separate the red cells from the supernatant. Spectra were then run on both the packed cells and supernatant to ensure copper absorption had occurred. A small amount of cell lysis had occurred in both the Cu^{2+} and CuL^+ samples as the colours of the supernatant were pale orange and light red respectively.

1.2.5(c) Data collection procedure for Aqua(2-formylpyridine thiosemicarbazonato)(saccharinato-N)copper(II) Hemihydrate

The title complex was synthesised as described in section 1.2.5(a). The crystal was of poor quality and displayed faces of the forms {1 0 $\bar{1}$}, {0 1 1}, {0 1 $\bar{1}$}, {0 $\bar{1}$ $\bar{1}$}, {0 $\bar{1}$ 1}, {0 0 1} and {$\bar{1}$ 0 1} with approximate dimensions of 0.010 x 0.026 x 0.063 cm. Cell dimensions of: $\underline{a}$ = 7.465(7), $\underline{b}$ = 9.245(7), $\underline{c}$ = 26.209(33) Å and β = 97.18(9)° were determined from the setting angles of 25 reflections centred on the diffractometer to give a cell volume of 1794.6 Å^3 and a molecular weight of 452.0 a.m.u. ($C_{14}H_{14}CuN_5O_{4.5}S_2$). The density was calculated to be 1.673 g cm^{-3} for four formula weights in the unit cell. Systematic absences (0$\underline{k}$0, $\underline{k}$ = 2n + 1 and $\underline{h}$0$\underline{l}$, h + l = 2n + 1) established the space group as P21/n. A total of 2533 reflections were collected on a Nicolet R3M four-circle automatic single-crystal diffractometer (at Canterbury University) with Mo–K_α radiation (μ (M_o-K_α) = 14.08 cm^{-1}). The $\omega/2\theta$ scan technique was employed (θ_{max} = 22.5°) with $\underline{h}$ $\underline{k}$ $\underline{l}$ ranges of: -8 → 7, 0 → 7, 0 → 28. Empirical absorption corrections were applied to this crystal [126].

Tables 1.2.10 and 1.2.11 summarise the relevant crystal and data collection parameters.

1.2.5(d) Structure solution and refinement

The copper atom site, located by direct methods [159], was in agreement with the Patterson synthesis and yielded a residual of 0.48. All non-hydrogen atoms were located in the subsequent electron density map phased by this copper site. Two cycles of full-matrix least-squares refinement with all atoms assuming isotropic thermal motion gave an R factor of 0.10. All hydrogens were located from a difference electron density synthesis; those in the pyridine and saccharin rings and on C(6) were added in calculated positions (C-H 1.08 Å). The values of R and R_w for the final cycle were 0.0537 and 0.0544 respectively for the 238 parameters and 2533 data for which $F^2 > 3\sigma(F^2)$. The function minimised was $\Sigma w(|F_o| - |F_c|)^2$ with the weight, w, being defined as $1.7509/(\sigma^2(F) + 0.00104\ F^2)$.

All non-hydrogen atoms were refined assuming anisotropic thermal motion with the atoms in the saccharin phenyl ring being treated as a rigid group (C–C 1.395 Å, C–H 1.08 Å). In the final refinement cycle the largest shift per esd was 0.003. The two highest peaks in the final difference electron density map of 0.60 $\bar{e}$ $Å^{-3}$ were associated with the residual electron density around the copper and thiosemicarbazonato sulphur atoms respectively.

Final atomic parameters and the observed and calculated structure factors are presented on the microfiche in the pocket inside the back cover of this thesis. The bond length and bond angle data are listed in Tables 1.2.2 and 1.2.3 respectively.

TABLE 1.2.10
$[CuL(sacc)H_2O]\cdot\frac{1}{2}H_2O$

CRYSTAL DATA

Compound:	Aqua(2-formylpyridine thiosemicarbazonato)(saccharinato-N)copper(II) Hemihydrate
Colour:	Green
Formula:	$C_{14}H_{14}CuN_5O_{4.5}S_2$
Formula weight:	452.0 g mol^{-1}
Space group:	$P2_1/n$
a:	7.465(7) Å
b:	9.245(7) Å
c:	26.209(33) Å
β:	97.18(9)°
V:	1794.6 $Å^3$
Z:	4
ρ_c:	1.673 g cm^{-3}
Crystal faces:	{1 0 $\bar{1}$}, {0 1 1}, {0 1 $\bar{1}$}, {0 0 $\bar{1}$}, {0 $\bar{1}$ $\bar{1}$}, {0 $\bar{1}$ 1}, {0 0 1}, {$\bar{1}$ 0 1}
Crystal dimensions:	0.010 x 0.026 x 0.063 cm
μ (M_o-K_α):	14.08 cm^{-1}
F(OOO):	912

TABLE 1.2.11
$[CuL(sacc)H_2O]\cdot \frac{1}{2}H_2O$

Parameters Associated with Data Collection

Radiation used:	Mo(K_α) (λ = 0.71069 Å)
Graphite monochromator used:	Yes
Scan type:	$\omega/2\theta$
Scan range:	3.2°
Scan speed:	4.88°/min
θ Range:	2 – 22.5°
Total number of reflections in data set:	2 533
Observed data criterion:	1 372 unique reflections with $F^2 > 3\sigma(F^2)$
Collection temperature:	153 K

1.2.5(e) Data collection procedure for 2, 2′-Bipyridyl(2-formylpyridine thiosemicarbazonato)copper(II) Perchlorate.

The title compound was synthesised as described in section 1.2.5(a). Faces of the forms {0 0 1}, {0 0 $\bar{1}$}, {$\bar{1}$ 1 0}, {1 $\bar{1}$ 0}, {1 1 0} and {$\bar{1}$ $\bar{1}$ 0} were displayed by the crystal which had approximate dimensions of 0.010 x 0.010 x 0.054 cm. The Nicolet R3M four circle automatic diffractometer with Mo-K_α radiation ($\mu(M_o\text{-}K_{\bar{\alpha}})$ = 12.90 cm^{-1}) used the setting angles of 25 reflections to calculate the cell dimensions of: $\underline{a}$ = 8.560(3), $\underline{b}$ = 9.452(4), c = 13.078(4) Å, α = 106.35(3), β = 94.66(3) and γ = 95.27(3)°. A cell volume of 1004.7$Å^3$ and a molecular weight of 498.4 a.m.u. gave a calculated crystal density of 1.647 g cm^{-3} for two formula weights in the unit cell. The diffraction symmetry established the crystal class as triclinic, with the space-group being P1 or P$\bar{1}$. Initially the centrosymmetric P$\bar{1}$ was chosen and final analysis showed this choice to be correct. A total of 2623 reflections were collected using the $\omega/2\theta$ scan technique (θ_{max} = 22.5°) with the $\underline{h}$ $\underline{k}$ $\underline{l}$ ranges of: -9 → 7, -10 → 9, 0 → 14. Data were corrected for absorption using the empirical technique [126].

Tables 1.2.12 and 1.2.13 summarise the relevant crystal and data collection parameters.

1.2.5(f) Structure solution and refinement

The copper and sulphur atom sites were located by direct methods [159] and returned a residual of 0.42. Subsequent electron and difference electron density maps revealed all non-hydrogen atoms and these were included with isotropic temperature factors yielding an R factor of 0.071 for two full-matrix least-squares cycles. A difference electron density synthesis revealed all hydrogen atom positions and these were included in the calculations; those in the pyridine and bipyridyl rings and on C(6) were fixed at 1.08 Å. For the 276 parameters and 2623 data for which $F^2 > 3\sigma(F^2)$ the values of R and R_w for the final refinement cycle were both 0.0412. The function minimised was $\Sigma w(|F_o| - |F_c|)^2$ with the weight, w, being defined as $3.0849/(\sigma^2(F) + 0.00014\ F^2)$.

All non-hydrogen atoms were refined assuming anisotropic thermal motion. The highest two peaks in the final difference electron density synthesis were both 0.70 $\bar{e}$ $Å^{-3}$ and associated with the residual electron density around the copper. The largest shift per esd of 0.004 was associated with a perchlorate oxygen.

Final atomic parameters and the observed and calculated structure factors are presented on the microfiche inside the back cover pocket of this thesis. The bond length and bond angle data are presented in Tables 1.2.2 and 1.2.3 respectively.

TABLE 1.2.12
[CuL(bipy)]ClO_4

CRYSTAL DATA

Compound:	2, 2'-Bipyridyl(2-formylpyridine thiosemicabazonato) copper(II) Perchlorate
Colour:	Green
Formula:	$C_{17}H_{15}CuClN_6O_4S$
Formula weight:	498.4 g mol^{-1}
Space group:	$P\bar{1}$
a:	8.560(3) Å
b:	9.452(2) Å
c:	13.078(4) Å
α:	106.35(3)°
β:	94.66(3)°
γ:	95.27(3)°
V:	1004.7 $Å^3$
Z:	2
ρ_c:	1.647 g cm^{-3}
Crystal faces:	{0 0 1}, {$\bar{1}$ 1 0}, {1 $\bar{1}$ 0}, {0 0 $\bar{1}$}, {1 1 0}, {$\bar{1}$ $\bar{1}$ 0}
Crystal dimensions:	0.010 x 0.010 x 0.054 cm
μ (Cu-$K_{\bar{\alpha}}$):	12.90 cm^{-1}
F(OOO):	502

TABLE 1.2.13
[CuL(bipy)]ClO_4

Parameters Associated with Data Collection

Radiation used:	Mo(K_α) (λ = 0.71069 Å)
Graphite monochromator used:	Yes
Scan type:	$\omega/2\theta$
Scan range:	1.6°
Scan speed:	3.91°/min
θ Range:	2 – 22.5°
Total number of reflections in data set:	2 623
Observed data criterion:	2 065 unique reflections with $F^2 > 3\sigma(F^2)$
Collection temperature:	153 K

CHAPTER 3

TERNARY O DONOR ATOM COPPER COMPLEXES OF LH/L⁻

1.3.1 INTRODUCTION

In the previous chapter, proposed mechanisms for antitumour activity involving the formation of sulphur and nitrogen donor atom adducts were discussed. *In vivo*, the possibility of oxygen donor adduct formation exists whereby the drug binds to the phosphato oxygens of nucleic acids. Several studies involving the interaction of binary copper(II) complexes (e.g. $Cu(bipy)^{2+}$) with model nucleic acids demonstrate that the copper complex can coordinate to the nucleotide via the phosphato oxygen atoms [160-162]. The possibility of such adduct formation *in vivo* is investigated in the present chapter through the synthesis *in vitro* of ternary complexes involving anionic oxygen donors (e.g. phosphate species, phenolate or molybdate).

In the literature at present, there appear to have been no crystallographic studies of copper(II) ternary phosphato or pyrophosphato complexes. This is most probably due to the unsuitability of the starting materials; $Cu_3(PO_4)_2{\cdot}3H_2O$ is insoluble in cold water and only slightly soluble in hot [96] and the $P_2O_7^{4-}$ anion is prone to hydrolysis [163]. In view of the above, the synthesis of such complexes is of interest, and in particular the single-crystal X-ray crystallographic structures of the pyrophosphato complex, $[(CuL)_4P_2O_7]{\cdot}12H_2O$, and the dihydrogenphosphato complex, $[Cu(LH)(H_2PO_4)]_2(H_2PO_4)_2(H_3PO_4)_2{\cdot}2H_2O$, are noteworthy. The complexes prepared in this chapter are listed in Table 1.3.1 with their elemental analyses and room temperature magnetic moment data.

Two general methods of synthesis were employed in this chapter. In the first, the acetate ion was metathetically displaced from a neutral, aqueous solution of $[CuL(CH_3COO)]_2$ to give anionic ligand complexes of the general formulation [CuL(OR)] (where OR = e.g. phenolate or $½(HPO_4^{2-})$). The second procedure was similar but acid solutions were used. Hence the

neutral ligand complexes $[Cu(LH)(H_2PO_4)]_2(H_2PO_4)_2 \cdot 3H_2O$ and $[Cu(LH)(H_2PO_4)]_2(H_2PO_4)_2(H_3PO_4)_2 \cdot 2H_2O$ were obtained.

TABLE 1.3.1

Analytical and Magnetic Data for Chapter 3

Complex[a]	Colour	Analyses (%)[b]				μ_{eff}[c]
		C	H	N	Other	
$[(CuL)_4P_2O_7] \cdot 12H_2O$	Dark Green	24.7 (24.7)	4.2 (3.9)	16.6 (16.5)	4.9 (4.6)[d]	1.83
$[(CuL)_2HPO_4] \cdot 6H_2O$	Green	24.3 (24.4)	4.3 (4.0)	15.8 (16.3)	4.5(4.5)[d]	1.92
$[Cu(LH)(H_2PO_4)]_2(H_2PO_4)_2 \cdot 3H_2O$	Green	18.5 (18.1)	3.8 (3.6)	12.0 (12.1)	12.8 (13.3)[d]	1.77
$[Cu(LH)(H_2PO_4)]_2(H_2PO_4)_2(H_3PO_4)_2 \cdot 5H_2O$[f]	Dark Green	14.4 (14.5)	3.5 (3.6)	9.8 (9.7)	16.0 (16.0)[d]	1.84
$[CuL(ptp)] \cdot 2H_2O$	Green	62.7 (62.6)	4.7 (5.1)	9.4 (9.1)		1.89
[CuL(tip)]	Green	22.3 (21.9)	1.4 (1.3)	8.3 (7.9)		2.26
$[(CuL)_2MoO_4]H_2O$	Green	25.3 (25.3)	3.0 (2.4)	16.8 (16.9)	14.7 (14.5)[e]	1.80

a see page x for abbreviations
b calculated values are given in parentheses
c measured at 293 K and quoted in B.M. per copper(II) ion
d %P
e %Mo
f crystal structure shows $2H_2O$ but the compound is very hygroscopic and may have picked up water during handling for analysis.

1.3.2 CRYSTAL STRUCTURE OF μ_4-Pyrophosphatotetrakis[(2-formylpyridine thiosemicarbazonato)copper(II)] Dodecahydrate

A thermal ellipsoid diagram of the title complex (abbreviated as $[(CuL)_4P_2O_7]\cdot 12H_2O$) showing the numbering scheme used is depicted in Figure 1.3.1. Bond length and angle data are given in Tables 1.3.2 and 1.3.3 respectively.

The complex $[(CuL)_4P_2O_7]\cdot 12H_2O$ crystallises as a discrete tetramer, with the pyrophosphato moiety bridging the four CuL^+ units. The coordination environment of each copper atom in the structure is similar and may be described as a distorted square-pyramid. Each copper is coordinated to the mono-anionic, tridentate, 2-formylpyridine thiosemicarbazonato ligand (L^-) in the equatorial plane via the pyridine nitrogen, imine nitrogen and thioamide sulphur. The remaining in-plane position is occupied by a pyrophosphato oxygen and the coordination sphere is completed by a weak bond to a sulphur atom of an adjacent ligand (see Figures 1.3.1 and 1.3.2). There is no sixth contact of any significance.

The planes of best-fit through the four equatorial donors around each of the four copper atoms show each copper to lie out of the plane towards its long-bonded apical sulphur, with a mean displacement of 0.114 Å*. Examination of the chi-squared values gives an indication of the degree of planarity for the equatorial donors. These values range from zero in the surprisingly planar donor set around Cu(2), to 4000 for Cu(4) where the average, absolute displacement for the four in-plane coordinating atoms from the mean-plane is 0.139 Å.

---

* Plane (i) S(1), N(11), N(12), O(21) $\chi^2 = 42$
0.3144X + 0.1164Y – 0.9421Z – 1.6810 = 0
[S(1) -0.012, N(11) -0.014, N(12) 0.015, O(21) 0.011, Cu(1) -0.130]
Plane (ii) S(2), N(21), N(22), O(11) $\chi^2 = 0$
0.0918X – 0.0101Y – 0.9957Z + 1.6015 = 0
[S(2) 0.000, N(11) 0.000, N(12) 0.000, O(11) 0.000, Cu(2) -0.103]
Plane (iii) S(3), N(31), N(32), O(12) $\chi^2 = 395$
0.2778X + 0.2604Y – 0.9247Z + 0.8668 = 0
[S(3) -0.039, N(31) -0.047, N(32) 0.049, O(12) 0.038, Cu(3) 0.111]
Plane (iv) S(4), N(41), N(42), O(22) $\chi^2 = 4000$
0.4349X – 0.1897Y – 0.8803Z + 1.2234 = 0
[S(4) -0.125, N(41) -0.152, N(42) 0.158, O(22) 0.119, Cu(4) 0.111]
Distances of atoms from the plane (Å) are given in square brackets.

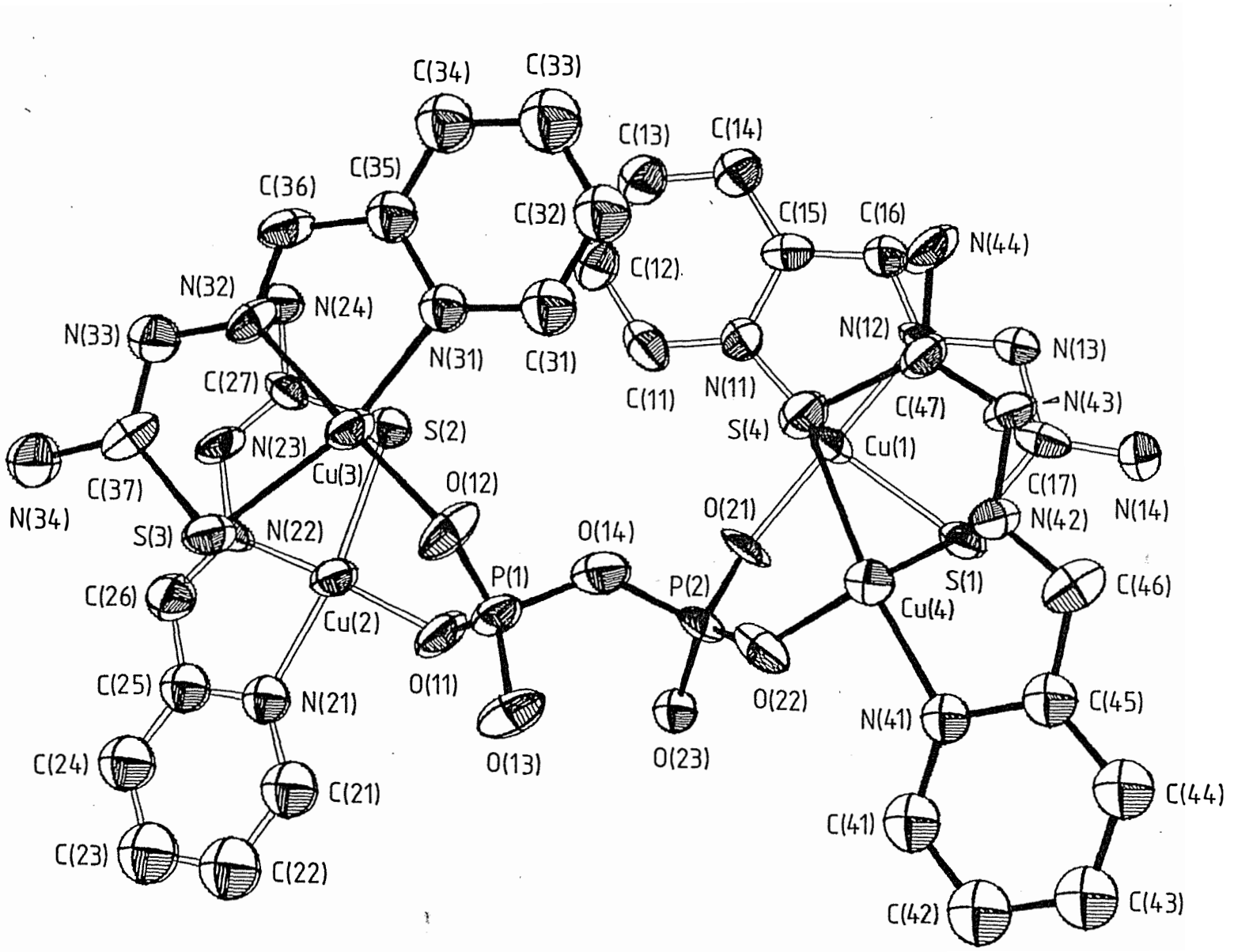

Figure 1.3.1: The tetramer $[(CuL)_4P_2O_7]\cdot 12H_2O$ showing the atom numbering scheme. The water molecules and hydrogen atoms have been omitted for clarity.

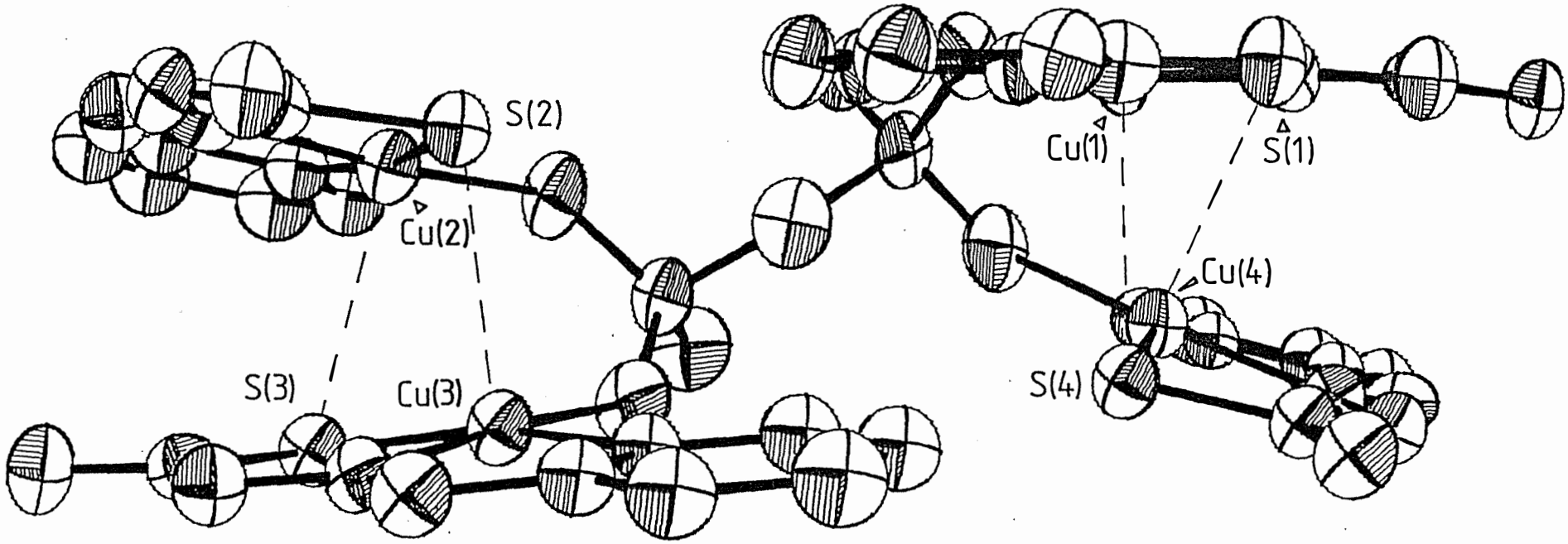

Figure 1.3.2: The tetramer $[(CuL)_4P_2O_7]\cdot 12H_2O$ showing the long, apical Cu-S bonds. The water molecules and hydrogen atoms have been omitted for clarity.

TABLE 1.3.2
Bond Lengths (Å) with Estimated Standard Deviations in Parentheses for the Complex $[(CuL)_4P_2O_7]\cdot 12H_2O$*

Cu(1)–N(11)	2.001(5)	Cu(2)–N(21)	1.998(6)
Cu(3)–N(31)	2.004(5)	Cu(4)–N(41)	2.016(6)
Cu(1)–N(12)	1.916(7)	Cu(2)–N(22)	1.974(8)
Cu(3)–N(32)	1.946(7)	Cu(4)–N(42)	1.950(7)
Cu(1)–S(1)	2.274(2)	Cu(2)–S(2)	2.264(3)
Cu(3)–S(3)	2.292(3)	Cu(4)–S(4)	2.284(2)
Cu(1)–O(21)	1.909(6)	Cu(2)–O(11)	1.910(7)
Cu(3)–O(12)	1.903(7)	Cu(4)–O(22)	1.902(7)
S(1)–C(17)	1.739(9)	S(2)–C(27)	1.773(9)
S(3)–C(37)	1.733(10)	S(4)–C(47)	1.741(9)
N(12)–N(13)	1.376(10)	N(22)–N(23)	1.340(10)
N(32)–N(33)	1.343(10)	N(42)–N(43)	1.330(9)
N(12)–C(16)	1.287(11)	N(22)–C(26)	1.293(12)
N(32)–C(36)	1.285(11)	N(42)–C(46)	1.305(12)
N(13)–C(17)	1.333(10)	N(23)–C(27)	1.334(11)
N(33)–C(37)	1.306(12)	N(43)–C(47)	1.318(11)
N(14)–C(17)	1.365(12)	N(24)–C(27)	1.315(11)
N(34)–C(37)	1.399(13)	N(44)–C(47)	1.329(11)
C(15)–C(16)	1.387(10)	C(25)–C(26)	1.417(12)
C(35)–C(36)	1.412(11)	C(45)–C(46)	1.417(10)
Cu(1)–S(4)	2.892(3)	Cu(2)–S(3)	2.900(3)
Cu(3)–S(2)	2.855(3)	Cu(4)–S(1)	2.891(3)
Cu(1)···Cu(4)	3.281(2)	Cu(2)···Cu(3)	3.233(2)

Pyrophosphato Bond Lengths (Å)

P(1)–O(11)	1.507(7)	P(2)–O(21)	1.518(8)
P(1)–O(12)	1.487(7)	P(2)–O(22)	1.508(8)
P(1)–O(13)	1.491(8)	P(2)–O(23)	1.505(7)
P(1)–O(14)	1.596(8)	P(2)–O(14)	1.601(7)

* C–C and C–N bond lengths in pyridine rings fixed at 1.395 Å
C–H and N(X3)–H(X3) bond lengths fixed at 1.08 Å (X = 1 – 4).

TABLE 1.3.3
Bond Angles (°) with Estimated Standard Deviations in Parentheses for the Complex $[(CuL)_4P_2O_7]\cdot 12H_2O$

N(11)–Cu(1)–N(12)	80.8(3)	N(21)–Cu(2)–N(22)	81.0(3)
N(31)–Cu(3)–N(32)	80.9(3)	N(41)–Cu(4)–N(42)	81.0(2)
N(11)–Cu(1)–S(1)	165.2(2)	N(21)–Cu(2)–S(2)	164.8(2)
N(31)–Cu(3)–S(3)	163.4(2)	N(41)–Cu(4)–S(4)	159.3(2)
N(11)–Cu(1)–O(21)	96.5(2)	N(21)–Cu(2)–O(11)	94.3(3)
N(31)–Cu(3)–O(12)	96.3(3)	N(41)–Cu(4)–O(22)	95.1(3)
N(12)–Cu(1)–S(1)	85.4(2)	N(22)–Cu(2)–S(2)	84.6(2)
N(32)–Cu(3)–S(3)	84.4(2)	N(42)–Cu(4)–S(4)	83.7(2)
N(12)–Cu(1)–O(21)	171.1(3)	N(22)–Cu(2)–O(11)	172.5(3)
N(32)–Cu(3)–O(12)	175.3(3)	N(42)–Cu(4)–O(22)	175.6(3)
S(1)–Cu(1)–O(21)	96.3(2)	S(2)–Cu(2)–O(11)	99.5(2)
S(3)–Cu(3)–O(12)	97.8(2)	S(4)–Cu(4)–O(22)	100.6(2)
N(11)–Cu(1)–S(4)	90.4(2)	N(21)–Cu(2)–S(3)	89.6(2)
N(31)–Cu(3)–S(2)	92.0(2)	N(41)–Cu(4)–S(1)	98.4(2)
N(12)–Cu(1)–S(4)	88.5(2)	N(22)–Cu(2)–S(3)	87.6(2)
N(32)–Cu(3)–S(2)	87.7(2)	N(42)–Cu(4)–S(1)	86.3(2)
S(1)–Cu(1)–S(4)	94.5(1)	S(2)–Cu(2)–S(3)	94.7(1)
S(3)–Cu(3)–S(2)	95.2(1)	S(4)–Cu(4)–S(1)	94.4(1)
O(21)–Cu(1)–S(4)	100.0(2)	O(11)–Cu(2)–S(3)	98.3(2)
O(12)–Cu(3)–S(2)	96.3(2)	O(22)–Cu(4)–S(1)	92.2(3)
Cu(1)–N(11)–C(11)	128.8(4)	Cu(2)–N(21)–C(21)	127.2(4)
Cu(3)–N(31)–C(31)	128.3(4)	Cu(4)–N(41)–C(41)	128.6(4)
Cu(1)–N(11)–C(15)	111.2(4)	Cu(2)–N(21)–C(25)	112.6(5)
Cu(3)–N(31)–C(35)	111.6(4)	Cu(4)–N(41)–C(45)	111.3(4)
N(11)–C(15)–C(16)	114.1(5)	N(21)–C(25)–C(26)	113.3(6)
N(31)–C(35)–C(36)	114.0(5)	N(41)–C(45)–C(46)	114.3(6)
C(15)–C(16)–N(12)	116.8(7)	C(25)–C(26)–N(22)	118.1(8)
C(35)–C(36)–N(32)	116.9(7)	C(45)–C(46)–N(42)	116.5(8)
C(16)–N(12)–Cu(1)	117.0(6)	C(26)–N(22)–Cu(2)	114.9(6)
C(36)–N(32)–Cu(3)	116.5(6)	C(46)–N(42)–Cu(4)	116.1(6)
N(13)–N(12)–Cu(1)	123.6(5)	N(23)–N(22)–Cu(2)	123.2(6)
N(33)–N(32)–Cu(3)	122.7(5)	N(43)–N(42)–Cu(4)	123.4(5)
N(12)–N(13)–C(17)	111.3(7)	N(22)–N(23)–C(27)	113.1(7)
N(32)–N(33)–C(37)	113.1(7)	N(42)–N(43)–C(47)	113.5(7)
C(16)–N(12)–N(13)	119.4(7)	C(26)–N(22)–N(23)	121.6(8)
C(36)–N(32)–N(33)	120.8(7)	C(46)–N(42)–N(43)	120.4(7)
N(13)–C(17)–S(1)	125.6(7)	N(23)–C(27)–S(2)	123.9(6)
N(33)–C(37)–S(3)	126.0(8)	N(43)–C(47)–S(4)	124.2(6)
N(13)–C(17)–N(14)	116.4(8)	N(23)–C(27)–N(24)	118.1(8)
N(33)–C(37)–N(34)	116.4(8)	N(43)–C(47)–N(44)	118.0(8)
S(1)–C(17)–N(14)	118.0(6)	S(2)–C(27)–N(24)	117.9(7)
S(3)–C(37)–N(34)	117.6(7)	S(4)–C(47)–N(44)	117.8(7)
C(17)–S(1)–Cu(1)	93.3(3)	C(27)–S(2)–Cu(2)	94.2(3)
C(37)–S(3)–Cu(3)	92.9(3)	C(47)–S(4)–Cu(4)	93.8(3)
Cu(4)–S(1)–Cu(1)	77.9(1)	Cu(3)–S(2)–Cu(2)	77.4(1)
Cu(2)–S(3)–Cu(3)	76.0(1)	Cu(1)–S(4)–Cu(4)	77.7(1)
Cu(4)–S(1)–C(17)	108.0(3)	Cu(3)–S(2)–C(27)	106.8(3)
Cu(2)–S(3)–C(37)	106.7(4)	Cu(1)–S(4)–C(47)	103.0(3)

Pyrophosphato Bond Angles (°)

O(11)–P(1)–O(12)	112.6(4)	O(21)–P(2)–O(22)	113.1(4)
O(11)–P(1)–O(13)	110.0(4)	O(21)–P(2)–O(23)	112.3(4)
O(11)–P(1)–O(14)	106.5(4)	O(21)–P(2)–O(14)	102.4(4)
O(12)–P(1)–O(13)	113.0(5)	O(22)–P(2)–O(23)	112.7(4)
O(12)–P(1)–O(14)	104.8(4)	O(22)–P(2)–O(14)	107.7(4)
O(13)–P(1)–O(14)	109.6(4)	O(23)–P(2)–O(14)	107.9(4)
P(1)–O(11)–Cu(2)	132.5(4)	P(2)–O(21)–Cu(1)	129.9(5)
P(1)–O(12)–Cu(3)	136.3(5)	P(2)–O(22)–Cu(4)	136.5(5)
P(1)–O(14)–P(2)	132.9(4)		

A significant distortion in the geometry around Cu(4) towards a trigonal bipyramidal structure is apparent by comparison of the bond angles with the equivalent angles for the other three copper atoms. The angles S(4)-Cu(4)-N(41) (159.3(2)°; average of the other comparable three angles is 164.5(9)°) and N(41)-Cu(4)-S(1) (98.4(2)°; average of the other three is 90.7(12)°) both show distortions towards 120°, whereas O(22)-Cu(4)-S(1) (angle of 92.2(3)°; average of the other three is 98.2(18)°) is distorted towards 90°. The remaining angles around Cu(4) are not significantly different from the average of the other three equivalent bond angles for their respective copper atoms. These changes all act to distort the coordination sphere around Cu(4) away from a square-pyramidal geometry towards a trigonal-bipyramidal configuration (see the comparison of $[CuL(bipy)]ClO_4$ with $[CuL(sacc)H_2O]\cdot\frac{1}{2}H_2O$ in Chapter 2). The reason/s for this change are not obvious as the donor sets are equivalent and steric interactions within the tetramer are expected to be equivalent. The difference may therefore lie in crystal packing forces.

There are several significant differences in the copper-donor bond lengths (e.g. Cu(1)-N(12) and Cu(2)-N(22) have values of 1.916(7) and 1.974(8) Å respectively) but no pattern is observed in these.

Each copper in this molecule is in the unusual position of being linked to the remaining three copper atoms. Figure 1.3.2 shows the tetramer may be considered as a pair of dimers, linked by the pyrophosphato moiety. Within each of these dimers, the two copper atoms are bridged by the axially coordinated sulphur atom. These axial bonds range in length from 2.855(3) to 2.900(3) Å with a mean value of 2.885 Å. In the structures of kethoxal-bis(thiosemicarbazone)copper(II) (CuKTS [164] - see Figure 1.3), diacetyl-bis(thiosemicarbazone)copper(II) (CuDAT [165]) and benzyl-bis(thiosemicarbazone)copper(II) (CuBBT [166]) a similar situation exists whereby two molecules interact in pairs (or for the former two examples, in chains) through Cu-S axial bonds of 3.101(2), 3.102 and 3.454(3) Å

respectively (the longer, chain forming, Cu-S interactions for CuKTS and CuDAT are 3.312(2) and 3.314 Å respectively). The angle between the normal to the plane containing the four equatorial donor atoms and the Cu-S axial bond in this study ranges from 6.1° for Cu(1)-S(4) to 2.7° for Cu(4)-S(1) (average of the four is 4.9°) showing the axially bound sulphur deviates only slightly from the z-axis. This results in Cu···Cu separations of 3.282 Å and 3.233 Å for Cu(1)···Cu(4) and Cu(2)···Cu(3) respectively. The Cu···Cu separations for the complexes CuKTS (3.835 and 3.904 Å [164]), CuDAT (3.833 and 3.896 Å [165]) and CuBBT (3.720 [166]) have a mean value of 3.84 Å, an increase of 0.58 Å over the average for the title complex.

Both of the pairs of copper atoms in the pyrophosphato complex also have a three-atom bridge from the pyrophatato group e.g. Cu(1)-O(21)-P(2)-O(22)-Cu(4). A number of phosphato three-atom bridges between two copper atoms have been reported where the phosphato group is attached to a nucleotide [161,162 and refs. therein] but no other three-atom bridges involving pyrophosphates could be found in the literature. The copper atoms in these latter structures are separated by over 5 Å and are bridged by two phosphato groups. The angle between the two coordinated oxygens and the phosphorus in these structures of 113.2° is not significantly changed from the equivalent angles (O(11)-P(1)-O(12) and O(21)-P(2)-O(22)) of 112.9° in the title complex.

In addition to these three-atom bridges, each copper in a 'dimer' has two, five-atom bridges to the coppers in the other 'dimer' with an average Cu···Cu separation of 7.31 Å (see Figure 1.3.1). In total, each copper is involved in a one-atom S bridge, a three-atom and two five-atom bridges via the coordinated pyrophosphato group. Not surprisingly, the magnetic behaviour of this complex can not be explained using a simple dimer model (see Chapter 3 discussion).

Bond lengths within the four anionic ligands, L^-, for an equivalent bond tend to show some variation but with the high esd's calculated these are not thought to be significant. Such small

differences are probably to be expected in view of the other variations observed (e.g. coordination geometry distortions).

The pyrophosphate in this structure appears to be unique in that no other ternary complexes with pyrophosphate as the anion could be found in the literature. A number of salts (e.g. $Na_4P_2O_7$ [167] and α-$Mg_2P_2O_7$ [168]) and binary compounds (e.g. α-$Cu_2P_2O_7$ [169] and α-$Co_2P_2O_7$ [170]) have however been studied by X-ray diffraction techniques, hence a comparison of the bonding parameters can be made.

The $P_2O_7^{4-}$ group comprises two slightly distorted PO_4 tetrahedra which share a common oxygen, O(14). Four of the six terminal oxygens are coordinated to four different copper atoms. The average Cu-O bond length of 1.906(7) Å is shorter than the values of 1.929, 1.935(13) and 1.95 Å found for the in-plane phosphato bonds in [Cu(5′-AMP)(bipy)H_2O]$_2$(NO_3)$_2$·6H_2O (5′-AMP is adenosine 5′-monophosphate [162]), [Cu(5′-UMP)(dpa)H_2O]$_2$·5H_2O (5′-UMP is uridine 5′-monophosphate, dpa is 2, 2′-dipyridylamine [161]) and for $Cu_2P_2O_7$ [171] respectively.

In all of these instances the copper(II) atom is essentially five coordinate with the fifth axial coordination site occupied by an oxygen from water or pyrophosphate anion (average Cu-$O_{(axial)}$ of 2.35 Å). This observed reduction in the in-plane Cu-O(phosphato) bond length in [(CuL)$_4$$P_2O_7$]·12$H_2O$ may therefore be a result of a weaker axial contact (Cu-$S_{(axial)}$ of 2.885(20) $Å_{av}$) accompanied by stronger in-plane coordination and/or the differences in the equatorial donor sets.

The two remaining oxygens are uncoordinated but are involved in hydrogen-bonding to water molecules. As a result of this, the six terminal P-O_t bonds (average bond length of 1.503(12) Å), show no significant bond length variation unlike some other $P_2O_7^{4-}$-containing compounds where there is a difference in the environments of these oxygens [170,172,173]. The two bridging P-O_b bonds (average bond length of 1.599(10) Å) are 0.096 Å longer than the P-O_t

bond (the P(1)-O(14)-P(2) bridge angle is 132.9(4)°). A correlation has been observed between the bridge angle and $\Delta d_{(om)}$ ($\Delta d_{(om)}$ is the difference between the experimentally observed bridging P-O_b bond length and the mean P-O_t bond length). As the P-O-P bridge angle widens, the bridging P-O_b bonds acquire some π character and the bond length decreases. The experimentally determined values of 132.9(4)° for P(1)-O(14)-P(2) and 0.072 Å for $\Delta d_{(om)}$ agree well with the other data reported for pyrophosphates [172].

The O-P-O bond angles which do not involve the bridging oxygen, O(14), are all greater than the tetrahedral value of 109° with an average value of 112.3(11)° being observed. The average O-P-O angle including O(14) is 106.5(26)°. Both these results are in accord with published data on such systems.

The $P_2O_7^{4-}$ anion can adopt either a staggered or an eclipsed conformation, with more than half of the published structures containing the staggered arrangement. Figure 1.3.3 shows the pyrophosphate anion in this structure, with the plane containing P(1), O(14) and P(2) running vertically. The two oxygens not bound to copper (O(13) and O(23)) are shown shaded. From this diagram it can be seen that the $P_2O_7^{4-}$ moiety adopts a staggered configuration. To be completely staggered the P(2)-O bonds should bisect the O-P(1)-O bond angles as the diagram is plotted, forming six angles of 60°. In this anion, the mean OPPO torsion angle is only 42° (see Figure 1.3.3). Factors such as the hydrogen-bonding network involving the pyrophosphate, and steric requirements for suitable bonding to copper may regulate this angle. The anion possesses approximate C_2 symmetry with the rotation axis passing through O(14) and bisecting the line joining P(1) and P(2). A truely staggered configuration of this anion should possess Cs symmetry, with the mirror plane containing P(1), O(14) and P(2). Some idea of the discrepancy from C_2 can be gained from examining the distances of pairs of rotationally related atoms from the P(1), O(14), P(2) plane*. The distances of these pairs of

* Plane (v) P(1), O(14), P(2)
0.1728X + 0.6324Y – 0.7551Z _ 2.8684 = 0
[O(11) 1.445, O(22) -1.423, O(12) -0.679, O(21) 0.547, O(13) -0.708, O(23) 0.915]
Distances of atoms from the plane (Å) are given in square brackets.

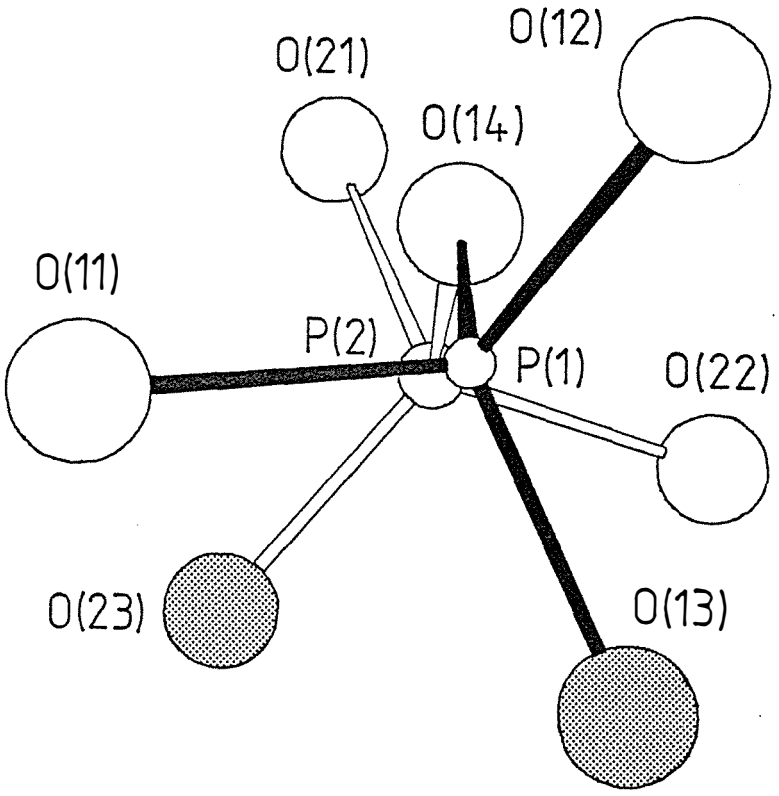

Figure 1.3.3: The $P_2O_7^{4-}$ moiety for $[(CuL)_4P_2O_7]\cdot 12H_2O$ showing the staggered arrangement. The two oxygen atoms not bound to copper are shown shaded.

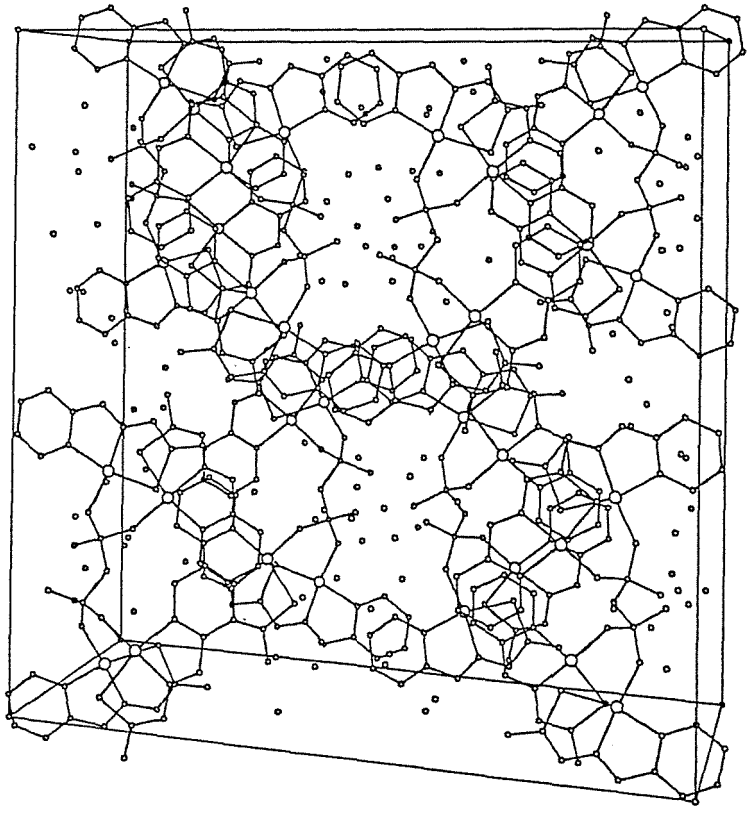

Figure 1.3.4: Unit-cell packing diagram for $[(CuL)_4P_2O_7]\cdot 12H_2O$

atoms (O(11) and O(22); O(12) and O(21); O(13) and O(23)) from the plane is greatest for O(13) and O(23) (29%), showing the symmetry to be only approximate.

An extensive hydrogen-bonding network involving the pyrophosphato oxygens, the thioamide and amine nitrogens and the water molecules helps to stabilise the crystal packing. All hydrogen-bonds are listed in Table 1.3.4 with their bond lengths. As the hydrogen positions were not located, N···O distances less than 3.2 Å, and O···O distances of less than 3.0 Å were considered as possible hydrogen-bonding contacts. Inspection of Table 1.3.4 reveals a number of distances involving the two disordered water molecules, O(112) and O(113), to be up to 0.4 Å shorter than the accepted conventional O-H···O value of 2.72 ± 0.04 Å [135]. Less credence was therefore placed on these. Also, the non-coordinated pyrophosphato oxygens, O(13) and O(23), both appear to have three contacts. No differentiation on the basis of the angles around these atoms could be made. This may be a reflection of disorder problems of the water molecules as the thermal parameters are relatively high.

The pyrophosphato moiety plays an integral role in the hydrogen-bonding scheme and, except for the bridging and one coordinated oxygen, (O(14) and O(12) respectively), all of the oxygen atoms are involved in hydrogen-bonds to water molecules. In the structure of [(thiaminepyrophosphato)(1,10-phenanthroline)aqua copper(II)] dinitrate hydrate [160] the ethyl ester pyrophosphate coordinates (in an eclipsed conformation) to the copper atom via two oxygens to form a six membered ring. Except for the two coordinated and the bridging oxygens, all the other pyrophosphato oxygens are involved in a hydrogen-bonding scheme. In the title complex $[(CuL)_4P_2O_7]\cdot 12H_2O$, not only are the two free oxygens (O(13) and O(23)), hydrogen-bound but also three of the coordinated pyrophosphato oxygens (O(11), O(21) and O(22)) are involved, in contrast with the previous example. This difference in the coordinated $P_2O_7^{4-}$ oxygen atoms does not appear to have affected the Cu-O bond distances. It may however account for the possibly significant difference in the P(1)-O(12) bond (1.487(7) Å) which is a little shorter than the other three comparable P-O bonds (viz. P(1)-O(11), P(2)-O(21) and P(2)-O(22) with an average bond length of 1.511(8) Å).

TABLE 1.3.4
Hydrogen-Bonding Distances (Å) for $[(CuL)_4P_2O_7]\cdot 12H_2O$

Atoms[a]	Distance (Å)	Symm[b]	T_x, T_y, T_z
N(14)···N(33)	2.965	7	0 $\bar{1}$ 0
N(14)···O(103)	3.033	7	0 $\bar{1}$ 0
N(24)···N(43)	2.997	7	0 0 0
N(24)···O(101)	2.873	1	0 0 0
N(34)···N(13)	2.952	7	0 0 0
N(34)···O(102)	3.096	1	0 0 0
N(44)···N(23)	3.048	7	0 $\bar{1}$ 0
N(44)···O(104)	3.139	1	0 0 0
O(11)···O(109)	2.817	6	0 0 0
O(21)···O(104)	2.822	6	0 0 0
O(22)···O(105)	2.895	1	0 0 0
O(13)···O(105)	2.780	1	0 0 0
O(13)···O(108)	2.693	1	0 0 0
O(13)···O(108)	2.802	3	0 0 0
O(23)···O(107)	2.662	8	$\bar{1}$ 0 $\bar{1}$
O(23)···O(109)	2.967	6	0 0 0
O(23)···O(113)[c]	2.542	1	0 0 0
O(101)···O(112)[c]	2.862	1	0 0 0
O(102)···O(106)	2.693	1	0 0 0
O(105)···O(107)	3.095	6	0 0 1
O(103)···O(107)	2.870	1	0 0 0
O(104)···O(110)	2.582	1	0 0 0
O(105)···O(105)	2.778	3	1 0 0
O(106)···O(109)	2.998	1	0 0 0
O(106)···O(110)	2.829	1	0 0 0
O(106)···O(110)	2.909	3	1 0 0
O(107)···O(108)	2.980	6	0 0 1
O(107)···O(112)[c]	2.486	1	0 0 0
O(108)···O(111)	2.742	6	0 0 1
O(109)···O(111)	2.901	3	1 0 0
O(110)···O(111)	2.621	1	0 0 0
O(111)···O(112)[c]	2.838	1	0 0 0
O(112)[c]···O(113)[c]	2.322	1	0 0 0
O(113)[c]···O(113)[c]	2.371	3	1 0 0

a the first atom is at symmetry position 1

b symmetry positions

1 (x, y, z)
2 ($\bar{x}$, $\bar{y}$, $\bar{z}$)
3 ($\bar{x}$, y, 0.5 - z)
4 (x, y, 0.5 + z)
5 (0.5 + x, 0.5 + y, z)
6 (0.5 - x, 0.5 + y, $\bar{z}$)
7 (0.5 - x, 0.5 + y, 0.5 - z)
8 (0.5 + x, 0.5 - y, 0.5 + z)

c disordered atom

Figure 1.3.4 shows the complicated packing involved in the unit-cell. A clearer picture of the stacking of the $[(CuL)_4P_2O_7]$ units can be gained however from Figures 1.3.5 and 1.3.6.

In Figure 1.3.5, two of the tetramers stack, one (the heavy bonds) over the top of the other. They are linked via mutually shared hydrogen-bonded water molecules and partial overlap of the pyridine rings. The closest approaches of the equivalent symmetry related pyridine ring atoms are 3.194 Å for C(43) to C(44) (symm 3; T_x, T_y,T_z 0 0 0 - see Table 1.3.4) and C(43) to C(41) at a distance of 3.297 Å (symm 2; T_x, T_y, T_z 0 0 0). The result, as can be seen in Figure 1.3.7, is a stacking of these pyridine rings, along the c axis, with approximately half of the ring involved in the overlap. The distances of closest approach between the carbon atoms in this stack alternates between 3.194 Å and 3.297 Å. These approaches appear to be sufficiently close for some π overlap between rings to be possible [97,161,174]. However, these interactions may help in the stabilisation of the crystal packing. A number of other inter-ligand contacts from 3.35 - 3.6 Å also occur (e.g. C(12)···C(11) - symm 6; T_x, T_y, T_z 0 0 0; 3.35 Å and C(17)···N(43) - symm 4; T_x, T_y, T_z 0 0 0; 3.34 Å) as part of the packing. In Figure 1.3.5 a number of hydrogen-bonds from the thioamide nitrogens and the terminal amine nitrogens (N(X3) and N(X4) respectively where X = 1-4) can be seen around the outside of the pair of tetramers. One of the amine interactions is with a thioamide nitrogen on a symmetry related tetramer; this molecule hydrogen-bonds back from its amine to the first thioamide nitrogen (average N···N contact of 2.991 Å). This results in pairs of tetramers being linked through such hydrogen-bonding contacts in a step-wise manner (see Figure 1.3.6). The hydrogen-bonds shown in this diagram are the same as those which appear in Figure 1.3.5 indicating the misleading conception of planarity for the pair of tetramers.

Each tetrameric unit is therefore hydrogen-bound via the pyrophosphato moieties and water molecules to another tetramer to give a stepped 'cyclic' structure with pyridine ring overlap. Reflection in the b-axis followed by a half-cell glide in c results in the stacking of these pairs of tetramers with a 'chain' of half-pyridine ring overlaps as shown schematically in Figure 1.3.7.

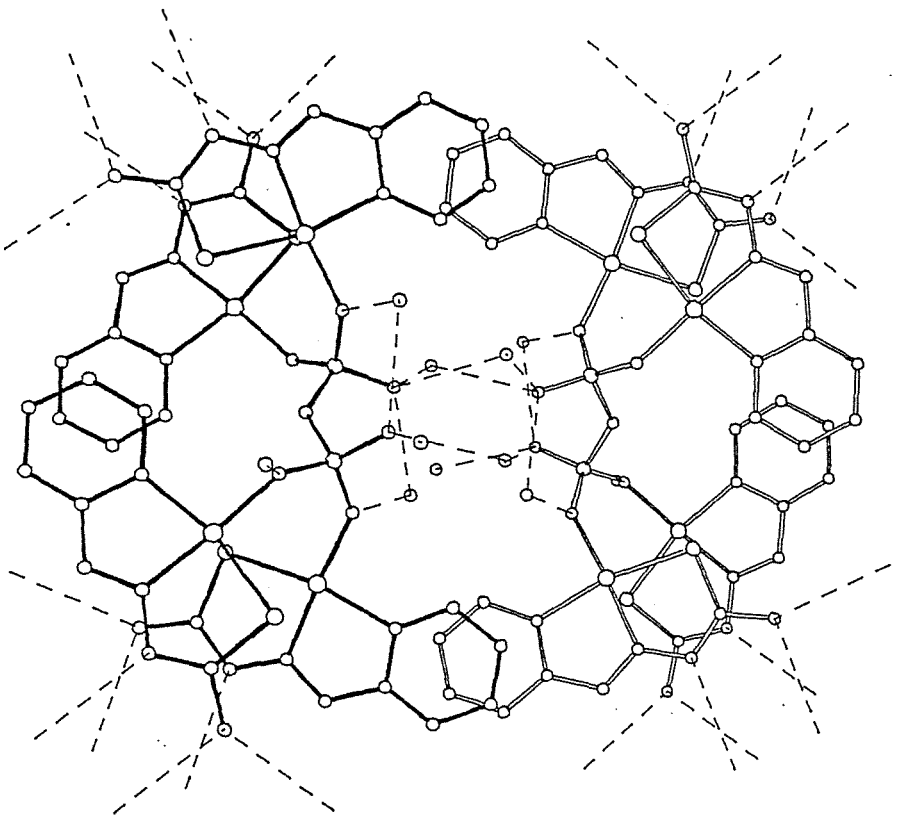

Figure 1.3.5: View of two $[(CuL)_4P_2O_7]\cdot 12H_2O$ tetramers with selected water molecules and hydrogen-bonds. Hydrogen atoms have been omitted for clarity.

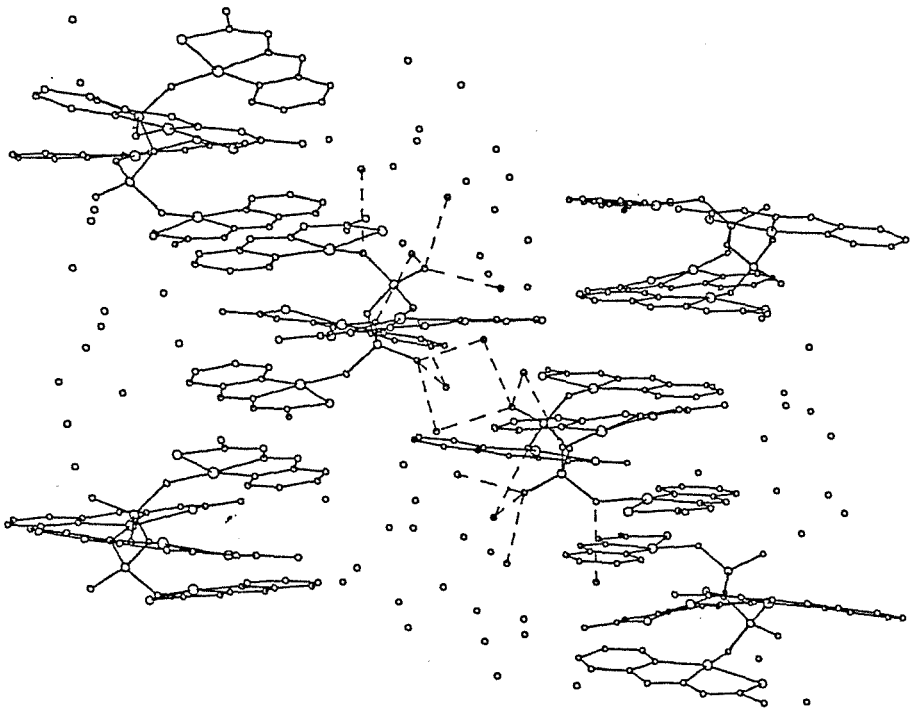

Figure 1.3.6: View showing the stacking for $[(CuL)_4P_2O_7]\cdot 12H_2O$ tetramers with the same hydrogen-bonds as Figure 1.3.5.

Each ligand hydrogen-bonds to the 'back' of another through its protonated nitrogens, linking tetramers in the ab plane. A large number of the water molecules have been found to occupy spaces left by the molecular packing. These are involved in a hydrogen-bonding network amongst themselves and with the pyrophosphato oxygens and amine nitrogens and help in the stabilisation of the structure. The overall effect, viewed down the c axis, as in Figure 1.3.5, is to form a honeycomb type of packing arrangement, the walls of which are made up of the overlapping pairs of tetramers and the cavity containing the pyrophosphate moieties and water molecules.

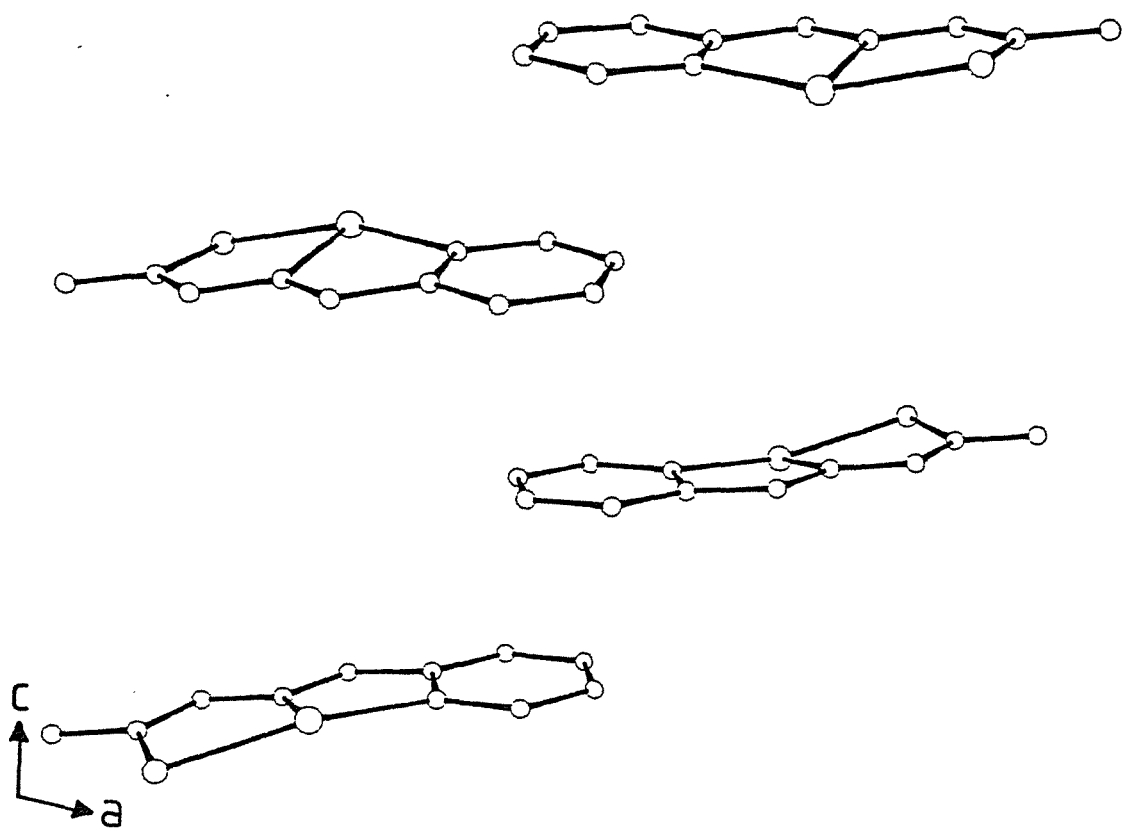

Figure 1.3.7: View of symmetry related CuL^+ moieties for $[(CuL)_4P_2O_7]\cdot 12H_2O$ showing the stacking and partial pyridine ring overlap.

1.3.3 CRYSTAL STRUCTURE OF Di-μ-dihydrogenphosphato-bis[(2-formylpyridine thiosemicarbazone)copper(II)] Bis(dihydrogenphosphate) Bis(trihydrogenphosphate) Dihydrate

A thermal ellipsoid diagram for the title complex (abbreviated as $[Cu(LH)(H_2PO_4)]_2(H_2PO_4)_2(H_3PO_4)_2.2H_2O$) showing the numbering scheme used is depicted in Figure 1.3.8. Bond length and bond angle data are given in Tables 1.3.5 and 1.3.6 respectively.

An attempt to synthesise a complex of the expected formulation $[Cu(LH)(PF_6)]_2(PF_6)_2$ from an aqueous solution of $[CuL(CH_3COO)]_2$ in HPF_6 resulted in dark green crystals after approximately two months (see Experimental section). The crystals analysed as $[Cu(LH)(H_2PO_4)]_2(H_2PO_4)_2(H_3PO_4)_2{\cdot}2H_2O$ instead, where the three inequivalent phosphates have been formed from the hydrolysis of the PF_6^- anions. There is precedence for such a hydrolysis [175] and for the existence of H_3PO_4 'solvates' of $H_2PO_4^-$ salts [176]. This phosphate complex crystallises as a discrete centrosymmetric dimer, bridged by two dihydrogenphosphato ($H_2PO_4^-$) ligands. The coordination environment around the copper(II) atom is very similar to that found in $[Cu(LH)(CF_3COO)]_2(CF_3COO)_2$ (in Chapter 1 (Figure 1.1.1) $[CuL(CH_3COO)]_2$ and $[Cu(LH)(SO_4)]_2$ [64]. The copper adopts a distorted square-pyramidal geometry comprised of the neutral, tridentate NNS constellation from LH (N(1), N(2) and S) and a dihydrogenphosphato oxygen, O(11), in the basal plane. The coordination sphere is completed by a more weakly coordinated bridging $H_2PO_4^-$ oxygen (O(11')) in the apical position. The copper atom lies out of the best-fit mean-plane calculated for the four basal atoms* by 0.092 Å towards the apical oxygen. There is a considerable distortion of these four coordinating atoms away from planarity with the average displacement from this plane being 0.118 Å with a chi-squared value of 27290. A weak sixth contact exists between the copper

* Plane (i) S, N(1), N(2), O(11)
-0.4446X – 0.0875Y – 0.8914Z + 1.3029 = 0
[S -0.106, N(1) -0.129, N(2) 0.133, O(11) 0.102, Cu 0.092]
Distances of atoms from the plane (Å) are given in square brackets.

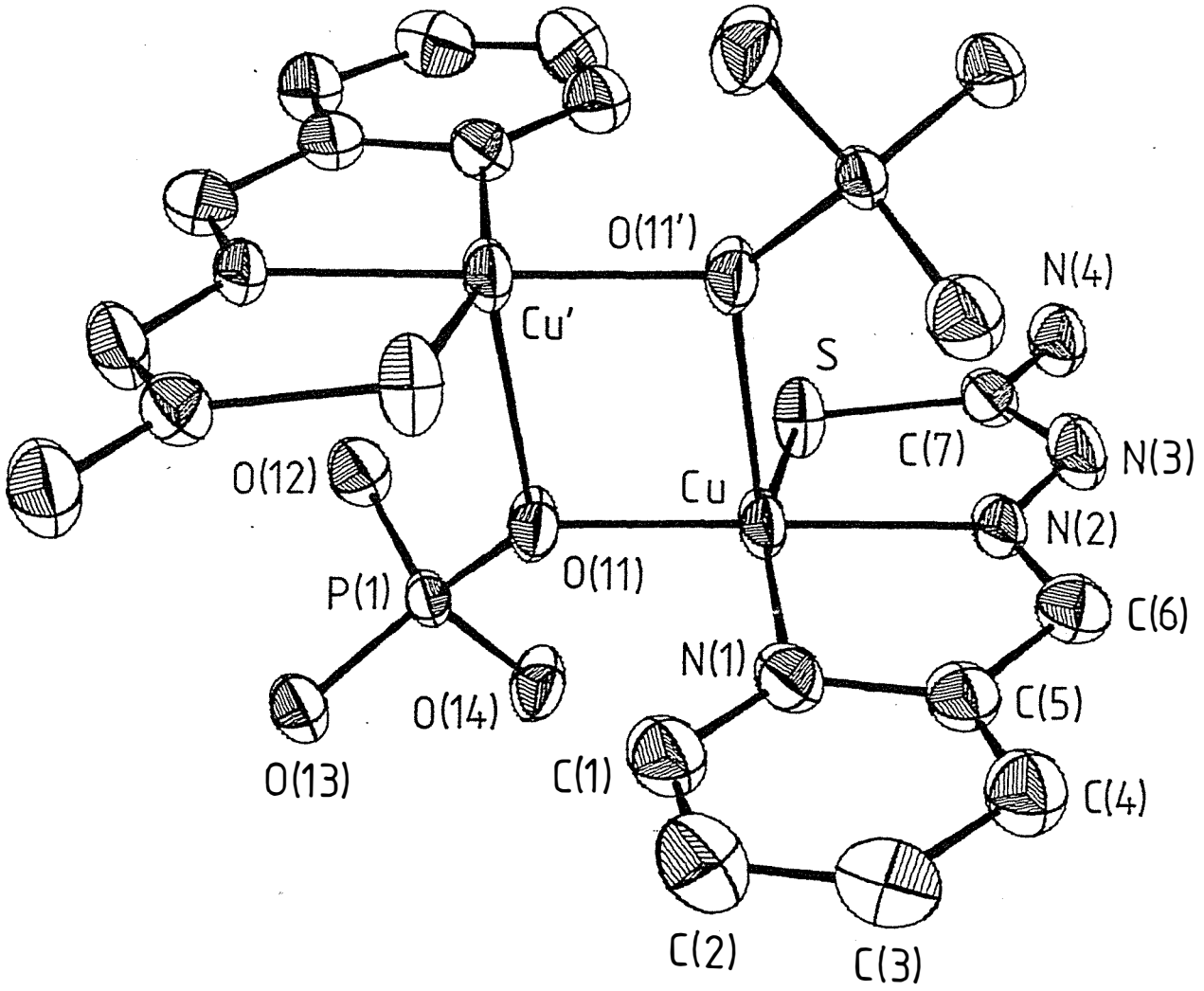

Figure 1.3.8: The dimeric cation for $[Cu(LH)(H_2PO_4)]_2(H_2PO_4)_2(H_3PO_4)_2{\cdot}2H_2O$ showing the atom numbering scheme. The non-coordinated phosphate and water molecules and hydrogen atoms have been omitted for clarity.

TABLE 1.3.5
Bond Lengths (Å) with Estimated Standard Deviations in Parentheses for the Complex $[Cu(LH)(H_2PO_4)]_2(H_2PO_4)_2(H_3PO_4)_2 \cdot 2H_2O$ *

Cu-N(1)	2.016(3)	Cu–N(2)	1.996(3)
Cu–S	2.283(1)	S–C(7)	1.714(3)
N(1)–C(1)	1.334(4)	N(1)–C(5)	1.376(4)
N(2)–N(3)	1.354(4)	N(2)–C(6)	1.282(4)
N(3)–C(7)	1.350(4)	N(4)–C(7)	1.313(4)
C(1)–C(2)	1.389(5)	C(2)–C(3)	1.364(5)
C(3)–C(4)	1.412(5)	C(4)–C(5)	1.374(4)
C(5)–C(6)	1.448(4)	Cu–O(11)	1.923(2)
Cu–O(11′)	2.444(6)	Cu···Cu′	3.295(3)
	Phosphato Bond Lengths (Å)		
P(1)–O(11)	1.522(2)	P(1)–O(12)	1.551(2)
P(1)–O(13)	1.509(2)	P(1)–O(14)	1.557(2)
P(2)–O(21)	1.525(3)	P(2)–O(22)	1.560(2)
P(2)–O(23)	1.504(2)	P(2)–O(24)	1.552(2)
P(3)–O(31)	1.495(3)	P(3)–O(32)	1.538(3)
P(3)–O(33)	1.556(3)	P(3)–O(34)	1.546(2)

* O–H bond lengths 0.93 – 1.02 Å, mean 0.96 Å
N–H bond lengths 0.73 – 0.95 Å, mean 0.84 Å
C–H bond lengths 1.06 – 1.13 Å, mean 1.09 Å

TABLE 1.3.6
Bond Angles (°) with Estimated Standard Deviations in Parentheses for the Complex $[Cu(LH)(H_2PO_4)]_2(H_2PO_4)_2(H_3PO_4)_2 \cdot 2H_2O$

N(1)–Cu–N(2)	80.7(1)	N(1)–Cu–S	161.2(1)
N(1)–Cu–O(11)	95.3(1)	N(1)–Cu–O(11′)	90.9(1)
N(2)–Cu–S	84.6(1)	N(2)–Cu–O(11)	175.5(1)
N(2)–Cu–O(11′)	95.3(2)	S–Cu–O(11)	99.8(1)
S–Cu–O(11′)	102.1(2)	O(11)–Cu–O(11′)	82.7(2)
Cu–O(11)–Cu′	97.3(2)	Cu–N(1)–C(1)	129.2(2)
Cu–N(1)–C(5)	112.5(2)	C(1)–N(1)–C(5)	117.9(3)
N(1)–C(1)–C(2)	122.9(2)	C(1)–C(2)–C(3)	119.1(3)
C(2)–C(3)–C(4)	119.6(3)	C(3)–C(4)–C(5)	118.1(3)
C(4)–C(5)–C(6)	124.0(3)	C(4)–C(5)–N(1)	122.4(3)
N(1)–C(5)–C(6)	113.6(3)	C(5)–C(6)–N(2)	116.6(3)
C(6)–N(2)–Cu	116.3(2)	N(3)–N(2)–Cu	119.9(2)
N(2)–N(3)–C(7)	117.2(3)	C(6)–N(2)–N(3)	123.7(3)
N(3)–C(7)–S	121.1(2)	N(3)–C(7)–N(4)	118.2(3)
S–C(7)–N(4)	120.6(2)	C(7)–S–Cu	96.3(1)
	Phosphate Bond Angles (°)		
O(11)–P(1)–O(12)	108.7(1)	O(11)–P(1)–O(13)	113.8(1)
O(11)–P(1)–O(14)	105.6(1)	O(12)–P(1)–O(13)	110.6(1)
O(12)–P(1)–O(14)	107.0(1)	O(13)–P(1)–O(14)	110.8(1)
O(21)–P(2)–O(22)	105.9(1)	O(21)–P(2)–O(23)	112.8(1)
O(21)–P(2)–O(24)	108.4(1)	O(22)–P(2)–O(23)	112.3(1)
O(22)–P(2)–O(24)	108.6(1)	O(23)–P(2)–O(24)	108.6(1)
O(31)–P(3)–O(32)	114.4(1)	O(31)–P(3)–O(33)	112.8(2)
O(31)–P(3)–O(34)	111.1(2)	O(32)–P(3)–O(33)	102.8(2)
O(32)–P(3)–O(34)	107.8(2)	O(33)–P(3)–O(34)	107.5(2)
Cu–O(11)–P(1)	128.7(1)	Cu′–O(11)–P(1)	130.3(2)

atom and the bridging dihydrogenphosphato group. This contact of 3.144(3) Å between Cu and O(14) (O(11)-Cu-O(14) angle of 51.2(3)°) is the longest found for the four centrosymmetric, anion bridged complexes of copper(II) with this ligand (see Table 1.3.7). The two acetato complexes in Table 1.3.7 display similar bond distances and angles, the differences being related to the different basicities of the anions. Analysis of the data presented, in going from the acetato complexes to those of the tetrahedral sulphato and dihydrogenphosphato anions, shows several major changes (e.g. an average Cu-O distance of 1.950(3) Å is found for the acetato containing complexes whereas an average value of 1.923(2) Å is observed for the SO_4^{2-} and $H_2PO_4^-$ analogues). A comparison with therefore be made with the sulphato complex.

Although the Cu-O bonds lengths from Table 1.3.7 are comparable, the bridging bond length, Cu-O′, is 0.138 Å longer for the $H_2PO_4^-$ complex than for the SO_4^{2-} case. In the case of the acetato complexes, the longer CF_3COO^- Cu-O′ bond compared with the CH_3COO^- was attributed to the weaker basicity of the trifluoroacetato anion. Analogous reasoning for the $H_2PO_4^-$ and SO_4^{2-} complexes would predict that the Cu-O′ bond of the sulphato anion will be the longer (pKa SO_4^{2-} = 1.92, pKa H_3PO_4 = 2.12 [96]). As this is not observed other factors must also be involved. The O-Cu-O′ angle for the title complex is 82.7(2)° compared with an average value of 76.3(11)° for the other three compounds in Table 1.3.7. This widening of the angle between the in-plane and axial, bridging anions of 6.4° may account for the previously discussed difference in the bridging Cu-O′ bond lengths. One effect is to bring the two copper atoms in the dimer closer together, as seen in the Cu···Cu′ distances of 3.295(2) Å for $[Cu(LH)(H_2PO_4)]_2(H_2PO_4)_2(H_3PO_4)_2.2H_2O$ and 3.46(9) Å for the average of $[Cu(LH)(SO_4)]_2$, $[Cu(LH)(CF_3COO)]_2(CF_3COO)_2$ and $[CuL(CH_3COO)]_2$. A possible cause of this change is altered crystal packing forces.

The 2-formylpyridine thiosemicarbazone ligand, LH, displays the expected tridentate (NNS) coordination mode with normal bonding parameters [64,this work]. The copper to phosphato

TABLE 1.3.7
Selected Bond Distance (Å) and Angle (°) Data for Centrosymmetric Anion Bridged Complexes of Copper(II) with LH/L⁻

	$[Cu(LH)(CF_3COO)]_2(CF_3COO)_2$	$[CuL(CH_3COO)]_2$[a]	$[Cu(LH)(SO_4)]_2$[a]	$[Cu(LH)(H_2PO_4)]_2(H_2PO_4)_2(H_3PO_4)_2$
Cu–O (Å)[b]	1.948(3)	1.951(1)	1.922(2)	1.923(2)
Cu–O′(Å)[c]	2.516(4)	2.427(2)	2.306(2)	2.444(6)
Cu···O″(Å)[d]	2.921(3)	2.925(2)	3.128(2)	3.144(3)
Cu···Cu′(Å)	3.557(4)	3.450(2)	3.376(2)	3.295(2)
O–Cu–O′(°)	75.1(2)	76.5(1)	77.3(1)	82.7(2)
O–Cu–O″(°)	49.7(2)	49.0(1)	50.3(1)	51.2(2)

a after [64]
b O is the inplane coordinated anion oxygen
c O′ is the apically coordinated bridging anion oxygen
d O″ is the weakly contacting anion oxygen in the sixth coordination position

TABLE 1.3.8

Hydrogen-Bonding Distances (Å) and Angles (°) for $[Cu(LH)(H_2PO_4)]_2(H_2PO_4)_2(H_3PO_4)_2 \cdot 2H_2O$

Bond D–H···A[a]	D–H(Å)	H···(Å)	D···A(Å)	D–H···A(°)	Symm[b]	T_x	T_y	T_z
O(12)–H(12)···O(31)	1.022	1.581	2.588	167.4	2	0	0	0
O(14)–H(14)···O(23)	0.974	1.558	2.529	174.9	4	1	0	0
O(22)–H(22)···O(32)	0.927	1.684	2.608	174.5	1	1	0	0
O(24)–H(24)···O(13)	0.951	1.587	2.539	179.9	1	0	0	0
O(32)-H(32)···O(21)	0.960	1.482	2.442	178.3	4	0	$\bar{1}$	0
O(33)–H(33)···O(13)	0.940	1.697	2.634	174.7	2	0	0	0
O(34)–H(34)···O(21)	0.969	1.662	2.630	176.7	3	$\bar{1}$	$\bar{1}$	$\bar{1}$
O(1)–H(101)···O(14)	0.925	2.061	2.986	177.5	4	0	0	0
O(1)–H(102)···O(31)	0.951	1.944	2.895	179.3	1	0	1	0
N(3)–H(31)···O(23)	1.080	1.693	2.735	160.5	1	$\bar{1}$	0	0
N(4)–H(41)···O(1)	0.830	2.054	2.855	162.4	1	0	0	0
N(4)–H(42)···O(24)	0.733	2.283	2.954	152.6	1	$\bar{1}$	0	0

a Donor–Hydrogen···Acceptor; D–H at symmetry position 1
b symmetry positions
1 (x, y, z)
2 ($\bar{x}$, $\bar{y}$, $\bar{z}$)
3 ($\bar{x}$, 0.5 + y, 0.5 - z)
4 (x, 0.5 - y, 0.5 + z)

oxygen bond distance of 1.923(2) Å in the plane agrees well with literature values for phosphato coordinated nucleotides to Cu(II) [160-162].

The complex appears to be unique in the literature at present in that it is the only reported ternary complex of copper containing dihydrogenphosphate anions for which a crystal structure has been determined. The paucity of data for such systems (as mentioned in the introduction) is most probably due to the insolubility of the $Cu_3(PO_4)_2 \cdot 3H_2O$ salt as a starting material [96]. It also appears to have the distinction of being the only complex presently to have coordinated and non-coordinated dihydrogenphosphate anions within the one structure.

The coordinated dihydrogenphosphato group in this complex links the two copper atoms in the dimer by a one-atom bridge. A literature survey of copper(II) complexes with unsubstituted or substituted phosphato moieties failed to reveal any single atom phosphato bridges. A number of nucleotide phosphates however are coordinated in dimeric complexes but invariably have three-atom bridges (e.g. Cu-O-P-O-Cu' [161,162,177-179]). The formation of a single atom bridge, again, appears to be a literature first. This follows the trend for the dimeric copper(II) complexes with this ligand where the unusual one oxygen atom bridging modes for both acetato and sulphato species have been observed [64,this work].

Within the phosphate ions, the P-O distances range from 1.495(3) to 1.560(2) Å with a mean value of 1.535(23) Å. This value agrees well with that found for $KH_5(PO_4)_2$ [176] in which there is strong hydrogen-bonding, and is in accord with a bond order of approximately 1.5. The P-O bond length data presented in Table 1.3.5 can be grouped into three categories. In the first of these, containing six of the twelve bonds, the P-O distance is significantly longer than the others. The oxygen atoms involved (O(12), O(14), O(22), O(24), O(33) and O(34)) have a mean P-O bond length of 1.554(5) Å and can be considered to belong to hydroxyl groups. The mean value for P-OH bonds in $KH_5(PO_4)_2$ [176 and refs. therein] of 1.555 Å is in close agreement with this result.

In the second group, containing the three oxygens O(13), O(23) and O(31) the mean P-O bond distance is 1.503(7) Å and these correspond to 'keto' (P=O) oxygens. The analogous bonds from ref. [176] are 1.502 Å, again in close agreement.

The average bonding distance of 1.528(9) Å for the remaining three oxygens, O(11), O(21) and O(32) is intermediate between the 'pure' hydroxyl and keto lengths found in the two previous groups. For O(11), this undoubtedly is due to its being involved in bonding to the copper centres but for the other two oxygens a different explanation must be invoked.

One possibility is that the hydrogen, H(32), formally assigned as bonded to O(32) and involved in a very short hydrogen-bond to O(21) (2.442 Å - see Table 1.3.8) actually participates in a symmetrical hydrogen-bond (i.e. may be shared equally between O(21) and O(32)). Whereas the location of the hydrogen atom positions from difference electron density maps for the title structure was generally straightforward, the hydrogen, H(32), attached to O(32) was difficult to locate. The final position chosen is close to O(32) and leaves no large residual peaks in the difference electron density map, but does not exclude the possibility of a symmetrical bond. Its existence is supported by the P(2)-O(21) and P(3)-O(32) bond distances which are both significantly shorter than the 'pure' P-OH bonds and longer than the P=O bonds. Also, the hydrogen-bond between O(32) and O(21) of 2.442 Å is significantly shorter than the average for the other interphosphate contacts of 2.588(45) Å and ranks amongst the shortest ever found [176,180,181]. A very similar situation exists in the compound $KH_5(PO_4)_2$ [176] where the possibility of a symmetrical hydrogen-bond has been postulated between two phosphate oxygens with a separation of 2.405 Å.

The O(21)···O(32) contact is only one of a number of hydrogen-bonds involved in the stabilisation and packing of the dimeric $[Cu(LH)(H_2PO_4)]_2(H_2PO_4)_2(H_3PO_4)_2.2H_2O$ units and the noncoordinated water and phosphate molecules. Table 1.3.8 lists the hydrogen-bonding data and in Figure 1.3.9 a stereoscopic view of the unit-cell packing is given. In this diagram it can be seen that rows of dimers related by the 2-fold screw axis along the c direction

are separated by a column of hydrogen-bonded di/trihydrogenphosphates. The dimers between these rows are all connected via a hydrogen-bonding network.

In Figures 1.3.10 (a), (b) and (c) the hydrogen-bonding scheme around each of the three phosphate anions is depicted. In Figure 1.3.10(a), the coordinated dihydrogenphosphato moiety is involved in a total of five contacts, four to the remaining two uncoordinated phosphate oxygens and one to the water molecule, O(1). Figures 1.3.10(b) and (c) show the hydrogen-bonds around the di/trihydrogenphosphates for P(2) and P(3) respectively. Two of the oxygens of P(2), namely O(23) and O(24), form hydrogen-bonds to the protons H(31) and H(42) of the protonated thioamide, N(3), and amine, N(4), nitrogens of the organic ligand with N···O distances of 2.735 and 2.954 Å respectively. These are a part of the seven contacts for the P(2) phosphate shown in the figure. With the P(3) anion the total number of contacts is six.

The water molecule is involved in three contacts. It is coordinated to O(14) and O(31) with hydrogen-bonding distances of 2.986 and 2.895 Å respectively, linking the two phosphates. In addition it is bound to the terminal amine nitrogen of the ligand at a distance of 2.855 Å. The overall effect of this hydrogen-bonding network is to form a stable and (apart from the previously mentioned possibly symmetric hydrogen-bond) well defined structure for this novel complex.

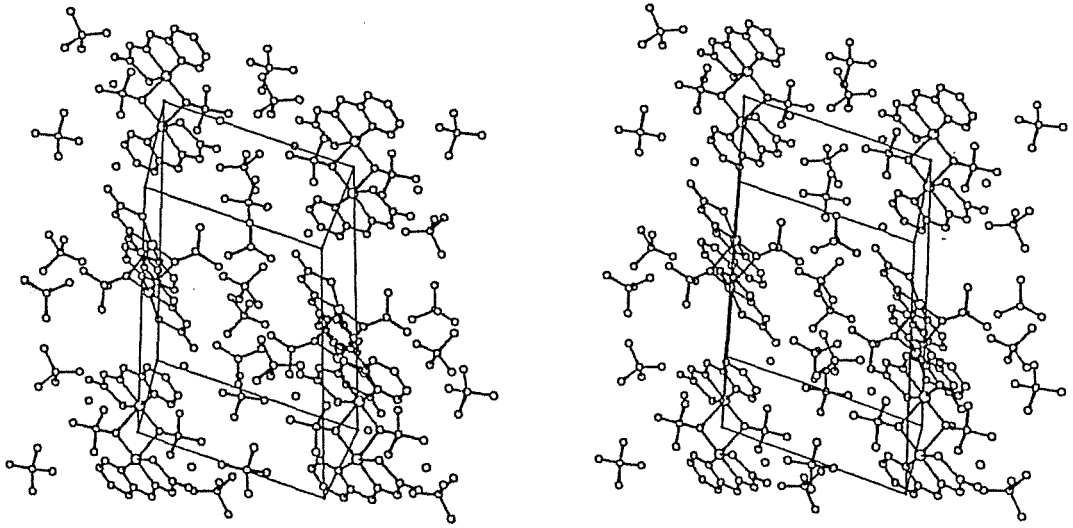

Figure 1.3.9: Stereo-view of the unit-cell packing diagram for $[Cu(LH)(H_2PO_4)]_2(H_2PO_4)_2(H_3PO_4)_2{\cdot}2H_2O$.

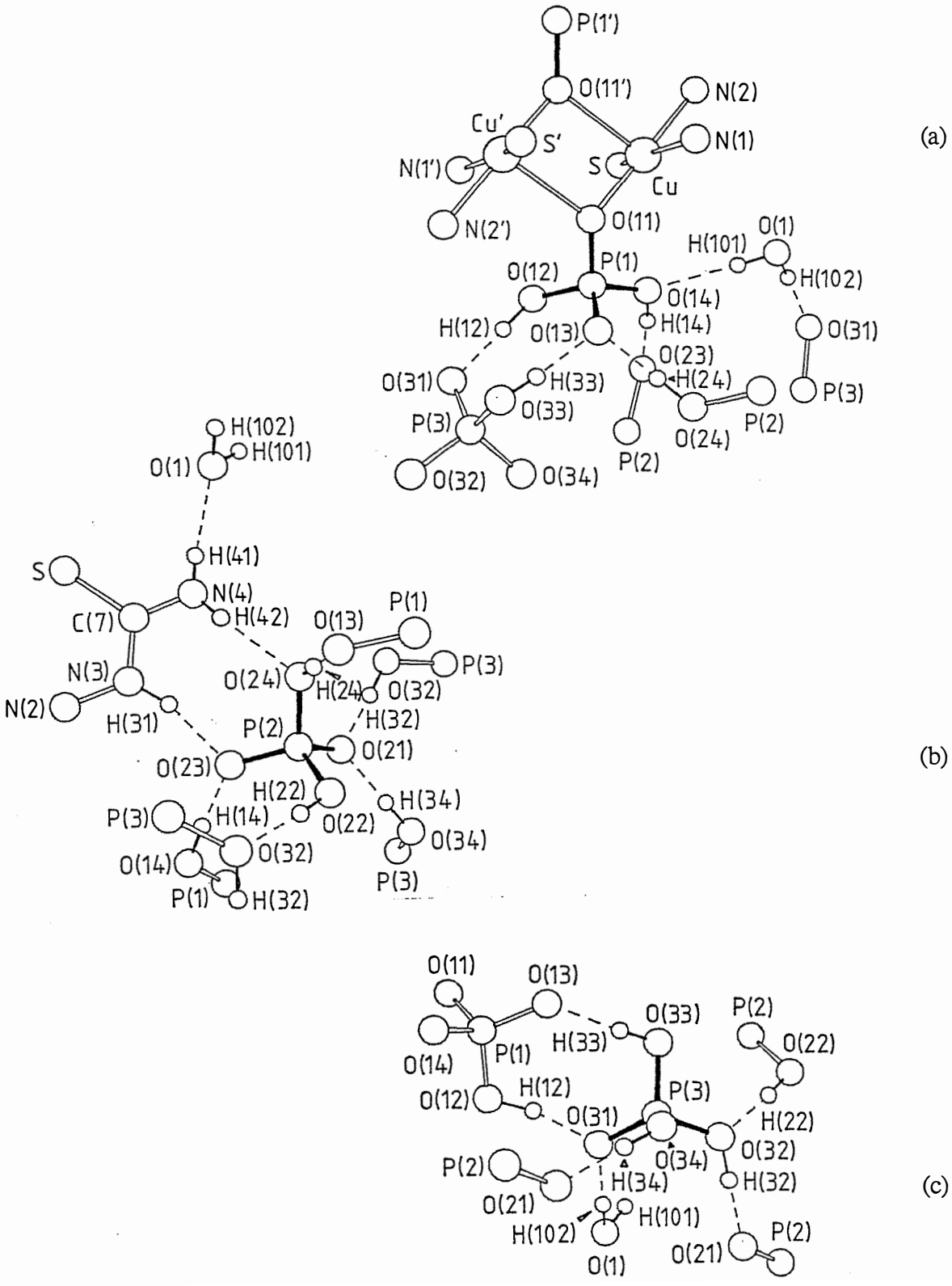

Figure 1.3.10: The hydrogen-bonding schemes around each of the three phosphate species for $[Cu(LH)(H_2PO_4)]_2(H_2PO_4)_2(H_3PO_4)_2{\cdot}2H_2O$

(a) the coordinated bridging $H_2PO_4^-$

(b) the non-coordinated '$H_2PO_4^-$' anion

(c) the non-coordinated 'H_3PO_4' molecule.

1.3.4 RESULTS AND DISCUSSION

1.3.4(a) Electronic Spectra

Analytical and room temperature magnetic moment data are presented in Table 1.3.1 whereas the electronic absorption maxima and molar conductance data are in Table 1.3.9.

The charge-transfer (c.t.) maxima positions in the solid state (mull transmittance) and solution are comparable with those in the preceding chapters. The maxima for the phenolato complexes, $[CuL(ptp)]\cdot 2H_2O$ and [CuL(tip)], do however show considerable broadening, with a tail running into the visible which tends to obscure any d-d transitions. This may result from a phenolato $\rightarrow$ copper(II) c.t. band being superimposed upon the low energy side of the S $\rightarrow$ Cu(II) c.t. band from the ligand. The assignment by Ainscough *et al.* [182] of an intense c.t. band around 410-545 nm, for a range of Cu(II) phenolato complexes, as $Op_\pi \rightarrow Cud\sigma^*$ adds credence to this.

The d-d maxima which fall in the range of 605-713 nm are consistent with the distorted square-pyramidal/tetragonal stereochemistry found for the structures of $[(CuL)_4P_2O_7]\cdot 12H_2O$, $[Cu(LH)(H_2PO_4)]_2(H_2PO_4)_2(H_3PO_4)_2\cdot 2H_2O$ and those in the two preceding chapters. The resolution of an additional weak band at 961 nm in the aqueous solution spectrum of $[(CuL)_4P_2O_7]\cdot 12H_2O$ may indicate the presence of the copper(II) centres in an elongated octahedral stereochemistry [105].

The molar conductance values in Table 1.3.9, as found in the preceding chapters, indicate that in dmso the complexes are non-electrolytes or only partially ionised. The two neutral ligand dihydrogenphosphato complexes in water are both strong acids and have conductance values consistent with extensive ionisation. The value of 579 s mol^{-1} l for $\frac{1}{2}([Cu(LH)(H_2PO_4)]_2(H_2PO_4)_2(H_3PO_4)_2\cdot 2H_2O)$ is consistent with approximately 9 charges

TABLE 1.3.9

Absorption Maxima and Conductance Data for Chapter 3

Complex[a]	Absorption Maxima (nm)[b] Charge Transfer	d–d	Molar Conductance[c] (s mol^{-1} l)	Solvent[d]
$[(CuL)_4P_2O_7]\cdot 12H_2O$	426	640 (sh)		m.t.
	412 (11 100)	628 (110; br)	4	dmso
	384	630 961(br;wk)		H_2O
$[(CuL)_2HPO_4]\cdot 6H_2O$	440	605		m.t.
	414	630 (sh)		dmso
	413			CH_3NO_2
$[Cu(LH)(H_2PO_4)]_2(H_2PO_4)_2$	404	713		m.t.
$\cdot 3H_2O$	415 (11 000)	635 (120; br)	3	dmso
	383 (10 100)	633 (170)	329	H_2O
$[Cu(LH)(H_2PO_4)]_2(H_2PO_4)_2$	394	670 (br)		m.t.
$(H_3PO_4)_2\cdot 2H_2O$	415 (13 800)	632 (200; br)	22	dmso
	385 (11 130)	637 (190; br)	579	H_2O
$[CuL(ptp)]\cdot 2H_2O$	427	654		m.t.
	413 (10 700)	(sh)	0	dmso
	406	(sh)		EtOH
[CuL(tip)]	415			m.t.
	415 (13 800)		9	dmso
	419			acetone
$[(CuL)_2MoO_4]H_2O$	430	600 (sh)		m.t.
	414 (12 000)	632 (200)	4	dmso

a see page X for abbreviations
b extinction coefficients given in parentheses (l mol^{-1} cm^{-1})
c for typical molar conductance ranges see Appendix 3
d m.t. = mull transmittance

per molecule. The measured pH of a 1.76×10^{-3} M solution of this complex is 2.34 pH units, therefore it was assumed that the ligand deprotonates and only the first ionisation of phosphoric acid occurs. If the following dissociation occurs;

$$\text{'Cu(LH)(H}_2\text{PO}_4)_2(\text{H}_3\text{PO}_4)\text{'} \xrightarrow{\text{H}_2\text{O}} \text{CuL}^+ + 2\text{H}^+ + 3(\text{H}_2\text{PO}_4^-)$$

only 6 charges result. The remaining 3 charges, by analogy with $[Cu(LH)(ClO_4)_2H_2O]\cdot 2H_2O$ and $[Cu(LH)(NO_3)_2H_2O]$ (see Chapter 1 discussion), are considered to result from acid adhering to the crystals. As this complex is hygroscopic and showed some solubility in common organic solvents, attempts to totally remove this excess acid were not undertaken. The calculated pH of this solution, assuming 4 protons to be ionised, is 2.15, in reasonable agreement with the measured value of 2.34. Similar reasoning was applied to account for the complex $[Cu(LH)(H_2PO_4)]_2(H_2PO_4)_2\cdot 3H_2O$ which has a molar conductance value (per copper atom) of 329 s mol^{-1} l in aqueous solution. This value is consistent with 5 charges but, as the complex ionisation accounts for only 4 charges, the remaining 1 may again result from adherent acid. The measured and calculated pH values for this complex in aqueous solution are 3.00 and 2.62 respectively.

1.3.4(b) Infrared Spectra

The primary use of the ir spectra again was in anion identification, therefore selected anion bands are presented in Table 1.3.10. The easily identifiable bands displayed by the complexes $[(CuL)_4P_2O_7]\cdot 12H_2O$ and $[(CuL)_2MoO_4]H_2O$ are indicative of the presence of the pyrophosphato [140] and molybdato [107] anions respectively. The positioning of the two broad peaks at 1 020 and ~980 cm^{-1} in the two dihydrogenphosphato complexes shows the anion to be monodentate [183]. The 980 cm^{-1} band is very broad and assymetric, possibly containing another absorption which is expected at ~934 cm^{-1}. An additional peak which may have been expected from the non-coordinated di/trihydrogenphoshates at ~1 080 cm^{-1} coincides with a ligand band and was not resolved. The appearance of three ir active absorptions at

TABLE 1.3.10

Selected Anion Infrared Bands for Chapter 3

Complex	bands (cm^{-1})		
$[(CuL)_4P_2O_7]\cdot 12H_2O$	1 153 (s;br)	1 085 (s)	933 (s)
$[(CuL)_2HPO_4]\cdot 6H_2O$	1 115 (s)	1 055 (m)	890 (m;br)
$[Cu(LH)(H_2PO_4)]_2(H_2PO_4)_2\cdot 3H_2O$	1 020 (s;br)	982 (s;br)	
$[Cu(LH)(H_2PO_4)]_2(H_2PO_4)_2$ $(H_3PO_4)_2\cdot 2H_2O$	1 020 (s;br)	980 (s;br)	
$[(CuL)_2MoO_4]H_2O$	894 (s)	817 (m)	

TABLE 1.3.11

Theoretical Values of 2J from μ_{eff} and g

Complex	μ_{eff}[a]	$g_{i(measured)}$[b]	2J[c](cm^{-1})
$[CuL(CH_3COO)]_2$	1.82	2.113	-9[d]
$[(CuL)_4P_2O_7]\cdot 12H_2O$	1.83	2.131	-14[e]
$[Cu(LH)F]_2F_2$	1.45	2.129	-250
$[Cu(LH)I]_2I_2$	0.43	2.073	-860
$[CuL(NO_3)]_2$	1.42	2.040	-240
$[CuL(ClO_4)]_2$	1.34	2.155	-320
$[CuL(ntp)]_2\cdot 6H_2O$	1.59	2.077	-150
$[Cu(LH)(SO_4)]_2$	1.86	2.170	-16
$[Cu(LH)(CF_3COO)]_2(CF_3COO)_2$	1.83	2.092	17
$[Cu(LH)(H_2PO_4)]_2(H_2PO_4)_2(H_3PO_4)_2\cdot 2H_2O$	1.84	2.158	-24

a measured at 293 K and quoted in B.M. per copper(II) ion

b isotropic g value calculated from the powder e.s.r. data

c calculated from $-2J = kT\ln\left(\frac{3.003\ g^2}{\mu_{eff}^2} - 3\right)$ after [188] where k is the Boltzmann's constant and T is the absolute temperature

d fitted value from variable temperature susceptibility data is -6.2 cm^{-1}

e fitted value from variable temperature susceptibility data is -6.0 cm^{-1}

1 115, 1 055 and 890 cm^{-1} in $[(CuL)_2HPO_4]\cdot 6H_2O$ is indicative of a bidentate phosphato anion [183]. The monohydrogenphosphate may therefore form a three-atom bridge between two copper centres or chelate to one copper atom. All spectra showed a large, broad absorption between ~3 000 and 3 500 cm^{-1}, consistent with the presence of water of crystallisation [107].

1.3.4(c) Magnetic Properties

A number of the room temperature magnetic moments presented in the first three chapters have been depressed (relative to the spin only value of 1.73 B.M.), typical of strongly antiferromagnetically coupled copper(II) complexes. Of the eight X-ray crystallographic structures carried out on copper(II) complexes with the ligand 2-formylpyridine thiosemicarbazone, four are anion bridged dimers (where the anions are SO_4^{2-} and CH_3COO^- [64] and $H_2PO_4^-$ and CF_3COO^- [this work]) and another is the tetrameric complex $[(CuL)_4P_2O_7]\cdot 12H_2O$. Although the room temperature moments for these five complexes have normal spin-only values, at low temperature, magnetic interaction between the two copper(II) centres should be possible. Because of this, the variable temperature magnetic susceptibilities of two of these complexes, $[CuL(CH_3COO)]_2$ and $[(CuL)_4P_2O_7]\cdot 12H_2O$, were kindly measured by Dr Keith S. Murray and Christopher Delfs of Monash University.

As displayed in Figure 1.3.11(a) for $[CuL(CH_3COO)]_2$, the molecular susceptibilities show a rapid increase as the temperature approaches 0 K, with a maxima at approximately 6 K. Below 6 K the susceptibilities decrease, as is typical of weakly antiferromagnetically coupled copper(II) complexes. The data were fitted very well by the Bleany-Bowers expression [184] for a spin coupled $S_1 = S_2 = ½$ system with best-fit parameters of $g = 2.114$, $2J = -6.2$ cm^{-1} and no monomer present. The magnetic moment vs. temperature plot depicted in Figure 1.3.11 (b) shows the moment to be nearly constant down to approximately 30 K. Below this temperature, the moment drops rapidly as spin-pairing of the two copper centres in the dimer occurs. This is consistent with the powder e.s.r. spectrum which does not show a signal corresponding to $\Delta Ms = 2$ at 110 K. The very low value of 2J, the singlet-triplet splitting

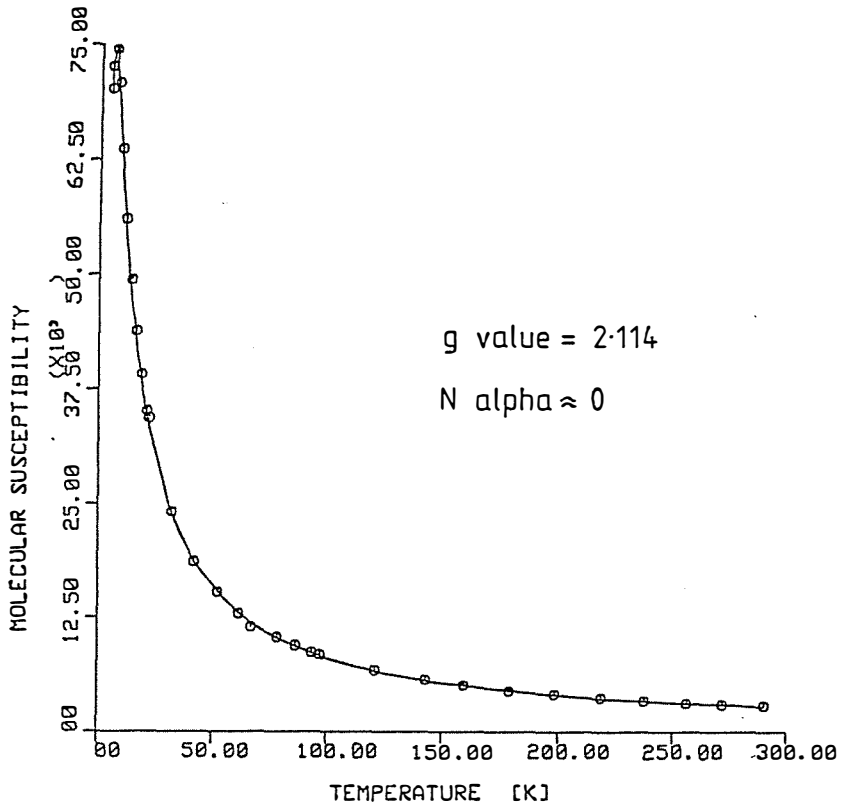

(a)

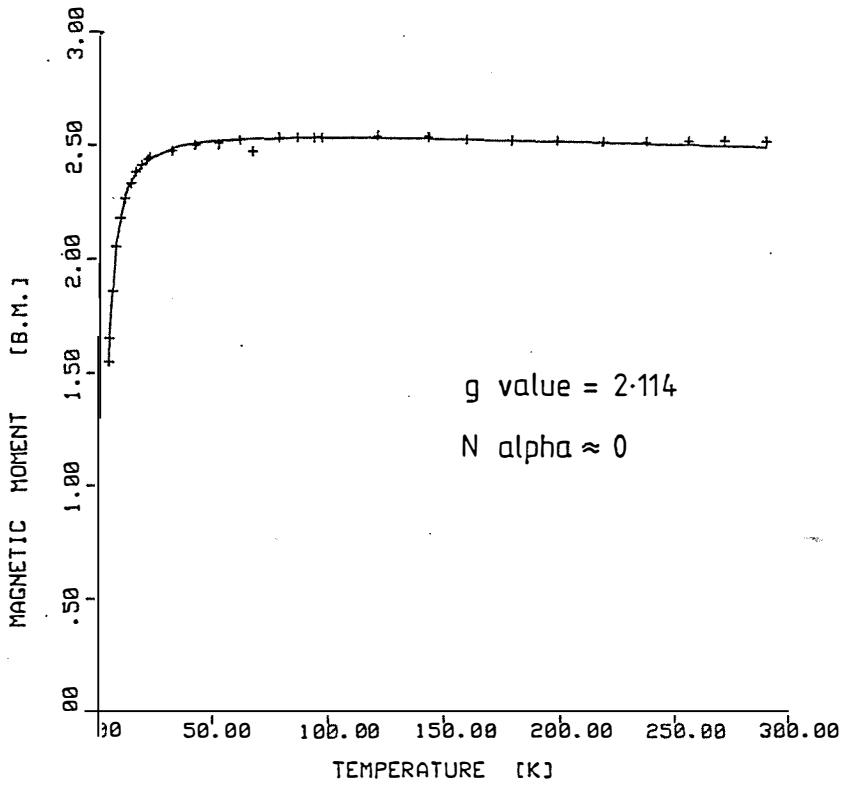

(b)

Figure 1.3.11: Temperature dependence of $[CuL(CH_3COO)]_2$ for (a) the molecular susceptibilities and (b) the magnetic moments. The solid lines are those calculated using the parameters given in the text.

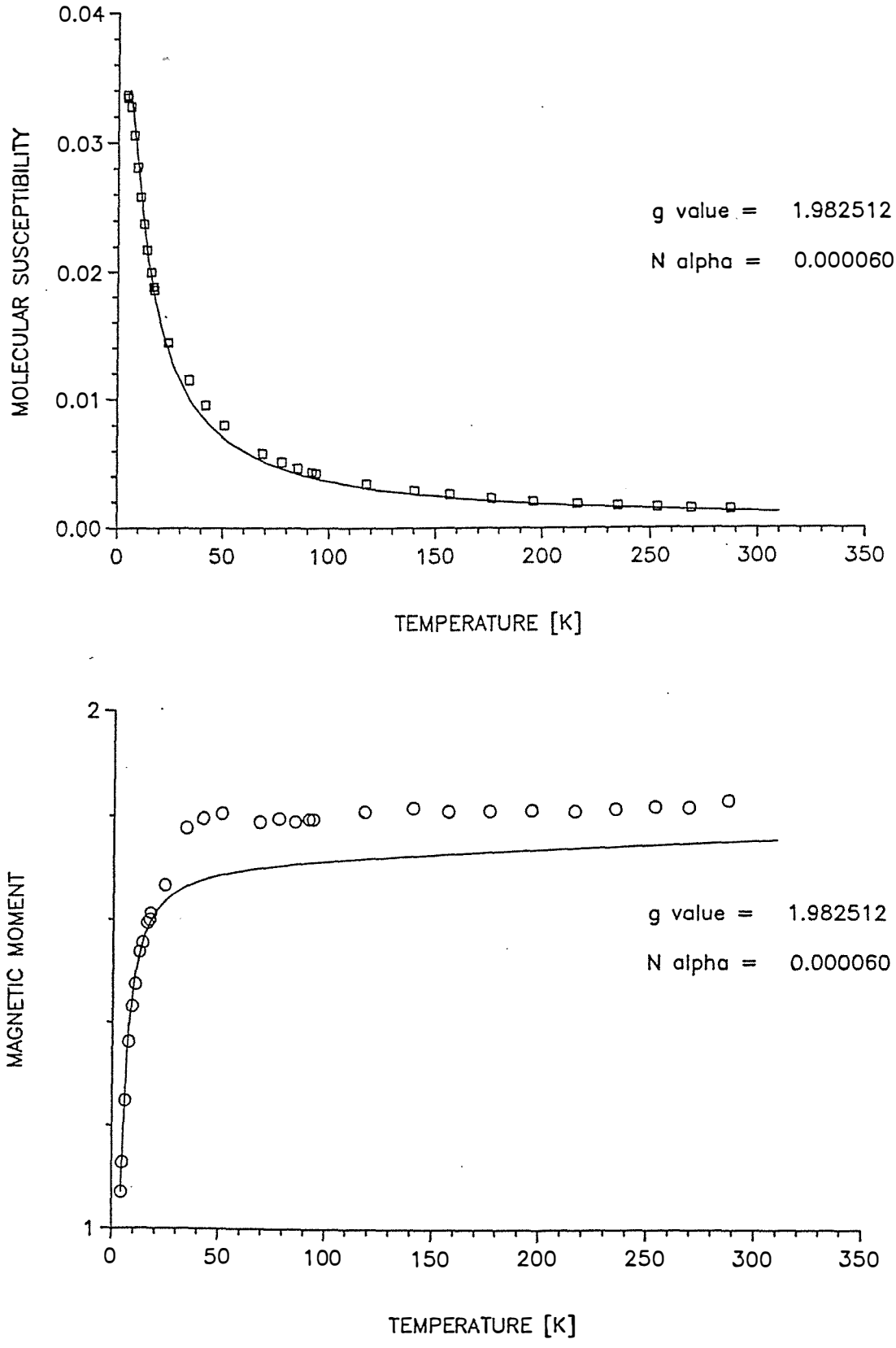

Figure 1.3.12: Temperature dependence of $[(CuL)_4P_2O_7]\cdot 12H_2O$ for (a) the molecular susceptibilities and (b) the magnetic moments. The solid lines are those calculated using the parameters given in the text.

energy, presumably arises because of poor overlap of the magnetic orbitals. This is in accord with the crystal structure [64,65] which shows the dimer to have acetato groups bridging the two copper atoms, stacking the two CuL(acetato) moieties. The in-plane Cu-O (acetato) bonding distance is 1.951(1) Å whereas the out of plane (apical) length is 2.427(2) Å with a Cu-O-Cu′ angle of 103.5(1)°. This long, off-axis, apical bond therefore may provide only weak overlap of the $d_{x^2-y^2}$ orbitals. A crystallographically similar situation exists in the structures of $[Cu(LH)(CF_3COO)]_2(CF_3COO)_2$, $[Cu(LH)(H_2PO_4)]_2(H_2PO_4)_2(H_3PO_4)_2{\cdot}2H_2O$ [this work] and $[Cu(LH)(SO_4)]_2$ [64], indicating analogous magnetic behaviour may occur in these complexes.

In the structure of $[Cu_2Cl_2(sap)_2]{\cdot}dmf{\cdot}H_2O$ (sapH = salicylaldehyde 2-amino-1-phenylethanol) the monoanionic, tridentate sap^- moiety coordinates in the plane with the fourth position occupied by a chloride ion (bond length of 2.261(2)Å) [185]. The complex is a dimer, with the chloride ion forming a long bridge (2.82(2)Å) between the Cu(II) centres giving a distorted square pyramidal geometry. The magnetic susceptibilities, measured down to 5·1K, showed a weak antiferromagnetic spin coupling which, on fitting to the Bleaney-Bowers equation, gave g = 2.09(2), 2J = -7.1(4) cm^{-1} and N_α = 131(10) x 10^{-6} c.g.s. units. These parameters are very similar to those found for $[CuL(CH_3COO)]_2$ and may therefore be typical of such step-like structures.

In contrast, the complex $[(CuL)_4P_2O_7]{\cdot}12H_2O$ shows coupling with a 2J value of -6.0 cm^{-1} and fits the Bleany-Bowers expression well at low temperature, as seen in Figure 1.3.12(b), but not at the higher temperatures. A better fit within the range 30-300 K may be obtained by increasing the calculated value of g from 1.983, but this makes the low temperature range worse. The experimentally determined value of the g_{iso} (from the powder e.s.r. data in Table 1.3.12) is 2.131, indicating the problem with the fitted model used probably lies in the low temperature range.

From the X-ray crystallographic structure presented in this chapter, the tetrameric molecule may best be thought of as a pair of dimers. It can be seen that each copper atom binds to a sulphur atom of the ligand L^- in the plane (see Figure 1.3.1), the average bond distance being 2.279 Å (from Table 1.3.2). This sulphur forms a long bridging bond to the other copper of the dimer directly above (or below) with an average bond length of 2.885 Å. In the structures of diacetyl-bis(thiosemicarbazonato)copper(II) [165] and kethoxal-bis(thiosemicarbazonato)copper(II) [186] similar Cu-S axial bonds (3.102 and 3.10 Å respectively) result in the 2J values of -27.2 cm^{-1} for the former and -32 cm^{-1} for the latter examples. In the crystal structure of aqua(pyridoxal thiosemicarbazonato)copper(II) chloride monohydrate [68], two of the centrosymmetrically related, monomeric units pack to give an elongated square-pyramid. The apical donor for this pyramid is the sulphur atom from the related molecule with a Cu-S distance of 3.066(2) Å. Unfortunately no magnetic data were reported for this complex.

The situation for $[(CuL)_4P_2O_7]\cdot 12H_2O$ is possibly complicated by the additional three-atom pyrophosphato bridge, linking the two copper atoms as well. A 2J value of -10.8 cm^{-1} has been calculated for the complex $[Cu(5'\text{-UMP})(dpa)H_2O]_2\cdot 5H_2O$ (where 5'-UMP is uridine 5'-monophosphate and dpa is 2, 2'-dipyridylamine [187]) in which the two copper(II) atoms in the dimer are linked via two, three-atom phosphato bridges in the plane. It is possible therefore, that the two copper atoms in a 'dimer' of the title complex can magnetically interact (although weakly) via both the one-atom sulphur and the three-atom phosphato bridges. In addition to the two previously mentioned magnetic pathways there is a possibility that each copper atom in a dimer could also interact very weakly with the two coppers in the other dimer via the five-atom pyrophosphato bridge. The five-atom bridge may account for the poor fit of the susceptibility and magnetic moment data at low temperature. It is not surprising therefore that the attempt to fit a simple dimer model to the variable temperature susceptibility data for this complex was not entirely satisfactory. Possibly a tetramer or two-dimer model will be necessary.

An estimate of the exchange integral, 2J, for antiferromagnetically coupled binuclear copper(II) complexes can be made from the room temperature magnetic moment data after the method of Thompson and Ramaswamy [188]. The 2J values calculated for the low moment and crystallographically studied dimeric complexes from the first three chapters are given in Table 1.3.11 (the ground state for these molecules is d_{x2-y2}). The calculated values of -9 and -14 cm^{-1} for $[CuL(CH_3COO)]_2$ and $[(CuL)_4P_2O_7]\cdot 12H_2O$ respectively agree well with the fitted values of -6.4 and -6.0 cm^{-1} considering the approximations made in the model. The large values obtained for $[Cu(LH)X]_2X_2$ (X is F^- or I^-) and $[CuLY]_2$ (Y is NO_3^- or ClO_4^-) reflect the low room temperature magnetic moments and warrant further investigation, both from crystallographic and magnetic investigations. A positive 2J value of 17 cm^{-1} results for $[Cu(LH)(CF_3COO)]_2(CF_3COO)_2$ because of the low g_i value.

1.3.4(e) Electron Spin Resonance Spectra

The powder and solution e.s.r. parameters presented in Table 1.3.12 are all consistent with an axial stereochemistry about the copper(II) centre (d_{x2-y2} ground state) and with an oxygen donor atom in the plane (giving an N_2OS donor set). This has been verified in the crystal structures of $[(CuL)_4P_2O_7]\cdot 12H_2O$ and $[Cu(LH)(H_2PO_4)]_2(H_2PO_4)_2(H_3PO_4)_2\cdot 2H_2O$ which show a square-pyramidally complexed copper atom with a phosphato oxygen completing the basal donor set (along with the tridentate NNS ligand, LH or L^-). Addition of an excess of adenosine 5'-triphosphate (ATP) to an aqueous solution of $[CuL(CH_3COO)]_2$ did not markedly change the e.s.r. parameters. This indicates that the ATP either did not coordinate or did so through a phosphato oxygen, rather than an adenosine nitrogen.

TABLE 1.3.12

E.s.r. Results for Selected Chapter 3 Complexes[a]

Complex	g_1	$g_\perp$	g_2	$g_{/\!/}(g_3)$	$A_{/\!/}(A_3)$[b]	Solvent
$[(CuL)_4P_2O_7]\cdot 12H_2O$		2.035		2.179		Powder
$[(CuL)_2HPO_4]\cdot 6H_2O$			2.069[c]			Powder
$[Cu(LH)(H_2PO_4)]_2(H_2PO_4)_2\cdot 3H_2O$		2.048		2.221		Powder
$[Cu(LH)(H_2PO_4)]_2(H_2PO_4)_2$ $(H_3PO_4)_2\cdot 2H_2O$		2.042		2.217		Powder
$[CuL(ptp)]\cdot 2H_2O$		2.072		2.202	185	dmso
$[CuL(CH_3COO)]_2$ + excess ATP[e]		2.055		2.206	187	H_2O[d]

a via simple first-order spectral analysis
b h.f. coupling constants in 10^4 cm^{-1}
c g_{iso} value
d containing 10% dmso
e ATP is adenosine 5'-triphosphate

1.3.4(e) General Discussion

The tetramer, $[(CuL)_4P_2O_7]\cdot 12H_2O$ appears to be the first crystallographically studied ternary pyrophosphato complex in the literature. The pair of 'dimers' formed in this compound also represent a different form of molecular packing. In the dimeric complexes of the acetato, trifluoracetato, sulphato and dihydrogenphosphato anions, dimerisation is achieved via an unusual one-atom oxygen bridge from the anion. The pyrophosphato complex however has a one-atom sulphur, a three-atom pyrophosphato and two five-atom pyrophosphato bridges linking the two copper centres. A number of other reported dimeric complexes of copper(II) thiosemicarbazones also have sulphur bridges [68,165,186]. The factors which govern the bridging mode are however unclear.

The dimeric complex, $[Cu(LH)(H_2PO_4)]_2(H_2PO_4)_2(H_3PO_4)_2\cdot 2H_2O$ appears to have the distinction of being the only ternary complex of Cu(II) with dihydrogenphosphate coordinated (in the literature at present) as well as the only one-atom phosphato bridge between two copper centres. The occurrence of both di and trihydrogenphosphates within the same structure is unusual also. For these reasons further study seems justified on this system. The complex is formed from the addition of $[CuL(CH_3COO)]_2$ to the acid HPF_6. The source of the phosphate however is from the hydrolysis of PF_6^- anions, an unexpected result and an unusual route for making a phosphato complex. The formation of the acidic, neutral ligand complex, rather than the insoluble $Cu_3(PO_4)_2\cdot 3H_2O$ salt, again testifies to the stability of this system in highly acidic conditions.

When phosphoric acid is added to $[CuL(CH_3COO)]_2$, the crystalline compounds formed are not the same as that from the hydrolysis of PF_6^-. Two morphologically distinct complexes can be synthesised with the general formualtion $[Cu(LH)(H_2PO_4)]_2(H_2PO_4)_2\cdot XH_2O$, depending upon the acid concentration. When 2M H_3PO_4 is used X is 3 and diamond shaped prisms crystallise, but if 3M acid is used X is 10 and hexagonal plates are obtained. The plates lack

the 'H_3PO_4 solvate' present in $[Cu(LH)(H_2PO_4)]_2(H_2PO_4)_2(H_3PO_4)_2 \cdot 2H_2O$. The reason/s for the synthesis of two distinct crystalline forms using phosphoric acid may result from different H_3PO_4 and/or CuL^+ concentrations in the solutions at the time of crystallisation.

The possibility of *in vivo* phosphate coordination has been demonstrated *in vitro* through the formation of stable, isolable adducts and the finding from e.s.r. spectroscopy that CuL^+ does not appear to coordinate the base nitrogens of ATP in solution. Attempts to isolate adducts of biologically relevant phosphates, e.g. ATP, were unsuccessful. An interesting and unexpected outcome from such a trial of an aqueous 1:1 mixture of CuL^+ and guanosine-5′-monophosphate (GMP) was the formation of mould on the solution surface after two months. These were identified as Penicillium and Acremonium, both common airborne moulds. They were undoubtedly feeding on the GMP but their presence was surprising as a number of thiosemicarbazones and their metal chelates have been shown to be fungicidal [47,60,189].

The isolation of the green phenolato complexes, $[CuL(ptp)] \cdot 2H_2O$ and [CuL(tip)], required the use of bulky, deactivated phenols (where ptp^- is paratritylphenolate and tip^- is 2,4,6-triiodophenolate). When less bulky phenols such as 3,4-dimethylphenol or 4(methylmercapto)phenol were used, a small amount of a black compound with no strong ir bands in the range 4 000 - 400 cm^{-1} was obtained, so the reaction was not followed up. From this it can be seen that merely having a phenolate in the presence of CuL^+ was not a guarantee of obtaining a stable adduct.

A number of complexes of the general formulation $[Cu(OR)_2L^1]$ and $[Cu(OR)_2L^2_2]$ (where OR is e.g. pentafluorophelolate or 2,4,6-tribromophenolate, L^1 is e.g. ethylenediamine or 2, 2′-bipyridyl and L^2 is e.g. pyridine or imidazole) have been isolated [182,190], but it appears that the two phenolato complexes from this work are the first ternary adducts involving a tridentate ligand to be prepared. Attempts to form the complex $[Cu(2L)(ptp)_2]$, where 2L is the neutral ligand 2-formylpyridine 2′-methylthiosemicarbazone (see Chapter 4) were unsuccessful. It is

possible therefore, that the tridentate ligand must be anionic to be able to isolate a phenolato adduct of Cu(II).

The formation of a phenolate to copper bond can be seen from the broadening of the charge transfer band in these complexes (see Electronic Spectra discussion). Unfortunately this broad, intense band all but obscures the d-d transitions (see Table 1.3.9). The mull transmittance d-d absorption maxima at 654 nm for $[CuL(ptp)]\cdot 2H_2O$ is very similar to a number of the complexes in this work with square-pyramidal stereochemistries, although the possibility of a square-planar structure has not been discounted. To achieve this configuration, assuming the phenolate is coordinated in the fourth in-plane position, the apical donor could be an oxygen from water (e.g. as in the structure of $[CuL(sacc)H_2O]\cdot \frac{1}{2}H_2O$ - see Chapter 2) or a bridged phenolate oxygen (e.g. as in the structure of $[Cu(LH)(CF_3COO)]_2(CF_3COO)_2$ - see Chapter 1). A dimeric, phenolate bridged copper(II) complex has been reported in the literature [191] so such a structure in these cases may be possible. These novel complexes deserve further attention.

The remarkable ability of the CuL^+ system to coordinate and stabilise both neutral and ionic moieties led to studies with further anions. One of these was $Mo_7O_{24}^{6-}$. This was chosen rather than MoO_4^{2-}, as polymeric molybdates are formed in weakly acidic solutions [192] and the pH of an approximately 6 mM solution of $[CuL(CH_3COO)]_2$ was measured to be 5.6. However, when an acidified solution of $Mo_7O_4^{6-}$ was added to CuL^+ (1:6), the complex isolated best fitted the analysis of $[(CuL)_2MoO_4]\cdot H_2O$, showing rearrangement had occurred in spite of the acidic conditions. When MoO_4^{2-} was added to CuL^+ (1:2) in aqueous solution a green complex with an identical ir spectrum was obtained and was not investigated further.

1.3.4(f) Summary

The crystallographic studies in this chapter show CuL^+ to be able to coordinate and form stable complexes with phosphates *in vitro*. Intracellularly, such adducts may therefore be important.

The variable temperature magnetic behaviour of two dimeric complexes was investigated and show only very weak antiferromagnetic interactions. Some idea of the magnetic spin coupling can however be obtained from the room temperature magnetic moment using the Thompson-Ramaswamy relationship [188].

It is clear that the CuL^+ system provides a remarkable vehicle to study uncommon anions, often in unusual coordination modes, many of which might not otherwise be investigated. Full advantage of this should be taken.

1.3.5 EXPERIMENTAL

1.3.5(a) Preparation of Complexes

$[(CuL)_4P_2O_7]\cdot 12H_2O$

To $[CuL(CH_3COO)]_2$ (200 mg, 0.66 mmols) in warm water (70 cm^3) was added $Na_4P_2O_7$ (176 mg, 0.66 mmols) in water (10 cm^3). The clear green solution which resulted was filtered and left for two days after which time dark green rod shaped crystals had separated. These were removed from solution and carefully dried on filter paper. Yield 45 mg (20%).

$[(CuL)_2HPO_4]\cdot 6H_2O$

Solid $Na_2HPO_4\cdot 12H_2O$ (500 mg, 1.40 mmols) was added to a hot solution of $[CuL(CH_3COO)]_2$ (302 mg, 1.00 mmols) in water (60 cm^3). The green precipitate which formed was filtered off and washed with water then vacuum dried. Yield 178 mg (52%).

$[Cu(LH)(H_2PO_4)]_2(H_2PO_4)_2\cdot 3H_2O$

To a phosphoric acid solution (2M, 5 cm^3) was added $[CuL(CH_3COO)]_2$ (271 mg, 0.90 mmols). The emerald green solution was heated until all of the solid had dissolved. One day later, green diamond shaped prisms had separated which proved to be hygroscopic. They were removed from solution and carefully dried on filter paper only. Yield 179 mg (43%). If the reaction was repeated using a more concentrated phosphoric acid solution (3M, 5 cm^3) with $[CuL(CH_3COO)]_2$ (265 mg, 0.88 mmols) green hexagonal plates separated after approximately three hours. These were filtered and washed with H_3PO_4 (3M) then diethyl ether. Yield 221

mg (48%). This complex was formulated as $[Cu(LH)(H_2PO_4)]_2(H_2PO_4)_2 \cdot 10H_2O$ from the analyses (%) C: 15.9 (15.9) H: 3.2 (4.2) N: 10.3 (10.6) (the calculated values are given in parentheses).

$[Cu(LH)(H_2PO_4)]_2(H_2PO_4)_2(H_3PO_4)_2 \cdot 2H_2O$

An attempt was made to synthesise the complex $[Cu(LH)(PF_6)]_2(PF_6)_2$ using the previous procedure, taking HPF_6 instead of H_3PO_4. A solution of approximately 2M HPF_6 was made by adding concentrated HPF_6 (2 cm^3) to water (10 cm^3). When $[CuL(CH_3COO)]_2$ (222 mg, 0.74 mmols) was added to this solution (5 cm^3) an emerald green solution resulted which was filtered and put aside. Eleven weeks later large, diamond shaped, hygroscopic crystals were removed and dried under vacuum. Yield 254 mg (62%). Analysis showed no F to be present but a higher than expected percentage of P. Subsequently the title formulation was verified by X-ray crystallography.

[CuLOR] (OR = ptp^- or tip^-)

To $[CuL(CH_3COO)]_2$ (200 mg, 0.66 mmols) in water (70 cm^3) which had been briefly boiled then filtered, was added dropwise paratritylphenol (ptpH) (227 mg, 0.67 mmols) or 2,4,6-triiodophenol (tipH) (320 mg, 0.68 mmols) in ethanol (15 cm^3) in which sodium metal (20 mg, 0.87 mmols) had previously been dissolved. The green precipitates which formed were immediately removed from solution and washed successively with water, ethanol and diethyl ether then vacuum dried. Yields $[CuL(ptp)] \cdot 2H_2O$ 283 mg (70%); [CuL(tip)] 364 mg (77%).

$[(CuL)_2MoO_4]H_2O$

For reasons outlined in the discussion, MoO_4^{2-} was not used as the starting product. Instead $(NH_4)_6Mo_7O_{24}\cdot 4H_2O$ (103 mg, 0.083 mmols) was dissolved in an acetic acid solution (10 cm^3, 0.05M). This was added slowly to a solution of $[CuL(CH_3COO)]_2$ (151 mg, 0.50 mmols) in water (75 cm^3) which had been filtered after the pH had been adjusted to 5 by adding acetic acid (0.05M). The green precipitated which formed immediately was separated and washed with water then vacuum dried. Yield 106 mg (32%).

1.3.5(b) Data collection procedure for μ_4-Pyrophosphatotetrakis[(2-formylpyridine thiosemicarbazonato)copper(II)] Dodecahydrate

The title complex was synthesised as described in section 1.3.5(a). A crystal of approximate dimensions 0.040 x 0.032 x 0.024 cm displayed faces of the forms {1 0 0}, {1 $\bar{1}$ 0}, {0 $\bar{1}$ 0}, {$\bar{1}$ $\bar{1}$ 0}, {$\bar{1}$ 0 0}, {$\bar{1}$ 1 0}, {0 1 0}, {1 1 0}, {0 0 1} and {0 0 $\bar{1}$}. Cell dimensions of: $\underline{a}$ = 29.074(6), $\underline{b}$ = 28.021(3), $\underline{c}$ = 13.374(3) Å and β = 102.93(2)° were determined from a least-squares refinement of the setting angles of 25 reflections. The calculated cell volume is 10619.4 Å^3 with a molecular weight of 1361.3 g mol^{-1} ($C_{28}H_{52}Cu_4N_{16}O_{19}P_2S_4$). For eight formula weights per unit cell, the density was calculated to be 1.703 g cm^{-3}. Systematic absences ($\underline{h}$ $\underline{k}$ $\underline{l}$, $\underline{h}$ + $\underline{k}$ = 2n + 1 and $\underline{h}$ 0 $\underline{l}$, $\underline{l}$ = 2n + 1) showed the space group to be the C centred (Cc or C2/c). Final analysis was consistent with C2/c. A total of 10503 reflections were collected on an Enraf-Nonius CAD-4 diffractometer with Cu-K_α radiation (μ(Cu-$K_{\bar{\alpha}}$) = 43.20 cm^{-1}) using the $\omega/2\theta$ scan technique (θ_{max} = 70°). The $\underline{h}$ $\underline{k}$ $\underline{l}$ limits were: -35 → 34, 0 → 34, 0 → 16.

The intensities of three standard reflections were monitored at hourly intervals during data collection to check for crystal decomposition. As the total loss of intensity was no greater than 2.4% corrections for decay were not applied. Analytical absorption corrections [124,125] were applied with the minimum and maximum transmission coefficients calculated as 0.2364 and 0.6726 respectively.

The relevant crystal and data collection parameters are summarised in Tables 1.3.13 and 1.3.14 respectively.

1.3.5(c) Structure solution and refinement

The structure was solved by a direct methods approach [159] and sites for the four Cu, four S, two P and 46 lighter atoms were eventually located from a series of electron density maps. A structure factor calculation which included these atoms returned a residual of 0.22. All remaining non-hydrogen atoms were located from a series of difference electron density syntheses. An R factor of 0.14 was returned from three full-matrix least-squares cycles of refinement assuming isotropic thermal motion for all atoms. One further refinement cycle in which anisotropic thermal behaviour was assumed for the Cu atoms yielded a residual of 0.12. Hydrogen atoms were added in calculated positions on all pyridine rings and methylene carbons at a fixed C-H bond length of 1.08 Å. In the final refinement cycle, all non-hydrogen atoms except the pyridine rings 2, 3 and 4 (these restrictions were imposed by the limitations of SHELX76 - G. M. Sheldrick 1976) were refined assuming anisotropic thermal motion. The respective R and R_w values for this cycle were 0.0873 and 0.0940 for the 534 parameters and 6096 data for which $F^2 > 5\sigma(F^2)$. The function minimised was $\Sigma w(|F_o| - |F_c|)^2$ with the weight, w, being defined as $9.4402/(\sigma^2(F) + 0.0014\ F^2)$. The largest parameter shift per esd was 0.09 for a disordered water molecule.

The highest peak in the final difference electron density map of 1.77 $\bar{e}$ $Å^{-3}$ was associated with residual electron density around Cu(2) (separation of 0.87 Å).

Final atomic parameters and the observed and calculated structure factors are on the microfiche in the back cover pocket of this thesis. The bond length and bond angle data are in Tables 1.3.2 and 1.3.3 respectively.

TABLE 1.3.13
$[(CuL)_4P_2O_7]\cdot 12H_2O$

CRYSTAL DATA

Compound:	μ_4-Pyrophosphatotetrakis[(2-formylpyridine thiosemicarbazonato)copper(II)] Dodecahydrate
Colour:	Green
Formula:	$C_{28}H_{52}Cu_4N_{16}O_{19}P_2S_4$
Formula weight:	1361.3 g mol^{-1}
Space group:	C2/c
a:	29.074(6) Å
b:	28.021(3) Å
c:	13.374(3) Å
β:	102.93(2)°
V:	10 619.4 $Å^3$
Z:	8
ρ_c:	1.703 g cm^{-3}
Crystal faces:	{1 0 0}, {1 $\bar{1}$ 0}, {0 $\bar{1}$ 0}, {$\bar{1}$ $\bar{1}$ 0}, {$\bar{1}$ 0 0}, {$\bar{1}$ 1 0}, {0 1 0}, {1 1 0}, [0 0 1}, {0 0 $\bar{1}$}
Crystal dimensions:	0.040 x 0.032 x 0.024 cm
μ (Cu-K_α):	43.20 cm^{-1}
F(OOO):	5 488

TABLE 1.3.14
$[(CuL)_4P_2O_7]\cdot 12H_2O$

Parameters Associated with Data Collection

Radiation used:	$Cu(K_\alpha)$ (λ = 1.5418)
Graphite monochromator used:	No
Incident beam collimator (diameter):	0.8 mm
ω scan angle:	$(1.00 + 0.142 \tan \theta)^\circ$
Horizontal aperture width:	$(1.80 + 0.80 \tan \theta)$mm
Vertical aperture height:	4 mm
Scan type:	$\omega/2\theta$
Prescan speed:	3
Prescan acceptance; relative $\sigma(F^2)/F^2$ required:	0.5
Final scan acceptance $\sigma(F^2)/F^2$:	0.018
Maximum time limit for final scan:	120 s
Intensity control frequency:	3 600 s
Orientation acceptance; maximum deviation of any scattering vector from its calculated position:	0.10°
θ Range:	1 – 70°
Total number of reflections in data set:	10 503
Observed data criterion:	6 096 unique reflections with $F^2 > 5\sigma(F^2)$
Collection temperature:	293 K

1.3.5(d) Data collection procedure for Di-μ-dihydrogenphosphato-bis[2-formylpyridine thiosemicarbazone)copper(II)] Bis(dihydrogenphosphate) Bis(trihydrogenphosphate) Dihydrate

The title complex was synthesised as described in section 1.3.5(a). As the compound is hygroscopic a crystal of approximate dimensions 0.047 x 0.025 x 0.010 cm was mounted in a capillary. A least-squares refinement of the setting angles of 25 reflections gave the cell dimensions of: $\underline{a}$ = 11.500(1), $\underline{b}$ = 10.238(1), $\underline{c}$ = 16.583(1) Å, β = 107.164(7)°. For a cell volume of 1865.5 $Å^3$ and a molecular weight of 1107.6 g mol^{-1} per dimer the density was calculated to be 1.972 g cm^{-3} for two formula weights in the cell. Systematic absences ($\underline{h}$ 0 $\underline{l}$, $\underline{l}$ = 2n + 1 and 0 $\underline{k}$ 0, k = 2n + 1) established the space group as $P2_1/c$. A total of 4071 reflections were collected on an Enraf-Nonius CAD-4 diffractometer with Cu-K_α radiation (μ(Cu-$K_{\bar{\alpha}}$) = 55.83 cm^{-1}) using the ω/2θ scan technique (θ_{max} = 75°); the $\underline{h}$ $\underline{k}$ $\underline{l}$ limits were: -14 → 13, 0 → 12, 0 → 20 respectively.

The intensities of three standard reflections were monitored at hourly intervals during the data collection. Their variation in intensity was ≤ 0.5% hence decay corrections were not applied to the data.

Two pairs of Freidel equivalent reflections with psi near 90° were used for the azamuthal scans so that empirical absorption corrections could be applied [126]. The minimum and maximum transmission coefficients calculated were 0.6759 and 0.9986 respectively.

The relevant crystal and data collection parameters are summarised in Tables 1.3.15 and 1.3.16 respectively.

1.3.5(e) Structure solution and refinement

The copper site was located from a Patterson map and a structure factor calculation based on this position gave an R factor of 0.59. All remaining non-hydrogen atoms were located from a series of electron density syntheses and refinement of these atoms assuming isotropic thermal motion returned a residual of 0.17. Three full-matrix least-squares cycles of refinement, assuming anisotropic thermal motion for the copper atom lowered the R factor to 0.10. All hydrogens were subsequently located from difference fourier syntheses and included in the calculations at fixed positions; (C-H, N-H 1.08 Å). In the final cycle all non-hydrogen atoms were refined assuming anisotropic thermal motion yielding values for R and R_w of 0.0598 and 0.0638 respectively for the 270 parameters and 3432 data with $F^2 > 3\sigma(F^2)$.

The function minimised was $\Sigma w(|F_o| - |F_c|)^2$, with the weight, w, being defined as $1.0000/(\sigma^2(F) + 0.1185\ F^2)$. The largest parameter shift per esd was 0.3 and the highest peak of 0.52 $\bar{e}$ $Å^{-3}$ in the final difference electron density map was associated with residual electron density around the copper atom.

Final atomic parameters and the observed and calculated structure factors are on the microfiche inside the pocket on the back cover of this thesis. The bond length and angle data are in Tables 1.3.5 and 1.3.6 respectively.

TABLE 1.3.15
$[Cu(LH)(H_2PO_4)]_2(H_2PO_4)_2(H_3PO_4)_2 \cdot 2H_2O$

CRYSTAL DATA

Compound:	Di-μ-dihydrogenphosphato-bis[(2-formylpyridine thiosemicarbazone)copper(II)] Bis(dihydrogenphosphate) Bis(trihydrogenphosphate) Dihydrate
Colour:	Green
Formula:	$C_{14}H_{34}Cu_2N_8O_{26}P_6S_2$
Formula weight:	1107.6 g mol^{-1}
Space group:	$P2_1/c$
a:	11.500(1) Å
b:	10.238(1) Å
c:	16.583(1) Å
β:	107.164(7)°
V:	1865.5 $Å^3$
Z:	2
ρ_c:	1.972 g cm^{-3}
Crystal dimensions:	0.047 x 0.025 x 0.010 cm
μ (Cu-K_α):	55.83 cm^{-1}
F(OOO):	1 112

TABLE 1.3.16
$[Cu(LH)(H_2PO_4)]_2(H_2PO_4)_2(H_3PO_4)_2 \cdot 2H_2O$

Parameters Associated with Data Collection

Radiation used:	$Cu(K_\alpha)$ (λ = 1.5418)
Graphite monochromator used:	No
Incident beam collimator (diameter):	0.8 mm
ω scan angle:	$(0.80 + 0.142 \tan \theta)^\circ$
Horizontal aperture width:	$(2.00 + 0.80 \tan \theta)$mm
Vertical aperture height:	4 mm
Scan type:	$\omega/2\theta$
Prescan speed:	3
Prescan acceptance; relative $\sigma(F^2)/F^2$ required:	0.5
Final scan acceptance $\sigma(F^2)/F^2$:	0.016
Maximum time limit for final scan:	120 s
Intensity control frequency:	3 600 s
Orientation acceptance; maximum deviation of any scattering vector from its calculated position:	0.08°
θ Range:	1 – 75°
Total number of reflections in data set:	4 071
Observed data criterion:	3 432 unique reflections with $F^2 > 3\sigma(F^2)$
Collection temperature:	293 K

CHAPTER 4

VARIATIONS ON THE Cu/LH SYSTEM

1.4.1 INTRODUCTION

Variation in the antitumour properties of the LH/Cu(II) system should result from changes in either the ligand or the metal. Hence four modified ligands (see below) and a selection of their copper(II) complexes were synthesised.

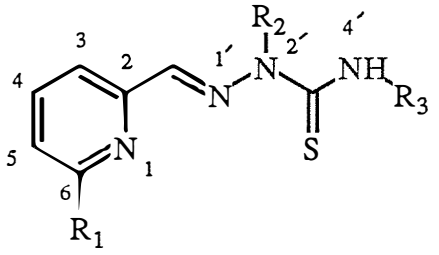

LH $R_1 = R_2 = R_3 = H$
6LH $R_1 = CH_3$, $R_2 = R_3 = H$
2'LH $R_2 = CH_3$, $R_1 = R_3 = H$
4'LH $R_3 = CH_3$, $R_1 = R_2 = H$

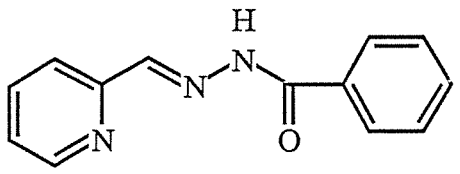

pbH

Figure 4.1 Ligands used in this chapter.

A range of complexes using the unmodified ligand, LH, were also prepared with other metals, namely $M(II)L_2$ and $M(II)(LH)Cl_2$ (where M(II) = Zn, Cd or Hg) and M(I)L and M(I)(LH)X (where M(I) = Ag, X = NO_3^- or ClO_4^- and M(I) = Au, X = Cl^-), by addition of the appropriate metal salt to a solution of LH in alcohol, either with, or without, base added.

As these ligands and their range of complexes were primarily synthesised for cytotoxicity testing, they were not characterised exhaustively. However, a number of physical techniques were employed including n.m.r. spectroscopy, and pKa and reduction potential measurements. The results of these studies will be presented in this chapter, whereas the cytotoxicity results will appear in Chapter 6 (Section 2).

1.4.2 RESULTS AND DISCUSSION

1.4.2(a) Electronic Spectra and Magnetic Properties

The magnetic moment data presented in Table 1.4.1 (along with the elemental analyses) are all considered to be normal according to the criteria discussed in Chapter 1.

The electronic absorption maxima and molar conductance data in Table 1.4.2, for the copper(II) complexes, generally parallel those of the analogous unsubstituted ligand complex. Differences observed between the complexes of 6LH and pbH with the analogous LH compounds may be attributed to (i) steric effects from the methyl group upon coordination for 6LH, (ii) the fact that pbH has an amide with an inductive phenyl ring attached to it rather than the thioamide and amine group associated with LH. The majority of the complexes show one d-d transition in the approximate range of 600-700 nm which, from the evidence presented in the preceding chapters is consistent with a square-pyramidal stereochemistry about the copper(II) centre. According to Hathaway [105], two d-d bands as observed at ~700 nm and ~1 300 nm for $[(Cu(pb))_2HPO_4]\cdot 2H_2O$, are consistent with a static, elongated, tetragonal-octahedral stereochemistry. The two absorption maxima observed in a number of the bipy complexes at ~650 nm and 900-1 000 nm may, by analogy with $[CuL(bipy)]ClO_4$, suggest a distorted trigonal-bipyramidal system.

TABLE 1.4.1

Analytical and Magnetic Data for Chapter 4

Complex[a]	Colour	Analyses (%)[b]				μ_{eff}[c]	Yield
(%)		C	H	N	Other		
6LH·H_2O	Yellow	44.9 (45.3)	5.6 (5.7)	26.8(26.4)	m.p. = 202-4° C[f]		77
2'L	Yellow	49.5 (49.3)	5.2 (5.2)	28.9 (29.1)	m.p. = 178-80° C[g]		81
4'LH	Yellow	49.5 (48.8)	5.2 (5.1)	28.9 (28.6)	m.p. = 244-9° C[h]		94
pbH· ¼ H_2O	White	67.8 (68.0)	5.0 (5.5)	18.3 (18.3)	m.p. = 130-40° C[i]		76
[Cu(6L)(CH_3COO)]$_2$·$2H_2O$	Dark Green	35.9 (36.0)	4.4 (4.2)	17.0 (16.8)		1.81	75
[Cu(4'L)(CH_3COO)]$_2$	Dark Green	37.7 (38.0)	3.9 (3.8)	17.9 (17.7)		1.85	65
[Cu(pb)(CH_3COO)]$_2$	Green	51.7 (51.9)	3.9 (3.8)	15.1 (15.1)		1.85	55
[Cu(6LH)(CF_3COO)]$_2$ (CF_3COO)$_2$·H_2O	Green	29.8 (29.8)	2.1 (2.1)	12.1 (11.6)		1.82	20
[Cu(4'LH)(CF_3COO)]$_2$ (CF_3COO)$_2$	Dark Green	28.8 (28.7)	2.4 (2.4)	11.1 (11.2)		1.85	77
[Cu(6L)pftp]$_2$	Green	36.1 (36.9)	2.0 (2.0)	13.6 (12.3)		1.84	55
[Cu(4'L)pftp]$_2$	Brown	36.7 (36.9)	2.0 (2.0)	12.2 (12.3)		1.89	64
[Cu(pb)pftp]$_2H_2O$	Green	46.1 (46.0)	2.0 (2.2)	8.3 (8.5)	19.1 (19.2)[d]	1.86	50
[Cu(6L)bipy]PF_6	Green	38.8 (38.7)	3.7 (3.1)	15.4 (15.1)		1.84	70
[Cu(4'L)bipy]PF_6	Dark Green	38.5 (38.7)	3.0 (3.1)	14.9 (15.1)		1.86	72
[Cu(pb)bipy]PF_6	Dark Green	46.9 (46.8)	3.4 (3.1)	11.6 (11.9)	19.5 (19.4)[d]	1.86	43
[Cu(pb)(bipy)pftp]H_2 O	Brown	52.3 (52.7)	2.8 (3.1)	10.7 (10.6)		1.75	
[Cu(6L)(dmap)$_2$]PF_6·$\frac{5}{2}H_2O$	Dark Green	37.8 (38.2)	4.6 (5.0)	17.0 (16.2)		1.95	45
[Cu(4' L)(dmap)$_2$]PF_6·H_2O	Green Brown	39.8 (39.7)	4.6 (4.7)	16.7 (16.9)		1.97	76
[Cu(6L)ptp]	Brown	66.3 (66.9)	4.7 (4.8)	8.1 (9.4)		1.65	59
[Cu(4' L)ptp]	Brown Yellow	67.5 (67.0)	4.8 (4.8)	9.0 (9.5)		1.75	89
[Cu(pb)ptp]	Green	73.1 (73.2)	4.7 (4.7)	7.0 (6.7)		1.88	87
[(Cu(6L))$_2$$HPO_4$]·$4H_2O$	Dark Green	28.2 (28.2)	4.6 (4.0)	16.7 (16.4)		1.87	13
[(Cu(4'L))$_2$$HPO_4$]·$5H_2O$	Dark Green	27.9 (27.5)	4.7 (4.2)	15.7 (16.0)		1.73	28
[(Cu(pb))$_2$$HPO_4$]·$2H_2O$	Brown	44.0 (44.1)	3.4 (3.6)	11.6 (11.9)		1.91	35
[Cu(pbH)Cl_2]	Pale Green	43.6 (43.4)	2.9 (2.8)	11.7 (11.7)	19.5 (19.7)[e]	1.87	94
[Cu(2'L)Cl_2]	Green	29.0 (29.3)	3.1 (3.1)	16.9 (17.1)	21.4 (21.6)[e]	1.79	81
[Cu(2'L)(NO_3)$_2$]	Green	25.4 (25.2)	2.6 (2.7)	22.3 (22.0)		1.80	62

TABLE 1.4.1 continued

Analytical and Magnetic Data for Chapter 4

Complex[a]	Colour	Analyses (%)[b]			
		C	H	N	Other
$[AgL]H_2O$	Tan	27.5 (27.6)	2.3 (3.0)	18.8 (18.4)	
$[Ag(LH)]NO_3 \cdot \frac{3}{2}H_2O$	Yellow	22.4 (22.3)	2.5 (3.0)	18.0 (18.6)	
$[Ag(LH)]ClO_4$	Yellow	22.2 (21.7)	2.6 (2.1)	15.0 (14.5)	
$[AuL] \cdot 4H_2O$	Yellow	18.5 (18.4)	2.7 (3.3)	12.3 (12.3)	
$[Au(LH)]Cl \cdot H_2O$	Yellow	19.5 (19.5)	2.7 (2.4)	13.8 (13.0)	
$[ZnL_2]$	Yellow	39.4 (39.7)	3.7 (3.3)	26.0 (26.4)	
$[Zn(LH)Cl_2]H_2O$	Pale Yellow	25.3 (25.1)	3.2 (3.0)	17.0 (16.8)	21.6 (21.2)[e]
$[CdL_2] \cdot \frac{1}{2}H_2O$	Yellow	34.8 (35.0)	3.4 (3.2)	24.0 (23.4)	
$[Cd(LH)Cl_2]$	White	23.4 (23.1)	3.0 (2.2)	15.2 (15.4)	18.9 (19.5)[e]
$[HgL_2] \cdot \frac{1}{2}H_2O$	Green	29.4 (29.6)	2.6 (2.7)	19.7 (19.7)	
$[Hg(LH)Cl_2]$	Yellow	19.2 (18.6)	2.3 (1.8)	12.4 (12.4)	
$[PbL_2] \cdot 2H_2O$	Yellow	28.1 (27.9)	3.0 (3.0)	17.9 (18.6)	
$[Zn(pb)_2] \cdot \frac{1}{2}H_2O$	Yellow	60.2 (59.9)	4.1 (4.1)	16.1 (16.1)	

a see page x for abbreviations
b calculated values are given in parentheses
c measured at 293 K and quoted in B.M. per copper(II) ion
d %F
e %Cl
f reported m.p. of 203-4° C [193]
g reported m.p. of 174-5° C [59]
h reported m.p. of 224-6° C [58
i reported m.p. of ~146° C [194]

TABLE 1.4.2

Absorption Maxima and Conductance Data for Chapter 4

Complex[a]	Absorption Maxima (nm)[b] Charge Transfer		d-d		Molar Conductance[c] ($s\ mol^{-1}\ l$)	Solvent[d]
$[Cu(6L)(CH_3COO)]_2 \cdot 2H_2C$	425		647			m.t.
	413	(12 000)	656 (220)		0	dmso
	385	(11 000)	658 (200)		66	H_2O
$[Cu(4'L)(CH_3COO)]_2$	420		630 (sh)			m.t.
	413	(13 100)	608 (200)		0	dmso
	385	(12 000)	626 (170)		58	H_2O
$[Cu(pb)(CH_3COO)]_2$	415		695 (br)			m.t.
	386	(16 400)	712 (100)		0	dmso
	381	(19 100)	695 (90)		3	EtOH
$[Cu(6LH)(CF_3COO)]_2$ $(CF_3COO)_2$	395		638			m.t.
	413	(12 700)	676 (260)		19	dmso
	414	(11 500)	609 (240)		6	acetone
$[Cu(4'LH)(CF_3COO)]_2$ $(CF_3COO)_2$	394		671			m.t.
	413	(14 500)	631 (190)		21	dmso
	417	(12 000)	574 (200)		5	acetone
$[Cu(6L)pftp]_2$	394		(sh)			m.t.
	400	(10 300)	667 (280)		11	dmso
	420	(sh)	650 (sh)			EtOH
$[Cu(4'L)pftp]_2$	461		(sh)			m.t.
	416	(11 500)	(sh)		0	dmso
	422	(10 400)	(sh)		2	EtOH
$[Cu(pb)pftp]_2H_2O$	422		673 (br)	900 (sh)		m.t.
	387	(12 500)	688 (110)		4	dmso
	389	(19 900)	680 (80; sh)		12	acetone
$[Cu(6L)bipy]PF_6$	406		644 (br)	928 (br)		m.t.
	392	(8 200)	669 (210)		32	dmso
	407	(12 000)	647 (300)	922 (90; br)	143	acetone
$[Cu(4'L)bipy]PF_6$	410		666	900 (sh)		m.t.
	413	(13 400)	610 (210; sh)		28	dmso
	410	(12 100)	630 (220; br)	900 (70; sh)	86	CH_3NO_2
$[Cu(pb)bipy]PF_6$	409		693	1070 (br)		m.t.
	386	(4 900)	693 (90)		20	dmso
	387	(15 600)	661 (12)	870 (70; sh)	62	CH_3NO_2
$[Cu(pb)(bipy)pftp]H_2O$	420			1150 (br)		m.t.
$[Cu(6L)(dmap)_2]PF_6 \cdot \frac{5}{2}H_2O$	388		650 (sh)	900 (sh)		m.t.
	400	(11 700; br)	653 (320)		31	dmso
	399		(sh)			CH_3NO_2
$[Cu(4'L)(dmap)_2]PF_6 \cdot H_2O$	424		650 (sh)	900 (sh)		m.t.
	413	(13 300)	(sh)		28	dmso
	420	(10 600)	(sh)			CH_3NO_2
[Cu(6L)ptp]	411		700 (sh)			m.t.
	396	(10 300)	(sh)		11	dmso
	393		(sh)			CH_3NO_2
[Cu(4'L)ptp]	440		711 (sh)			m.t.
	413	(12 000)	(sh)		0	dmso
	412	(10 200)	(sh)		4	EtOH
[Cu(pb)ptp]	421		770 (sh)			m.t.
	387	(13 900)	670 (110; sh)		0	dmso
	380		709			EtOH

TABLE 1.4.2 continued

Complex[a]	Absorption Maxima (nm)[b] Charge Transfer		d-d		Molar Conductance[c] (s mol^{-1} l)	Solvent[d]
$[(Cu(6L))_2HPO_4]\cdot 4H_2O$	414		648 (br)			m.t.
	401	(11 800)	(sh)		14	dmso
$[(Cu(4'L))_2HPO_4]\cdot 5H_2O$	426		670 (br)			m.t.
	413	(11 200)	(sh)		9	dmso
	416		630 (br)			EtOH
$[(Cu(pb))_2HPO_4]\cdot 2H_2O$	395		710	1300 (br)		m.t.
	387		710	1280 (br)		dmso
	391		694	1270 (br)		CH_3NO_2
$[Cu(pbH)Cl_2]$	382		837 (br)			m.t.
	390	(16 600)	758 (90)		24	dmso
	384		740			EtOH
$[Cu(2'L)Cl_2]$	382		714 (br)			m.t.
	308	(17 700)	703 (230)		26	dmso
	345	(8 400; sh)	670 (170)		233	H_2O
$[Cu(2'L)(NO_3)_2]$	367		654 (br)			m.t.
	308	(19 200)	682 (200)		66	dmso
	345	(6 700; sh)	667 (170)		224	H_2O
$[ZnL_2]$	380	(2 500; sh)			3	dmso
$[Zn(LH)Cl_2]H_2O$					5	dmso
					240	H_2O
$[CdL_2]$	400	3 500; sh)			2	dmso
$[Cd(LH)Cl_2]$					10	dmso
$[HgL_2]\cdot \frac{1}{2}H_2O$	(sh)				8	dmso
$[Hg(LH)Cl_2]$					3	dmso

a see page x for abbreviations
b extinction coefficients given in parentheses (l mol^{-1} cm^{-1})
c for typical molar conductance ranges see Appendix 3
d m.t. = mull transmittance

1.4.2(b) Electron Spin Resonance Spectra

The e.s.r. spectral parameters for selected compounds are given in Table 1.4.3 and, where three g values are resolved in the solid state, indicate a rhombic stereochemistry.

The powder and solution $g_{//}$ values for the $Cu(pb)^+$ species are greater than those observed for the corresponding CuL^+ compounds in accord with the substitution of the carbonyl/carbonylate oxygen of pb^- with the thione/thiolate sulphur in L^-. The comparatively low $A_{//}$ values of 158 and 147 x 10^{-4} cm^{-1} for $[Cu(pb)(CH_3COO)]_2$ and $[Cu(pbH)Cl_2]$ respectively could be due to a distortion of the equatorial donor sets from planarity, or to increased covalency. Distortion is thought to be the reason, as the N_2O donor set of pbH is considered to be 'harder' (i.e. more ionic) than the N_2S set of LH. As the solid state $g_{//}$ parameters for the two thiolato complexes, $[Cu(pb)pftp]_2H_2O$ (2.203) and $[Cu(pb)(bipy)pftp]H_2O$ (2.234) are both reduced compared with that for $[Cu(pb)(CH_3COO)]_2$ (2.272), it is assumed the thiolato sulphur is interacting with the copper(II) centre.

The appearance of a $\Delta M_s = 2$ signal (g = 4.251) in $[Cu(pb)(CH_3COO)]_2$ suggests the formulation of this complex as a dimer is justified. Further structural and magnetic studies of this complex would seem warranted.

1.4.2(c) E.s.r. Spectra of $Cu(2'L)^{2+}$ and $Cu(pb)^+$ with Blood Components

Several significant differences in the spectral parameters for $Cu(2'L)^{2+}$ and $Cu(pb)^+$ with human blood components were noted (see Table 1.4.4) when compared with those for CuL^+ (which were discussed in Chapter 2). When CuL^+ interacted with red cells, two species were formed. The low-field component was consistent with a sulphur adduct whereas the high-field species was assumed to result from nitrogen coordination. However, both $Cu(2'L)^{2+}$ and

TABLE 1.4.3

Selected E.s.r. Results for Chapter 4 Complexes[a]

Complex	g_1	$g_\perp$	g_2	$g_{/\!/}(g_3)$	$A_{/\!/}(A_3)$[b]	G[c]	Solvent
$[Cu(6L)bipy]PF_6$	2.016		2.078	2.165			powder
$[Cu(6L)(dmap)_2]PF_6\cdot\frac{5}{2}H_2O$	2.017		2.121				powder
$[Cu(4'L)bipy]PF_6$	2.038		2.076	2.134			powder
$[Cu(4'L)pftp]$		2.055		2.151	174	2.8	dmf
$[Cu(pb)(CH_3COO)]_2$		2.053		2.272			powder
$\Delta M_s = 2$			4.251				powder
		2.076		2.259	158	3.4	dmso
$[Cu(pb)bipy]PF_6$			2.093[d]				powder
$[Cu(pb)(bipy)pftp]H_2O$	2.029		2.114	2.234			powder
$[Cu(pbH)Cl_2]$		2.066		2.308			powder
			2.084	2.374	147	4.4	dmso
$[Cu(pb)pftp]_2H_2O$	2.045		2.093	2.203			powder

a via simple first-order spectral analysis
b h.f. coupling constants in 10^{-4} cm^{-1}
c $G = (g_{/\!/} - 2)/(g_\perp - 2)$
d g_{iso} value

TABLE 1.4.4

E.s.r. Results for $Cu(2'L)^{2+}$ and $Cu(pb)^+$ with Human Blood Components[a]

Sample		$g_\perp$	$g_{/\!/}$	$A_{/\!/}$[b]	α^2 [c]
$Cu(2'L)^{2+}$ in saline solution		2.075	2.197	179	0.77
$Cu(2'L)^{2+}$ and red cells		2.064	2.210	200	0.83
$Cu(2'L)^{2+}$ and red cells thawed then rerecorded		2.064	2.209	196	0.82
$Cu(2'L)^{2+}$ in red cell supernatant			no signal		
$Cu(2'L)^{2+}$ and plasma	Equal	2.049	2.164	159	0.66
	Equal	2.049	2.190	199	0.81
$Cu(pb)^+$ in saline solution		2.081	2.316	158	0.83
$Cu(pb)^+$ and red cells		2.062	2.209	201	0.83
$Cu(pb)^+$ and red cells thawed then rerecorded		2.062	2.211	201	0.84
$Cu(pb)^+$ in red cell supernatant			no signal		
$Cu(pb)^+$ and plasma	Equal	2.058	2.131	153	0.62
	Equal	2.058	2.187	202	0.81

a via simple first-order spectral analysis
b h.f. coupling constant in 10^{-4} cm^{-1}
c $\alpha^2 = (A_{/\!/}/0.036) + (g_{/\!/} - 2) + 3/7(g_\perp - 2) + 0.04$

$Cu(pb)^+$ display only one high-field species which is nearly equivalent for these two, and different from that for CuL^+. This suggests that the coordination environment around the $Cu(2L)^{2+}$ and $Cu(pb)^+$ moieties is the same when they interact with the red cells or that the copper(II) has been removed from these complexes. Two nearly equivalent high-field species are also observed when this pair interact with human plasma, which may indicate a similar interaction is occurring here. Intuitively, the differences between the monoanionic NNS tridentate arrangement in L^-, and either the neutral NNS tridentate of 2L, or the monoanionic NNO constellation of pb^-, should result in different binding properties with copper(II). The binding constant for Cu(II) with LH is 16.9 log units [128] but those for $Cu(2L)^{2+}$ and $Cu(pb)^+$ have not been determined. It is feasible therefore that in the presence of cellular components, the ligands from $Cu(2L)^{2+}$ and $Cu(pb)^+$ could be displaced e.g.

$$CuL_{EXTERNAL} + L_{CELL} \rightleftarrows CuL_{CELL} + L_{EXTERNAL} .$$

The product CuL_{CELL} would then be common to both complexes and may account for the similar spectral parameters observed. Another difference is the lack of an e.s.r. detectable signal in the red cell supernatant fraction for these complexes (see Table 1.4.4). As the instrumental gain needed for the two complexes in saline solution and those for the equivalent compound in the red cell fractions were approximately the same, it is assumed the majority of the copper is still in the divalent state. Hence the absence of a signal in the supernatant fraction suggests all of the copper(II) has been incorporated into the red cell component.

The incubation of plasma with $Cu(2L)^{2+}$ and $Cu(pb)^+$, in both cases, results in two equally intense species. The low-field components have $g_{//}$ and α^2 values which are consistent with a thiolato adduct. The low $A_{//}$ values of 159 and 153 x 10^{-4} cm^{-1} for $Cu(2L)^{2+}$ and $Cu(pb)^+$ respectively are also in accord with the 'softer' covalent bonding of sulphur. Unlike the high-field plasma components discussed above, the thiolato adducts for the two complexes are not the same. In this case therefore, the ligands are probably still coordinated to the copper. Whether this is a stable adduct or an intermediate species before the ligands are displaced is

uncertain. The significance of these differences in reactivities between the blood components and the copper complexes for the ligands 2'L and pbH with LH (which are paralleled in their cytotoxicities) will be discussed in Chapter 6.

1.4.2(d) Protonation Constants of the Ligands and their Copper(II) Complexes

The pKa values presented in Table 1.4.5 were obtained spectrophotometrically. Plots of pH vs. absorbance similar to that for $[Cu(4'L)(CH_3COO)]_2$ (see Figure 1.4.1) were obtained. By fitting the data to the equation $pH = pKa + \log\left(\frac{A_A - A_{APP}}{A_{APP} - A_B}\right)$ (where A_A, A_B and A_{APP} are the absorptions of the protonated, deprotonated and any intermediate species respectively) the pKa can be determined. The magnitude of the error for the pKa values presented in Table 1.4.5 was estimated from the standard deviation for that pKa determination. The accuracy of the determinations for the ligands was hindered by the high pH's needed for pK_{ii} (see Table 1.4.5 for a definition of the pK_a processes). At high pH, the ionic strength may have increased sufficiently (c.f. the background electrolyte concentration) and if the ionisation has not gone to completion the absolute values calculated will have large errors. The complexes in a number of cases did not exhibit ideal behaviour (isobestic points were spread). The low pK_{iii} values may also have the same inherent problems as for the above mentioned pK_{ii} determinations (i.e. high acid concentration for pK_{iii}). In spite of these problems, the values calculated are both internally consistent and realistic.

Petering *et al.* in 1977 [128] determined log protonation constants for CuL^+ of 2.40 and 8.30, and presumed them to characterise the protonation of CuL(OH), and the protonation of CuL^+ at the terminal amine (N(4)) nitrogen, respectively. However, a dissociation constant of 2.40 for a copper(II) hydroxy species is quite unrealistic (see below). Two years later, in a more comprehensive publication by the same group [57], the assignment of this value had been changed. It was now assumed to result from the protonation of the terminal N(4) nitrogen

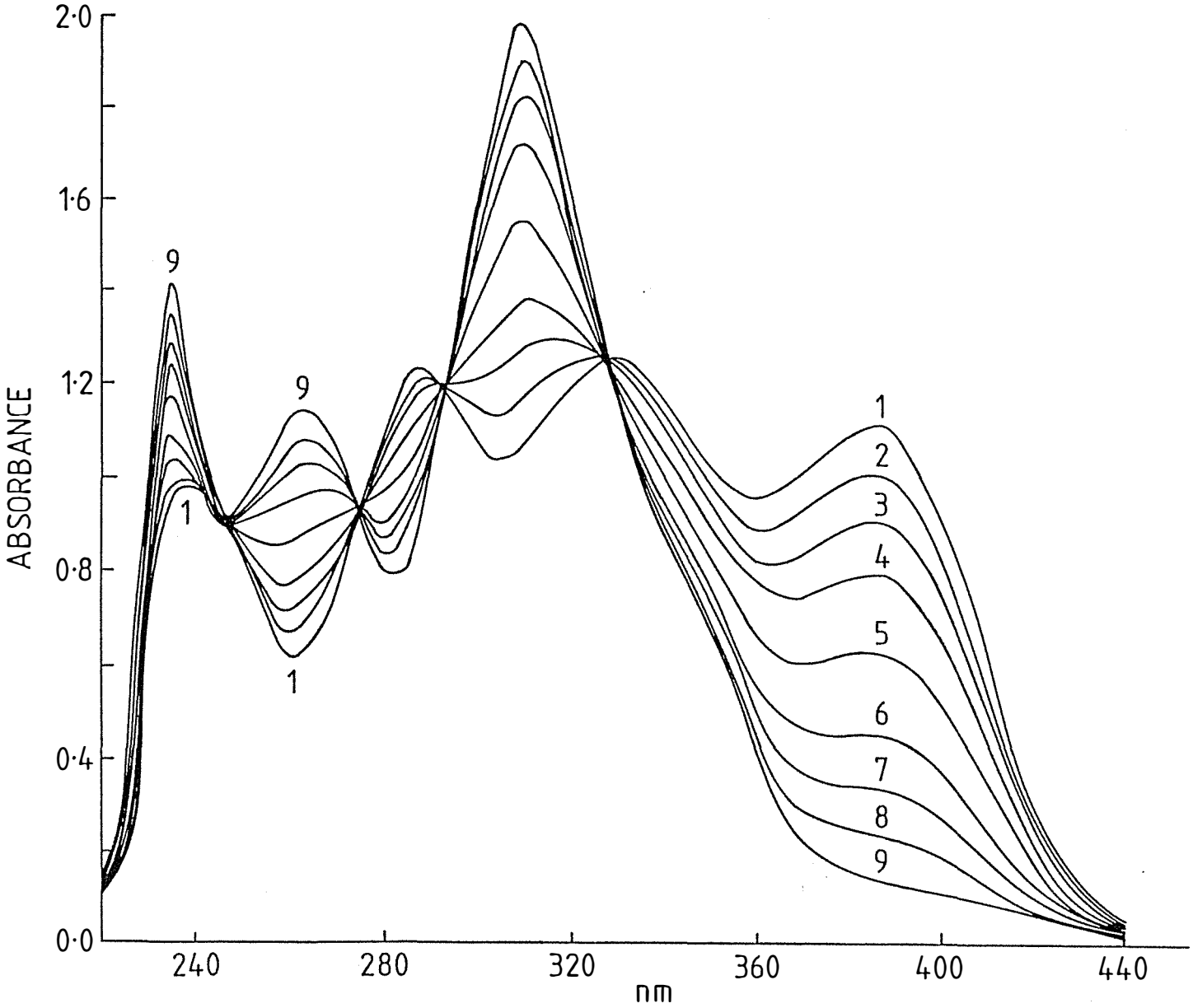

Figure 1.4.1: Spectral forms for $Cu(4'L)^+$ as a function of pH: c = 9.52 x 10^{-5} M; pH values of (1) 6.12, (2) 3.29, (3) 2.93, (4) 2.69, (5) 2.38, (6) 2.10, (7) 1.91, (8) 1.69, (9) 1.35.

TABLE 1.4.5

Protonation Constants and Reduction Potentials for Selected Section 1 Compounds

Compound[a]	pKa Values[b]		Isobestic Points (nm)			$E_{½}$ (mV)[d]
LH	i	3.6 ± 0.2	276	330		
	ii	11.5 ± 0.2	250	328		
6LH	i	4.6 ± 0.2	274	332		
	ii	11.1 ± 0.5	254	333		
4′LH	i	3.9 ± 0.2	273	332		
	ii	11.8 ± 0.5	250	334		
2′L	i	4.1 ± 0.2	278	333		
$[CuL(CH_3COO)]_2$	iii	2.4 ± 0.2	269	292	333	-150 ± 20
	iv	8.8 ± 0.5	285	315	370	
$[Cu(6L)(CH_3COO)]_2$	iii	2.8 ± 0.5	265	305	365	-210 ± 20
	iv	9.1 ± 0.5	290	330	376	
$[Cu(4'L)(CH_3COO)]_2$[c]	iii	2.7 ± 0.2	275	295	328	-260 ± 20
	iv	8.9 ± 0.5	285	313	370	
$[Cu(2'L)Cl_2]$[c]	iv	7.3 ± 0.5	247	277	313	-270 ± 20
$[CuL(pftp)]_2 \cdot 4H_2O$						0 ± 50
$[CuL(pctp)]_2$						-70 ± 50
$[CuL(bipy)]PF_6$						-70 ± 20
$[Cu(pbH)Cl_2]$						340 ± 20

a see page x for abbreviations

b pKa numbers refer to the processes

i e.g. $LH + H^+ \overset{pk_i}{\rightleftarrows} LH_2^+$

ii e.g. $L^- + H^+ \overset{pk_{ii}}{\rightleftarrows} LH$

iii e.g. $CuL^+ + H^+ \overset{pk_{iii}}{\rightleftarrows} Cu(LH)^{2+}$

iv e.g. $CuL(OH) + H^+ \overset{pk_{iv}}{\rightleftarrows} CuL(H_2O)^+$

using LH and CuL^+ as examples

c measured at 18° C. All others recorded at 24° C

d run in dmf with 0.1 M teap and quoted vs. the H electrode

(assigned the value of 8.30 in their first paper) as the log protonation constant for thiourea is 2.03 (no reference given). A reported value for pK_1 of thiourea found by this author is -1.2 [156] and the pKa values for thioamides are reported to be in the range -2.2 to -3.4 [195]. The assignment thus seems dubious and, as will be shown, there is another reason to doubt it. The protonation constant of 8.30 in Petering's second paper was now assigned to be the pKa of a bound water molecule (given the value of 2.40 in their first publication).

The protonation constants for the free ligand, LH, have been calculated by Petering *et al.* [57] and Tosi *et al.* [79] and were assigned to the deprotonation of the pyridine nitrogen (3.60 and 3.61 ± 0.2 for the above ordered references) and the deprotonation of the thiolate group (10.97 and 11.50 ± 0.2) by both groups.

In the present study, the protonation constants were determined for LH and the three methylated variations of this (6LH, 4′LH and 2′LH) as well as their copper complexes (see Table 1.4.5). The pKa's calculated for LH and CuL^+ agree quite well with the previously discussed values by Petering and Tosi [57,79]. The values of pK_i for the ligands range from 3.6 to 4.6 and, in accord with the previous references, are assigned to the protonation of the pyridine ring N, e.g.

$$LH + H^+ \overset{pk_i}{\rightleftarrows} LH_2^+$$

Verification of this comes from the pKa values of pyridine-2-carboxaldoxime (3.54 - 3.69), pyridine (5.47 - 5.75) and 2-methylpyridine (5.81 - 6.13) [156]. Pyridine-2-carboxaldoxime has a conjugated C=N in the 2-position, as does LH (pk_i of 3.6 ± 0.2) and is possibly the reason for the close agreement between the two. The effect of adding a sterically hindering methyl in the 6-position can be seen by the increase of the pKa value of pyridine on going to 2-methylpyridine. A similar effect is observed for the pair LH and 6LH with pKa's of 3.6 ± 0.2 and 4.6 ± 0.2 respectively.

The second protonation constant for the ligands, pK_{ii}, is assigned to the thiol group, e.g.

$$L^- + H^+ \overset{pk_{ii}}{\rightleftarrows} LH$$

In the ligand 2L, the methyl group on N(3) has replaced this proton, therefore pK_{ii} should not be observed. As this is indeed the case, credence is added to the assignment.

The copper complexes also exhibit two protonation steps (except for $Cu(2L)^{2+}$ which has one). The lower of the two pKa ranges, that of pK_{iii}, can not be due to the protonation of the pyridine as this is complexed. That the complex integrity remains in highly acidic solutions is demonstrated by Figure 1.4.1 where, even at a pH of 1.35 the spectrum shows no evidence of decomposition. This stability towards acid has also been demonstrated in the literature by spectroscopic means [57,79,128], and in this work, by the crystallisation of species from 1-4 M acids (see the previous three chapters). The absence of a pK_{iii} value for $Cu(2L)^{2+}$ suggests therefore that this protonation is at N(3) and not N(4) as proposed by Petering *et al.* [57]. The low value for pK_{iii} would then explain why it was not possible to form the neutral ligand complex $[Cu(LH)(CH_3COO)]_2(CH_3COO)_2$ (pKa of CH_3COOH is 4.75 [96]) whereas $[Cu(LH)(CF_3COO)]_2(CF_3COO)_2$ was synthesised (pKa of CF_3COOH is -0.26 [95] - see Chapter 1 for the crystal structure of this complex). The assignment by Petering [57] then, of this protonation to the terminal N(4) nitrogen would seem highly unlikely. Also, if it is not observed in the free ligand, then upon complexation where conjugation adds a small amount of double bond character to the C(7)-N(4) bond and hence a small positive change to N(4) (see Figure 1.12(b)), it is even less likely to occur.

The assignment of the higher protonation constant for the copper complexes, pK_{iv}, to the deprotonation of coordinated water is reasonable in light of the pK_1 values measured for the reaction:

$$Cu^{2+} + H_2O \overset{pk_1}{\rightleftarrows} Cu(OH)^+ + H^+$$

which range from 7.71 to 8.1 [196-198]. Complexation to the anionic ligands in CuL^+, $Cu(6L)^+$ and $Cu(4L)^+$ reduces the effective charge on the copper centre to one, reducing its polarisability with the result that the pKa value, pK_{iv}, should increase (relative to Cu^{2+}). The value obtained by Petering was 8.3 for CuL^+ whereas in this work it was 8.8 ± 0.5. In both cases the value is greater than for Cu^{2+}, as predicted. Using a similar argument, the pK_{iv} value for the dipositive complex $Cu(2'L)^{2+}$ should be lower than for the three unipositive compounds, and again this is observed (pK_{iv} for $Cu(2'L)^{2+}$ is 7.3 ± 0.5).

A point worthy of note is that the deprotonation for the free ligands (the thiol/thioamide proton) LH, 6LH and 4'LH has an average pK_{ii} value of 11.5 compared with 2.6 for pK_{iii}, the equivalent proton in the copper complexes. This is a change of approximately 9 log units. Thus the addition of copper to these ligands has changed this proton from being a very weak base in the free organic compound, to an acid, stronger than acetic acid, in the complex. The high molar conductance values, in conjunction with low aqueous pH values, for the neutral ligands discussed in the first three chapters, is a demonstration of this effect.

No correlation between the pKa values presented here and the cytotoxic activity for these compounds, to be presented in Section 2, Chapter 6 could be found (possibly due to the small number of data, their associated errors and/or the cell line used).

1.2.4(e) Reduction Potentials

The half-wave reduction potentials ($E_{½}$) for this work were determined polarographically using a dropping mercury electrode (d.m.e.) apparatus made by Dr Graham Bowmaker at Auckland University. Determinations were carried out in dmf solutions with a 0.1 M tetraethylammonium perchlorate (teap) carrier electrolyte vs. a saturated calomel electrode. Values were recorded at room temperature and corrected relative to the hydrogen electrode.

The d.m.e. method was chosen in preference to cyclic voltammetry for this work (electrodes used for cyclic voltammetry: reference = calomel; working = glassy carbon; auxiliary = platinum) as the former gave reproducible, reversible polarograms (although not ideal) in contrast to the latter when run on the same solutions. Dmf with teap was used as high complex concentrations could be obtained, the solvent has a large working range (window) and in aqueous solution the carrier electrolyte (KCl or $NaClO_4$) often caused precipitation of the chloride or perchlorate complex (even when 10% dmf or dmso was present).

The $E_{½}$ value for $[CuL(CH_3COO)]_2$ was determined by Petering *et al.* [57,128] to be 2 ± 10 mV in aqueous solution and to be a one electron process. A value of 4 ± 20 mV was obtained in this work (using the d.m.e. with the $[CuL(CH_3COO)]_2$ in 10% dmso/90% H_2O and 0.2 M KCl as the carrier electrolyte), is in good agreement with this. However, when dmf with teap was used, this value became -150 ± 20 mV (see Table 1.4.5). The difference between these determinations was due to the different solvent systems employed.

The thiolato adducts $[CuL(pftp)]_2 \cdot 4H_2O$ and $[CuL(pctp)]_2$ have $E_{½}$ values of 0 ± 50 and -70 ± 50 mV respectively. These values have become more positive, relative to $[CuL(CH_3COO)]_2$, due to the 'soft' thiolato sulphur coordinated in the plane. The $E_{½}$ for $[CuL(bipy)]PF_6$ (-70 ± 20 mV) has also increased, possibly due to the bipy being able to π bond and accept electron density from filled orbitals on the metal and facilitate the addition of an electron to the complex [128]. Also important may be the flexibility of bipy, allowing distortion of a copper(I) species to a more energetically favoured non-planar geometry. On going from the NNS tridentate constellation for CuL^+ to the NNO for $Cu(pbH)^{2+}$ the reduction potential has increased from -150 ± 20 to 340 ± 20 mV.

Several studies have revealed the importance of the reduction of CuKTS and its analogues in the biological activities of these complexes [56,199]. The general trend observed is; the more easily reduced the species, the more active it is; i.e. if the complex is so stable that it can resist

reduced *in vivo*, it is not active. Such a trend was not observed for the CuL^+ complexes, again possibly because of too few data.

1.2.4(f) Nuclear Magnetic Resonance Spectra

The n.m.r. spectra for LH and its analogues were recorded to fully characterise them and to shed some light upon the solution species present for the diamagnetic d^{10} transition metal (e.g. Zn(II), Cd(II), Hg(II), Ag(I), Au(I)) complexes of LH. All spectra were recorded in D_6-dmso and expressed in parts per million (p.p.m.) downfield (higher frequency) from either tetramethylsilane (TMS; δ_H and δ_C) or upfield from nitromethane (CH_3NO_2; δ_N).

Complete assignments for the ligand, LH, were made possible from the two-dimensional ^1H-^1H shift correlation spectrum (cosy) and the ^1H-^{13}C shift correlation spectrum (hetcor) (Figures 1.4.2 and 1.4.3) respectively), the J-resolved spectrum (Figure 1.4.4) and from a comparison with known pyridine compounds. The electron withdrawing α-thiosemicarbazone side-chain on the pyridine in LH was found to have very similar chemical shifts within the pyridine ring to those of 2-formylpyridine and 2-acetylpyridine (see Table 1.4.6). On this basis the pyridine carbons were assigned. The two remaining carbons, C(6) and C(7), were easily identified, as the electron deficient thioamide carbon, C(7), should be at higher frequency than the imine carbon C(6). As well, C(7) is a quaternary carbon and should have no ^1H-^{13}C coupling in the hetcor spectrum whereas C(6) has a tertiary structure and will be coupled. Such a pattern was observed. From the hetcor spectrum the protons were assigned according to their couplings to the carbon atoms. The splitting patterns observed in Figures 1.4.2, 1.4.3 and 1.4.4 due to the proton couplings within the pyridine ring agree with the assignments made. As an example, the H on C(1) will be coupled strongly to the H on C(2) ($J_{1,2}$ = 4.9 Hz) less strongly to the H on C(3) ($J_{1,3}$ = 1.8 Hz) and corresponding to its proximity to the H on C(4), more weakly still to it ($J_{1,4}$ = 1.0 Hz). Therefore, the coupling to these three protons results in a doublet of doublets of doublets (ddd) as shown in Figure 1.4.5(a) and the ^1H data in Table 1.4.7. In Figure 1.4.2, what appears to be a 1:2:1 triplet of doublets at 7.81 p.p.m. for C(3) is

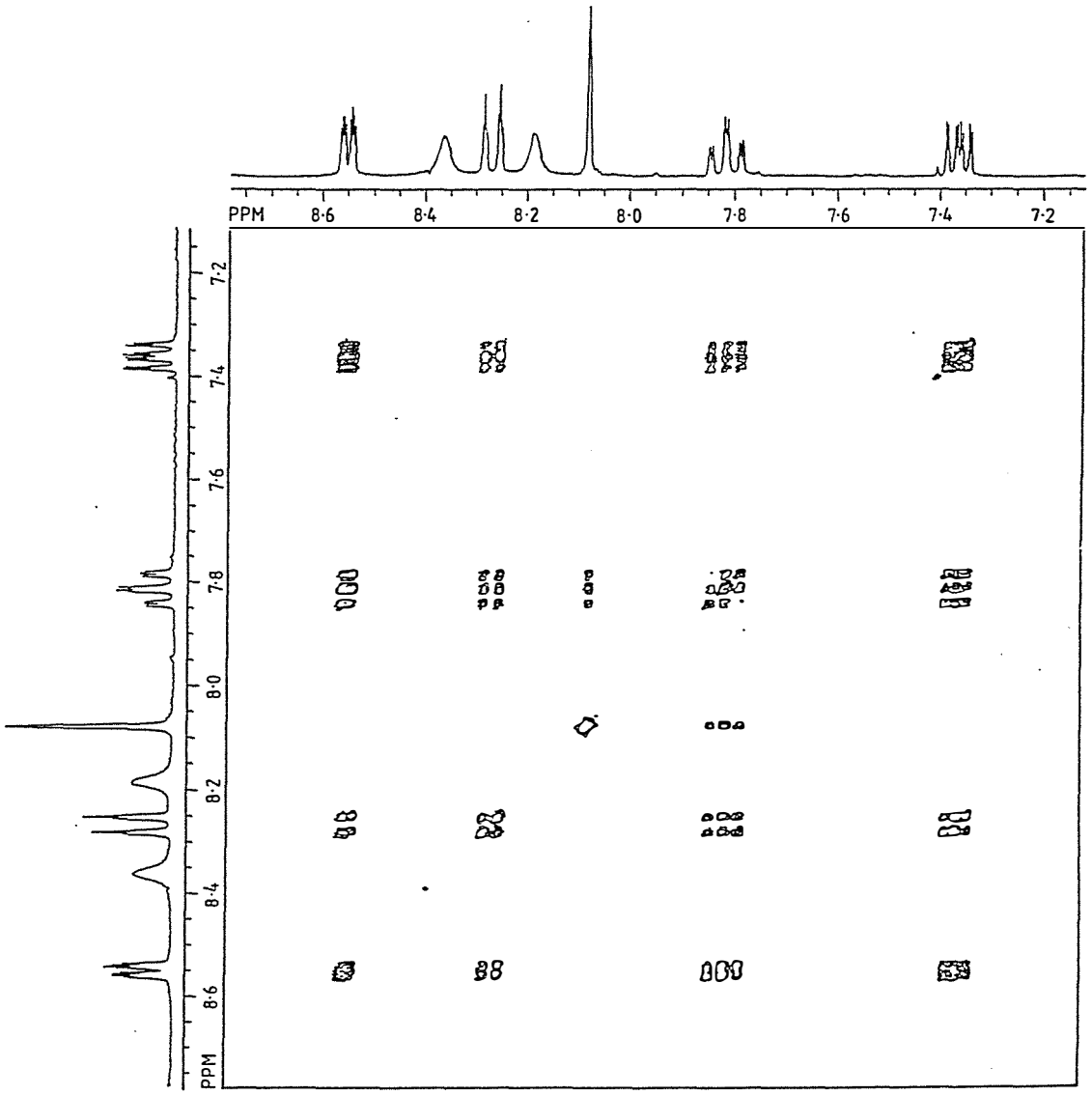

Figure 1.4.2: ^{1}H–^{1}H shift correlation (cosy) spectrum for LH; run in D_6-dmso vs. TMS

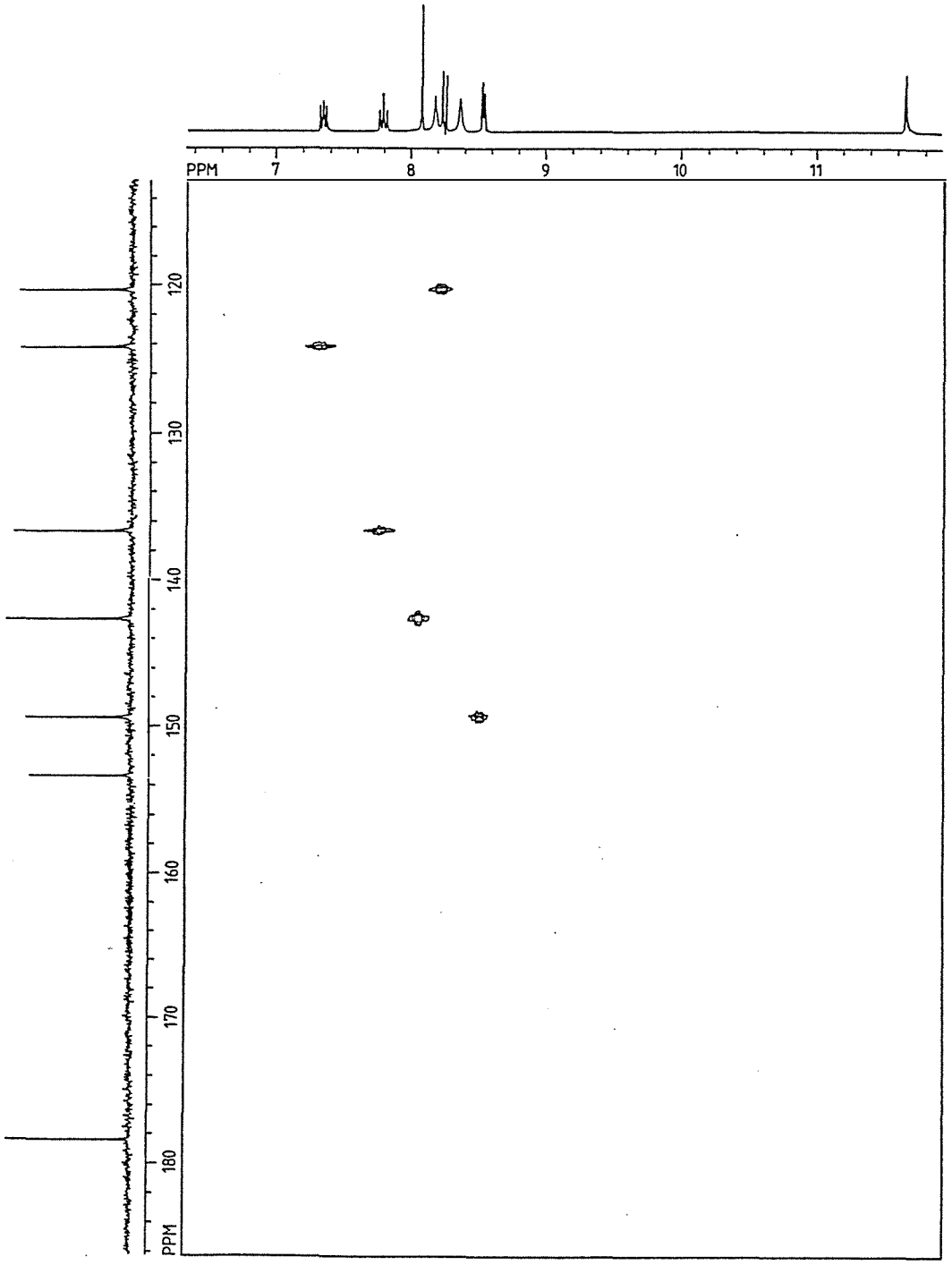

Figure 1.4.3: $^{1}H-^{13}C$ shift correlation (hetcor) spectrum for LH; run in D_6-dmso vs. TMS.

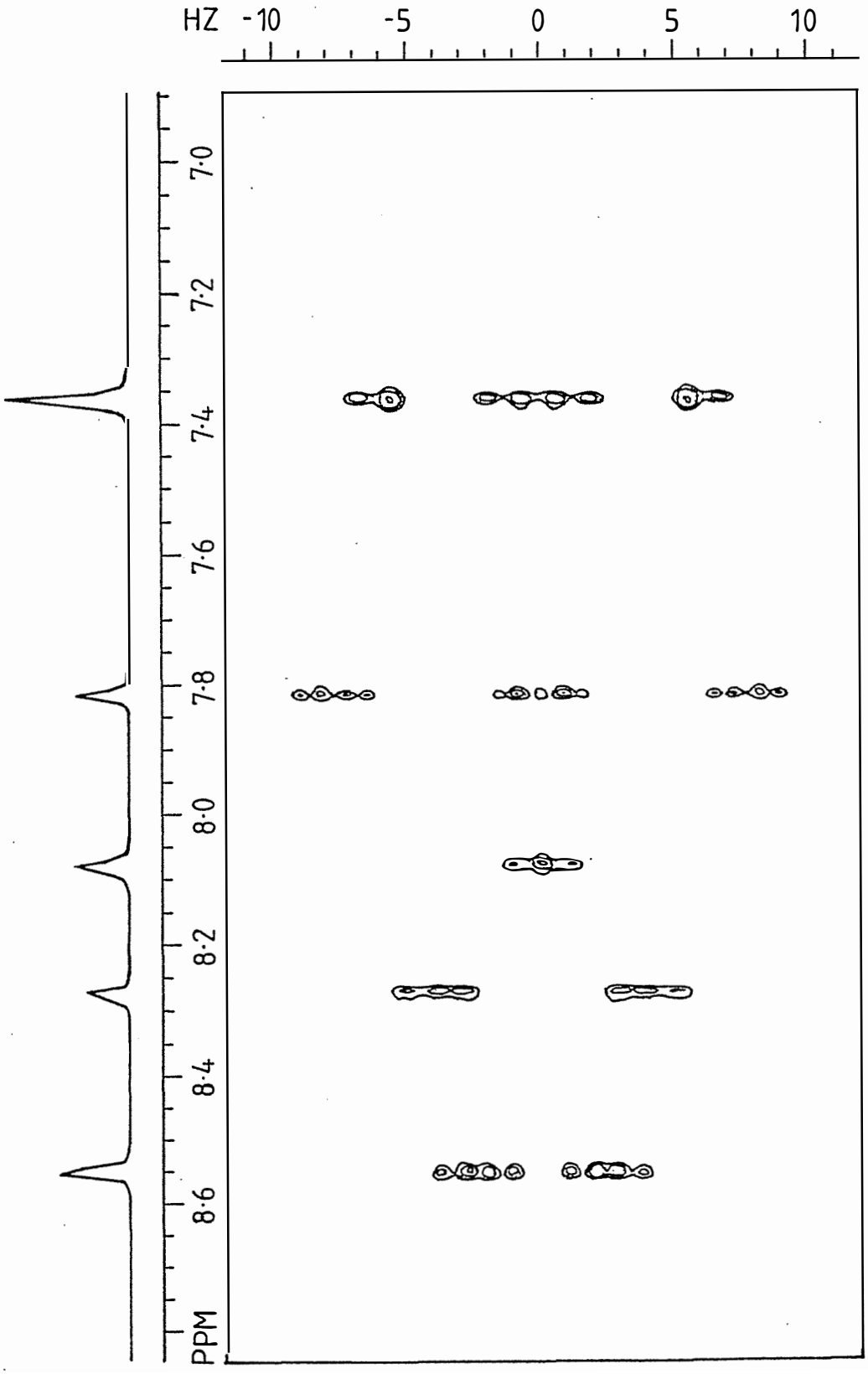

Figure 1.4.4: J-resolved spectrum for LH with the decoupled ^{1}H spectrum; run in D_6-dmso vs. TMS.

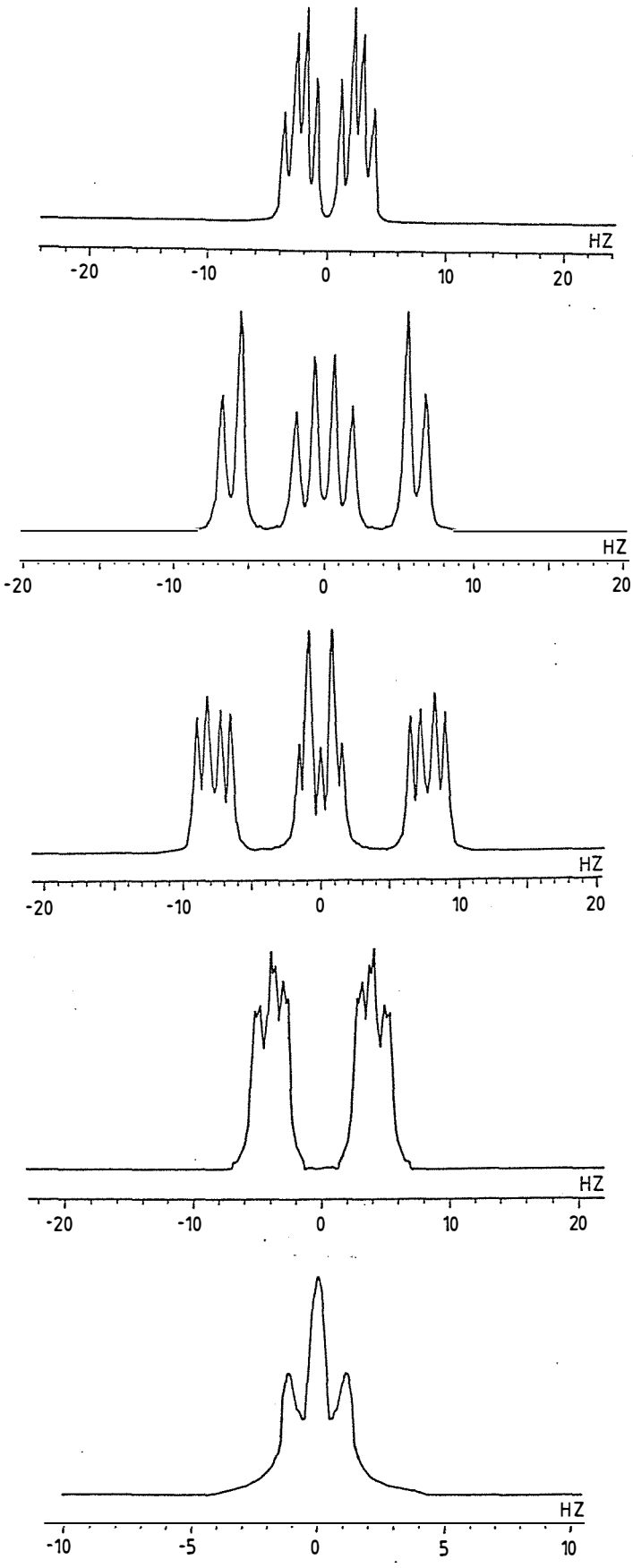

Figure 1.4.5: Slices through the J-resolved peaks for LH for the H attached to carbon atom number (a) C(1); (b) C(2); (c) C(3); (d) C(4); (e) C(6) (see Table 1.4.6 for atom labels).

TABLE 1.4.6

Selected Nuclear Magnetic Resonance Data for LH Type Compounds

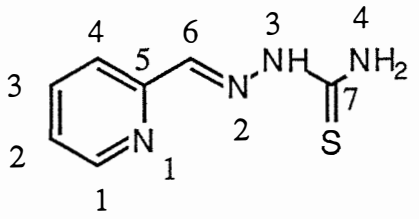

Carbon and Nitrogen Numbering Scheme Used

^{13}C N.m.r. Data for LH Type Compounds[a]

Compound	C(1)	C(2)	C(3)	C(4)	C(5)	C(6)	C(7)	CH_3
LH	149.3	124.2	136.6	120.3	153.3	142.6	178.4	
LH + Na[b]	149.1	122.5	136.2	119.4	155.8	142.1	181.6	major
	149.8	123.3	137.5	122.2	153.7	140.9	185.6	minor
6LH	157.8	123.7	136.9	117.7	152.6	143.0	178.4	23.9
4'LH	149.4	124.1	136.5	120.1	153.4	142.0	178.0	30.9
2'L [b, c]	149.3	124.2	136.7	120.8		140.8		32.4
					153.3		180.9	
	149.2	124.1	136.5	120.7		140.7	–	32.7
$[Zn(LH)Cl_2]H_2O$	149.1	124.3	137.0	120.5	153.1	142.2	178.4	–
$[ZnL_2]$	146.3	124.2	136.5	123.6	149.1	138.9	183.5	–
pyridine-2-aldehyde[d]	150.3	127.9	137.1	121.6	153.0	–	–	–
2-acetylpyridine[d]	148.5	127.0	137.4	121.5	154.3	–	–	–

^{15}N N.m.r. Data for LH Compounds[e]

Compound	N(1)	N(2)	N(3)	N(4)
LH	-67.1	-54.8	-209.3	-271.0
$[Zn(LH)Cl_2]H_2O$[f]	-81.7	-53.9	-208.8	-267.9
	-83.3			-270.6
	-117.2			
$[ZnL_z]$[g]	-73.1	-40.0[h]		

a spectra recorded in D_6-dmso and expressed in p.p.m. downfield from TMS (δ_C)
b two species observed
c both species are approximately of equal intensity with only one peak being observed for C(5) and C(7)
d after [200]
e spectra recorded in D_6-dmso and expressed in p.p.m. upfield from CH_3NO_2 (δ_N)
f three and two peaks asigned to N(1) and N(4) respectively
g complex not soluble enough to resolve all peaks
h peak marginally bigger than the background noise

TABLE 1.4.7

^{1}H N.m.r. Data for LH Type Compounds[a]

Compound[b]	Hydrogen atached to atom								
	C(1)	C(2)	C(3)	C(4)	C(6)	N(3)	N(4)		CH_3
LH[e]	8.55 ddd	7.36 ddd	7.81 tdd	8.27 dtd	8.08 s	11.65 s	8.18 s	8.36 s	–
6LH	–	7.13 d	7.61 t	7.94 d	8.02 s	11.64 s	8.15 s	8.31 s	2.39 s
4LH	8.55 ddd	7.36 ddd	7.84 ddd	8.24 dt	8.08 s	11.69 s	8.67 s		3.02 s
2L	8.59 ddd	7.36 ddd	7.81 dd	8.38 d	7.77 s	–	8.46 s	8.6[c] s	3.80 s
$[Zn(LH)Cl_2]H_2O$	8.56 d	7.38 t	7.84 t	8.27 d	8.08 s	11.67 s	8.20 s	8.37 s	–
$[ZnL_2]$	8.41 s	7.27 dd	7.54 d	7.82[c] d	7.86[c] s	–	7.09 s		–

a spectra recorded in D_6-dmso and expressed in p.p.m. downfield from TMS (δ_H)
s = singlet, d = doublet, t = triplet

b same numbering scheme as Table 1.4.6

c assignment uncertain

e coupling constants for LH (Hz): $J_{1,2} = 4.9$, $J_{1,3} = 1.8$, $J_{1,4} = 1.0$, $J_{2,3} = 7.4$, $J_{2,4} = 1.0$, $J_{3,4} = 8.1$, $J_{3,6} = 0.9$, $J_{4,6} = 0.5$. Similar values were observed for the other compounds in this table.

revealed to be more complicated than this in Figure 1.4.5(c). The 1:2:1 triplet pattern is not exact due to the coupling constants $J_{2,3}$ and $J_{3,4}$ being slightly different (7.4 and 8.1 Hz respectively). What is revealed now is a quartet (doublet of doublets) indicating that the hydrogen on C(3) interacts with two more protons with inequivalent coupling constants. One of these is $J_{1,3}$ (1.8 Hz) and surprisingly the other is $J_{3,6}$ (0.9 Hz). This was unexpected (but shown in the cosy spectrum) as the coupling is through five bonds. Similar couplings have however been observed before [202]. A weaker four bond coupling assumed to be between the hydrogens on C(4) and C(6) of approximately 0.5 Hz, is revealed by the splitting on the doublet of triplets in Figure 1.4.5(d) and the unresolved 'wings' on Figure 1.4.5(e). Why the coupling through five bonds from the hydrogen on C(6) to that on C(3) is larger than the four bond coupling to the hydrogen as C(4) is unknown.

The peaks which appear at 11.65, 8.36 and 8.18 p.p.m. in the hetcor spectrum of LH are not coupled to carbon atoms. Integration of the proton spectrum reveals eight peaks or multiplets which integrate as one hydrogen. Therefore, the two hydrogens on the terminal nitrogen, N(4), are inequivalent and were accordingly assigned to the pair of broad, non carbon coupled peaks at 8.18 and 8.36 p.p.m. That these two hydrogens are inequivalent indicates rotation about the C(7)-N(4) bond is restricted. This may be due to partial double bond character from electron delocalisation in the side chain as found in the X-ray crystallographic structures of 5-hydroxy-2-formylpyridine thiosemicarbazone [91] and 2-formylthiophene thiosemicarbazone [92] and/or hydrogen-bonding (either inter- or intramolecular).

The highest field peak at 11.65 p.p.m. was subsequently attributed to the thioamide group. The possibility that this hydrogen might be on either N(3), if the ligand was in the keto tautomer,or S, if in the thiol form, was investigated by running the D_6-dmso solution ir spectrum of LH. No ir band within 100 cm^{-1} of the expected range of 2 450 - 2 650 cm^{-1} for an SH stretch was observed [107]. The ligand would therefore appear to be in the thione form, in agreement with studies on related systems [91,92,195]. There is precedent for such a high–

field resonance for a hydrogen on a nitrogen, as others involved in conjugated systems display comparable values [203].

When sodium metal is dissolved in D_6-dmso the very strong base D_5-dmso is formed. Addition of LH to such a sample resulted in partial deprotonation, giving two solution species as observed in the ^{13}C n.m.r. spectrum (see Table 1.4.6). The major component has only slightly changed chemical shifts, therefore appears to be LH. The minor species however shows more marked alterations consistent with the deprotonated L^- anion. The thioamide carbon, C(7), has been deshielded, moving to higher frequency by 7.2 p.p.m. compared with LH. A similar effect is seen for C(5), C(3) and C(1) whereas shielding of C(6) and C(4) is observed. The effect is, as expected, less pronounced further from the site of deprotonation. These findings are consistent with the charge delocalised resonance structures which can be drawn for this structure and help to confirm the minor species as being the deprotonated ligand.

The ^{13}C spectrum of the neutral ligand complex formulated as $[Zn(LH)Cl_2]H_2O$ shows resonances which are similar to the uncomplexed ligand, LH, but shifted by up to 0.4 p.p.m. (e.g. for C(3) and C(6) - see Table 1.4.6). The effect is illustrated more dramatically for the non-isotopically enriched ^{15}N spectra of LH and $[Zn(LH)Cl_2]H_2O$. The resonance assigned to the pyridine nitrogen, N(1)*, of -67.1 p.p.m. in LH is no longer present in the zinc complex. Instead two peaks shifted to lower frequency at -81.7 and -83.3 p.p.m. and possibly a third at -117.2 p.p.m. appear. The terminal amine nitrogen, N(4), resonance which appears as a single resonance in LH at -271.0 p.p.m. is now split into two peaks which have been shifted slightly to higher frequency at -267.9 and -270.6 p.p.m. in $[Zn(LH)Cl_2]H_2O$. Both the imine, N(2), and thioamide, N(3), nitrogens have been shifted to higher frequency also, with values of -54.8 and -209.3 p.p.m. in the ligand and -53.9 and -208.8 p.p.m. in the zinc complex respectively. These changes are all considered to indicate that in solution the ligand, LH, is interacting with the zinc.

* ^{15}N resonances were assigned from, where possible, analogous pyridines (-62 to -70 p.p.m.), imines (-41 to -58 p.p.m.) and a thiourea ($CHCONHC(S)NH_2$). All resonances are in p.p.m. upfield from CH_3NO_2 (δ_N) after [201].

In the deprotonated zinc complex [ZnL_2], the resonances attributed to N(3) and N(4) could not be resolved, most probably due to the poor solubility of the complex in D_6-dmso. The two peaks which were resolved at -73.1 and -40.0 p.p.m. were assigned to N(1) and N(2) respectively (compared with the values of -81.7 and -53.9 p.p.m. in [$Zn(LH)Cl_2$]H_2O for the same ordered compounds). The respective shielding and deshielding observed for N(1) and N(2) compared with the free ligand can be rationalised in terms of the delocalised resonance charge distribution. The resonance structures for L^- show N(1) would have a net negative charge whereas N(2) would be positive, in agreement with the observed shifts. This factor therefore appears to be more important than the donation of a lone pair to the zinc in a sigma bond which, in the case of N(1), would tend to deshield the nitrogen (i.e. become less negative), in opposition to the observed shift. The resonance structures would also predict the shielding of N(3) and N(4) if these were resolved.

Unfortunately the ^{13}C and ^{1}H n.m.r. spectra for the other d^{10} metal complexes with this ligand (see Table 1.4.1) proved to be too complicated to interpret and the silver complexes decomposed in D_6-dmso. They were therefore not investigated further.

1.4.2(g) Summary

The four variations of the ligand LH and their copper(II) complexes, as well as a range of complexes of LH (where the metal was varied) were primarily synthesised for the cytotoxicity trials. Limited studies using a number of spectroscopic and physical techniques were however applied. The blood component e.s.r. spectra for $Cu(2L)^{2+}$ and $Cu(pb)^{+}$ displayed a number of differences when compared with CuL^{+}, possibly because of the decomposition of the former species in the presence of the biological media. The protonation data for LH and its analogues, as well as their copper(II) complexes, revealed a possible discrepancy with reported data, but more importantly showed the acidity of the thioamide proton to be reduced by approximately 9 pH units upon coordination to copper(II). Electrochemistry demonstrated the relative ease of reduction of the thiolato $[CuLSR]_2$ and bipy $[CuL(bipy)]^{+}$ adducts compared with $[CuL(CH_3COO)]_2$. A complete n.m.r. characterisation of the ligand LH was possible using a number of techniques and revealed the ligand to interact with Zn(II) in solution, when both neutral and deprotonated. Also, an unusual five-bond hydrogen coupling was observed between the hydrogen on the methylene group and the pyridine ring in LH. However, as will be discussed in Chapter 6, no correlations between the cytotoxic activities of these compounds and the parameters measured in this chapter were found.

1.4.3 EXPERIMENTAL

As the majority of procedures in this section were entirely analogous to those in the preceding three chapters for the corresponding LH compounds, the only preparations to be outlined will be those where a different method was used. Yields for those reactions not specified here are included in Table 1.4.1.

1.4.3(a) Preparation of Complexes

$[Cu(pb)(bipy)pftp]H_2O$

A solution of pentafluorothiophenol (0.12 cm^3, 0.88 mmols) and sodium metal (25 mg, 1.09 mmols) in ethanol (5 cm^3) was prepared. This was then added dropwise to a solution containing $[Cu(pb)(CH_3COO)]_2$ (347 mg, 1.00 mmols) and bipyridyl (164 mg, 1.05 mmols) in ethanol (20 cm^3). The thick brown precipitate which immediately formed was stirred and warmed for 2 minutes then filtered and washed with ethanol and diethyl ether before being vacuum dried. Yield 376 mg (57%).

$[Cu(pbH)Cl_2]$

To a solution of pbH (500 mg, 2.22 mmols) in hot ethanol (20 cm^2) was added $CuCl_2 \cdot 2H_2O$ (380 mg, 2.23 mmols) in ethanol (10 cm^3). The resulting pale green precipitate was heated and stirred for 5 minutes then filtered, washed with ethanol and diethyl ether and dried under vacuum. Yield 748 mg (94%).

$[Cu(2'L)X_2]$ (X = Cl^- or NO_3^-)

A solution of either $CuCl_2 \cdot 2H_2O$ (0.89 g, 5.22 mmols) or $Cu(NO_3)_2 \cdot 3H_2O$ (1.26 g, 5.20 mmols) in ethanol (20 cm^3) was added to a solution of 2'L (1.00 g, 5.15 mmols) in ethanol (60 cm^3). The green products which formed were heated briefly then filtered, washed with hot ethanol and diethyl ether and vacuum dried. Yields $[Cu(2'L)Cl_2]$ 1.377 g (81%); $[Cu(2'L)(NO_3)_2]$ 1.213 g (62%).

$[AgL]H_2O$

To a filtered solution containing LH (400 mg, 2.22 mmols) and sodium (58 mg, 2.52 mmols) in methanol (40 cm^3) was added $AgNO_3$ (390 mg, 2.30 mmols) in water (10 cm^3). The tan precipitate which formed at once was left to settle before being filtered, washed with methanol and water, then dried under vacuum. Yield 493 mg (77%).

$[Ag(LH)]X$ (X = NO_3^- or ClO_4^-)

A solution of $Ag(NO_3)$ (480 mg, 2.83 mmols) or $Ag(ClO_4)$ (586 mg, 2.83 mmols) in water (10 cm^3) was added slowly to a warm solution of LH (500 mg, 2.77 mmols) in methanol (50 cm^3). The resultant solutions were left to cool after which the yellow complexes were filtered off and washed successively with water, ethanol and diethyl ether and vacuum dried. Yields $[Ag(LH)]NO_3 \cdot \frac{3}{2}H_2O$ 858 mg (88%); $[Ag(LH)]ClO_4$ 748 mg (70%).

For the next two procedures it was necessary to reduce the Au(III) starting salt to Au(I) before the ligand, LH, was added (according to the method from [204]). The reducing agent used for this was 2, 2'-thiodiethanol ($S(CH_2CH_2OH)_2$).

$[AuL]\cdot 4H_2O$

To $NaAuCl_4\cdot 2H_2O$ (200 mg, 0.50 mmols) in methanol (5 cm^3) was added dropwise $S(CH_2CH_2OH)_2$ (0.16 cm^3, 1.60 mmols) in methanol (5 cm^3). The resulting solution was warmed gently. To this was added a solution of LH (92 mg, 0.51 mmols) and sodium (15 mg, 0.65 mmols) in methanol (10 cm^3). The pale yellow solution was stirred and warmed briefly then left for 4 hours. The crystalline yellow product which had separated was removed from the mother liquor and washed with methanol only, before being dried under vacuum. Yield 108 mg (46%).

$[Au(LH)]Cl\cdot H_2O$

The previous procedure was repeated, except no sodium metal was added to the ligand solution, to give a pale yellow complex. Yield 124 mg (57%).

$[ML_2]$ (M = Zn, Cd or Hg)

To a solution of LH (300 mg, 1.66 mmols) and sodium (44 mg, 1.91 mmols) in methanol (20 cm^3) was added a solution of $ZnCl_2$ (115 mg, 0.84 mmols), $CdCl_2$ (153 mg, 0.83 mmols) or $HgCl_2$ (226 mg, 0.83 mmols) in hot water (20 cm^3) plus 5 drops of 2M HCl. The bright yellow Zn and Cd and the green Hg complexes were filtered and washed with hot water and hot methanol, then vacuum dried. Yields $[ZnL_2]$ 318 mg (90%); $[CdL_2]\cdot \frac{1}{2}H_2O$ 334 mg (84%); $[HgL_2]$ 298 mg (63%).

$[M(LH)Cl_2]$ (M = Zn, Cd or Hg)

To a hot solution of LH (300 mg, 1.66 mmols) in methanol (40 cm^3) was added dropwise $ZnCl_2$ (227 mg, 1.67 mmols), $CdCl_2$ (316 mg, 1.72 mmols) or $HgCl_2$ (462 mg, 1.70 mmols)

in hot water (20 cm^3) plus 5 drops of 2M HCl. The solution was then heated for ½ hour then cooled. The white or pale yellow products which separated were filtered and washed with hot water and methanol, then vacuum dried. Yields $[Zn(LH)Cl_2]H_2O$ 346 mg (62%); $[Cd(LH)Cl_2]$ 244 mg (40%); $[Hg(LH)Cl_2]$ 501 mg (67%).

PbL_2

The title complex was synthesised inadvertently while trying to desulphurise the ligand LH. The general procedure used was for the desulphurisation of thioureas to give cyanimides according to [205]. To LH (0.5 g, 2.77 mmols) in water (10 cm^3) was added KOH (1.55 g, 27.6 mmols) in water (10 cm^3) and the solution was boiled. To this was added $Pb(CH_3COO)_2 \cdot 3H_2O$ (1.05 g, 2.77 mmols) in water (10 cm^3). The yellow precipitate which separated immediately was filtered off, washed with water, then dried under vacuum. Yield 507 mg (61%).

$[Zn(pb)_2]$

A solution of $ZnCl_2$ (142 mg, 1.04 mmols) in ethanol (10 cm^3) was added to a solution of pbH (450 mg, 2.00 mmols) and sodium (54 mg, 2.35 mmols) in ethanol (20 cm^3). The title complex separated as a fine yellow powder which was filtered and washed successively with hot water, ethanol and diethyl ether, then vacuum dried. Yield 379 mg (73%).

1.4.3(b) Protonation Constants

The protonation constants were carried out spectrophotometrically due to the insolubility of the compounds. A one litre 5 - 8 x 10^{-5} M solution of the appropriate ligand or complex in 0.1 M KCl was prepared by initially dissolving it in dmso (10 cm^3) so the final concentration of dmso was 1%. Spectra were recorded as a function of pH by the addition of ≤ 50 µl of acid (HCl) or base (KOH) to a 10 cm^3 sample of compound solution. Plots similar to that for

$[Cu(4L)(CH_3COO)]_2$ in Figure 1.4.1 were obtained. The data at several wavelengths about the most intense bands were fitted to the equation

$$pH = pKa + \log\left(\frac{A_A - A_{APP}}{A_{APP} - A_B}\right)$$

where A_A and A_B are the absorption of the protonated and deprotonated species respectively and A_{APP} is the absorption at any intermediate pH value [76]. A plot of pH vs. log $[(A_A - A_{APP})/(A_{APP} - A_B)]$ yields a line with the y intercept being the pKa value. The pH meter was calibrated using buffer solutions of pH - 2.0, 4.01, 7.00 and 12.4 and the spectra were recorded in 1 cm quartz cells.

1.4.3(c) Electrochemistry

The half-wave reduction potentials for all complexes in this work were determined polarographically using a dropping mercury electrode (made by Dr Graham Bowmaker at Auckland University). Dmf was chosen as the solvent as the complexes are generally not soluble in aqueous solution. Tetraethylammonium perchlorate (0.1 m) was the carrier electrolyte used. All solutions were degassed by bubbling dry nitrogen through them for 5 minutes prior to the polarogram being recorded at room temperature. Typical settings used for e.g. $[CuL(CH_3COO)]_2$ in dmf are: set = 0.4 V; range = -1.20 V; rate = 2 mV/s; current = 20 μA.

1.4.4 SECTION 1 SUMMARY

The 2-formylpyridine thiosemicarbazone ligand (LH) coordinates as a tridentate NNS species to copper(II) either in the neutral, LH, or deprotonated, L^-, forms. The complexes are stable in strong, non-oxidising acid solutions and can bind a large range of anions, often in unusual coordination modes. Ternary adducts between CuL^+ and potentially biologically relevant model sulphur, nitrogen and oxygen donors were synthesised and their possible roles in antitumour mechanisms were discussed. Variations of the CuL^+ system were made for the cytotoxicity trials by using substituted ligands or different metals. The ligands and their complexes were characterised, where applicable, by a number of physicochemical techniques including X-ray crystallography, e.s.r. (of the copper complexes and their interactions with blood components), n.m.r., ir and electronic absorption spectroscopies as well as protonation constants and electrochemistry. The results of these studies have been presented in the preceding four chapters of Section 1.

SECTION 2

STUDIES ON THE SALICYLALDEHYDE BENZOYLHYDRAZONE (sbH_2) SYSTEM

Background

The discovery last century of the antiinflammatory and analgesic properties of acetylsalicylic acid (aspirin) [206,207] has lead to a large body of research into the chemistry and properties of salicylates. More recently, it has been shown that the copper complexes of non-steroidal antiinflammatory agents are more effective than the parent drugs [208,209]. This lead to the suggestion that copper complexes were the active metabolites of these drugs. To test this, Sorenson *et al.* [21] compared the analgesic properties of salicylic acid (see Figure 2.1(a), anthranilic acid and 3, 5-diisopropylsalicylic acid (dipsH) against their respective copper(II) complexes. The complex $Cu(dips)_2$ proved to be only as effective as dipsH whereas the copper complexes of the former two compounds were more effective than their organic counterparts. The compound $Cu(dips)_2$, is however one of the most promising of a number of lipid soluble copper complexes of salicylates for which the observed activities must be attributed to the complexed form of Cu [210]. The range of activities displayed by these salicylates includes anticancer, anticarcinogenic, antiinflammatory, antiarthritic, anticonvulsant, antidiabetic, antimutagenic, radioprotectant and superoxide and peroxide scavenging [7,15,23,29,207,210-215].

Interest has not been limited to salicylic acids. A number of hydrazones of aromatic aldehydes with an ortho-hydroxy group (salicylaldehydes - see Figure 2.1(b)) have been synthesised as models for biological systems. The coenzyme, pyridoxal phosphate (plp see Figure 2.1(c)), is important because of the multiplicity of different enzymatic reactions that are dependent upon its presence. The initial combination of pyridoxal phosphate with an amino acid to form a Schiff-base is a common feature of these two-component dependent amino acid transformations [216]. Because of this, a number of Schiff-base compounds of pyridoxal and its analogues, with a range of amino acids and hydrazides have previously been synthesised, often with the aim of elucidating the mechanism of action for these vitamin B_6 containing enzymes [216-218].

(a)

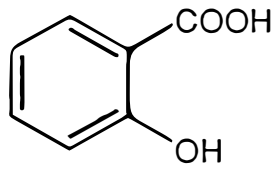

Salicylic acid

(b)

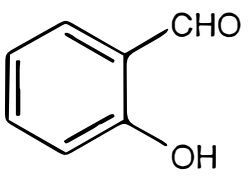

Salicylaldehyde (salH)

(c)

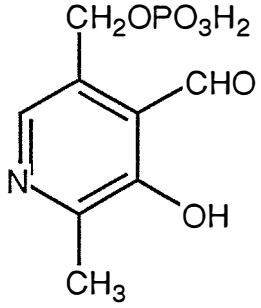

Pyridoxal phosphate (plp)

(d)

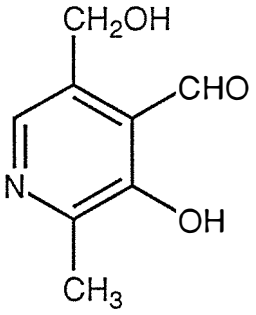

Pyridoxal

(e)

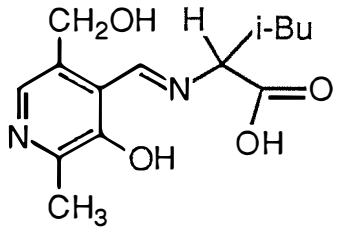

Pyridoxal leucine (plH_2)

(f)

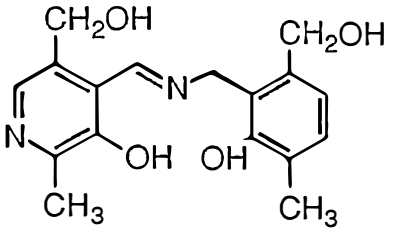

Pyridoxal pyridoxamine (ppH_2)

(g)

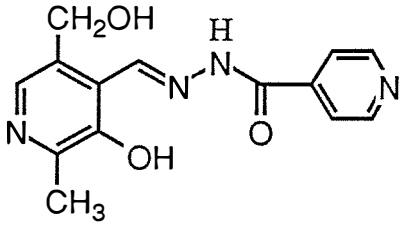

Pyridoxal isonicotinoyl hydrazone ($pihH_2$)

(h)

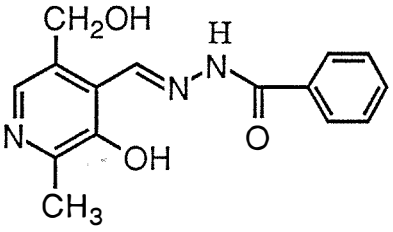

Pyridoxal benzoylhydrazone ($pbhH_2$)

(i)

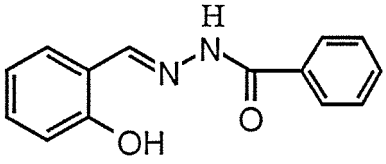

Salicyclaldehyde benzoylhydrazone (sbH_2)

(j)

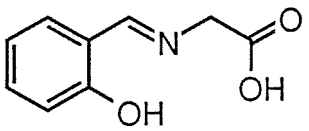

Salicylaldehyde glycine ($salglyH_2$)

Figure 2.1 The structures of selected compounds related to salicylic acid.

Amino acid hydrazones of salicylaldehyde, abbreviated as salα (where α is gly (glycine), ala (alanine), val (valine), leu (leucine), phen (Phenylalanine), phegly (phenylglycine) and lys (lysine)) and their copper(II) complexes have been studied as models for catalytic intermediates of the interaction pyridoxalphosphate with amino acids [219]. As well, complexes of the type $Cu(sal\alpha R)_2$ (where αR is an ester of an amino acid) undergo several reactions including oxidation, ester exchange and racemisation all of which are catalysed by the copper [220]. $Cu(salgly)\cdot xH_2O$ in particular has been investigated, with the single-crystal X-ray structures of both the hemi- and tetrahydrates being solved [221]. The chemistry of Cu(salgly) has also been probed. The addition of excess thiourea to copper(II) systems usually results in the reduction of the Cu. However, the [Cu(salgly)thiourea] ternary complex has been isolated as a stable solid and studied crystallographically [42]. Adducts of imidazole, 2-propylimidazole, pyridine, pyrazole and 2,5-dimethylpyrazole with Cu(salgly) have been prepared [219] as well as the pyridine, γ-collidine and N-methylimidazole adducts of a range of Cu(salα) complexes [217]. These adducts were studied both in the solid state and in solution. E.s.r. spectroscopy was used to try to gain some insight into the influence of neutral ligands on the structure of Cu(II) complexes with tridentate Schiff-base ligands related to plp. Also, complexes of these ligands may provide useful information which could help to elucidate the roles of plp *in vivo* e.g. the absorption of zinc by the intestine involves pyridoxine phosphate [222].

In 1982 Johnson *et al.* [223] evaluated a range of tridentate ONO hydrazones as iron-chelating drugs *in vivo*. At the time of their publication the only iron-chelating agent in clinical use was desferrioxamine B (dfo), a naturally occurring, hexadentate trihydroxamic acid. Five of these agents, represented in figure 2.1(e)–(i), are the four hydrazones of pyridoxal (plH_2, ppH_2, $pihH_2$ and $pbhH_2$) and salicylaldehyde benzoylhydrazone (sbH_2). All of these gave increased radio-iron excretions when compared with dfo at equivalent doses, but for sbH_2 the compound was toxic (LD_{50} of 75 mg/kg) when administered at high pH (as a suspension in water its LD_{50} is 800 mg/kg). It was also noted however, that $pihH_2$ and in particular sbH_2 appeared to be unusually potent inhibitors of DNA synthesis and cell growth in a variety of human and rodent cell lines grown in culture [223]. This will be discussed further.

Because of the interest in the iron-complexing ability of these tridentate ligands, several studies, including the X-ray crystallographic structures of $[Fe(pihH_2)Cl_2]Cl$ and $[Fe(pihH_2)Cl_2(H_2O)]Cl{\cdot}H_2O$ [224,225], have been carried out by others [226-228]. None of the complexing agents however appears to be in clinical use at present.

Another area which has gained prominence recently, has been that of naturally occurring and synthetic peptides. The reason for this probably stems from the isolation of the human plasma tripeptide glycyl-L-histyl-L-lysine (GHL). GHL has been shown to be growth-modulating [17,18], and to possess multiple wound-healing properties [19]. Its biological activities however, are dependent upon the presence of copper. GHL appears to function as a chelate of copper although the tripeptide chelates virtually any transition metal [18]. In the absence of copper, GHL is not wound-healing and does not give reproducible results in growth-modulating experiments. Also it functions synergistically with copper and iron ions to promote the growth of cultured hepatoma cells, as well as promoting the incorporation of copper into these cells [18].

In the X-ray crystallographic structure of $[Cu(GHL)]{\cdot}14H_2O$, GHL coordinates as a planar, tridentate, dianionic ligand, with the three nitrogen donor atoms being supplied by the glycine amino N, the first peptide N and the histidine imidazole N [229]. The lysyl side-chain is not involved in bonding to the copper but may shield it from water molecules and aid in the recognition of receptors that function in the uptake of copper into cells. Each Cu atom has a pseudo-square-pyramidal coordination geometry with the remaining in-plane and apical sites being occupied by carboxyl terminal oxygens. It was noted by Pickart [17] that a homology similarity between the tripeptide and the copper transport sites on albumin and α-fetoprotein exists. These proteins bind the Cu through a histidyl residue adjacent to a basic residue, and it was therefore suggested that GHL may act as a copper transport factor.

To further investigate this hypothesis, Pickart [18] synthesised analogues of GHL-Cu. These included the benzoyl, nicotinoyl, isonicotinoyl and picolinoyl hydrazones of pyridoxal and of salicylaldehyde (see Figure 2.1 for some examples). When they were tested for their inhibition of DNA synthesis, all were active, but salicylaldehyde benzoylhydrazone (sbH_2) and 2-formylpyridine-2′-pyridylhydrazone (papH see Figure 2.2) were by far the most potent.

(a) (b)

Figure 2.2 The structures of (a) salicylaldehyde benzoylhydrazone (sbH_2)
(b) 2-formylpyidine-2′-pyridylhydrazone (papH).

When tested on certain cell lines, the copper complexes of sbH_2 ($[Cu(sbH)Cl]H_2O$) and papH ($[Cu(papH)Cl_2]$) showed up to 100-fold increased potency when compared with the free organics. It was concluded that the remarkable activities of these hydrazone analogues of the Cu(GHL) binding region were inhibiting some specific process in the cells.

Studies on sbH_2 Analogues and their Complexes

In 1952 sbH_2 was shown to have modest bacteriostatic properties, although these were not sufficient to encourage further study at that time [230]. The more recent interest into this potentially tridentate ligand and its transition metal complexes, stems from the above mentioned properties as well as several others. These include;

(i) its use as an iron complexing agent for treatment of Fe overloading [223,227,228]

(ii) its use as a model for pyridoxalphosphate/amino acid intermediates and for the binding sites of albumin, fetoprotein and GLH [7,19,216,217,219,220,229]

(iii) the ability of sbH_2 but more significantly, Cu(sbH)Cl to inhibit DNA synthesis and cell growth [231,232]

(iv) the anomalous magnetic behaviour of related Cu(II) [228,233-238], Fe(III) [239] and Cr(III) [240] systems as a consequence of di- or polymeric structures

(v) the testing of Ni/sbH_2 and analogues as colouring agents in carbonless copying paper [241] and

(vi) to study the mode of coordination and the stereochemistry of these versatile hydrazones by forming a range of complexes [242-244].

Iskander *et al.* [244] prepared copper(II) chelates of, amongst others, salicylaldehyde aroylhydrazones (including sbH_2 and congeners as well as saH_2 - see Figure 2.5.11) for reason (vi) above. The complexes, formulated as Cu(XsbH)Cl·yH_2O (where the para substituent X = $0CH_3$, NO_2 and OH) and Cu(saH)Cl·H_2O were synthesised and displayed normal magnetic moments at room temperature. However, the neutral Cu(Xsb) complexes invariably had depressed moments. Pyridine adducts of both the neutral Cu(Xsb) and cationic $Cu(XsbH)^+$ complexes were isolated with the respective formulations of Cu(Xsb)py and Cu(XsbH)Cl·py and had normal moments. The stereochemistry of the compounds was inferred from magnetic, electronic and ir data. A more limited study upon the same lines as Iskander's utilising neutral copper(II) complexes of ONO tridentate ligands (including sbH_2

and analogues) was also carried out by Biradar and Havinale [235]. Again, all complexes showed subnormal moments.

Because of the biological relevance of both the copper and iron complexes of sbH_2, Johnson *et al.* [245,246] determined the single-crystal X-ray structures of $[Cu(sbH)Cl]H_2O$ and $\{Fe(sbH)Cl_2(CH_3OH)]$. In both structures, the ligand was shown to coordinate as a planar, tridentate moiety through the phenolic oxygen, imine nitrogen and amide carbonyl oxygen. The copper complex was four coordinate and planar with the chloride ion in the remaining site, whereas the iron was six coordinate with *cis*-chlorides and a coordinated methanol molecule. After the initial report of these structures plus the very promising reports on their biological activities, little more had been published when this work was initiated. However, during the course of this research two papers by Mohan *et al.* [226,247] were published. In these, a range of 3- and 5-substituted (into the salicylaldehyde ring) sbH_2 ligands were synthesised and their Fe(II), Fe(III), Mn(II), Co(II), Ni(II), Cu(II), Zn(II) and Pt(II) complexes prepared. Testing of the antitumour properties of these compounds against the P388 lymphocytic leukaemia test system in mice gave no significant activity at the dosages used. The same group also tested the closely related 3- and 5-substituted salicylaldehyde o-hydroxybenzoylhydrazones and their metal complexes (as above) and again found no significant activity at the dosages used [227]. A range of other potentially tridentate hydrazones have been synthesised and investigated, often for their anomalous magnetic behaviour [109,233,234] but little if anything was done to test their biological activities.

Possible Antitumour Mechanisms

The mechanism/s of biological activity for the hydrazones is at best vague. As with the thiosemicarbazones (see Section 1 Introduction), the copper complexes of these ligands tend to be more active than the free ligands. Hence, it has been suggested that the active form of the drug is in fact the metal complex. It is thought that copper intake, absorption, circulation and distribution may play a significant role in cellular utilisation [211]. Mobilisation of copper may

then result from the addition of a preformed complex or from the sequestering of biologically bound copper by the exogenous ligand. The physiological response might therefore be a result of:

(i) the coordinatively unsaturated copper complex binding to critical cellular targets e.g. DNA (intercalation, base or phosphate binding) or proteins

(ii) the complex being able to dismutate pro-oxidation states of oxygen e.g. superoxide, peroxide or singlet oxygen

(iii) the mobilisation of copper to, and the activation of, copper dependent enzymes e.g. superoxide dismutase

(iv) the facilitation of the absorption of the complex into cells whereupon the complex decomposes and either the copper, the ligand or both exert their biological effects.

A study on the interaction of the copper antitumour drug [Cu(papH)Cl_2] (see Figure 2.2(b) for the structure of papH) with DNA indicated intercalation did not occur [76]. Instead, the results were more consistent with outside (phosphate) binding. The ligand N-salicyloyl-N'-(2-furylthiocarbonyl) hydrazine was found to possess better antitumour activity than its copper complex and the appearance of the tumour mass was considered to be indicative of involvement of the host's immune system [248]. Sorenson [207,210,249,250] in his studies on copper salicylates found them to have superoxide dismutase mimetic properties, whereas another study [109] found that the copper complexes of ligands derived from salicylaldehyde and a range of amino pyridines did not react with superoxide in dmso solutions.

These findings reveal the interaction of ligands and their copper complexes with biologically relevant systems are complicated and not well understood. Considerably more research is needed, both to synthesise new compounds and to elucidate the physiological mechanisms of their action.

The Present Study

In the present study, the aim was to synthesise a range of substituted salicylaldehyde benzoylhydrazone (sbH_2) analogues and a selection of their transition metal complexes, primarily for cytotoxicity testing. Any correlations between the observed activities and selected measurable properties of the compounds have been investigated.

This section has two chapters. In the first, Chapter 5, the preparation of the ligands and their complexes is outlined and the X-ray crystallographic structures of three copper complexes will be presented. The physicochemical and structural properties of the compounds will be discussed with reference to their solid-state and solution properties. In Chapter 6, all of the cytotoxicity results for this work will be presented. Correlations between the cytotoxicities and, where possible, the lipophilicities and electronegativities of substituents will be discussed. As well, the significance of the copper in the complexes, as opposed to other metals, as well as that of the free ligand, is investigated.

CHAPTER 5

STUDIES ON sbH_2 CONGENERS AND THEIR COMPLEXES

2.5.1 INTRODUCTION

As previously stated, the tridentate ONO ligands based on salicylaldehyde benzoylhydrazone (sbH_2) and their transition metal complexes have been prepared in this work primarily for cytotoxicity trials. No ternary adducts were synthesised, partly due to the acidity of the second (amide) proton which was easily removed to form the highly insoluble species $[Cu(sb)]_2$. The study was therefore restricted to the interaction of the substituted sbH_2 congeners with $CuCl_2$ and simple metal salts with sbH_2 itself (see Tables 2.5.1 and 2.5.2). In spite of these limitations, a number of interesting and unusual properties of these compounds were observed. Three different complexes from a mixture of $CuCl_2$ and sbH_2 in ethanol were isolated, depending upon the pH, viz.

$$Cu(sbH_2)X_2 \xrightarrow{-HX} Cu(sbH)X \xrightarrow{-HX} Cu(sb)$$

The green complex formulated as $[Cu(sbH)Cl]H_2O$ has previously been studied crystallographically [245]. The non-hydrated form has also been reported but was brown [244]. Both were reported to have normal magnetic moments. In the present study, a brown form was also synthesised but had a depressed moment. A large number of the copper complexes of sbH_2 congeners also had reduced moments and subsequently were formulated as dimers. Because of the interesting magnetic properties of these complexes, the X-ray crystallographic structure of the low moment, dimeric compound formulated as $[Cu(sbH)ClO_4(H_2O)]_2$ was carried out. However, the crystals were not the same as the bulk sample, and were shown to be $[Cu(sbH)ClO_4(EtOH)]_2$. Two other crystal structures were also determined and these compounds, as well as others, were characterised spectroscopically.

Synthesis of the Compounds

The Ligands

The ligands (see Table 2.5.1) were generally synthesised by condensing the appropriate salicylaldehyde with the benzoylhydrazone to give the Schiff-base. A number of the substituted salicylaldehydes were prepared according to literature methods (see experimental section). The substituted benzoylhydrazones which were generally not commercially available had to be synthesised from the appropriate benzoic acid by first converting it to an ester and then to the hydrazide.

The Complexes

The complexes (see Table 2.5.2) were prepared by addition of ethanolic solutions of the metal salt to the hydrazone which usually afforded the desired complex e.g.

$$CuCl_2 + sbH_2 \xrightarrow{EtOH} \tfrac{1}{2}[Cu(sbH)Cl]_2$$

If, however, base was added to the reaction mixture the dianionic ligand copper(II) complex was obtained e.g.

$$CuCl_2 + sbH_2 \xrightarrow{Na/EtOH} \tfrac{1}{2}[Cu(sb)]_2$$

To prepare the neutral ligand complexes formulated as $[Cu(sbH_2)X_2]$ ($X = Cl^-$ or Br^-), the copper salt was first dissolved in the appropriate concentrated acid e.g.

$$CuCl_2/HCl + sbH_2 \xrightarrow{EtOH} [Cu(sbH_2)Cl_2(H_2O)]$$

The ligands prepared in this chapter are presented in Table 2.5.1 and their transition metal complexes are given in Table 2.5.2, along with their analytical and room temperature magnetic moment data.

TABLE 2.5.1

Analytical and Physical Data for Chapter 5 Ligands

Ligand[a]	Colour	Analyses (%)[b]			Melting Point (°C)
		C	H	N	
sbH_2	White	69.9 (70.0)	5.0 (5.0)	11.7 (11.7)	170-1
$3msbH_2{\cdot}H_2O$	White	66.4 (66.1)	5.8 (6.0)	10.3 (10.3)	184-6
$3mosbH_2$	White	62.8 (62.5)	5.6 (5.6)	9.8 (9.7)	100-10
$5msbH_2$	White	70.6 (70.8)	5.7 (5.6)	11.2 (11.0)	191-2
$5csbH_2$	White	61.1 (61.2)	4.1 (4.0)	10.3 (10.2)	220-1
$5nsbH_2$	Yellow	58.7 (58.9)	3.9 (3.9)	14.6 (14.7)	302-5
$s2mbH_2$	White	70.6 (70.8)	5.5 (5.6)	11.1 (11.0)	167-70
$s3mbH_2$	White	71.0 (70.8)	5.6 (5.6)	11.1 (11.0)	173-6
$s4mbH_2{\cdot}H_2O$	White	66.1 (66.1)	6.0 (5.9)	10.4 (10.3)	199-200
$s4fbH_2{\cdot}H_2O$	White	61.4 (60.8)	4.1 (4.8)	10.2 (10.1)	196-7
$s4cbH_2{\cdot}H_2O$	White	57.8 (57.4)	4.4 (4.5)	9.7 (9.6)	208-9
$s4BbH_2{\cdot}H_2O$	Pale orange	50.6 (49.9)	3.9 (3.9)	8.3 (8.3)	219-25
$s4abH_2$	Gold	66.1 (65.9)	5.1 (5.1)	16.2 (16.5)	220-40
$s4mobH_2$	White	66.4 (66.7)	5.2 (5.2)	10.4 (10.4)	184-7
$s2hbH_3$	White	65.6 (65.6)	4.7 (4.7)	11.0 (11.0)	284-7
$s4hbH_3$	White	65.4 (65.6)	4.8 (4.7)	11.2 (11.0)	272 (dec.)
$s4nbH_2$	Yellow	58.5 (58.9)	3.9 (3.9)	15.1 (14.7)	292-6 (dec.)
$5ms4mbH_2$	White	71.4 (71.6)	6.1 (6.0)	10.4 (10.4)	212-4
$5m4cbH_2$	White	62.4 (62.1)	4.6 (4.4)	9.7 (9.5)	254-6
$5ms4abH_2{\cdot}H_2O$	Gold	62.6 (62.7)	6.0 (6.0)	14.6 (14.6)	115-9 (dec.)
$5cs4mbH_2$	White	62.3 (62.4)	4.5 (4.6)	9.7 (9.7)	228
$3c5csbH_2{\cdot}H_2O$	Pale Yellow	51.7 (51.4)	3.7 (3.7)	8.5 (8.6)	214-7
$b5nbH_2$	White	58.5 (58.6)	4.5 (4.6)	14.6 (14.6)	210-3
bsH_2	White	69.9 (70.0)	5.0 (5.0)	11.9 (11.7)	248-51
psH_2	Pale Yellow	64.6 (64.7)	4.5 (4.6)	17.3 (17.4)	217-20
saH_2	White	60.7 (60.7)	5.6 (5.7)	15.7 (15.7)	203-5
$saaH_2$	Yellow	70.0 (69.9)	5.0 (4.8)	11.7 (11.5)	215-8

a see Figure 2.5.11 for an explanation of the ligand abbreviations and the basic structure forms
b calculated values are given in parentheses
dec. decomposed

TABLE 2.5.2

Analytical and Magnetic Data for Chapter 5 Complexes

Complex[a]	Colour	Analyses (%)[b]				μ_{eff}[c]
		C	H	N	Other	
$[Cu(sb)]_2$	Green	55.9 (55.7)	3.3 (3.4)	9.2 (9.3)		1.16
$[Cu(sbH)Cl]_2$	Brown	49.5 (49.7)	3.2 (3.3)	8.1 (8.3)		1.24
$[Cu(sbH_2)Cl_2(H_2O)]$	Khaki	43.2 (42.8)	3.6 (3.6)	7.2 (7.1)		1.85
$[Cu(sbH)Br]_2$	Brown	44.6 (43.9)	2.9 (2.9)	7.3 (7.3)		1.27
$[Cu(sbH_2)Br_2]_2H_2O$	Yellow	35.7 (35.6)	2.7 (2.8)	6.1 (5.9)		1.59
$[Cu(sbH)ClO_4(H_2O)]_2$	Green	39.7 (40.0)	3.1 (3.1)	6.5 (6.7)		1.25
$[Cu(sbH)NO_3]_2$	Brown	45.8 (46.1)	3.1 (3.1)	11.5 (11.5)		1.24
$[(Cu(sbH))_2SO_4]$	Green	47.7 (47.9)	3.3 (3.2)	8.0 (8.0)		1.50
$[(Cu(sbH)H_2O)_2SiF_6]\cdot 2H_2O$	Green	40.1 (41.0)	3.7 (3.7)	6.6 (6.8)	15.2 (13.9)[d]	1.81
$[Cu(3msbH)Cl]H_2O$	Green	48.1 (48.6)	4.0 (4.1)	7.7 (7.6)		1.85
$[Cu(3mosbH)Cl]\frac{5}{2}H_2O$	Green-Yellow	43.5 (43.6)	3.6 (4.4)	6.7 (6.8)		1.94
$[Cu(5msbH)Cl]_2$	Brown	51.2 (51.1)	3.7 (3.7)	7.8 (7.8)		1.25
$[Cu(5csbH)Cl]$	Green	45.3 (45.1)	2.4 (2.7)	7.5 (7.5)		1.83
$[Cu(5nsbH)Cl]$	Green	43.6 (43.9)	2.6 (2.9)	10.9 (11.0)		1.99
$[Cu(s2mbH)Cl]_2$	Brown	50.8 (51.1)	3.9 (3.7)	8.0 (8.0)		1.23
$[Cu(s3mbH)Cl]_2$	Brown	51.1 (51.1)	3.7 (3.7)	7.8 (8.0)		1.25
$[Cu(s4mbH)Cl]\cdot\frac{1}{2}H_2O$	Green	50.5 (49.9)	4.7 (3.9)	7.1 (7.8)		1.77
$[Cu(s4fbH)Cl]$	Green	46.9 (47.2)	2.8 (3.1)	7.8 (7.9)		1.74
$[Cu(s4cbH)Cl]$	Green	45.1 (45.1)	2.6 (2.7)	7.5 (7.5)		1.83
$[Cu(s4BbH)Cl]$	Dark Green	40.4 (40.3)	2.6 (2.7)	6.7 (6.7)		1.92
$[Cu(s4abH)Cl]_2\cdot 3H_2O$	Green	44.0 (44.2)	3.4 (4.0)	10.8 (11.1)		1.65
$[Cu(s4mobH)Cl]H_2O$	Green	46.6(46.6)	3.8 (3.9)	7.3 (7.3)		1.93
$[Cu(s2hbH)]_2$	Pale Green	52.9 (52.9)	3.2 (3.8)	9.0 (8.8)		1.35
$[Cu(s4hbH_2)Cl]_2H_2O$	Khaki	46.5 (46.3)	3.3 (3.3)	7.5 (7.7)		1.27
$[Cu(s4nbH)Cl]$	Dark Green	43.9 (43.9)	2.6 (2.9)	11.1 (11.0)		1.86
$[Cu(5ms4mbH)Cl]_2$	Tan	52.6 (52.5)	4.3 (4.1)	7.5 (7.7)		1.21
$[Cu(5ms4cbH)Cl]$	Green	46.8 (46.6)	3.1 (3.1)	7.4 (7.3)		1.81
$[Cu(5ms4abH)Cl]_2H_2O$	Brown	47.9 (47.9)	4.1 (4.0)	10.7 (11.2)		1.18
$[Cu(5cs4mbH)Cl]$	Green	46.6 (46.6)	3.1 (2.9)	7.2 (7.3)		1.79
$[Cu(3c5csbH)Cl]$	Green	41.3 (41.3)	2.2 (2.2)	6.7 (6.9)	26.0 (26.1)[e]	1.83
$[Cu(b5nbH)Cl]$	Green	44.0 (43.6)	2.6 (3.1)	11.0 (10.9)	9.4 (9.2)[e]	1.97
$[Cu(bs)]_2$	Dark Green	55.6 (55.7)	3.4 (3.4)	9.6 (9.3)		1.63
$[Cu(psH)Cl]$	Green	45.6 (46.0)	2.6 (3.0)	12.1 (12.4)		2.05
$[Cu(saH)Cl(H_2O)]$[f]	Green	36.7 (36.7)	3.3 (3.8)	9.5 (9.5)		1.83
$[Cu(saa)]$	Brown	55.8 (55.7)	3.3 (3.4)	9.2 (9.3)		1.78
$[Cu(sal)_2]$	Green	55.2 (55.0)	3.2 (3.3)			1.81
$[Cu(5msal)_2]$	Green	57.5 (57.5)	4.1 (4.2)			1.83
$[Zn(sbH)_2]H_2O$	Yellow	59.6 (59.8)	4.3 (4.3)	10.0 (10.0)		–
$[Zn(saH)_2]$	Pale Yellow	51.4 (51.5)	4.6 (4.7)	13.3 (13.3)		–
$[Ni(sbH)NO_3]\cdot\frac{1}{2}H_2O$	Pale Green	46.0 (45.6)	4.2 (3.3)	10.4 (11.4)		2.91
$[Co(sbH)NO_3]\cdot\frac{1}{2}H_2O$	Orange	46.3 (45.6)	4.0 (3.3)	10.6 (11.4)		4.57
$[Fe(sbH)_2]NO_3\cdot H_2O$	Dark Red	55.0 (54.7)	4.2 (4.0)	11.7 (11.4)		5.03
$[Fe_2(sb)_3]\cdot 4H_2O$	Red	55.7 (56.1)	4.4 (4.3)	9.3 (9.3)	11.7 (12.4)[g]	6.07
$[Cr(sbH)(sb)]$	Brown	62.9 (63.5)	4.2 (4.0)	10.6 (10.6)		3.76

a see Figure 2.5.11 for abbreviations
b calculated values are given in parentheses
c measured at 293K and quoted in B.M. Per copper(II) ion
d %F
e %Cl
f the X-ray structure for this complex shows it to be $[Cu(saH)Cl(H_2O)]H_2O$ although both samples are from the same preparation
g %Fe

2.5.2 CRYSTAL STRUCTURE OF μ-Hexafluorosilicato-bis[aqua(salicylaldehyde benzoylhydrazonato(1-))copper(II)] Dihydrate

A thermal ellipsoid diagram of the title complex (abbreviated as $[(Cu(sbH)H_2O)_2SiF_6]\cdot 2H_2O$) is given in Figure 2.5.1, showing the numbering scheme used. Bond length and bond angle data are given in Tables 2.5.3 and 2.5.4 respectively.

The complex $[(Cu(sbH)H_2O)_2SiF_6]\cdot 2H_2O$ was synthesised from a reaction mixture of $CuF_2.2H_2O$ in concentrated HF and sbH_2 in ethanol (see Experimental section). In order to heat the solution, it was briefly transferred to a pyrex beaker and the above complex resulted. The source of the SiF_6^{2-} therefore is from the action of the HF upon the silica in the glass.

The complex $[(Cu(sbH)H_2O)_2SiF_6]\cdot 2H_2O$ crystallises as a discrete centrosymmetric dimer with the two copper(II) centres bridged by the coordinated SiF_6^{2-} moiety with the silicon atom lying on the inversion centre. The copper adopts a distorted square-pyramidal geometry, the base of which is comprised of the tridentate salicylaldehyde benzoylhydrazono (ONO) moiety with the fourth in-plane position being occupied by a water molecule. In the fifth apical position is a more weakly coordinated F from the bridging SiF_6^{2-} anion. The closest sixth contact is to C(4) of a symmetry related molecule at 3.13 Å, which thus effectively blocks this position (see Figure 2.5.4).

The four basal atoms, N(1), O(1), O(2) and O(3) show a small tetrahedral distortion, with the dihedral angle, ω, between the planes of best fit containing Cu, O(1) and N(1)* and Cu, O(2) and O(3)§ being 8.1°. However, this is not expected to influence the spectroscopic properties

---

* Plane (i) Cu, O(1), N(1)
-0.7723X + 0.3186Y – 0.5496Z + 11.9127 = 0
[O(2) 0.11, O(3) -0.26]

§ Plane (ii) Cu, O(2), O(3)
-0.8217X + 0.1868Y – 0.53852 + 12.2255 = 0
[N(1) -0.26, O(1) 0.08]

Distances of the atoms from the plane (Å) are given in square brackets.

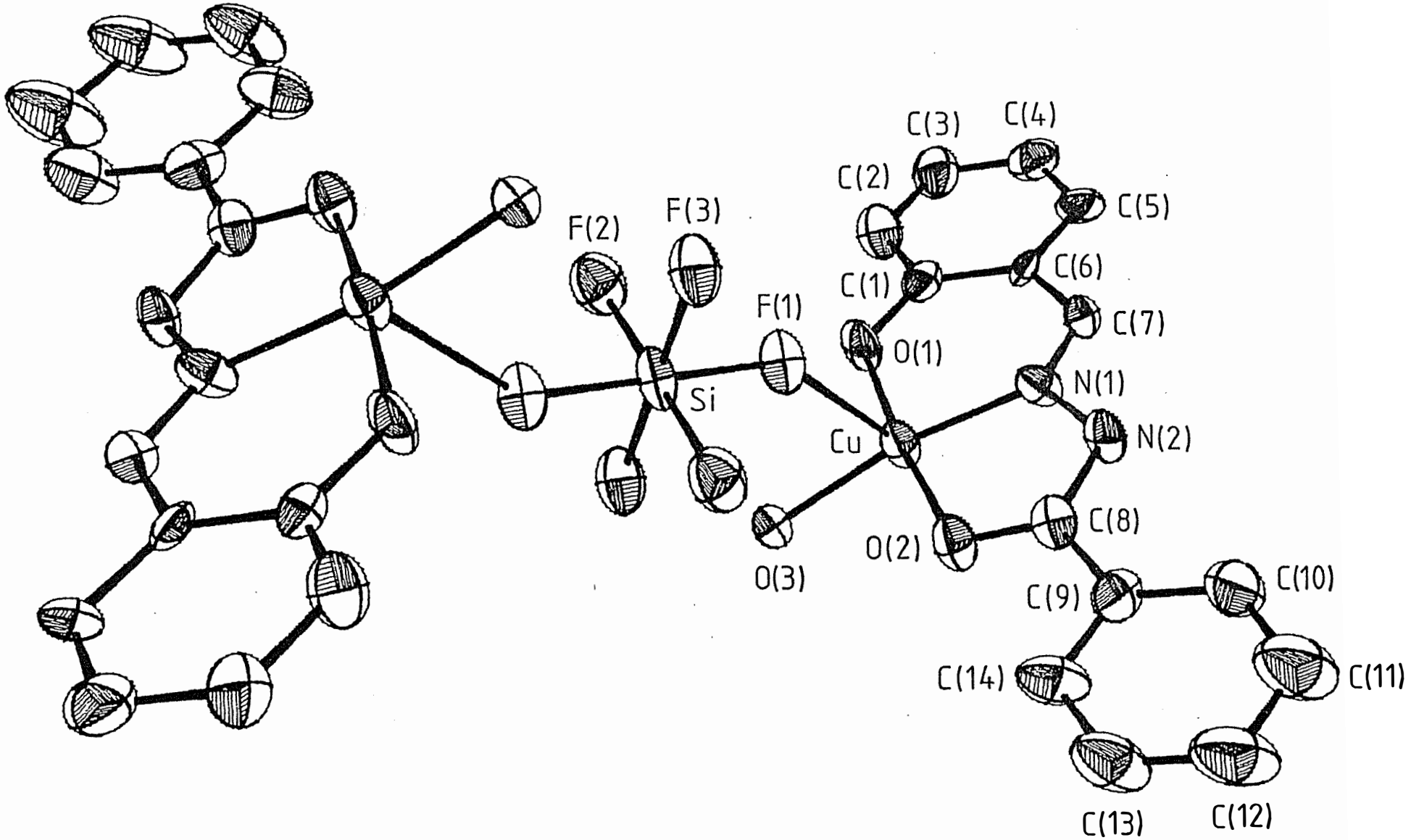

Figure 2.5.1: The dimer $[(Cu(sbH)H_2O)_2SiF_6]\cdot 2H_2O$ showing the atom numbering scheme. The non-coordinated water molecules and hydrogen atoms have been omitted for clarity.

TABLE 2.5.3
Bond Lengths (Å) with Estimated Standard Deviations in Parentheses for the Complexes $[(Cu(sbH)H_2O)_2SiF_6]\cdot 2H_2O$ and $[Cu(sbH)ClO_4(EtOH)]_2$*

	$[(Cu(sbH)H_2O)_2SiF_6]\cdot 2H_2O$			$[Cu(sbH)ClO_4(EtOH)]_2$
Cu–O(1)	1.891(8)			1.930(9)
Cu–O(2)	1.960(8)			1.987(11)
Cu–N(1)	1.909(9)			1.910(11)
Cu–O(3)	1.940(7)		Cu–O(1′)	1.938(11)
Cu–F(1)	2.523(5)		Cu–O(3)	2.289(9)
			Cu–O(11)	2.687(12)
O(1)–C(1)	1.344(11)			1.366(14)
C(1)–C(2)	1.395			1.407(18)
C(2)–C(3)	1.395			1.451(18)
C(3)–C(4)	1.395	Fixed		1.420(23)
C(4)–C(5)	1.395			1.338(24)
C(5)–C(6)	1.395			1.468(20)
C(1)–C(6)	1.395			1.383(20)
C(6)–C(7)	1.446(13)			1.431(20)
C(7)–N(1)	1.297(16)			1.261(14)
N(1)–N(2)	1.391(13)			1.359(15)
N(2)–C(8)	1.351(15)			1.327(16)
O(2)–C(8)	1.254(11)			1.325(17)
C(8)–C(9)	1.476(12)			1.406(19)
C(9)–C(10)	1.395			1.417(25)
C(10)–C(11)	1.395			1.370(30)
C(11)–C(12)	1.395	Fixed		1.489(29)
C(12)–C(13)	1.395			1.281(30)
C(13)–C(14)	1.395			1.428(27)
C(9)–C(14)	1.395			1.342(20)
Cu···Cu	8.075			2.999(4)

Hexafluorosilicato and Ethanol Bond Lengths (Å)

Si–F(1)	1.714(6)	C(20)–O(3)	1.377(22)
Si–F(2)	1.681(7)	C(20)–C(21)	1.303(40)
Si–F(3)	1.687(6)		

* C–H and N–H bond lengths fixed at 1.08 Å
O–H bond lengths 0.983-1.255, mean 1.08 Å
Cl–O bond lengths 1.235-1.587 Å, mean 1.46 Å

TABLE 2.5.4
Bond Angles (°) with Estimated Standard Deviations in Parentheses for the Complexes $[(Cu(sbH)H_2O)_2SiF_6]\cdot 2H_2O$ and $[Cu(sbH)ClO_4(EtOH)]_2$*

	$[(Cu(sbH)H_2O)_2SiF_6]\cdot 2H_2O$			$[Cu(sbH)ClO_4(EtOH)]_2$
O(1)–Cu–N(1)	92.4(4)			93.4(4)
O(2)-Cu-N(1)	81.8(4)			80.3(4)
O(1)-Cu-O(2)	173.3(3)			172.8(3)
O(1)-Cu-O(3)	93.4(3)		O(1)-Cu-O(1′)	78.3(4)
O(2)-Cu-O(3)	92.8(3)		O(2)-Cu-O(1′)	107.3(4)
N(1)-Cu-O(3)	170.4(3)		N(1)-Cu-O(1′)	166.3(3)
O(1)-Cu-F(1)	94.4(3)		O(1)-Cu-O(11)	94.1(4)
O(2)-Cu-F(1)	84.3(2)		O(2)-Cu-O(11)	82.5(3)
O(3)-Cu-F(1)	80.0(2)		O(1′)-Cu-O(11)	79.6(4)
N(1)-Cu-F(1)	107.1(3)		N(1)-Cu-O(11)	90.3(4)
			O(1)-Cu-O(3)	90.5(4)
			O(2)-Cu-O(3)	93.8(4)
			O(1′)-Cu-O(3)	92.6(4)
			N(1)-Cu-O(3)	98.3(4)
			O(11)-Cu-O(3)	170.0(3)
Cu-O(1)-C(1)	127.7(5)			126.8(8)
O(1)-C(1)-C(2)	117.0(7)			118.8(11)
O(1)-C(1)-C(6)	122.9(7)			120.2(12)
C(6)-C(1)-C(2)	120.0			120.9(11)
C(1)-C(2)-C(3)	120.0			116.7(13)
C(2)-C(3)-C(4)	120.0	Fixed		120.8(14)
C(3)-C(4)-C(5)	120.0			119.4(14)
C(4)-C(5)-C(6)	120.0			120.0(15)
C(5)-C(6)-C(1)	120.0			120.0(14)
C(5)-C(6)-C(7)	115.3(7)			114.0(13)
C(1)-C(6)-C(7)	124.6(8)			129.9(12)
C(6)-C(7)-N(1)	122.1(9)			126.5(12)
C(7)-N(1)-Cu	128.9(7)			125.8(10)
C(7)-N(1)-N(2)	118.1(9)			120.2(11)
Cu-N(1)-N(2)	112.4(7)			113.9(8)
N(1)-N(2)-C(8)	113.2(8)			116.8(12)
N(2)-C(8)-O(2)	120.0(9)			115.7(13)
N(2)-C(8)-C(9)	119.8(8)			123.6(13)
O(2)-C(8)-C(9)	120.2(10)			120.7(12)
Cu-O(2)-C(8)	112.6(8)			113.3(8)
C(8)-C(9)-C(10)	123.0(7)			120.4(14)
C(8)-C(9)-C(14)	116.9(6)			122.5(14)
C(10)-C(9)-C(14)	120.0			117.1(16)
C(9)-C(10)-C(11)	120.0			123.6(19)
C(10)-C(11)-C(12)	120.0	Fixed		116.1(23)
C(11)-C(12)-C(13)	120.0			119.2(24)
C(12)-C(13)-C(14)	120.0			122.8(21)
C(13)-C(14)-C(9)	120.0			120.9(17)
			Cu-O(1)-Cu′	100.5(3)

Hexafluorosilicato and Ethanol Bond Angles (°)

F(1)-Si-F(2)	89.9(3)	Cu-O(3)-C(20)	132.0(12)
F(1)-Si-F(3)	89.0(3)	O(3)-C(20)-C(21)	120.8(17)
F(2)-Si-F(3)	90.4(3)	Cu-O(11)-Cl	132.7(7)
Cu-F(1)-Si	144.0(3)		

* O-Cl-O bond angles 96.1 - 128.2°, mean 109°.

of the complex. In [Cu(sbH)Cl]H_2O [245], which appears to be the only other structure of a copper complex with this ligand to date, the metal was found to be approximately square planar. The fourth position in the plane wasoccupied by the chloride ion and there were no close axial bonding contacts. The Cu related bond lengths for this, the title and some analogous complexes (the two other complexes from this work will be discussed in turn after this structure) are presented in Table 2.5.5 for comparison. From this it can be seen that the Cu-ligand (Cu-O(1), Cu-O(2) and Cu-N(1)) bond distances are not significantly different between [(Cu(sbH)H_2O)$_2SiF_6$]·2H_2O and [Cu(sbH)Cl]H_2O in spite of the differences in their coordination geometries. A small difference is however observed between the Cu-O(1) bond lengths for these Cu(sbH)$^+$ compounds and the related Cu(salgly) complexes (using average bond lengths; Cu-O(1) 1.891(8) Å for Cu(sbH)$^+$ and 1.932(6) Å for Cu(salgly). This is probably due to the different ligands involved and that salgly^{2-} is coordinating as a dianionic moiety whereas sbH$^-$ is monoanionic. The in-plane Cu-water (bond length of 1.940(7) Å) in the title complex was not present in [Cu(sbH)Cl]H_2O. Instead the chloride ion was coordinated and the water molecule was 3.851 Å distant. The water may be equatorially bound in [(Cu(sbH)H_2O)$_2SiF_6$]·2H_2O as SiF_6^{2-} is expected to be a weaker base (c.f. the crystal structure in Chapter 1 of [Cu(LH)(ClO_4)$_2H_2O$]·2H_2O where the water is coordinated in the plane whereas the more weakly basic ClO_4^- ions are in the axial positions). Small variations in the bond angles were observed between the structures of [(Cu(sbH)H_2O)$_2SiF_6$]·2H_2O and [Cu(sbH)Cl]H_2O but due to the large errors associated with these, they were not considered to be of major significance.

The apically coordinated F(1), in [(Cu(sbH)H_2O)$_2SiF_6$]·2H_2O, is more weakly coordinated (Cu-F(1) 2.523(5) Å) than the four basal atoms, as is often seen for such copper(II) complexes undergoing Jahn-Teller distortions. F(1) does not form the apex of an ideal square pyramid, being displaced towards the other half of this dimer i.e. the angle between the normal to the

TABLE 2.5.5

Copper Bond Lengths in $Cu(sbH)^+$ and Some Related Complexes

Complex[b]	Copper Bond[a] Cu-O(1)	Cu-O(2)	Cu-N(1)	Cu-X(in-plane)	Cu-X(axial)	Ref.
$[(Cu(sbH)H_2O)_2SiF_6]\cdot 2H_2O$	1.891(8)	1.960(9)	1.909(9)	1.940(7)[c]	2.523(5)[d]	This work
$[Cu(sbH)ClO_4(EtOH)]_2$	1.930(9)	1.987(11)	1.910(11)	1.938(11)[e]	2.289(9)[f] 2.687(12)[g]	This work
$[Cu(sbH)Cl]H_2O$	1.891(8)	1.962(8)	1.933(9)	2.211(4)[h]	–	HYD 6
$[Cu(saH)Cl(H_2O)]H_2O$	1.909(2)	1.987(2)	1.936(2)	1.974(2)[c]	2.622(1)[h]	This work
$[Cu(salgly)]\cdot 4H_2O$	1.936(6)	1.959(6)	1.913(7)	1.965(6)[c]	2.352[c,i]	HYD 29
$[Cu(salgly)]\cdot 2H_2O$	1.928(6)	1.953(6)	1.947(7)	2.016(6)[c]	–	HYD 33

a using the numbering scheme in Figure 2.5.1
b sbH^- is the anion of salicyladehyde benzoylhydrazone
saH^- is the anion of salicylaldehyde acetylhydrazone
$salgly^{2-}$ is the dianion of salicyladehyde glycine
c $X = H_2O$
d $X = F$ of SiF_6^{2-}
e dimer, bridged throught he phenolic oxygen
f $X = O$ of ethanol
g $X = O$ of ClO_4^-
h $X = Cl^-$
i standard deviation not given

TABLE 2.5.6

Comparison of Salicylaldehyde Benzoylhydrazonato and Salicylaldehyde Acetylhydrazonato Bond Lengths (Å)

Bond	sbH^- [a]	saH^- [b]	Experimentally Determined Bond Lengths (Å)[c]		
C(6)-C(7)	1.446(13)	1.445(3)	C-C	1.541	
C(8)-C(9)	1.476(12)	1.487(5)	C=C	1.337	
C(7)-N(1)	1.297(16)	1.290(4)	C-N	1.472	
C(8)-N(2)	1.351(15)	1.334(4)	C···N	1.322	Partial Double Bond
C(1)-O(1)	1.344(11)	1.353(2)	C-O	1.43	
C(8)-O(2)	1.254(11)	1.255(4)	C=O	1.23	
N(1)-N(2)	1.391(13)	1.384(4)	N-N	1.44	
			N=N	1.24	

a $[(Cu(sbH)H_2O)_2SiF_6]\cdot 2H_2O$
b $[Cu(saH)Cl(H_2O)]$
c after [88]

plane of best fit containing the four basal donors and copper* and the Cu-F(1) bond is 14.5°. That the SiF_6^{2-} anion coordinates at all is unexpected, as will be discussed shortly.

The salicylaldehyde benzoylhydrazone ligand, sbH_2, coordinates to the copper atom as a monoanionic (sbH^-), tridentate moiety through the phenolic oxygen, O(1), the imine nitrogen, N(1) and the amide oxygen, O(2). This coordination mode has also been observed in the X-ray crystallographic structures of $[Cu(sbH)Cl]H_2O$ and $[Fe(sbH)Cl_2(MeOH)]$ [245].

In the closely related system, $[Cu(pshH_2)Cl]H_2O$ (where $pshH_3$ is pyridoxal salicyloylhydrazone [251]) the ligand coordinates as a monoanionic ONO tridentate moiety, although the amide proton (on N(2)) has been transferred to the heterocyclic N atom of the pyridoxal ring. A similar proton shift is also observed in the crystallographic structures of $[Fe(pihH_2)Cl_2]Cl$ and $[Fe(pihH_2)Cl_2(H_2O)]Cl\cdot H_2O$ (where $pihH_2$ is pyridoxal isonicotinoylhydrazone [224,225]: see Figure 2.1(g)) except this ligand has the heterocyclic N of the isonicotinoyi function protonated also, resulting in it having a net neutral charge. The amide proton therefore appears to be quite acidic when complexed.

Upon coordinating with the Cu(II) ion, sbH^- forms a five† and a six§ membered chelate ring, both of which are approximately planar and inclined at an angle of 4.5° to each other. The complexed ligand as a whole is also approximately planar, with the biggest deviation from the

* Plane (iii) Cu, O(1), O(2), O(3), N(1)
-0.7993X + 0.2504Y – 0.5462Z + 12.1447 = 0
[Cu 0.033, O(1) 0.08, O(2) 0.08, O(3) -0.09, N(1) -0.10]

† Plane (iv) Cu, O(2), N(1), N(2), C(8)
-0.7513X + 0.2969Y – 0.5894Z + 12.1686 = 0
[Cu -0.004, O(2) 0.01, N(1) 0.01, N(2) 0.00, C(8) -0.01]

§ Plane (v) Cu, O(1), N(1), C(1), C(6), C(7)
-0.6987X + 0.3406Y – 0.6291Z + 12.0816 = 0
[Cu -0.080, O(1) 0.06, N(1) 0.06, C(1) 0.01, C(6) -0.06, C(7) 0.01]

Distances of atoms from the plane (Å) are given in square brackets.

plane of best fit† (including the copper) being 0.18 Å for N(2). A similar situation was also found to be present for [Cu(sbH)Cl]H_2O [245].

A comparison of the bond lengths within the coordinated sbH^- ligand (excluding the phenyl rings) for the title complex is presented in Table 2.5.6 (along with [Cu(saH)Cl(H_2O)] and shows extensive delocalisation to be present. This may help to account for the observed planarity of the $Cu(sbH)^+$ system. The C(6) - C(7) and C(8) - C(9) bond distances are not significantly different (1.446(13) and 1.476(12) Å respectively) and are intermediate between a formal single- and double-bond. The N(1)-N(2) bond is also observed to have some double-bond character. More double-bond character is present in the C(7)-N(1) bond than in C(8)-N(2), as judged from their bond lengths (1.297(16) and 1.351(15) Å respectively). This is more consistent with canonical form (b) in Figure 2.5.2. In support of this also, is the C(8)-O(2) bond length of 1.254(11) Å which approaches the value of 1.23 Å expected for a formal C=O bond.

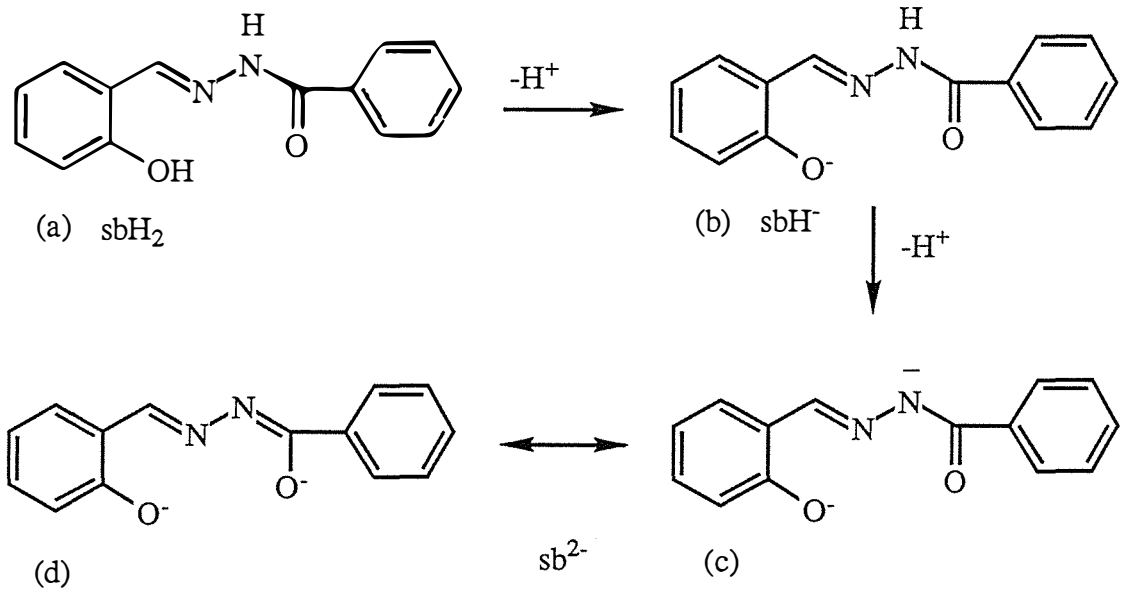

Figure 2.5.2 Some canonical forms of salicylaldehyde benzoylhydrazone (sbH_2)

† Plane (vi) Cu, O(1), O(2), N(1), N(2), C(1) - C(14)
-0.6710X + 0.3798Y – 0.6367Z + 11.9266 = 0
[Cu -0.084, O(1) 0.05, O(2) -0.09, N(1) 0.15, N(2) 0.18, C(1) 0.04, C(2) -0.03, C(3) -0.11, C(4) -0.11, C(5) -0.04, C(6) 0.04, C(7) 0.13, C(8) 0.03, C(9) 0.03, C(10) -0.04, C(11) -0.09, C(12) -0.08, C(13) -0.02, C(14) 0.04]
Distances of atoms from the plane (Å) are given in square brackets.

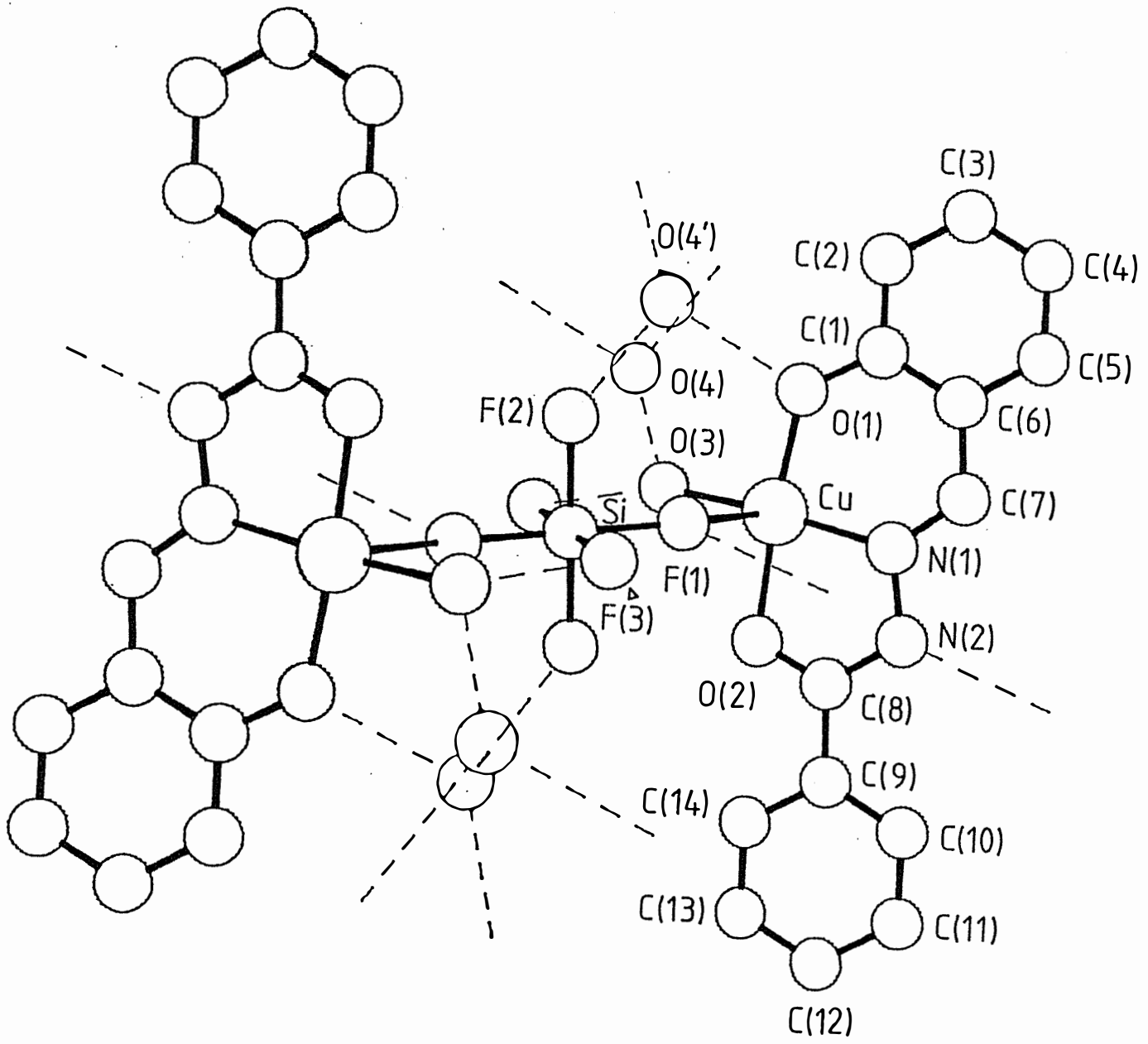

Figure 2.5.3: The dimer $[(Cu(sbH)H_2O)_2SiF_6]\cdot 2H_2O$ showing the atom numbering scheme and the hydrogen-bonding scheme.

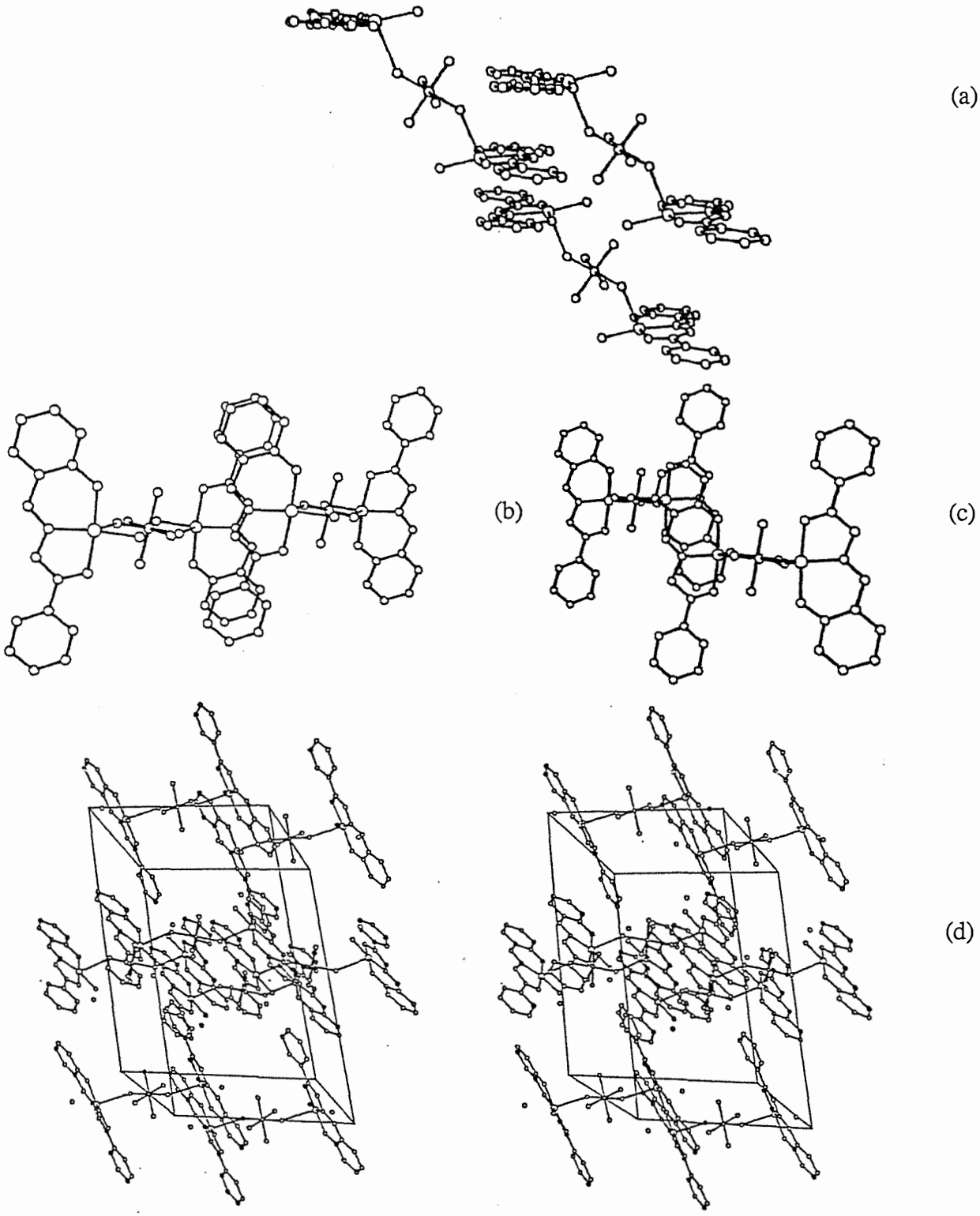

Figure 2.5.4: (a) Side-view of three $[(Cu(sbH)H_2O)_2SiF_6]\cdot 2H_2O$ molecules. The non-coordinated water molecules and hydrogen atoms have been omitted for clairyt in (a), (b) and (c)

(b) plan-view of the top two stacked molecules from (a)

(c) plan-view of the bottom two stacked molecules from (a)

(d) stereo-view of the unit-cell packing diagram.

TABLE 2.5.7
Hydrogen-Bonding Distances (Å) and Angles (°) for $[(Cu(sbH)H_2O)_2SiF_6]\cdot 2H_2O$

Atoms[a]	Distance (Å)	Symm[b]	T_x, T_y, T_z
F(1)···N(2)	2.77	6	1 0 1
F(2)···O(4)	2.80	6	1 $\bar{1}$ 1
F(3)···O(3)	2.68	2	1 0 1
O(1)···O(4)	2.66	6	1 $\bar{1}$ 1
O(3)···O(4)	2.63	1	0 0 0

a the first atom is at symmetry position 1

b symmetry positions

1	(x, y, z)
2	($\bar{x}$, $\bar{y}$, $\bar{z}$)
3	($\bar{x}$, y, 0.5 – z)
4	(x, $\bar{y}$, 0.5 + z)
5	(0.5 + x, 0.5 + y, z)
6	(0.5 – x, 0.5 – y, $\bar{z}$)
7	(0.5 – x, 0.5 + y, 0.5 – z)
8	(0.5 + x, 0.5 – y, 0.5 + z)

Atoms	Angle (°)	Atoms	Angle (°)
N(1)–N(2)···F(1)	115	C(8)–N(2)···F(1)	127
Si–F(1)···N(2)	120	Cu–F(1)···N(2)	94
Si–F(2)···O(4)	118	Si–F(3)···O(3)	114
Cu–O(1)···O(4)	111	C(1)–O(1)···O(4)	117
Cu–O(3)···F(3)	110	Cu–O(3)···O(4)	124
F(3)···O(3)···O(4)	114	F(2)···O(4)···O(1)	109
F(2)··· O(4)···O(3)	141	O(1)···O(4)···O(3)	103

Hexafluorosilicate is not a common anion. A literature search revealed several divalent metal complexes of the general formulation $M(II)(H_2O)_6SiF_6$ (where M(II) = Mg, Co, Ni, Fe, Mn, Zn and Cu [252-254 and refs. therein) but only six non-salt like complexes containing SiF_6^{2-} were located. Of these six, two were copper(I) complexes [255,256] and in only one structure, $[Co(viz)_4SiF_6]$ [257] (viz = N-vinylimidazole), was the hexafluorosilicate coordinated. In this complex, the Co(II) has four N atoms from the viz moieties coordinated equatorially and two F atoms belonging to different SiF_6^{2-} anions completing the tetragonal coordination sphere. The SiF_6^{2-} anions connect the $Co(viz)_4^{2+}$ cations by forming infinite linear chains.

In $[Cu(sbH)H_2O)_2SiF_6]\cdot 2H_2O$, the SiF_6^{2-} also coordinates to the copper atom in an apical position (Cu-F(1) 2.523(5) Å) bridging the centrosymmetrically related halves of the dimer. The Fs form a regular octahedron around the Si, with the F-Si-F bond angles being equal to 90° (within the limits of their esd's) as has been found in all previously reported structures [252-257]. The Si-F(1) bond length of 1.714(6) Å is marginally longer (0.03 Å) than the two non-coordinated Si-F bonds (Si-F(2) 1.681(7) and Si-F(3) 1.687(6) Å). In $[Co(viz)_4SiF_6]$ a similar pattern is observed whereby the coordinated F has an Si-F bond length 0.032 Å longer than the two equivalent non-complexed Fs (1.699(2) and 1.667(1) Å respectively). When the SiF_6^{2-} is not coordinated, as in $[Co(H_2O)_6]SiF_6$ and $[Fe(H_2O)_6]SiF_6$ (phos 12), the Si-F bonds are 1.643(5) and 1.706(9) Å respectively. In these two structures, each F is involved in two hydrogen-bonds to water molecules. However, in $[Co(H_2O)_6]SiF_6$, one of these contacts is longer and correspondingly results in the shorter Si-F bonding distance observed.

In $[(Cu(sbH)H_2O)_2SiF_6]\cdot 2H_2O$ each F of the SiF_6^{2-} anion is involved in one hydrogen bond. The hydrogen-bonding scheme for one dimer is shown in Figure 2.5.3 with the relevant data listed in Table 2.5.7; in Figure 2.5.4(d) the stereo-view of the unit-cell is given. The contacts involving the F atoms of 2.80 Å for F(2)···O(4) and 2.68 Å for F(3)···O(3) (as well as 2.77 Å for F(1)···N(2)) lie within the experimentally determined F···O(H_2O) range of 2.68 to 2.88 Å [252-254] found in other structures. The coordinated water molecule, O(3), in addition to its

contact with F(3), is hydrogen-bonded to the non-complexed water, O(4) (O(3)··· O(4) 2.63 Å). O(4) forms two more contacts; one is the above mentioned hydrogen-bond to F(2) and the other is to the phenolato oxygen O(1) (O(1)···O(4) 2.66 Å).

Another possible interaction which may however be significant is overlap of the molecular π clouds. Estimates of the effective thickness of an aromatic ring range from 3.4 - 3.7 Å [97,174]. Contacts within or less than this range between π delocalised systems may therefore be important. In Figure 2.5.4(a), it can be seen that stacking of the complexed ligand moieties occurs. The dimeric units are related to each other by inversion centres and appropriate translations, effectively maintaining the planar ligands in a parallel arrangement. In Figure 2.5.4(b) a plan-view of the top two dimers from (a) is given, demonstrating the almost ideal alignment of the phenyl rings. The planes of the two ligands are 3.63(1) Å apart and result in a Cu···Cu separation of 5.74(1) Å. A similar view for the bottom two dimers is given in Figure 2.5.4(c). The overlap here does not include the benzoyl, phenyl ring of the ligand (C(9) - C(14)) but the two delocalised ring systems are significantly closer than for the previous pair of planes. Now they are 3.21(1) Å apart with a Cu···Cu separation of 6.04(1) Å. Columns of stacked ligands are therefore formed with alternating distances between the best-fit least-squares planes of 3.63(1) and 3.21(1) Å. This appears to be important in the stabilisation and molecular packing of the dimeric $[(Cu(sbH)H_2O)_2SiF_6]\cdot 2H_2O$ complex. The planar stacking of the ligands and the partial double-bond character in the C(8)-C(9) bond appears to be forcing the benzoyl ring (C(9) - C(14)) to be coplanar with the remainder of the ligand (see plane (vi)). These would seem to be more important than the expected steric interactions between C(14)···O(2) and C(10)···N(2) which might otherwise rotate this ring.

The close approach of the π systems to each other may provide a mechanism by which the copper(II) atoms can magnetically interact. The separation of the two copper atoms within a dimer is 8.08 Å whereas the Cu···Cu distances between the stacked ligands are 5.74(1) and 6.04(1) Å (see above).However, as will be shown, the room temperature magnetic moment and the powder e.s.r. spectrum at -160° C do not indicate magnetic exchange.

2.5.3 CRYSTAL STRUCTURE OF Bisethanoldiperchloratobis-(μ-[salicylaldehyde benzoylhydrazonato (1-)]-μ-O, N, O')dicopper(II)

The title complex, abbreviated as $[Cu(sbH)ClO_4(EtOH)]_2$, is depicted in the thermal ellipsoid diagram, Figure 2.5.5, showing the numbering scheme used. Tables 2.5.3 and 2.5.4 contain the bond length and bond angle data respectively.

The complex $[Cu(sbH)ClO_4(EtOH)]_2$ crystallised from the ethanolic mother liquor of a reaction which yielded the compound formulated as $[Cu(sbH)ClO_4(H_2O)]_2$. It is therefore not the same as the bulk sample, but may still be representative of its structure. Decomposition of the title complex during the data collection occurred and may have been due to loss of the coordinated ethanol molecule. However, attempts to recrystallise $[Cu(sbH)ClO_4(H_2O)]_2$ from ethanol to give $[Cu(sbH)ClO_4(EtOH)]$ were unsuccessful.

The title complex crystallises as a centrosymmetric dimer, with the coordinated tridentate, anionic sbH^- ligand bridging the two copper(II) centres via the phenoxy oxygen, O(1) (see Figure 2.5.6). A similar side-by-side planar structure was reported for acetylacetone-mono-(o-hydroxyanil)copper(II) [234]. In this complex, the ligand also coordinates as an ONO tridentate moiety and bridges the two copper(II) centres through the phenoxy oxygen , resulting in a Cu···Cu separation of 2.989(3) Å and the observed magnetic moment of 1.37 B.M.. In this current work, the Cu···Cu distance is 2.999(4) Å whereas the magnetic moment of the bulk sample ($[Cu(sbH)ClO_4(H_2O)]_2$) is 1.25 B.M.. The assumption that the bulk sample has a structure similar to $[Cu(sbH)ClO_4(EtOH)]_2$ therefore appears reasonable.

The coordination sphere of the copper atom can be described as elongated tetragonal. The anionic ligand, sbH^-, coordinates in the plane as previously observed [this work, 245] via the phenolato oxygen, O(1), the imine nitrogen N(1) and the amide carbonyl oxygen, O(2) (see Figures 2.5.5 and 2.5.6). The fourth equatorial donor atom is supplied by the bridging

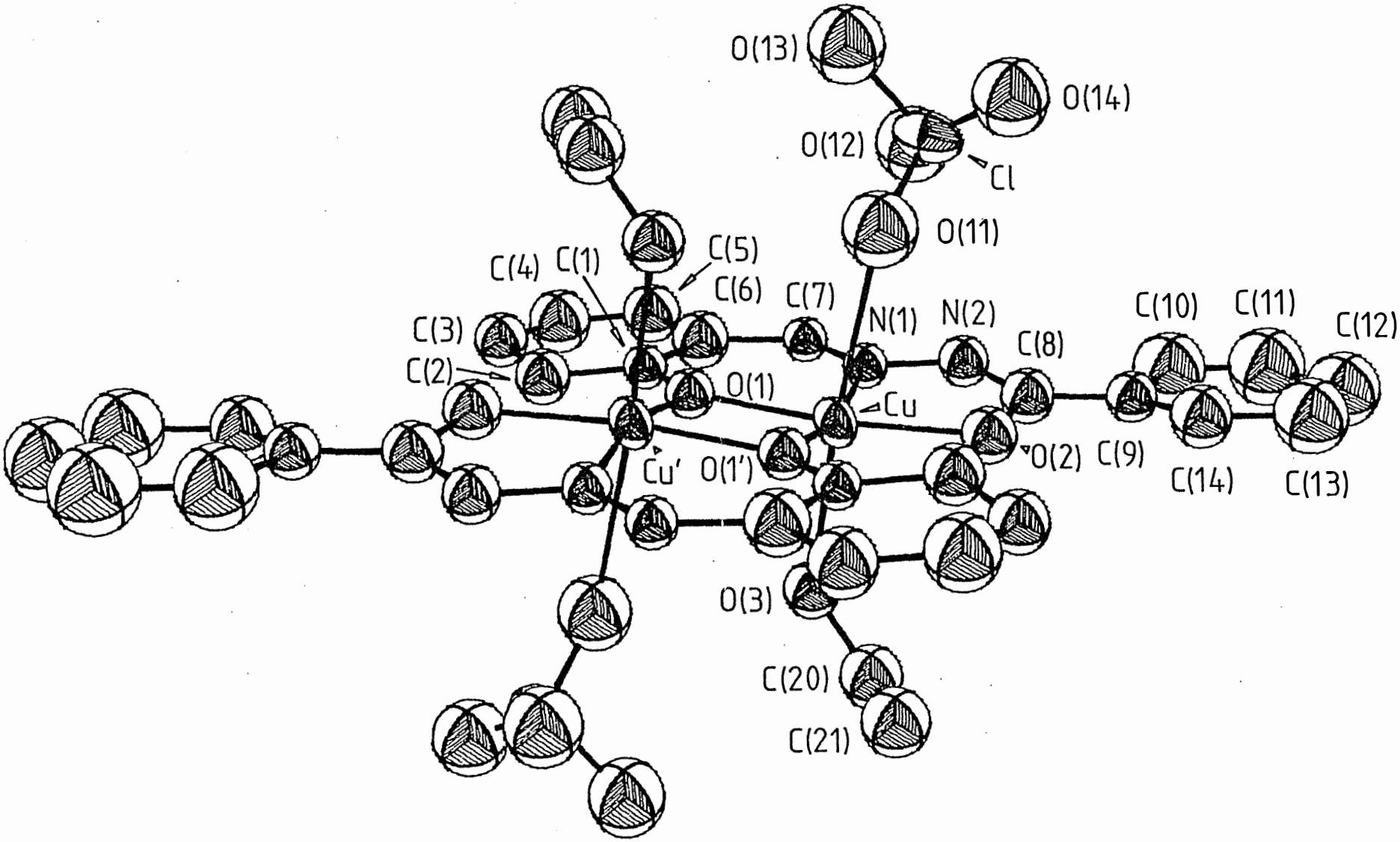

Figure 2.5.5: The dimer $[Cu(sbH)ClO_4(EtOH)]_2$ showing the atom numbering scheme.

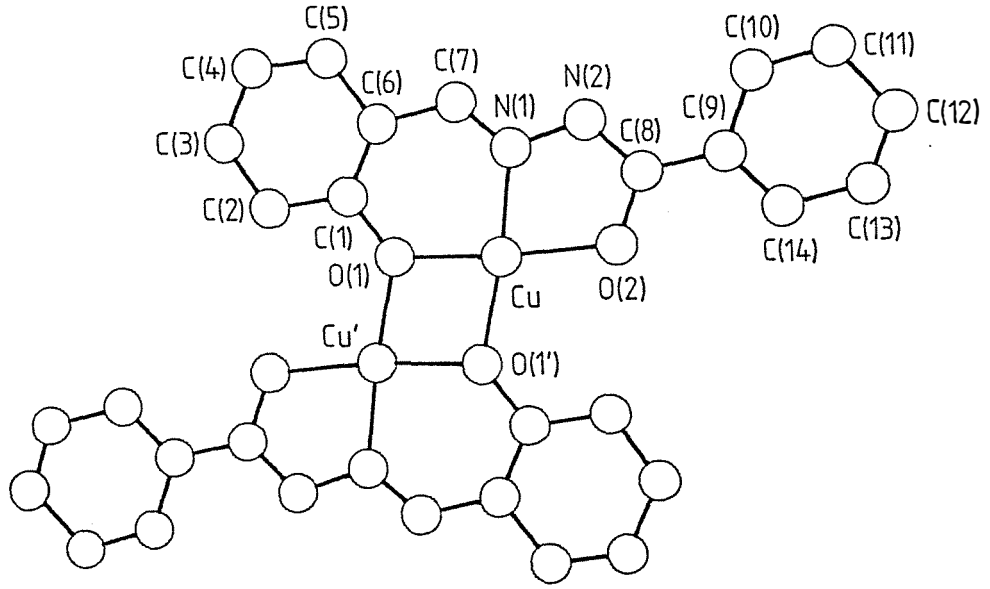

Figure 2.5.6: The dimer $[Cu(sbH)ClO_4(EtOH)]_2$ showing the atom numbering scheme and planar side-by-side structure. The axially coordinated ClO_4^- and EtOH groups have been omitted for clarity.

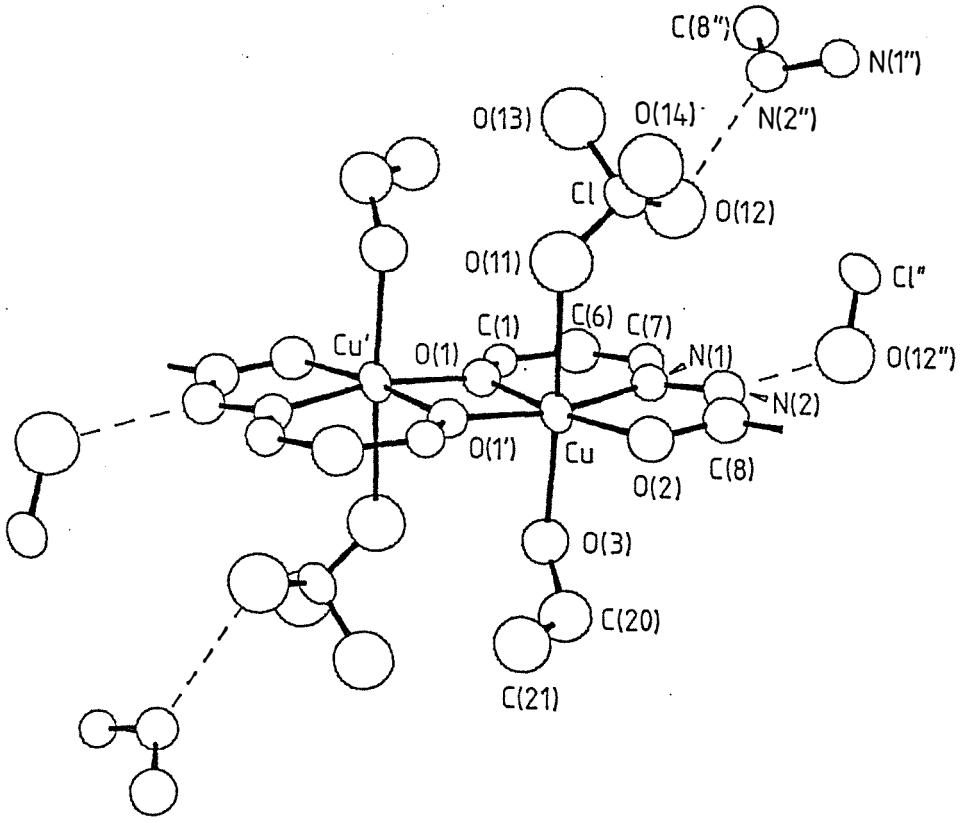

Figure 2.5.7: Cut-away view of the dimer $[Cu(sbH)ClO_4(EtOH)]_2$ showing the hydrogen-bonding scheme.

phenolato oxygen (O(1′)) from the other symmetry related half of the dimer. A comparison of the bonding distances of these four donors in Table 2.5.5 shows the Cu-O(1) bond (1.930(9) Å) to be marginally longer than the equivalent distance determined for the other two complexes of this ligand ($1.891(8)_{ave}$ Å). The addition of the two axial donors in $[Cu(sbH)ClO_4(EtOH)]_2$ may have slightly reduced the equatorial bond strengths, resulting in the observed lengthening of the Cu-O(1) bond distance.

The two axial positions are occupied by a perchlorato group (Cu-O(11) 2.687(12) Å) and a rarely observed coordinated ethanol molecule (Cu-O(3) 2.289(9) Å).

Both O(3) and O(11) are more weakly coordinated than the in-plane donors, as is often observed for Cu(II) complexes exhibiting Jahn-Teller distortions. These axially bound oxygen atoms are approximately perpendicular to the line joining the respective donor to the copper atom and the plane of best-fit* containing the four equatorial donors, O(1), O(2), O(1′) and N(1), and the copper atom. This can be seen in these angles for O(3) and O(11) of 2.9 and 7.9° respectively. The copper atom does not sit in the rather buckled plane of the equatorial donors, but is displaced 0.11 Å towards the closer of the two axial donor atoms, O(3) (of the ethanol molecule).

The monoanionic ligand, sbH^-, has some significant changes in its bond lengths and angles when compared with $[(Cu(sbH)H_2O)_2SiF_6]\cdot 2H_2O$ [this work]. The O(2)-C(8) bond length in the title complex is 1.325(17) Å compared with 1.254(11) Å in $[(Cu(sbH)H_2O)_2SiF_6]\cdot 2H_2O$, an increase of 0.071 Å. The adjacent C(8)-C(9) bond has correspondingly increased from 1.406(19) to 1.476(12) Å for the above ordered respective complexes. The angles between the carbon and nitrogen atoms joining the two phenyl rings have all increased, to some extent, in $[Cu(sbH)ClO_4(EtOH)]_2$ when compared with $[(Cu(sbH)H_2O)_2SiF_6]\cdot 2H_2O$ e.g. C(6)-C(7)-

* Plane (i) Cu, O(1), O(2), O(1′), N(1)
0.1552X + 0.9195Y – 0.3611Z – 0.0234 = 0
[Cu 0.11, O(1) 0.05, O(2) 0.04, O(1′) -0.10, N(1) -0.10]
Distances of the atoms from the plane (Å) are given in square brackets.

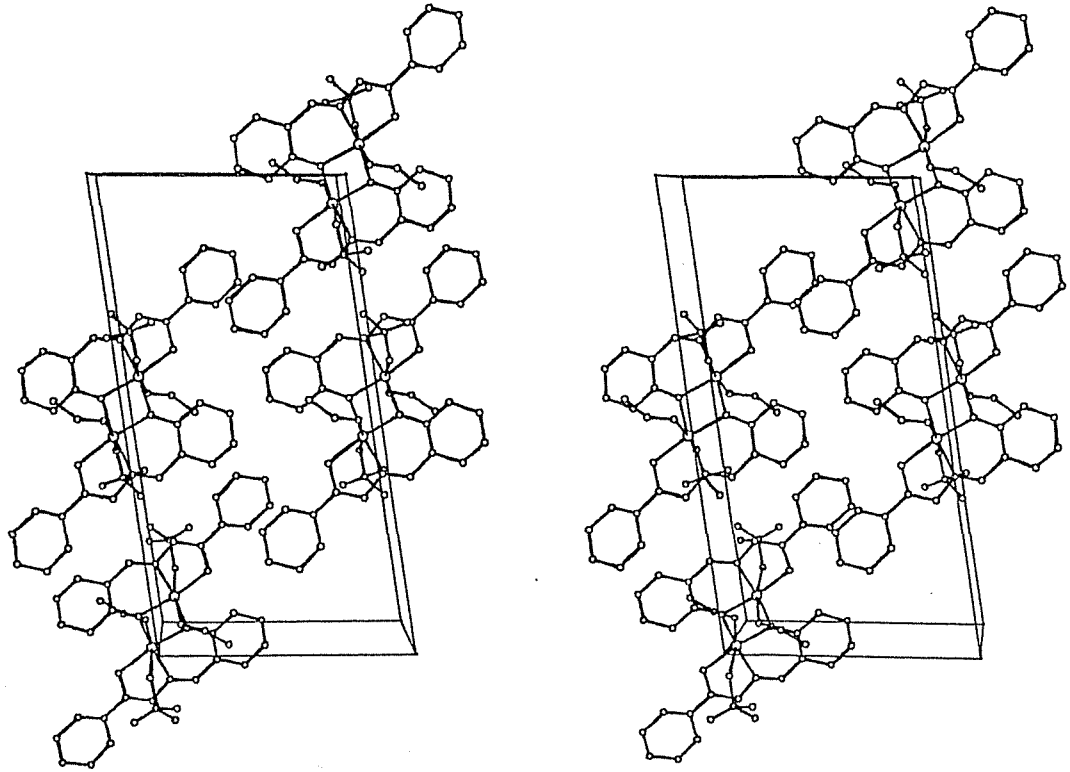

Figure 2.5.8 Stereo-view of the unit-cell packing diagram for $[Cu(sbH)ClO_4(EtOH)]_2$.

N(1) has increased 4.4° and N(1)-N(2)-C(8) by 3.6°.These changes in the bonding distances and angles are consistent with increased delocalisation in the ligand, giving the atoms more sp^2 character.

Both the perchlorato and ethanol moieties are disordered, which may be a reflection on the limited hydrogen-bonding network present. Only one contact between N(2) and O(12) of 2.89 Å (symm (x, 0.5 - y, 0.5 + z), T_x, T_y, T_z 0 0 0; Cl–O(12)···N(2) 117°, N(1)-N(2)···O(12) 109°, C(8)-N(2)···O(12) 133°) appears to be significant (see Figure 2.5.7). The coordinated ethanol molecule is still protonated and it is possible a hydrogen-bond between this proton on O(3) and the coordinated perchlorato oxygen, O(11), occurs (C(20)-O(3)···O(11) 115°, Cl-O(11)···O(3) 126°). The O(3)···O(11) separation is 2.94 Å, only 0.06 Å shorter than the Cu ···Cu′ distance of 3.00 Å. Therefore, this is at best, a weak contact but it may help to stabilise the coordinated ethanol molecule. The packing diagram is given in the stereo-view of the unit-cell, Figure 2.5.8.

2.5.4 CRYSTAL STRUCTURE OF Aquachloro(salicylaldehyde acetylhydrazonato(1-))copper(II) Hydrate

A thermal ellipsoid diagram of the title complex (abbreviated as [Cu(saH)Cl(H_2O)]H_2O is depicted in Figure 2.5.9, showing the numbering scheme employed. Tables 2.5.8 and 2.5.9 contain the bond distance and bond angle data respectively.

The complex [Cu(saH)Cl(H_2O)]H_2O crystallises as a discrete monomer. The coordination geometry adopted by the copper(II) atom may best be described as a distorted square-pyramid. The monoanionic tridentate, ONO, ligand saH^- coordinates in three of the basal positions, the fourth being occupied by a water molecule. Completing the coordination sphere in the apical position is a more weakly coordinated chloride ion, typical of the Jahn-Teller distortions seen for this geometry. The closest sixth approach is from C(4) of a symmetry related molecule at 3.520 Å. In [Cu(sbH)Cl]H_2O [245] (as described in the crystal structure description of [(Cu(sbH)H_2O)$_2SiF_6$]·2H_2O) the ligand again coordinates as an anionic, tridentate species in the plane. However, unlike [Cu(saH)Cl(H_2O)]H_2O, in [Cu(sbH)Cl]H_2O the fourth position in the plane is occupied by the chloride ion with the water molecule remaining uncoordinated, to give a square planar geometry. A comparison of the bond lengths around the copper centres for these complexes, presented in Table 2.5.5, shows the Cu-ligand distances not to be significantly different. Replacement of a phenyl ring in sbH^- with a methyl group in saH^-, in this case, does not appear to have significantly changed the ligating properties of the latter. Differences in the bond angles around the copper centre, when compared with [(Cu(sbH)H_2O)$_2SiF_6$]·2H_2O and [Cu(sbH)Cl]H_2O appear to result from changes in the copper geometry. The best-fit least-squares plane* through the four basal and copper atoms shows the copper atom to lie 0.156 Å out of the plane, towards the chloride ion.The chloride is bonded

* Plane (i) Cu, O(1), O(2), O(3), N(1)
0.8566X – 0.0083Y – 0.5158Z + 1.2676 = 0
[Cu -0.156, O(1) 0.003, O(2) -0.006, O(3) 0.078, N(1) -0.080]
Distances of the atoms from the plane (Å) are given in square brackets.

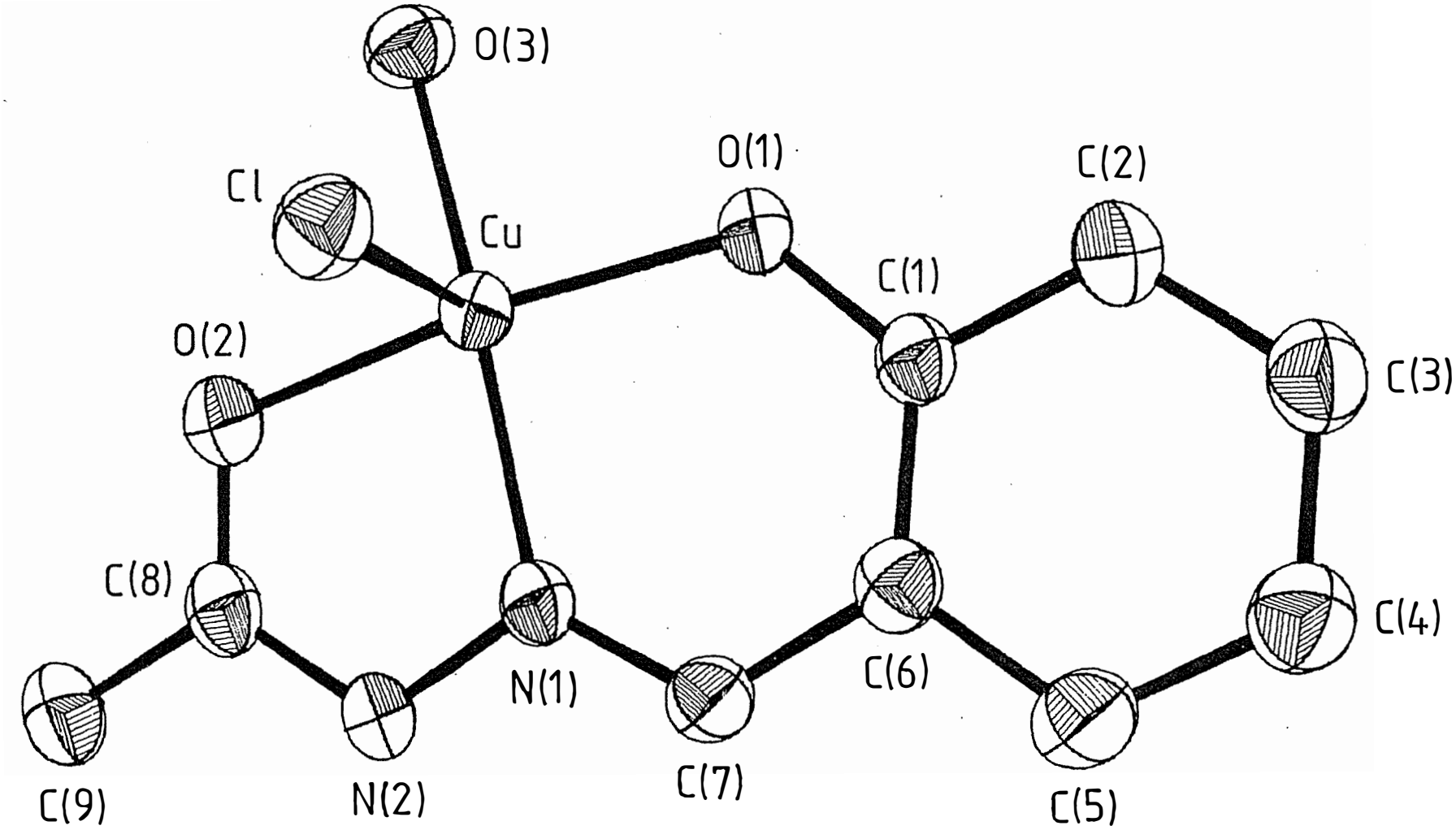

Figure 2.5.9: The monomer $[Cu(saH)Cl(H_2O)]H_2O$ showing the atom numbering scheme. The non-coordinated water molecule and hydrogen atoms have been omitted for clarity.

TABLE 2.5.8

Bond Lengths (Å) with Estimated Standard Deviations in Parentheses for the Complex $[Cu(saH)Cl(H_2O)]H_2O$*

Cu-O(1)	1.909(2)	Cu-O(2)	1.987(2)
Cu-O(3)	1.974(2)	Cu-N(1)	1.936(2)
Cu-Cl	2.622(1)	O(1)-C(1)	1.353(2)
C(6)-C(7)	1.445(3)	C(7)-N(1)	1.290(4)
N(1)-N(2)	1.384(4)	N(2)-C(8)	1.334(4)
C(8)-C(9)	1.487(5)	C(8)-O(2)	1.255(4)

* C-C bond lengths within the phenyl ring were fixed at 1.395 Å
C-H and N-H bond lengths fixed at 1.08 Å
O-H bond lengths 0.845 - 0.929 Å, mean 0.887 Å

TABLE 2.5.9

Bond Angles (°) with Estimated Standard Deviations in Parentheses for the Complex $[Cu(saH)Cl(H_2O)]H_2O$#

O(1)-Cu-N(1)	92.1(1)	O(2)-Cu-N(1)	81.3(1)
O(1)-Cu-O(2)	169.3(1)	O(1)-Cu-O(3)	93.3(1)
O(2)-Cu-O(3)	91.1(1)	N(1)-Cu-O(3)	164.7(1)
O(1)-Cu-Cl	95.1(1)	O(2)-Cu-Cl	94.2(1)
O(3)-Cu-Cl	94.8(1)	N(1)-Cu-Cl	99.0(1)
O(1)-C(1)-C(2)	115.4(1)	O(1)-C(1)-C(6)	124.5(1)
C(1)-C(6)-C(7)	124.3(1)	C(5)-C(6)-C(7)	115.7(1)
C(6)-C(7)-N(1)	121.8(3)	C(7)-N(1)-Cu	129.5(2)
C(7)-N(1)-N(2)	119.1(3)	Cu-N(1)-N(2)	111.4(2)
N(1)-N(2)-C(8)	115.1(3)	N(2)-C(8)-C(9)	117.8(3)
N(2)-C(8)-O(2)	120.0(3)	C(9)-C(8)-O(2)	122.2(3)
C(8)-O(2)-Cu	112.2(2)	C(1)-O(1)-Cu	125.7(2)

\# Internal angles for the phenyl ring were fixed at 120°

almost directly above the copper atom as seen by the angle between the Cu-Cl bond and the normal to plane (i) being 2.0°.

The monoanionic saH$^-$ ligand coordinates through the phenolic oxygen, O(1), the imine nitrogen, N(1), and the amide carbonyl oxygen, O(2), as seen in Cu(sbH)$^+$ complexes [this work, 245]. This tridentate equatorial coordination mode creates a five* and a six§ membered chelate ring. These are approximately planar and inclined at an angle of 5.5° to one another (compared with 4.5° for $[(Cu(sbH)H_2O)_2SiF_6]\cdot 2H_2O$). The plane of best fit† through the complexed ligand, including the copper atom, shows the molecule to be approximately planar with the biggest deviation from the plane being 0.163 Å for O(2).

A comparison of the equivalent ligand bonding distances between $[Cu(saH)Cl(H_2O)]H_2O$ and $[(Cu(sbH)H_2O)_2SiF_6]\cdot 2H_2O$ (also $[Cu(sbH)Cl]H_2O$) shows there are no significant differences in the bond lengths. This was surprising as the difference between having a methyl or a phenyl group substituted on C(8) was expected to alter the electronic properties of the ligand. The subtleties of these changes may not be readily noticeable in bond distance data where standard deviations of ~0.01 Å are observed. However, complexation to the copper atom may override any changes which might otherwise have occurred. In the title complex (as mentioned previously) the water molecule is coordinated equatorially and the chloride ion is in an apical position, whereas in $[Cu(sbH)Cl]H_2O$ [246] the chloride ion is coordinated in the plane and the water is not bound. In view of the similarities of the bonding distances between these two complexes, the differences in the coordination spheres may result from crystal packing forces.

---

* Plane (ii) Cu, O(2), N(1), N(2), C(8)
0.9079X – 0.0878Y – 0.4098Z + 0.5196 = 0
[Cu 0.013, O(2) -0.019, N(1) -0.010, N(2) 0.001, C(8) 0.016]

§ Plane (iii) Cu, O(1), N(1), C(1), C(6), C(7)
0.8736X + 0.0404Y – 0.4850Z + 0.9429 = 0
[Cu -0.089, O(1) 0.102, N(1) 0.035, C(1) -0.021, C(6) -0.081, C(7) 0.053]

† Plane (iv) Cu, O(1), O(2), N(1), N(2), C(1) - C(9)
0.8981X + 0.0020Y – 0.4397Z + 0.9659 = 0
[Cu -0.151, O(1) 0.156, O(2) -0.163, N(1) 0.003, N(2) 0.054, C(1) 0.104, C(2) 0.056, C(3) -0.054, C(4) -0.117, C(5) -0.070, C(6) 0.041, C(7) 0.097, C(8) -0.019, C(9) 0.064]

Distances of atoms from the plane (Å) are given in square brackets.

In Figure 2.5.10 a stereo-view of the hydrogen-bonding in the unit-cell is given and in Table 2.5.10 the hydrogen-bonding contacts and angles are listed. As with the hydrogen-bonding schemes for[$(Cu(sbH)H_2O)_2SiF_6]\cdot 2H_2O$ [this work] and $[Cu(sbH)Cl]H_2O$ [245], the coordinated phenoxy oxygen, O(1), is involved in a contact to a non-coordinated water molecule (O(1)···O(4) 2.768 Å). The coordinated water molecule, O(3), has a strong hydrogen-bond to O(4) also of 2.662 Å. The chloride ion forms two contacts, one to the coordinated water, O(3), in a symmetry related molecule (Cl···O(3) 3.102 Å) and the other to the protonated amide nitrogen, N(2), again in a symmetry related molecule (Cl···N(2) 3.129 Å). The effect is to link the monomers via this hydrogen-bonding network into a rigid structure. It should also be noted that the phenyl ring (C(1) - C(6)) stacks approximately parallel to the five membered chelate ring (Cu, N(1), N(2), C(8), O(2)) of a symmetry related molecule with the atoms of adjacent rings showing closest approaches ranging from 3.398 Å (C(5)···C(8)) to 3.520 Å (C(4)···Cu). This may result in a weak π overlap between the two rings but it is probably of greater significance in the crystal packing than the electronic properties of the compound.

A noticeably short distance of 3.248 Å between Cl and O(4) exists but it is accompanied by unfavorable bond angles and an explanation of its role in the overall hydrogen-bonding network is difficult. The hydrogen-bonding scheme for the chloride ion in $[Cu(saH)Cl(H_2O)]H_2O$ is similar to that in $[Cu(sbH)Cl]H_2O$ where a contact to a water molecule (Cl···O 3.332 Å) and a short, but unfavorable distance to a symmetry related water molecule (Cl···O 3.389 Å) exist. The amide nitrogen however is hydrogen-bonded to the water molecule (N···O 2.766 Å) whereas in the title complex this contact is to the chloro group. This difference in the hydrogen-bonding networks may therefore account for the previously discussed differences in the copper coordination sphere between $[Cu(saH)Cl(H_2O)]H_2O$ and $[Cu(sbH)Cl]H_2O$ [245].

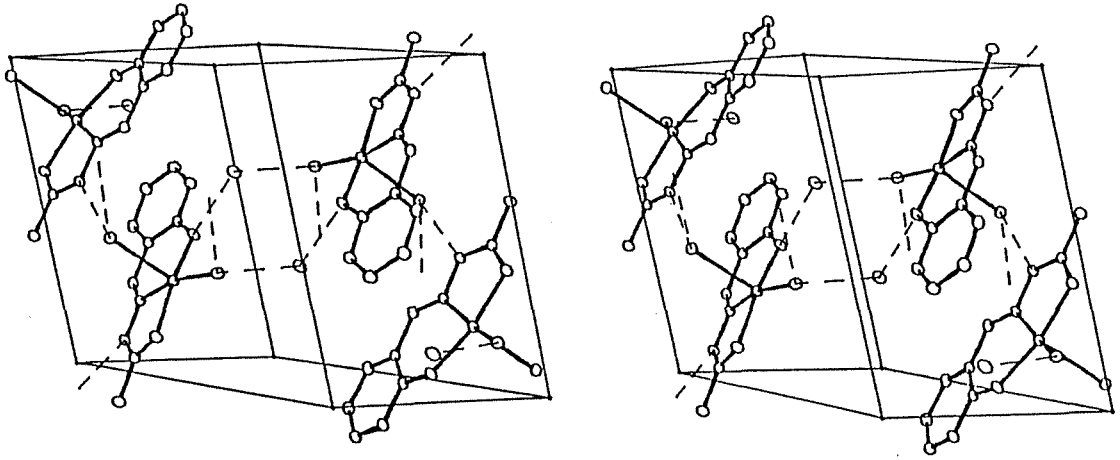

Figure 2.5.10: Stereo-view of the unit-cell packing diagram for [Cu(saH)Cl(H_2O)]H_2O showing the hydrogen-bonding scheme.

TABLE 2.5.10
Hydrogen-Bonding Distances (Å) and Angles (°) for $[Cu(saH)Cl(H_2O)]H_2O$

Atoms[a]	Distance (Å)	Symm[b]	T_x, T_y, T_z
Cl···O(3)	3.102	2	0 1 1
Cl···N(2)	3.129	3	0 0 0
O(1)···O(4)	2.768	2	1 1 1
O(3)···O(4)	2.662	1	0 0 0

a the first atom is at symmetry position 1

b symmetry positions

1 (x, y, z)
2 ($\bar{x}$, $\bar{y}$, $\bar{z}$)
3 ($\bar{x}$, 0.5 + y, 0.5 – z)
4 (x, 0.5 – y, 0.5 + z)

Atoms	Angle (°)	Atoms	Angle (°)
Cu–Cl···O(3)	139.1	Cu-Cl···N(2)	100.7
O(3)···Cl···N(2)	91.4	N(1)-N(2)···Cl	121.4
C(8)-N(2)···Cl	123.1	Cu-O(1)···O(4)	114.9
C(1)-O(1)··· O(4)	114.1	Cu-O(3)··· Cl	121.0
Cu-O(3)··· O(4)	116.0	Cl···O(3)···O(4)	102.9
O(1)···O(4)···O(3)	108.7		

2.5.5 RESULTS AND DISCUSSION

2.5.5(a) Complex Stability

The ligand sbH_2 can coordinate to a transition metal as a neutral (sbH_2), monoanionic (sbH^-) or dianionic (sb^{2-}) tridentate ONO moiety:

$$Cu(sbH_2)X_2 \xrightarrow{-HX} Cu(sbH)X \xrightarrow{-HX} Cu(sb)$$

What form of the ligand is coordinated is regulated by both the pH and apparently in some cases how the complex is prepared. Addition of non-basic copper salts (e.g. $CuCl_2$ and $Cu(NO_3)_2$) to sbH_2 in ethanol results in monoanionic complexes of the type Cu(sbH)X. However, when $Cu(CH_3COO)_2$ is used, a green complex whose formulation is intermediate between that of Cu(sbH)(CH_3COO) and Cu(sb) is obtained. Addition of any base to a solution of $Cu(sbH)^+$ immediately results in the precipitation of the highly insoluble complex formulated as $[Cu(sb)]_2$ through loss of the amide proton. Even heating the monoanionic complexes $[Cu(sbH)Cl]_2$ or $[Cu(sbH)ClO_4(H_2O)]_2$ in the basic solvent dmf results in the formation of this product. The amide proton is therefore relatively acidic when sbH_2 is complexed to Cu(II). This meant that ternary adducts of anionic ligands (e.g. phenolates, thiolates) as prepared in Section 1 of this work, could not be synthesised in an analogous fashion.

It appears that the only ternary adducts of Cu(II) with sbH_2 (or its congeners) prepared to date have been the pyridine (py) complexes Cu(sXbH)Cl·py (where X = H and 2-OH) and Cu(sXb)py (where X = H, 4-CH_3O, 4-NO_2 and 2-OH) [244]. However, a number of monomeric adducts, with a range of neutral Lewis-bases, have been prepared on related systems e.g. Cu(salgly)(LB) (where LB = thiourea, pyridine, N-methylimidazole, γ-collidine, imidazole and pyrazole [42,217,219]). Addition of a potentially coordinating moiety to such structurally related systems does not necessarily guarantee adduct formation. For the ONO tridentate system (N-n-propanol-salicylaldiminato)copper(II), and several of its substituted

congeners, recrystallisation of the complexes from pyridine did not result in adducts being formed; the products retaining their dimeric structure in the solid state [238].

When an alcoholic solution of sbH_2 is added to $CuCl_2$ in an excess of concentrated HCl (giving the $CuCl_4^{2-}$ anion) the khaki complex $[Cu(sbH_2)Cl_2(H_2O)]$, containing the neutral protonated ligand is isolated. Surprisingly this could not be prepared by protonating the preformed complex $[Cu(sbH)Cl]_2$ in 2 M HCl. Instead the green complex which separated fitted the formulation $[Cu(sbH)Cl]\cdot\frac{3}{2}H_2O$ (C 46.3 (46.0); H 3.9 (3.8); N 7.7 (7.6); Cl 9.7 (10.0)% :calculated figures are given in parentheses). When $CuBr_2$ in concentrated HBr was used as above, the purple colour due to the $CuBr_4^{2-}$ anion was immediately lost upon its addition to the sbH_2 solution. However, as excess HBr was used, and apparently not all the copper was complexed to sbH_2, a deep purple colour remained after all the $CuBr_4^{2-}$ had been added. It was from this solution three days later that a small amount of the yellow product, $[Cu(sbH_2)Br_2]_2H_2O$ was removed. After two further weeks, the purple solution had deposited large, clear crystals (which continued to separate until the solution was finally discarded). From a mass spectral analysis of this organic compound and its melting point (80-3° C) it was identified as 3, 5-dibromosalicylaldehyde (literature melting point 82-3.5° C [96]). The sbH_2 ligand had therefore been hydrolysed and the salicylaldehyde dibrominated, although not necessarily in that order. The fate of the benzoyl hydrazide is uncertain.

When the above procedure was repeated using CuF_2 in concentrated HF with sbH_2, and the green solution which resulted from this was briefly heated in a glass beaker, a green complex was isolated. The X-ray crystallographic structure of this compound showed it to be $[(Cu(sbH)H_2O)_2SiF_6]\cdot 2H_2O$. The SiF_6^{2-} ion was therefore generated by the action of the HF upon the silica (SiO_2) of the glass. When this final reaction was repeated in plastic containers and left for two weeks the resulting green complex could not be identified.

Figure 2.5.11

Abbreviations used for Ligands in Chapters 5 and 6

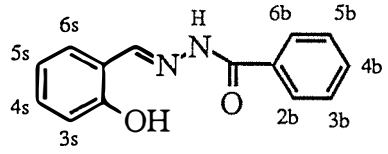

Ligand	3s	4s	5s	6s	2b	3b	4b	5b	6b
sbH_2									
$3msbH_2$	CH_3								
$3mosbH_2$	OCH_3								
$5msbH_2$			CH_3						
$5csbH_2$			Cl						
$5nsbH_2$			NO_2						
$s2mbH_2$					CH_3				
$s3mbH_2$						CH_3			
$s4mbH_2$							CH_3		
$s4fbH_2$							F		
$s4cbH_2$							Cl		
$s4BbH_2$							Br		
$s4abH_2$							NH_2		
$s4mobH_2$							OCH_3		
$s2hbH_3$					OH				
$s4hbH_3$							OH		
$s4nbH_2$							NO_2		
$5ms4mbH_2$			CH_3				CH_3		
$5ms4cbH_2$			CH_3				Cl		
$5ms4abH_2$			CH_3				NH_2		
$5cs4mbH_2$			Cl				CH_3		
$3c5csbH_2$	Cl		Cl						

m = methyl = CH_3
mo = methoxy = OCH_3
f = fluoro = F
c = chloro = Cl
B = bromo = Br
a = amino = NH_2
n = nitro = NO_2
h = hydroxy = OH

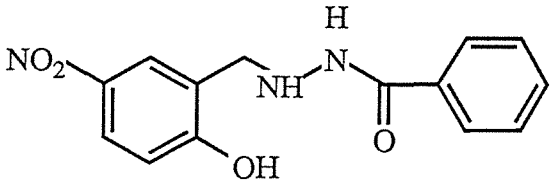

N-Benzoyl, N′-2-hydroxy-5-nitro benzyl hydrazide ($b5nbH_2$)

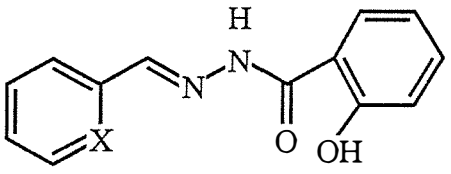

X = CH Bezaldehyde salic ylhydrazone(bsH_2)
X = N 2-formylpyridine salicylhydrazone (paH_2)

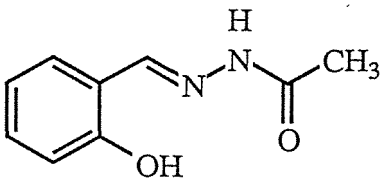

Salicylaldehyde acetylhydrazone (saH_2)

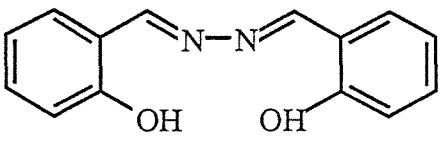

Salicylaldehyde azine ($saaH_2$)

TABLE 2.5.11

Absorption Maxima and Conductance Data for Chapter 5

Complex[a]	Absorption Maxima (nm)[b] Charge Transfer		d-d	Molar Conductance[c] ($s\ mol^{-1}\ l$)	Solvent[d]
$[Cu(sb)]_2$	396		615 (br)		m.t.
	393	(16 700)	650 (120)	1	dmso
$[Cu(sbH)Cl]_2$	395		750 (br)		m.t.
	394	(15 300)	675 (80; br)	18	dmso
	404		703		EtOH
$[Cu(sbH_2)Cl_2(H2O)]$	386		820 (br)		m.t.
	393	(11 700)	870 (70; br)	35	dmso
	409		713		EtOH
$[Cu(sbH)Br]_2$	398		733 (br)		m.t.
	394	(16 200)	681 (90)	28	dmso
	399		690		EtOH
$[Cu(sbH_2)Br_2]_2H_2O$	405		835 (br)		m.t.
	380	(4 000; sh)	670 (10; br)	4	dmso
	380	(5 000; sh)	709 (10; br)	6	EtOH
$[Cu(sbH)ClO_4(H_2O)]_2$	395		667		m.t.
	393	(15 700)	683 (90)	37	dmso
	401	(11 700)	706 (100)	39	EtOH
$[Cu(sbH)NO_3]_2$	396		702		m.t.
	394	(13 900)	692 (90)	6	dmso
	406		700 (br)		EtOH
$[(Cu(sbH))_2SO_4]$	401	(br)	695 (br)		m.t.
	394	(15 500)	671 (110)	5	dmso
	400		688		EtOH
$[(Cu(sbH)H_2O)_2SiF_6]\cdot 2H_2O$	419		653		m.t.
	400	(10 500)	666 (110)	4	dmso
	391		675		EtOH
$[Cu(3msbH)Cl]H_2O$	433		677		m.t.
	400	(14 900)	675 (70)	17	dmso
	405	(10 900)	703 (110)	31	EtOH
$[Cu(3mosbH)Cl]\cdot\frac{5}{2}H_2O$	406		767 (br)		m.t.
	402	(11 800)	695 (80)	24	dmso
	405	(8 300)	695 (100)	30	EtOH
$[Cu(5msbH)Cl]_2$	401		743 (br)		m.t.
	409	(9 400)	677 (75)	16	dmso
	414	(11 000)	700 (110)	27	EtOH
[Cu(5csbH)Cl]	424		660 (sh)		m.t.
	405	(12 200)	681 (80)	17	dmso
	411		691		EtOH
[Cu(5nsbH)Cl]	398		640		m.t.
	390	(28 300)	682 (120)	21	dmso
$[Cu(s2mbH)Cl]_2$	400		750 (br)		m.t.
	393	(11 000)	680 (70)	12	dmso
	395	(10 200)	706 (110)	32	EtOH
$[Cu(s3mbH)Cl]_2$	397		744 (br)		m.t.
	393	(13 000; br)	695 (80; br)	18	dmso
	397	(16 200)	694 (110)	22	EtOH
$[Cu(s4mbH)Cl]\cdot\frac{1}{2}H_2O$	420		681		m.t.
	393	(14 300)	686 (70)	12	dmso
	399	(13 500)	706 (100; br)	21	EtOH

TABLE 2.5.11 continued

Complex[a]	Absorption Maxima (nm)[b] Charge Transfer		d-d	Molar Conductance[c] ($s\ mol^{-1}\ l$)	Solvent[d]
[Cu(s4fbH)Cl]	409		682 (br)		m.t.
	392	(10 300; br)	685 (72)	17	dmso
	400		698		EtOH
[Cu(s4cbH)Cl]	413		e		m.t.
	396	(13 800)	679 (70)	14	dmso
[Cu(s4BbH)Cl]	419		670 (sh)		m.t.
	397	(9 800; br)	674 (70)	18	dmso
	404		704		EtOH
$[Cu(s4abH)Cl]_2 \cdot 3H_2O$	420	(sh)	682		m.t.
	409	(19 600)	744 (90)	28	dmso
	405		691		EtOH
$[Cu(s4mobH)Cl]H_2O$	422		663		m.t.
	405	(14 300)	700 (85)	12	dmso
	395	(18 000)	698 (110)	20	EtOH
$[Cu(s2hbH)]_2$	415		615		m.t.
	400	(14 400)	666 (120)	0	dmso
	390	(br)	e		$CHCl_3$
$[Cu(s4hbH_2)Cl]_2H_2O$	391		706 (br)		m.t.
	404	(11 100; br)	727 (90)	18	dmso
	403	(11 100; br)	670 (sh)		EtOH
[Cu(s4nbH)Cl]	429		660 (br)		m.t.
	427	(12 500)	660 (80; br)	16	dmso
	417		e		EtOH
$[Cu(5ms4mbH)Cl]_2$	405		735 (br)		m.t.
	412	(7 600; br)	700 (80)	17	dmso
	416		700		EtOH
[Cu(5ms4cbH)Cl]	433		e		m.t.
	408	(9 800; br)	674 (73)	17	dmso
	416		e		EtOH
$[Cu(5ms4abH)Cl]_2H_2O$	428		710 (br)		m.t.
	419	(19 600)	715 (110)	19	dmso
	411		640 (br; sh)		EtOH
[Cu(5cs4mbH)Cl]	419		650 (br; sh)		m.t.
	406	(15 000)	676 (80)	16	dmso
	408		691		EtOH
$[Cu(3c5csbH)Cl]_2$	430		700 (sh)		m.t.
	411	(14 400)	688 (90)	24	dmso
	411		705		EtOH
[Cu(b5nbH)Cl]	403		630 (br)		m.t.
	392	(26 600)	673 (120)	21	dmso
	382	(br)	680 (br)		EtOH
$[Cu(bs)]_2$	f				m.t.
	305	(18 800)	629 (100; br)	4	dmso
	306		e		$CHCl_3$
[Cu(psH)Cl]	408		669 (br)		m.t.
	379	(22 200)	754 (100)	0	dmso
	393		709		CH_3NO_2
$[Cu(saH)Cl(H_2O)]H_2O$	391	500 (sh)	760 (br)		m.t.
	389	(4 800)	798 (81)	19	dmso
	395		701 (br)		EtOH
[Cu(saa)]	422		e		m.t.
	412		e		dmso

TABLE 2.5.11 continued

Complex[a]	Absorption Maxima (nm)[b] Charge Transfer		d-d		Molar Conductance[c] (s mol^{-1} l)	Solvent[d]
$[Cu(sal)_2]$	412		672 (br)			m.t.
	385	(7 700)	694 (70)		0	dmso
	385		e			CH_3NO_2
$[Cu(5msal)_2]$	419		660 (sh)			m.t.
	398	(6 700)	695 (70)		0	dmso
	377	(1 600)	634 (90)		0	CH_3NO_2
$[Ni(sbH)NO_3]\cdot\frac{1}{2}H_2O$	395		617	932		m.t.
	415	(9 800)	e		30	dmso
	404			910 (br)		EtOH
$[Co(sbH)NO_3]\cdot\frac{1}{2}H_2O$	398		520 (sh)	1 230 (br)		m.t.
	399	(8 200)	e		26	dmso
	396		e			Acetone
$[Fe(sbH)_2]NO_3\cdot H_2O$	425	(br)	463 (sh)	600 (sh)		m.t.
	390	(11 400)		615 (500)	32	dmso
	e			547 (br)		EtOH
$[Fe_2(sb)_3]\cdot 4H_2O$	429	(br)		669 (br)		m.t.
	435	(4 400; br)	e		1	dmso
[Cr(sbH)(sb)]	429		450 (sh) 578 (sh)	627 (sh)		m.t.
	429	(17 800)	520 (610; sh) 550 (370; sh) 615 (150; sh)		6	dmso
	406	(br)	440 (sh)	615 (sh)		EtOH

a see Figure 2.5.11 for abbreviations
b extinction coefficients given in parentheses (1 mol^{-1} cm^{-1})
c for typical molar conductance ranges see the Appendix 3
d m.t. = mull transmittance
e not resolved
f featureless tail in the n.i.r.

2.5.5(b) Electronic Spectra

The mull transmittance charge transfer (c.t.) maxima presented in Table 2.5.11 range from 386 to 433 nm for all complexes and may be assigned to an O → Cu c.t. transition possibly with a ligand internal c.t. component. In solution, the position of this band is not shifted significantly for the majority of the complexes. The main exception to this is the complex $[Cu(sbH)Br_2]_2H_2O$, formulated as a dimer due to its low magnetic moment. Upon dissolution, the c.t. band observed at 405 nm for the solid sample shifts to higher energy, ~380 nm. This band is a shoulder on a high intensity absorption assumed to be a ligand internal $\pi \rightarrow \pi^*$ transition (at ~340 nm). The extinction coefficient of 4 000 l mol^{-1} cm^{-1} in dmso is considerably reduced compared with the other Cu(II) complexes of this ligand (average of 14 400 l mol^{-1} cm^{-1}) indicating the solution species for this neutral ligand complex is different. It is possible that in solution the phenolate oxygen is protonated and coordinates as such, or is displaced by solvent with the ligand coordinating as a bidentate species.

The c.t. shoulder at ~380 nm may therefore be a Br(σ) → Cu transition. This is consistent with the positioning and intensity of this band [258,259] and that it is not observed in the complex $[Cu(sbH_2)Cl_2(H_2O)]$. Drawing analogies between the two neutral ligand complexes $[Cu(sbH_2)Cl_2(H_2O)]$ and $[Cu(sbH_2)Br_2]_2H_2O$ may not be valid, as the latter has been formulated as a dimer due to the low magnetic moment observed (1.59 B.M. at room temp.). Differences between the solution d-d maxima positions and intensities are also observed. The complex $[Cu(sbH_2)Cl_2(H_2O)]$ displays a band at 870 nm in dmso with an extinction coefficient of 70 l mol^{-1} cm^{-1}, possibly indicative of a distorted (elongated) tetragonal stereochemistry. On the other hand $[Cu(sbH_2)Br_2]_2H_2O$ has this maxima at 670 nm with a much reduced value of 10 l mol^{-1} cm^{-1} for the extinction coefficient, more consistent with a nearly 'regular' octahedral coordination sphere. A comparison between these two species must therefore be treated with caution.

The d-d absorption maxima in the solid state range from 615 to 835 nm for the copper(II) complexes, indicative of a range of coordination geometries. In the crystal structures of $[(Cu(sbH)H_2O)_2SiF_6]\cdot 2H_2O$ and $[Cu(saH)Cl(H_2O)]H_2O$ the copper centres were both shown to be square pyramidal. The mull transmittance d-d band for these respective complexes are however at 653 and 760 nm showing that even within a particular geometry a large variation in the absorption position can occur. In general though, complexes exhibiting maxima greater than approximately 700 nm were tentatively assumed to have a tetragonal geometry whereas those below 700 nm were considered to result from a square-pyramidal or a square-planar stereochemistry. It is interesting to note that the copper complexes of sbH_2 congeners formulated as dimers (due to their low magnetic moments) exhibit an average solid state electronic maxima at 725 nm (range from 667 to 835 nm) whereas the monomeric complexes (excluding $[Cu(3mosbH)Cl]\cdot\frac{5}{2}H_2O$ 767 nm) average 664 nm (range from 640 to 682 nm).

The spectra for the four complexes $[Ni(sbH)NO_3]\cdot ½H_2O$, $[Co(sbH)NO_3]\cdot ½H_2O$, $[Fe(sbH)_2]NO_3\cdot H_2O$ and [Cr(sbH)(sb)] are all consistent with six coordinate species [112,192]. The presence of three resolved shoulders on the c.t. band for [Cr(sbH)(sb)] may indicate more d-d absorptions than might otherwise be expected. Hence the stereochemistry appears to be less than a regular octahedron.

The molar conductance values for the complexes as formulated in Table 2.5.11 show that they are, at most, only partial electrolytes. In the strongly coordinating solvent, dmso, it was assumed that any di- or polymeric structures would not be retained. It is possible, therefore, that in solution the anions are still weakly associated with the monomeric complex species.

2.5.5(c) Infrared Spectra

The ir spectra proved to be complicated and only the bands which could be selected with some degree of certainty are presented in Table 2.5.12. The ν(N-H) band of secondary amides (e.g. sbH_2) in the solid state appears around 3 270 cm^{-1} [260a]. However in the solid state this may

be split or shifted due to hydrogen-bonding. Possible absorptions due to ν(N-H) and ν(O-H) have therefore been grouped together as they may overlap. It has however been assumed that peaks above ~3 500 cm^{-1} are due to ν(O-H) of H_2O rather than phenol. The latter is expected to have a weak, sharp band within the range 3 600 - 3 500 cm^{-1} due to intermolecular hydrogen-bonding or a broad, diffuse resonance within the range 3 200-2 500 cm^{-1} due to intramolecular hydrogen-bonds [260a]. The ligands did not display a band above 3 500 cm^{-1} whereas a number of the hydrated complexes did.

The ligand $b5nbh_2$ and its associated copper complex [Cu(b5nbH)Cl] (see Figure 2.5.11) have no imine (-CH=N-) bond, but instead a saturated linkage (-CH_2-NH-) exists. The bands at 3 430 and 3 380 cm^{-1} in $b5nbH_2$ and 3 555 cm^{-1} in [Cu(b5nbH)Cl] may therefore be due to ν(N-H) (as these compounds are not hydrates). The shift to higher wave number of the bands in the free ligand to give one band in the complex indicates coordination through an amine nitrogen occurs.

The amide(I) band, ν(C=O), which occurs above 1 630 cm^{-1} for the ligands and the ν(C=N) + amide(II) band (see Table 2.5.12, footnote c) at ~1 620 cm^{-1} in Table 2.5.12, shift upon complexation to ~1 600 and ~1 550 cm^{-1} respectively, indicating coordination through the carbonyl O and imine N. This has also been observed previously but the assignment of the complexed band at 1 600 cm^{-1} varies between authors (ν(C=O) [240,242,244,260]; ν(C=N) [226,235,247]). The appearance of the ν(C=O) band (and ν(N-H)) indicates that in the solid state the ligand exists in the keto form (see Figure 2.5.2(b)). In the complexes of the monodeprotonated ligands ($Cu(sbH)^+$ and its congeners) the appearance of the band at ~1 600 cm^{-1} shows the carbonyl moiety to still be present. This has also been confirmed by X-ray crystallographic studies on both iron(III) [245] and copper(II) [245, this work] complexes of sbH^-.

In the dianionic ligand complex $[Cu(sb)]_2$, no bands attributable to ν(N-H) or ν(C=O) were located. The strong resonance at 1 623 cm^{-1} has however been assigned to the stretching

TABLE 2.5.12

Selected Infrared Absorption Bands for Chapter 5

Compound[a]	ν(N-H) + ν(O-H)			ν(C=O)[b]	ν(C=N) + Amide(II)[c]		Anion
sbH_2	3 250(m)			1 670(s)	1 620(m)	1606(m)	–
$5nsbH_2$	3 320(m)			1 630(s)	1 600(s)		–
$b5nbH_2$	3 430(m)	3 380(m)		1 640(s)	–		–
saH_2	3 175(w)			1 675(s)	1 620(m)		–
$[Cu(sb)]_2$	–			–	1 623(s)	1 600(s)	–
$[Cu(sbH)Cl]_2$	d			1 600(s)	1 553(s)		d
[Cu(sbH)Br]	d			1 600(s)	1 550(s)		d
$[Cu(sbH_2)Cl_2(H_2O)]$	3 530(w)	3 310(w)	3 160(w)	1 600(s)	1 550(s)		d
$[Cu(sbH_2)Br_2]_2H_2O$	3 520(w)	3 330(w)	3 150(w)	1 602(s)	1 545(s)		d
$[Cu(sbH)ClO_4(H_2O)]_2$	3 500(w)	3 205(w)		1 605(s)	1 550(s)		1 155(m), 1 085 (s)
$[(Cu(sbH)H_2O)_2SiF_6]\cdot 2H_2O$	3 500(m)	3 340(w)		1 600(s)	1 545(s)		730(vs)
	3 230(w)	3 090(vw)					
[Cu(5nsbH)Cl]	3 160(m)	3 070(w)		1 600(s)	1 550(s)		d
[Cu(b5nbH)Cl]	3 555(m)			1 610(s)	–		d
$[Zn(sbH)_2]H_2O$	3 160(m)			1 610(s)	1 570(s)	1 547(s)	-
$[Ni(sbH)NO_3]\cdot \frac{1}{2}H_2O$	3 470(w)	3 330(w)	3 200(w)	1 605(s)	1 565(s)		1 300(br), 1 045(s)
$[Co(sbH)NO_3]\cdot \frac{1}{2}H_2O$	3 290(w)	3 150(w)		1 610(s)	1 570(s)		1 300(br), 1 040(m)
$[Fe(sbH)_2]NO_3]\cdot H_2O$	3 400(vbr)	3 170(w)		1 605(s)	1 545(s)		1 305(s; br)
$[Fe_2(sb)_3]\cdot 4H_2O$	3 420(br)	3 170(w)		–	1 610(s)		–
[Cr(sbH)(sb)]	3 400(vbr)	3 130(w)		1 600(s)	1 555(s)		–
$[Cu(saH)Cl(H_2O)]H_2O$	3 490(s)	3 290(s; br)		1 605(s)	1 570(s)		d

a see Table 2.5.11 for abbreviations
b amide(I) band
c Amide(II) = δ(N-H) + ν(C-N): (N-H deformation)
d not able to be resolved

vibration mode of the conjugated C=N-N=C system [244]. Such behaviour is considered diagnostic for the enolisation of the hydrazone residue (see Figure 2.5.2 (d)) [261]. The appearance of a strong, sharp band (unassigned) at 1 515 cm^{-1} in $[Cu(sb)]_2$ which was not observed in $[Cu(sbH)Cl]_2$ seems to be characteristic of the dianionic ligand and was also observed in the complexes [Cr(sbH)(sb)] and $[Fe_2(sb)_3]\cdot 4H_2O$.

The two complexes formulated as having neutral ligands viz. $[Cu(sbH_2)Cl_2(H_2O)]$ and $[Cu(sbH_2)Br_2]_2H_2O$, display additional bands in the range 3 330-3 150 cm^{-1} when compared with $[Cu(sbH)Cl]_2$. Also, the strong absorptions between 1 600-1 300 cm^{-1} in the $Cu(sbH_2)^{2+}$ complexes tend to show less splitting and are sharper than the corresponding sbH^- complexes. These differences may therefore be used, albeit with caution, in differentiating the three possible forms of the ligand when complexed.

Anion bands generally overlapped with the numerous ligand and complex bands and were difficult to assign. The two resolvable peaks in $[Cu(sbH)ClO_4(H_2O)]_2$ at 1 155 and 1 085 cm^{-1} indicate an ionic or weakly coordinated unidentate perchlorato group [107]. This is not inconsistent with the weak, axial bonding observed in the crystal structure of $[Cu(sbH)ClO_4(EtOH)]_2$ [this work].

The very strong, broad band at ~730 cm^{-1} for $[(Cu(sbH)H_2O)_2SiF_6]\cdot 2H_2O$ (superimposed on a number of weaker peaks) demonstrates the presence of the SiF_6^{2-} anion [140]. As with the ClO_4^- ion, the NO_3^- ion complexes have bands (~1 300 and ~1 040 cm^{-1}) which indicate only weak covalency [107]. The partial association of these anions, as indicated by the ir band positions, may explain the molar conductivity values for these complexes which show only limited ionisation in dmso (see Table 2.5.11).

2.5.5(d) Magnetic Properties

Much interest in tridentate ligands has been stimulated by the anomalous magnetic behaviour of their paramagnetic transition metal complexes. It was not until 1961 however that a structure of a copper complex (acetylacetone-mono(o-hydroxyanil)copper(II) see Figure 2.5.12(a)) with a low moment (1.37 B.M.) was studied crystallographically and shown to have a structure different to that of copper(II) carboxylates [234] (see Figure 2.5.12 (a) and (b)). Structure (a) involves two planar, copper(II) dianionic ligand moieties side-by-side, linked by the phenolato oxygen bridges. The observed Cu···Cu separation of 2.989(3) Å (2J of -298 cm^{-1} [233]) is intermediate between that of $[Cu(CH_3COO)_2H_2O]_2$ (2.64 Å) (see Figure 2.5.12(b) where R = CH_3: 2J of -300 cm^{-1} [233]) and the value of 3.3 Å found for $[CuCl_2(pyridine\ N\text{-}oxide)]_2$ (see Figure 2.5.12(c): 2J of -650 cm^{-1} [237,262]). Possible mechanisms of spin pairing for the complexes $[Cu(CH_3COO)_2H_2O]_2$ and $[CuCl_2(pyridine\ N\text{-}oxide)]_2$ include a direct metal-metal bond and superexchange via the bridging oxygen atoms [237 and refs. therein].

Since 1961, a large number of copper(II) complexes of tridentate ligands of O and N donor atoms have been prepared, many of which have sub-normal room temperature magnetic moments [40,235-238,244 and refs. therein]. Although a number of these complexes have had the temperature dependence of their magnetic susceptibilities investigated down to liquid nitrogen temperatures, very few appear to have been studied by X-ray diffraction techniques. The structures of these complexes have, by analogy with Figure 2.5.12(a), been assumed to be side-by-side dimers.

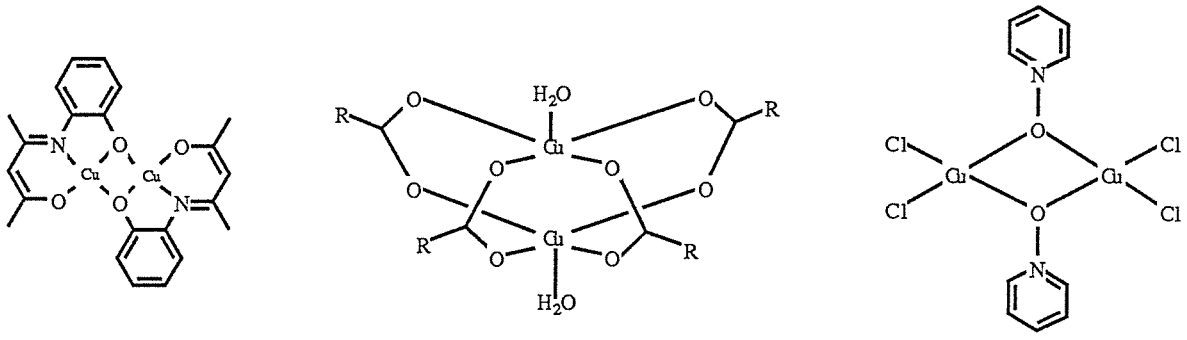

(a) (b) (c)

Figure 2.5.12

Figure 2.5.12 Schematic diagrams for the structures of the dimeric complexes
(a) acetylacetone-mono(o-hydroxyanil)copper(II) (after [234])
(b) copper(II) carboxylate (after [192])
(c) (pyridine N-oxide)copper(II) chloride (after [237,262]).

A number of copper(II) complexes of sbH_2, its substituted congeners and closely related ligands have previously been prepared [235,244,247]. Complexes of the dianionic ligands were shown invariably to have depressed magnetic moments e.g. for $[Cu(sb)]_2$ values of; 1.38 B.M. (at 300 K) [244], 1.31 B.M. (at 298 K) [235] and from this study, 1.16 B.M. were obtained. However, ternary adducts of the dianionic ligand complexes (e.g. [Cu(sb)pyridine]) and monoanionic ligand complexes (e.g. $[Cu(sbH)Cl]H_2O$) displayed normal magnetic properties at room temperature and down to 78 K [244,247]. These compounds were therefore assigned monomeric or only very weakly interacting dimeric structures.

In this study, 30 copper(II) complexes of either sbH_2 or its substituted analogues were prepared. Of these, 15 had magnetic moments which were considered to be indicative of spin coupling between the Cu(II) centres (see Table 2.5.2). It is interesting to note that of these complexes, 9 were brown (or khaki/yellow) and 6 were green, whereas the 15 'normal' moment compounds were green (with the exception of $[Cu(sbH_2)Cl_2(H_2O)]$ which was khaki).

TABLE 2.5.13

E.s.r. Parameters for Selected Chapter 5 Complexes[a]

Complex	g_1	$g_\perp$	g_2	$g_{/\!/}(g_3)$	$A_{/\!/}(A_3)$[b]	G[c]	2J[d]	Solvent
$[Cu(sb)]_2$		2.055		2.222	202	4.0	-390	powder
		2.061		2.253	192			dmso
		2.055		2.236	187			pyridine
		2.064		2.183	166			conc. NH_3[e]
$[Cu(sbH)Cl]_2$		2.073		2.277	165	3.8	-360	powder
	Major	2.070		2.288	176			dmso
	Minor	2.070		2.357	176			
		2.056		2.234	186			pyridine
		2.058		2.241	169			dmso + en[f]
$[Cu(sbH_2)Cl_2(H_2O)]$	2.064		2.078	2.304		4.3		powder
		2.076		2.289	178			dmso
$[Cu(sbH)Br]_2$		2.064		2.270	178	4.2	-350	powder
$[Cu(sbH_2)Br_2]_2H_2O$		2.062		2.274		4.4	-180	powder
		2.077		2.286	177			dmso
$[Cu(sbH)ClO_4(H_2O)]_2$	Major	2.088		2.327	128	3.7	-370	powder
	Minor	2.088		2.384	156	4.4		
$\Delta Ms = 2$		4.279		4.456	~65			powder
	Major	2.070		2.287	177			ethanol
	Minor	2.070		2.224	173			
$[Cu(sbH)NO_3]_2$		2.061		2.270	183	4.4	-360	powder
$[(Cu(sbH))_2SO_4]$		2.070		2.284	169	4.1	-230	powder
$\Delta Ms = 2$			4.210					powder
$[(Cu(sbH)H_2O)_2SiF_6]\cdot 2H_2O$		2.050		2.259		5.2		powder
$[Cu(5msbH)Cl]_2$		2.084		2.263	129	3.1	-360	powder
		2.075		2.293	179			dmso
$[Cu(5nsbH)Cl]$			2.128[g]					powder
		2.073		2.293	177			dmso
$[Cu(s2mbH)Cl]_2$			2.068[g]				-350	powder
		2.074		2.285	179			dmso
$[Cu(s3mbH)Cl]_2$		2.071		2.282	160	4.0	-360	powder
		2.074		2.290	179			dmso
$[Cu(s4abH)Cl]_2\cdot 3H_2O$	2.042		2.070	2.244		4.4	-140	powder
		2.073		2.287	179			dmso

TABLE 2.5.13 continued

Complex	g_1	$g_\perp$	g_2	$g_{/\!/}(g_3)$	$A_{/\!/}(A_3)$[b]	G[c]	2J[d]	Solvent
$[Cu(s4mobH)Cl]H_2O$	2.042		2.082	2.203		3.3		powder
$[Cu(s2hbH)]_2$		2.064		2.237	196	3.7	-300	powder
		2.071		2.255	189			dmso
$[Cu(s4hbH_2)Cl]_2H_2O$		2.074		2.282	163	3.8	-350	powder
		2.072		2.288	179			dmso
$[Cu(5ms4mbH)Cl]_2$[h]		2.076		2.287	165	3.8	-380	powder
$\Delta Ms = 2$			4.279					powder
		2.076		2.289	178			dmso
	Major	2.071		2.289	178			ethanol
	Minor	2.071		2.224	173			
$[Cu(5ms4abH)Cl]_2H_2O$		2.069		2.269	176	3.9	-390	powder
$[Cu(b5nbH)Cl]$		2.045		2.172		3.8		powder
		2.071		2.255	189			dmso
$[Cu(saH)Cl(H_2O)]H_2O$		2.044		2.236		5.4		powder
		2.078		2.289	177			dmso
$[Cu(bs)]_2$			2.063[g]				-120	powder
$[Cu(saa)]$	2.055		2.100	2.208		2.7		powder
$[Fe(sbH)_2]NO_3{\cdot}2H_2O$	4.103							powder
	4.265		8.2					dmso
$[Fe_2(sb)_3]{\cdot}4H_2O$	2.035							powder
	4.271		8.1					dmso
$[Cr(sbH)(sb)]$			3.077					powder
			3.610					dmso

a via simple first-order spectral analysis

b h.f. coupling constant in 10^4 cm^{-1}

c $G = (g_{/\!/} - 2)/(g_\perp - 2)$

d $-2J = kT \ln\left(\frac{3.0003\ g^2}{\mu_{eff}^2} - 3\right)(cm^{-1})$ [188]

e contains 10% dmso and concentrated aqueous NH_3

f Cu: en = 1:5 (en = ethylenediamine)

g g_{iso} value

The crystal structure of $[Cu(sbH)ClO_4(EtOH)]_2$, determined in this work, shows the monoanionic ligand to coordinate in the plane, with the phenolato oxygens bridging the two copper(II) centres (see Figure 2.5.6). The axial sites are occupied by weakly bound perchlorato and ethanol moieties. The separation of the two copper centres of 2.999(4) Å and the arrangement of the ligands is very similar to that found in the previously mentioned acetylacetone-mono(o-hydroxyanil)copper(II). It may therefore be representative of the structure formed in the low moment complexes with similar ligands.

The reaction of $CuCl_2$ with sbH_2 in ethanol yielded the green complex $[Cu(sbH)Cl]H_2O$ when carried out by Iskander *et al.* [244] and Johnson *et al.* [246]. The crystallographic structure was determined by the latter group and was shown to have a monomeric, square-planar copper(II) geometry. Upon heating, this complex, as well as Cu(sbH)Cl·pyridine, gave a brown complex of the formulation [Cu(sbH)Cl]. Both the green and the brown complexes displayed normal room temperature magnetic moments (1.81 and 1.80 B.M. respectively). When this initial reaction was repeated in this study, using 95% ethanol, the complex obtained was brown and had a magnetic moment of 1.24 B.M. It is therefore formulated as a dimer and is envisaged to have a side-by-side phenolato bridged structure as found in $[Cu(sbH)ClO_4(EtOH)]_2$. The calculated values of 2J given in Table 2.5.13 using the Thompson-Ramaswamy equation [188] for the low moment copper(II) complexes, range from -120 to -390 cm^{-1}. Appreciable coupling between the metal centres is apparent although, as mentioned previously, the mechanism by which the spin pairing occurs is not yet fully understood. The side-by-side, planar, dimeric structures observed for Cu(II) complexes of tridentate N and O donor atoms (e.g. see Figures 2.5.6 and 2.5.12(a)) results in significantly greater magnetic overlap ($d_{x^2-y^2}$ orbitals) than the stacked, off-axis dimers investigated in the first section of this work (e.g. $[Cu(LH)(CF_3COO)]_2(CF_3COO)_2$ - Figure 1.1.1). This can be seen by comparing approximate 2J values of -300 and -6 cm^{-1} for the previously ordered complexes.

The magnetic moments for the complexes $[Ni(sbH)NO_3]\cdot\frac{1}{2}H_2O$, $[Co(sbH)NO_3]\cdot\frac{1}{2}H_2O$ and [Cr(sbH)(sb)] of 2.91, 4.57 and 3.76 B.M. respectively are all considered to be normal for high-spin octahedral geometries [112,192]. For the former two compounds this would imply a di- or polymeric structure as the ligand contributes three coordinating atoms and the anion (NO_3^-) a maximum of two. From its formulation and normal moment, the complex [Cr(sbH)(sb)] seems to have both a mono- and dianionic ligand coordinated. The two ligands are most probably bound orthogonally to the pseudo-octahedral metal atom (N_2O_4 donor set) giving monomeric complexes. This structure has also been proposed for a series of Cr(III) complexes with sbH_2 and analogous ligands, only for these complexes both ligands are monoanionic e.g. $[Cr(sbH)_2]Cl$ [240].

The iron(III) complex $[Fe(sbH)_2]NO_3\cdot H_2O$, although formulated as a monomer, has a magnetic moment of 5.03 B.M., reduced from the expected spin only value of 5.9 B.M. [192]. As some degree of spin pairing seems to be occurring (at room temp.) the complex may be dimeric. The previously prepared complexes $Fe(II)(XsbH_2)SO_4\cdot H_2O$ and $Fe(III)(XsbH)Cl_2\cdot H_2O$ (where X = H, 3-CH_3O, 3-NO_2, 5-Cl, 5-Br, 5-CH_3 and 5-NO_2) are all high spin and have moments which are almost independent of temperature down to 78 K [226]. The ferric complex, Fe(sb)Cl, however was shown to have behaviour indicative of intermolecular antiferromagnetic exchange with μ_{eff} ranging from 5.68 B.M. at 300 K to 4.40 B.M. at 78 K and a calculated value for 2J of -7.3 cm^{-1}. In contrast to this, the ferric complex formulated as the dimer $[Fe_2(sb)_3]\cdot 4H_2O$ [this work] has a moment of 6.07 B.M., consistent with a normal, high spin Fe(III) complex at room temperature.

2.5.5(e) Electron Spin Resonance Spectra

The e.s.r. parameters in Table 2.5.13 show a number of interesting features which have not previously been reported for these or structurally related complexes. A high proportion of the copper complexes with sub-normal magnetic moments, indicating some degree of spin coupling at room temperature, have powder spectra which would normally be interpreted as

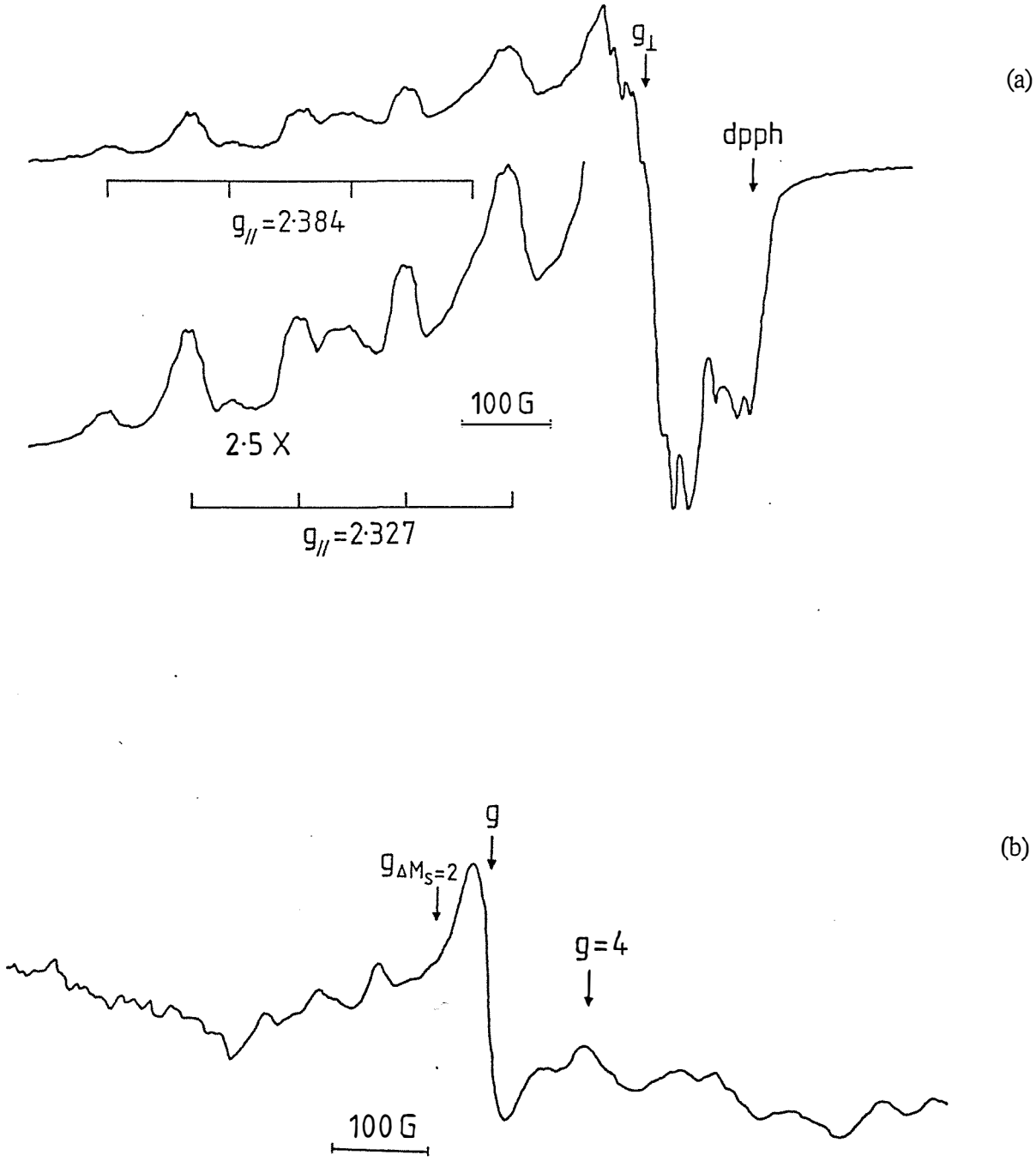

Figure 2.5.13: Powder e.s.r. spectra for $[Cu(sbH)ClO_4(H_2O)]_2$ at 110 K (a) g = 2 (ΔMs = 1) and (b) g = 4 (ΔMs = 2) regions.

being magnetically dilute. The calculated values of G are for the most part greater than 4 which is meant to indicate only slight misalignment of the tetragonal axes or minimal exchange coupling [105]. Therefore, these results also appear to be anomalous, indicating non-magnetically interacting copper centres. Not only are $g_{//}$ and $g_{\perp}$ resolved in the powder spectra, but in a number of cases $A_{//}$ is as well, as shown in Figure 2.5.13(a) for the dimer $[Cu(sbH)ClO_4(H_2O)]_2$ (where two species were detected). In several cases in the powder spectra, $\Delta Ms = 2$ transitions, indicative of magnetic coupling, were observed. In Figure 2.5.13(b) this transition is shown for $[Cu(sbH)ClO_4(H_2O)]_2$. For two magnetically interacting copper(II) nuclei a seven line hyperfine pattern is expected* . This is weakly resolved in this spectrum (with two of the hyperfine features being obscured by the strong absorption) giving g values of 4.279 and 4.557 and A ~65 x 10^{-4} cm^{-1}. The two g values are approximately twice the values seen for the $\Delta Ms = 1$ transition (2.088 and 2.327) whereas the value of A is nearly half of that for $\Delta Ms = 1$ (128 x 10^{-4} cm^{-1}) as is expected [263].

The 110 K powder spectrum of the brown, low-moment complex $[Cu(sbH)Cl]_2$ has the e.s.r. parameters of $g_{//} = 2.277$, $g_{\perp} = 2.073$ and $A_{//} = 165$ x 10^{-4} cm^{-1}. Mohan *et al.* [247], for the hydrated green monomer, obtained an axial type spectrum at room temperature with the values $g_{//} = 2.302$ and $g_{\perp} = 2.093$ ($g_1 = 2.042$, $g_2 = 2.144$) highlighting the difference between these two complexes.

The majority of powder spectra in Table 2.5.13 for the copper complexes have values of $g_{//}$~ 2.27 and $g_{\perp}$ ~2.07 therefore they are considered to be indicative of axial geometries. In two cases the value of $A_{//}$ was reduced (128 x 10^{-4} cm^{-1} for $[Cu(sbH)ClO_4(H_2O)]_2$ and 129 x 10^{-4} cm^{-1} for $[Cu(5msbH)Cl]_2$) when compared with the average value for the complexes of ~175 x 10^{-4} cm^{-1}. As the in-plane donor atoms are assumed to be approximately equivalent in these dimeric complexes (NO_3), the difference may be due to a tetrahedral distortion of the equatorial donor sets. The crystal structure of $[Cu(sbH)ClO_4(EtOH)]_2$ showed a tetrahedral distortion of

---

* Number of hyperfine lines = 2nI + 1. For a Cu(II) dimer n = 2 and $I = \frac{3}{2}$.

$\omega = 8.1°$ for the equatorial donor atoms. It is possible therefore the above two complexes have a similar in-plane distortion.

In dmso, values for $g_{//}$ and $A_{//}$ of ~2.29 and 180 x 10^{-4} cm^{-1} respectively are observed for most complexes, showing the solution species to be approximately equivalent. A second minor species was invariably observed in these spectra. The parameters for this product for $[Cu(sbH)Cl]_2$ are $g_{//} = 2.357$ and $A_{//} = 176 \times 10^{-4}$ cm^{-1} and typify those observed, therefore, except for this example, were not included in Table 2.5.13. The increased value of $g_{//}$ for the minor species, as compared with the major product (e.g. for $[Cu(sbH)Cl]_2$ $g_{//} = 2.357$ (minor) and 2.288 (major)), is consistent with a more solvated species being present.

The complex [Cu(b5nbH)Cl] is the saturated (i.e. imine reduced) analogue of [Cu(5nsbH)Cl] (see Figure 2.5.11), therefore it is expected to have the amine coordinated as compared with the imine in the $Cu(sbH)^+$ congeners. The powder g_{iso} values for [Cu(b5nbH)Cl] and [Cu(5nsbH)Cl] are 2.087 and 2.128 respectively whereas the $g_{//}$ values in dmso are 2.255 and 2.293 for the same ordering. The significant increase in the g values on changing from a neutral saturated to a neutral unsaturated nitrogen donor atom has been noted previously [264].

Upon dissolving the complexes $[Cu(sb)]_2$ and $[Cu(sbH)Cl]_2$ in the coordinating solvent pyridine, or upon addition of Lewis-bases (e.g. aqueous NH_3 or ethylenediamine (en)) to a dmso solution of the appropriate complex, adducts are formed. None of these were isolated, although the pyridine (py) adducts Cu(sb)py and Cu(sbH)Cl·py have previously been prepared as stable complexes but not studied using e.s.r. spectroscopy [244]. It was assumed therefore, as these adducts had been isolated and the spectral parameters of $[Cu(sb)]_2$ in concentrated aqueous NH_3 solution ($g_{//} = 2.183$, $A_{//} = 166 \times 10^{-4}$ cm^{-1}) were different to $CuCl_2$ in concentrated aqueous NH_3 solution ($g_{//} = 2.249$ $A_{//} = 184 \times 10^{-4}$ cm^{-1}), the ligand (sbH^- or sb^{2-}) was still coordinated. The spectral parameters for $[Cu(sbH)Cl]_2$ in py are nearly identical to those of $[Cu(sb)]_2$ in the same solvent. This may be a genuine result although upon

warming $[Cu(sbH)Cl]_2$ in py to dissolve it, deprotonation may have occurred to give solvated $[Cu(sb)]_2$.

The spectral parameters for the nitrogen adducts in Table 2.5.13 are very similar to those found for the closely related system Cu(salgly) with the nitrogen donors pyridine, N-methylimidazole and γ-collidine (spectra run in dioxane or dioxane:H_2O 3:1) [217].

It seems plausible that for these complexes (this work, [217]) assuming a tetragonal solution species, N_2O_2 equatorial donor sets are present as the data fall within the expected range for such copper(II) systems on a plot of $g_{//}$ vs. $A_{//}$ [264]. (Caution must be exercised however as this plot applies to Cu(II) centres with tetragonally or tetrahedrally disposed donor sets and does not include 5-coordinate species).

The ferric complex $[Fe(sbH)_2]NO_3 \cdot 2H_2O$ has one powder g value of 4.103 whereas in dmso one strong absorption at g - 4.265 and a weak maxima at g = 8.2 are observed. The solution spectrum is typical of high-spin iron(III) in a rhombic environment [265]. The ferric complex $[(Fe_2(sb)_3] \cdot 4H_2O$ displays a similar spectrum in dmso (g values of 4.271 and 8.1) however the powder spectrum is unusual. Instead of the expected resonance at g ~4.2, with a signal width of ~2 000 G, as observed in $[Fe(sbH)_2]NO_3 \cdot 2H_2O$, a g value of 2.035 is obtained with a very broad signal of ~8 000 G. The Cr(III) complex [Cr(sbH)(sb)] shows one broad absorption in the solid state at 3.077 which shifts to 3.610 in a dmso solution. A regular octahedral Cr(III) resonance is expected to have g at 1.98 [266 and refs. therein] therefore the stereochemistry is non-regular, as shown in the electronic spectra (see Table 2.5.11).

2.5.5(f) Nuclear Magnetic Resonance Spectra

N.m.r. spectra of selected ligands were recorded in D_6-dmso and are given in p.p.m. downfield from TMS in Tables 2.5.14 and 2.5.15. The assignments for the unsubstituted sbH_2 were made from a consideration of the ^1H-^{13}C (Figure 2.5.14) and ^1H-^1H shift correlation spectra, the J-resolved spectrum (Figure 2.5.15) and from published data on related systems (e.g. salicylaldehyde and benzoic acid [267-269]). The assigned values for the substituted sbH_2 congeners were then made using predictions of expected shifts upon the sbH_2 system [268,269]. Due to the complexity of some spectra and the uncertainty in a number of cases in the values of C(3) and C(5), these assignments are tentative.

There are four possible structural conformers hydrazones such as these can adopt, due to restricted rotation about the C-N bonds (but not N-N) caused by delocalisaton [270]; these are given in Figure 2.5.16.

Palla *et al.* [270] have stated that such hydrazones do not exhibit Z-E isomerization on the -N=C double bond, with the compounds maintaining the less sterically hindered E form (R′ *syn* to the nitrogen lone pair electrons). Benzoylhydrazones (R and R′ are aromatic) exist only in the form 2 (R *anti* to the nitrogen lone pair electrons) whereas acetylhydrazones (R = CH_3 and R′ aromatic) exist in solution as a mixture of conformers 1 and 2.

In solution sbH_2 and all of its congeners are correspondingly predicted to be in the E-form conformer 2, therefore all n.m.r. spectral shifts relate to this stereochemistry. Another reason to favour this particular arrangement is hydrogen-bonding interactions. As R′ in Figure 2.5.16 is 2-hydroxyphenyl, stabilisation resulting from hydrogen-bonding contacts between the hydroxy hydrogen and the nitrogen lone-pair and/or carbonyl oxygen may be possible (see Figure 2.5.18 also).

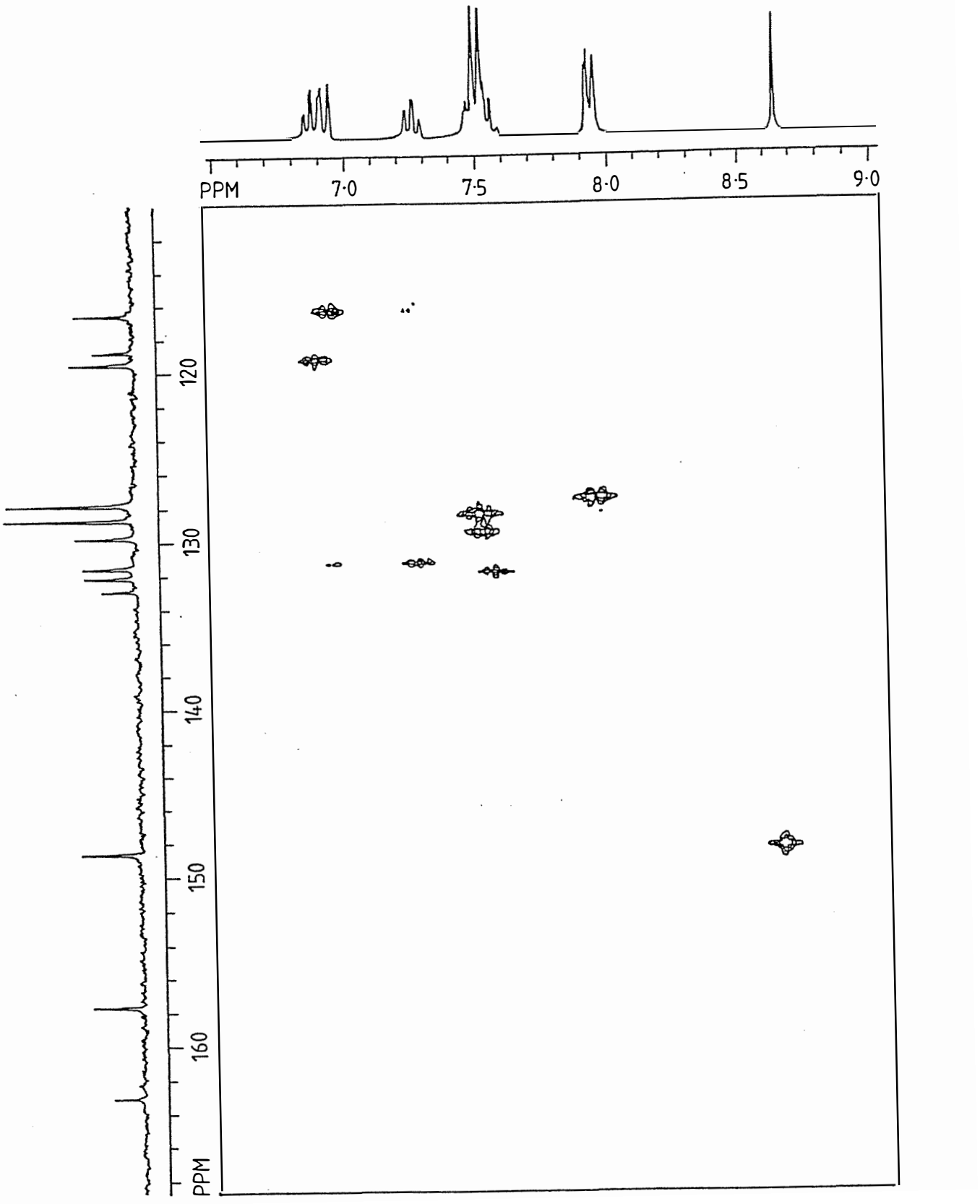

Figure 2.5.14: ^{1}H–^{13}C shift correlation (hetcor) spectrum for sbH_2; run in D_6-dmso vs. TMS.

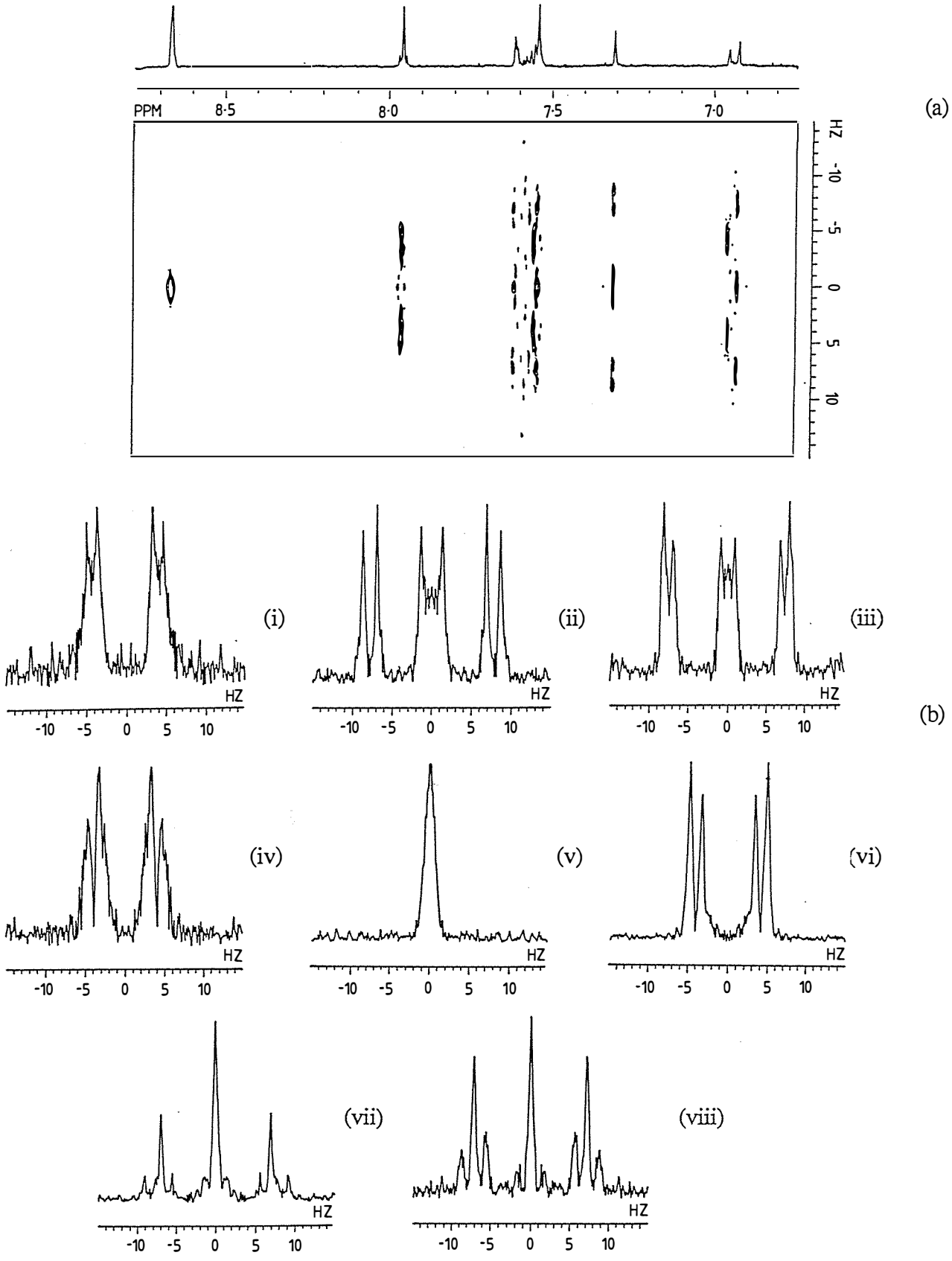

Figure 2.5.15: (a) J-resolved spectrum for sbH_2 with the decoupled ^1H spectrum and (b) slices through the J-resolved peaks for sbH_2 for the H attached to carbon atom number (i) C(2); (ii) C(3); (iii) C(4); (iv) C(5); (v) C(7); (vi) C(10); (vii) C(11); (viii) C(12).

TABLE 2.5.14

^{13}C N.m.r. Data for Chapter 5[a]

Ligand[b]	1	2	3[c]	4	5[c]	6	7	8	9	10	11	12	13	14	CH_3	
sbH_2	157.5	116.4	131.5	119.4	132.0	118.7	148.4	162.9	132.8	127.7	128.6	129.6	128.6	127.7	–	
$3msbH_2$	156.2	125.2	132.2	119.0	132.6	117.3	150.3	163.0	132.7	127.8	128.7	128.8	128.7	127.8	15.6	
$3mosbH_2$	147.4	148.1	113.9	119.2	121.1	119.0	148.6	163.2	132.9	127.8	128.7	132.1	128.7	127.8	55.9	
$5msbH_2$	155.5	116.4	132.0	128.0	132.2	118.4	148.6	163.1	132.9	127.8	128.6	129.6	128.6	127.8	20.0	
$5csbH_2$	156.2	118.3	132.1	123.1	132.1	120.7	146.1	163.1	132.8	127.8	128.6	130.8	128.6	127.8	–	
$5nsbH_2$	162.6	117.1	123.8	139.9	126.6	120.0	144.4	163.1	132.7	127.7	128.6	132.1	128.6	127.7	–	
$s2mbH_2$	157.7	116.6	129.9	119.5	130.3	118.7	148.5	165.2	134.7	136.4	130.9	131.5	125.8	127.7	19.5	
$s3mbH_2$	157.7	116.5	131.4	119.4	132.6	118.7	148.5	163.1	132.8	128.2	137.9	129.7	128.5	124.9	21.0	
$s4mbH_2$	157.8	116.6	130.0	119.5	130.0	118.8	148.6	163.1	131.4	127.8	129.2	142.3	129.2	127.8	21.1	
$s4fbH_2$	157.6	116.5	130.5	119.4	131.5	118.7	148.5	161.9	129.3	129.6	115.6	164.4	115.6	129.6	–	
$s4cbH_2$	157.7	116.6	129.7	119.4	131.5	118.7	148.9	162.0	129.7	128.7	129.7	137.1	129.7	128.7	–	
$s4BbH_2$	157.6	116.5	131.5	119.4	131.9	118.7	148.8	162.1	129.7	129.8	131.6	125.9	131.6	129.8	–	
$s4abH_2$	157.6	116.5	129.8	119.0	131.1	118.8	147.3	163.1	121.6	129.6	112.9	152.7	112.9	129.6	–	
$s4mobH_2$	157.6	116.5	129.8	119.3	131.2	118.7	148.1	162.4	124.8	129.7	113.8	162.3	113.8	129.7	55.4	
$s4hbH_3$	157.7	116.6	130.1	119.5	131.3	118.8	148.2	163.0	123.4	130.1	115.4	161.3	115.4	130.1	–	
$s4nbH_2$	157.6	116.5	129.4	119.4	131.7	118.6	149.3	161.2	138.5	129.2	123.7	149.1	123.7	129.2	–	
$5ms4mbH_2$	155.4	116.3	130.0	128.0	132.1	118.4	148.2	162.8	129.5	127.7	129.1	142.2	129.1	127.7	20.0	21.1
$5ms4cbH_2$	155.4	116.3	131.6	128.0	132.3	118.4	148.6	161.9	129.4	128.7	129.6	136.9	129.6	128.7	20.0	
$5ms4abH_2$	155.4	116.4	131.9	128.1	131.9	118.6	147.4	163.2	119.0	129.7	113.0	152.7	113.0	129.7	20.0	
$5cs4mbH_2$	156.1	118.3	129.8	123.0	129.8	120.7	145.9	162.9	130.7	127.8	129.1	142.2	129.1	127.8	21.1	
$3c5csbH_2$	152.3	121.5	132.2	122.9	128.4	120.7	147.0	163.0	132.3	127.8	128.6	130.2	128.6	127.8	–	
$b5nbH_2$	162.5	115.3	124.7	139.3	125.7	125.9	49.3	165.7	133.1	127.1	128.3	131.3	128.3	127.1	–	
pbH	–	149.6	124.5	136.9	120.0	153.3	148.1	163.5	133.2	127.8	128.6	132.0	128.6	127.8	–	
saH_2[e]	156.6	116.3	127.2	119.5	131.0	120.0	141.5	171.7			Conformer 1 40%				20.4	
	157.5	116.5	129.7	119.4	131.3	118.6	146.7	165.7			Conformer 2 60%				21.4	

a spectra recorded in D_6-dmso and listed in p.p.m. down-field from TMS. Assignments for sbH_2 and saH_2 are from hetcor and cosy spectra whereas the remainder are tentatively assigned on the predicted shifts due to the particular substituents [268,269].

b numbering scheme used is the same as for the crystallography (e.g. see Figure 2.5.1)

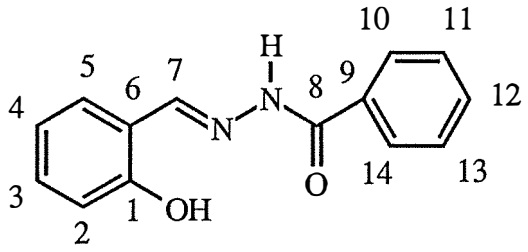

c assignments for C(3) and C(5) are uncertain in a number of cases

d $^1J_{CF}$ = 250 Hz, $^2J_{CF}$ = 21.5 Hz

e two E-form conformers are present; see Figure 2.5.18.

TABLE 2.5.15

Selected ^1H N.m.r. Data for Chapter 5[a]

Hydrogen atom attached to atom

Compound	O(1)	C(2)	C(3)	C(4)	C(5)	C(7)	N(2)	C(10)	C(11)	C(12)	CH_3
sbH_2[f]	12.13	6.96	7.31	6.93	7.57	8.64	11.30	7.94	7.54	7.60[c]	
	s	dd	td	td	dd	s	s	dd	tt	tt	
saH_2 1	e	e	7.59	e	7.22	8.29	11.26	–	–	–	2.18
2			7.45		7.22	8.34	11.64				1.98
			dd		m	s	s				s

a spectra recorded in D_6-dmso and expressed in p.p.m. downfield from TMS
s = singlet, d = doublet, t = triplet, m = multiplet
b same numbering scheme as Table 2.5.14
c assignment uncertain
e not resolved
f coupling constants for sbH_2 (Hz): $J_{2,3} = 8.3$ $J_{2,4} = 1.2$ $J_{3,4} = 7.2$ $J_{3,5} = 1.9$ $J_{4,5} = 7.2$ $J_{10,11} = 7.5$ $J_{10,12} = 1.3$ $J_{11,12} = 7.0$.

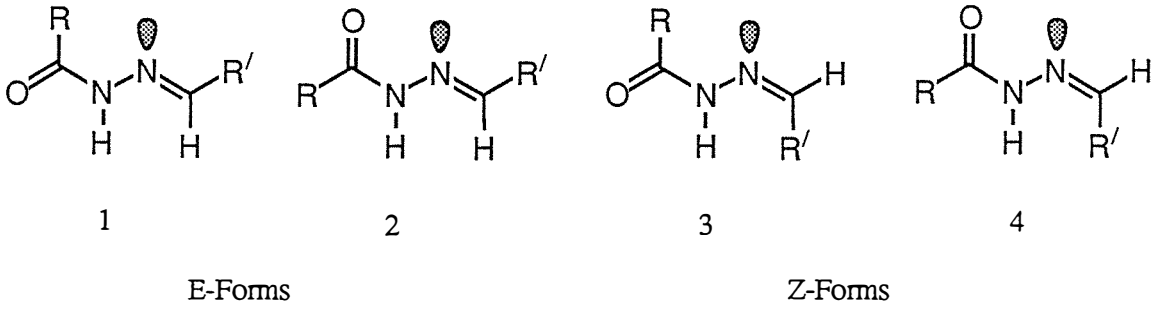

1 2 3 4

E-Forms Z-Forms

Figure 2.5.16 Possible conformers for hydrazones (after [270]).

In their paper, Palla *et al.* [270], assigned the NH proton resonance for a selection of N-aroyl and N-acylhydrazones (which did not contain any hydroxy groups) within a range of 11.08 to 11.83 p.p.m. By analogy, the peak at 11.30 p.p.m. in sbH_2 is assigned to the NH proton, therefore the resonance at 12.13 p.p.m. belongs to the hydrogen on the highly electronegative OH group. The remaining protons were classified according to their couplings in the hetcor spectrum although those on C(5) and C(12) were poorly resolved, even in the decoupled spectrum (Figure 2.5.15(a)).

Selected regions of the hetcor and cosy spectra of the acylhydrazone, salicylaldehyde acetylhydrazone (saH_2), shown in Figure 2.5.17, reveal (as discussed above) that two conformers are present in solution. The ^{13}C, and where possible the ^{1}H shifts for these conformers (1 and 2) are listed in Tables 2.5.14 and 2.5.15 respectively. From these values it can be seen that all atoms in the two isomers are made inequivalent. Palla *et al.* reasonably excluded keto/enol tautomerism as the source of such isomers as the signals coalesced on warming and were unaffected by dilution with basic solvents (e.g. pyridine).

Integration of the resolvable pairs of peaks in ^{1}H spectrum of saH_2 gives 60% for conformer 2. This same value was also obtained upon integration of the appropriate peaks of a ^{13}C spectrum (203 scans with no proton decoupling during the pulse delay of 30 s to remove the Nuclear

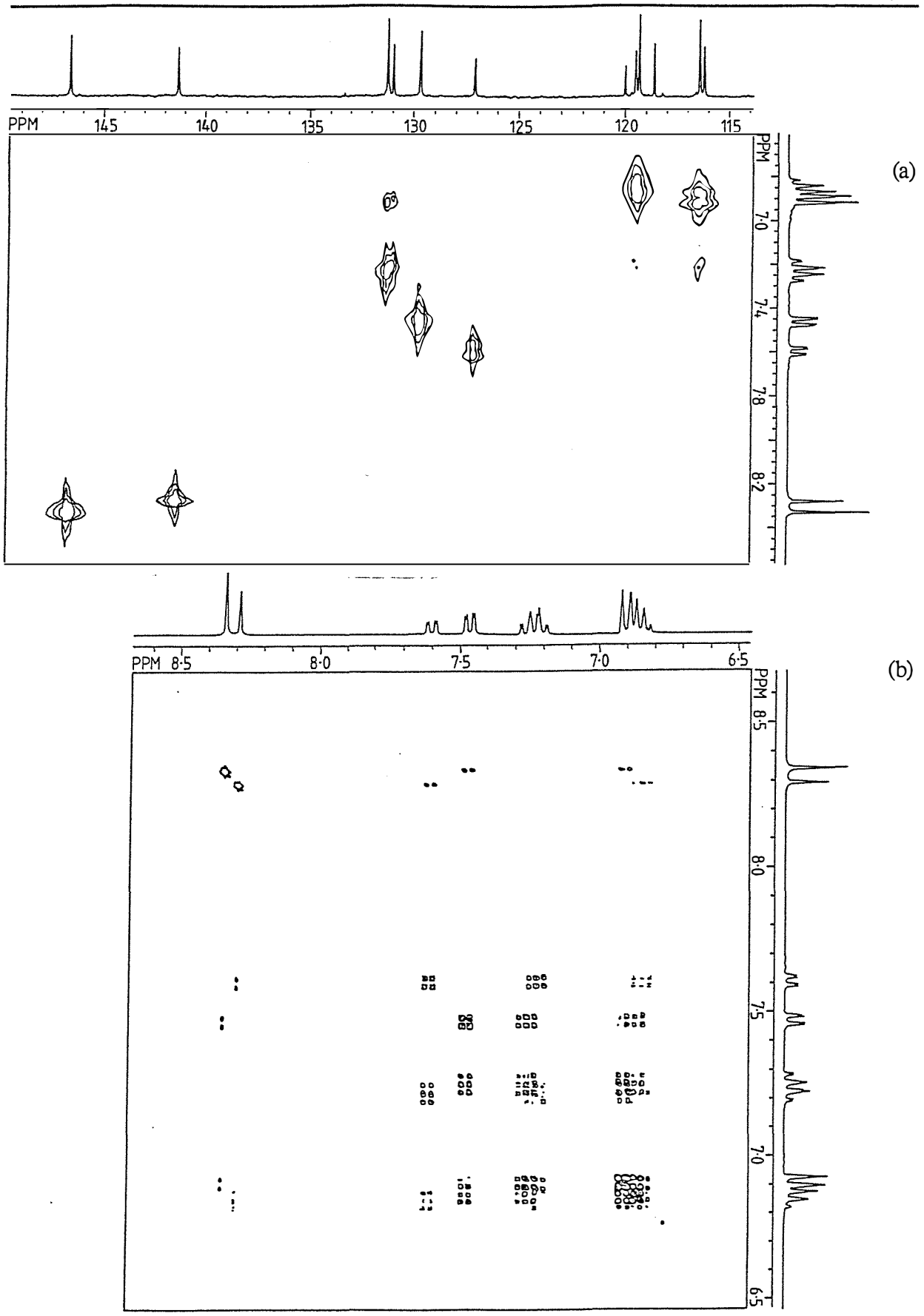

Figure 2.5.17: (a) $^{1}H-^{13}C$ shift correlation (hetcor) spectrum and (b) $^{1}H-^{1}H$ shift correlation (cosy) spectrum for saH_2; run in D_6-dmso vs. TMS.

Overhauser Effect). The percentage of conformer 2 obtained by Palla *et al.* [270] for the closely related compound benzaldehyde acetylhydrazone was 36%. The difference observed here may be caused by the above mentioned hydrogen-bonding contacts between the hydroxy group and the amide oxygen which would help to stabilise conformer 2 in saH_2 (see Figure 2.5.18). To help verify this, the compound where the hydroxy group has been methylated (anisaldehyde benzoylhydrazone - aaH white solid m.p. = 132-3° C) was prepared. The percentage of the conformer postulated to be involved in the hydrogen-bonding was found to have changed from 60% in saH_2 to 32% in aaH. This is the expected change due to the removal of the potential hydrogen-bond between the hydroxy and carbonyl groups for aaH with the value of 32% for conformer 2 now being comparable to those found by Palla *et al.* [270]. The presence of a pair of sharp peaks at 11.29 and 11.14 p.p.m. in the ^1H spectrum of aaH affirms these as resulting from the NH proton as the hydroxy hydrogen is no longer present.

Conformer 1 40% Conformer 2 60%

Figure 2.5.18 The two E-form conformers for salicylaldehyde acetylhydrazone (saH_2) showing possible intramolecular hyrogen-bonding contacts.

2.5.5(g) Summary

An extended range of ligands based on salicylaldehyde benzoylhydrazone (sbH_2) were synthesised and their copper(II) complexes prepared. As well, a selection of transition metal complexes of the parent sbH_2 ligand were made and the copper(II) complexes of the neutral ($Cu(sbH_2)^{2+}$), monoanionic ($Cu(sbH)^+$) and dianionic (Cu(sb)) forms of the ligand. Strongly acidic solutions of Cu(II) and sbH_2 can result in hydrolysis of the Schiff-base ligand whereas

acidic solutions of Cu(II) and sbH_2 can result in hydrolysis of the Schiff-base ligand whereas addition of base to a solution $Cu(sbH)^+$ results in the loss of the remaining (amide) proton and the highly insoluble complex $[Cu(sb)]_2$ is formed. The electronic and infrared spectra proved to be indefinitive in structural analysis. For the free ligands the n.m.r. spectra revealed two E-form conformers for the ligand salicylaldehyde acetylhydrazone (saH_2) to be present in solution.

X-ray crystallographic structures of three complexes were solved, and in one of these, $[Cu(sbH)ClO_4(EtOH)]_2$, a side-by-side dimeric arrangement of the $Cu(sbH)^+$ moieties was found. This structure may result in magnetic spin pairing of the Cu(II) centres, accounting for the sub-normal room temperature magnetic moments observed in half of the complexes. The solid state e.s.r. spectra of these low moment copper complexes, in a number of cases, gave parameters normally associated with magnetically dilute samples for the $\Delta Ms = 1$ transition, yet displayed the $\Delta Ms = 2$ transition. Adduct formation with several Lewis-bases was detected using e.s.r. spectroscopy, in accord with previously prepared ternary complexes of sbH_2 and related ligand systems. The unusual and intriguing spectroscopic and magnetic properties of this system have in the past only been superficially studied and deserve further investigation.

2.5.6 EXPERIMENTAL

2.5.6(a) Ligand Syntheses

All ligands, barring one, in this chapter were prepared by Schiff-base condensation of the appropriate aldehyde with its hydrazide. However, due to most of the substituted salicylaldehydes and benzoic acid hydrazides (benzoylhydrazides) not being readily commercially available, these were synthesised. All of the salicyclaldehyde benzoylhydrazone (sbH_2) congeners were prepared in an analogous manner, therefore the general procedure will be outlined here. Any of the preparations may be scaled up or down as desired and only the ligands prepared by a different synthetic route will be listed.

sbH_2 congeners

A solution of the appropriate benzoic acid (0.05 mmols) in methanol or ethanol (30 cm^3: the alcohol used depended on which gave the highest melting point solid or lowest boiling point liquid ester), containing concentrated sulphuric acid (0.5 cm^3), was refluxed overnight. If the ester produced was a liquid it was washed with water then a concentrated HCO_3^- solution. If satisfactory phase separation of the alcohol, ester, water mixture was not achieved CCl_4 (1-5 cm^3) was added. The ester was then dried over anhydrous Na_2SO_4 and the CCl_4 (if any) removed on a water bath. Finally, the ester was distilled, with only the fraction over the literature boiling point being retained. If the ester was a solid, excess alcohol was removed on a water bath then the product was recrystallised from alcohol or an alcohol/water mixture. To convert the ester to its hydrazide, a 4-5 fold excess of hydrazine hydrate was added to the ester, the mixture heated and ethanol added slowly until a solution was formed. This was then refluxed for several hours (or overnight) after which it was taken to dryness on a rotary evaporator. The solid product was then recrystallised from water, or if necessary, from 50%

aqueous ethanol. The crystalline solid was then dried on a vacuum line for up to a day. Overall yields of the hydrazide from the benzoic acid were generally in the range 10-40%.

The substituted salicylaldehydes were either obtained commercially or were kindly prepared by Miss Anna Wallace using literature procedures [271,272].

The general procedure used to prepare the Schiff-bases is as follows for sbH_2.

To a solution of benzoylhydrazide (8.00 g, 58.8 mmols) in 33% ethanol (100 cm^3 v/v) was added salicylaldehyde (6.20 cm^3, 59.4 mmols) in ethanol (10 cm^3). The mixture was refluxed for 1 hour then water (50 cm^3) added and the solution was left to cool. The white crystalline product was filtered and washed successively with H_2O, cold ethanol and diethyl ether then dried under vacuum. Yield 12.25 g (87%) with typical yields being of this order. If the melting point range of these ligands was greater than 3-4° C they were subsequently recrystallised from aqueous ethanol. Even after recrystallisation, the ligands $3mosbH_2$ and $s4abH_2$ had large melting point ranges (100-10 and 220-40° C respectively) but the analysis figures and mass spectra were consistent with their formulations and they were used without further purification.

All benzoylhydrazides, salicylaldehydes and salicylaldehyde benzoylhydrazones were analysed by mass spectrometry and were shown to be of high purity.

saH_2

Using entirely the same procedure as above, ethyl acetate (20 cm^3, 0.20 mols) was refluxed with hydrazine hydrate (30 cm^3, 0.60 mols) in ethanol (30 cm^3). Yield of hydrazide 13.6 g (90%). To the acetylhydrazide (6.11 g, 82.4 mmols) was added the salicylaldehyde (9 cm^3, 86.2 mmols) solution with the yield of recrystallised product being 11.26 g (77%).

bsH_2 and psH_2

To a filtered solution of salicylhydrazide (10.0 g, 65.7 mmols) in hot methanol (120 cm^3) was added either benzaldehyde (6.9 cm^3, 67.9 mmols) or 2-formylpyridine (6.5 cm^3, 68.3 mmols). This mixture was refluxed for 2 hours, cooled and the solid product filtered off, washed with methanol and diethyl ether then vacuum dried. Yields bsH_2 12.03 g (76%); psH_2 12.76 g (81%).

$saaH_2$

This ligand was initially inadvertently synthesised while trying to reduce salicylaldehyde hydrazone (shH: 2-$(HO)C_6H_4CH{=}NNH_2$). To a solution of shH (5.0 g, 36.7 mmols) in tetrahydrofuran (50 cm^3) was added cyclohexene (10 cm^3, 98.6 mmols) and 1 large spatula of palladium on activated charcoal. This was refluxed for 3 days, filtered through celite, then concentrated (to 20 cm^3). On cooling yellow crystals, identified by mass spectrometry as salicylaldehyde azine, the title compound, separated. Yield 1.09 g (25%). The product can simply be prepared by the following method. To hydrazine hydrate (1.00 cm^3, 46.9 mmols) in ethanol (5 cm^3) was added excess salicylaldehyde (5 cm^3, 46.9 mmols) in ethanol (20 cm^3). The yellow precipitate which formed immediately was heated for 5 minutes then filtered, washed with ethanol and vacuum dried. Yield 4.91 g (99%).

$b5nbH_2$

A solution of 2-hydroxy-5nitrobenzyl bromide (2.01 g, 8.66 mmols) in ethanol (20 cm^3) was added dropwise to a solution of benzoylhydrazide (3.51 g, 25.8 mmols) in ethanol (20 cm^3). This mixture was refluxed for 1 day then concentrated (to 20 cm^3). The white product which separated on cooling was dissolved in a NaOH solution (60 cm^3, 0.5 M) and extracted three times with diethyl ether to remove any unreacted starting products. The yellow aqueous layer

was acidified with concentrated HCl solution until no more colour remained. The white title compound was filtered, washed with water then vacuum dried. It was then recrystallised from ethanol. Yield 1.17 g (47%). An attempt to synthesise the un-nitrated starting product 2-hydroxybenzyl bromide, by brominating 2-hydroxybenzyl alcohol with Hbr (50% w/w) resulted in a white insoluble compound. This was identified from mass spectrometry as a polyether with repeating units of $(2\text{-}(O)C_6H_4CH_2\text{-})_n$.

2.5.6(b) Complex Syntheses

A large proportion of the transition metal complexes prepared in this section were synthesised using the same procedure, therefore one representative example will be given. All methods different to this will be given subsequently.

[Cu(sbH or congener)X] (except $5nsbH_2$ and $s4nbH_2$ (X = Cl^-, Br^-, ClO_4^- or NO_3^-), [Cu(saH)Cl(H_2O)], [Cu(psH)Cl] and [M(II)(sbH)NO_3]·½H_2O (M = Ni or Co)

A solution of sbH_2 (500 mg, 2.08 mmols) in ethanol (30 cm^3) was added to $CuCl_2{\cdot}2H_2O$ (340 mg, 1.99 mmols) in ethanol (10 cm^3). The brown precipitate which separated was filtered and washed with ethanol and diethyl ether then vacuum dried. Yield 616 mg (92%). Yields for this reaction ranged from 10 to 92%.

[Cu(5nsbH)Cl] and [Cu(s4nbH)Cl]

Due to solubility problems, for these preparations the above procedure was repeated except the ligand was dissolved in a mixture of dmf (40 cm^3) and ethanol (100 cm^3). Yields [Cu(5nsbH)Cl] 513 mg (63%); [Cu(s4nbH)Cl] 483 mg (60%).

$[Cu(sb)]_2$

The general procedure was repeated except sodium metal (96 mg, 4.17 mmols) was added to the ethanolic solution of sbH_2. Yield 467 mg (68%).

$[Cu(sbH_2)Cl_2(H_2O)]$ and $[Cu(sbH_2)Br_2]_2H_2O$

A solution of $CuCl_2{\cdot}2H_2O$ (359 mg, 2.11 mmols) in concentrated HCl (10 cm^3) and ethanol (10 cm^3) or $CuBr_2$ (467 mg, 2.09 mmols) in concentrated HBr (10 cm^3) and ethanol (10 cm^3) was added to sbH_2 (500 mg, 2.08 mmols) in ethanol (30 cm^3). The solutions which formed were heated briefly then filtered and left over the weekend during which time unstable yellow-brown crystals of the title complexes grew. These were removed from solution and washed with a solution of ethanol and the respective concentrated acid (4:1) then with diethyl ether and dried under vacuum. Yields $[Cu(sbH_2)Cl_2(H_2O)]$ 384 mg (47%); $[Cu(sbH_2)Br_2]_2H_2O$ 301 mg (31%).

$[(Cu(sbH)H_2O)_2SiF_6]{\cdot}2H_2O$

In an attempt to form a related complex to the previous two compounds the above procedure was repeated using $CuF_2{\cdot}2H_2O$ (288 mg, 2.08 mmols) in concentrated HF (10 cm^3) and ethanol (10 cm^3). In order to heat the green mixture, it was transferred to a glass beaker and upon heating, a green precipitate separated. This was identified as the title complex through the X-ray crystallographic structure of a poor quality crystal obtained from the mother-liquor. Yield 560 mg (66%).

[(Cu(sbH))$_2$SO$_4$]

The general procedure was repeated except the Cu(SO$_4$)·5H$_2$O (527 mg, 2.11 mmols) was dissolved in water (10 cm^3). Yield 484 mg (66%).

[Cu(b5nbH)Cl]

To b5nbH$_2$ (500 mg, 1.74 mmols) in ethanol (40 cm^3) was added sodium metal (45 mg, 1.96 mmols) in ethanol (10 cm^3). The dark green precipitate was heated for 5 minutes then filtered and washed with ethanol and diethyl ether. Yield 321 mg (48%).

[Cu(bs)]$_2$

A solution of bsH$_2$ (240 mg, 1.00 mmols) in boiling methanol (80 cm^3) was added to Cu(CH$_3$COO)$_2$H$_2$O (200 mg, 1.00 mmols) in methanol (20 cm^3) and was refluxed for 1 hour. The fine green precipitate which had formed was filtered and washed with methanol and diethyl ether then vacuum dried. Yield 166 mg (55%).

[Cu(saa)]

Sodium metal (65 mg, 2.83 mmols) was dissolved in ethanol (20 cm^3) and to this was added saaH$_2$ (294 mg, 1.22 mmols). A solution of CuCl$_2$·2H$_2$O (219 mg, 1.28 mmols) in ethanol (10 cm^3) was added to this with heat. The brown precipitate which formed was filtered and washed with ethanol then diethyl ether and dried under vacuum. Yield 357 mg (97%).

[Cu(sal)$_2$] and [Cu(5msal)]

To a solution of $Cu(CH_3COO)_2H_2O$ (300 mg, 1.50 mmols) in water (20 cm^3) and ethanol (20 cm^3) was added either salicylaldehyde (salH) (0.33 cm^3, 3.10 mmols) in ethanol (5 cm^3) or 5-methylsalicylaldehyde (5msalH) (410 mg, 3.01 mmols) in ethanol (10 cm^3). The mixture was stirred for 5 minutes then filtered and washed with water then 1:1 ethanol:diethyl ether and dried under vacuum. Yields [Cu(sal)$_2$] 264 mg (58%); [Cu(5msal)$_2$] 227 mg (45%).

[Zn(sbH)$_2$]H$_2$O and [Zn(saH)$_2$]

$ZnCl_2$ (140 mg, 1.03 mmols) in ethanol (10 cm^3) was filtered then added to a solution of sbH_2 (500 mg, 2.08 mmols) and sodium metal (51 mg, 2.22 mmols) in ethanol (20 cm^3) or saH_2 (373 mg, 2.09 mmols) and sodium metal (53 mg, 2.30 mmols) in ethanol (20 cm^3). The yellow precipitates which formed were heated for 5 minutes then filtered and washed successively with boiling water, ethanol and diethyl ether then vacuum dried. Yields [Zn(sbH_2]H_2O 469 mg (80%); [Zn(saH)$_2$] 292 mg (70%).

[Fe(sbH$_2$)$_2$]NO$_3$·H$_2$O and [Cr(sbH)(sb)]

Although the formulation of these complexes are different, they were both prepared using the same preparative procedure with a 1:1 stoicheometry of metal to ligand. To a solution of sbH_2 (500 mg, 2.08 mmols) in ethanol (20 cm^3) was added either $Fe(NO_3)_3·9H_2O$ (847 mg, 2.10 mmols) or $Cr(NO_3)_3·9H_2O$ (837 mg, 2.09 mmols) in ethanol (10 cm^3). This mixture was heated for 5 minutes, the precipitate filtered and given a cursory wash with ethanol then thoroughly with an ethanol:diethyl ether mix (1:4) and vacuum dried. Yields [Fe(sbH_2)$_2$]NO_2·H_2O 270 mg (42%); [Cr(sbH)(sb)] 301 mg (55%). When the stoicheometric ratios of Cr(III) and sbH_2 were reacted together (as above) the same product was obtained.

$[Fe_2(sb)_3]\cdot 4H_2O$

To a solution of sbH_2 (500 mg, 2.08 mmols) and sodium metal (96 mg, 4.17 mmols) was added $Fe(NO_3)_3\cdot 9H_2O$ (855 mg, 2.12 mmols) in ethanol (10 cm^3). The title complex formed as a red precipitate after heating for 5 minutes. This was left to cool then the product was filtered off and washed successively with hot water, ethanol and diethyl ether then vacuum dried. Yield 433 mg (69%).

2.5.6(c) Data collection procedure for μ-Hexafluorosilicato-bis[aqua(salicylaldehyde benzoylhdrazonato)copper(II)] Dihydrate

The title complex was prepared as described in section 2.5.6(b). The crystal which had approximate dimensions of 0.040 x 0.044 x 0.060 cm displayed faces of the forms {0 0 1}, {1 $\bar{1}$ 0}, {1 1 0}, {0 0 $\bar{1}$}, {$\bar{1}$ 1 0}, [$\bar{1}$ $\bar{1}$ 0}.

The Nicolet R3M four circle automatic diffractometer with Mo-K_α radiation (μ(Mo–Kα) = 13.95 cm^{-1}) used the setting angles of 25 reflections to calculate the cell dimensions of: $\underline{a}$ = 13.677(5), $\underline{b}$ = 11.876(3), $\underline{c}$ = 20.336(7) Å and β = 105.92(3)°. A crystal density of 1.714 g cm^{-3} was calculated from the cell volume of 3 176.4 $Å^3$ and a molecular weight of 819.8 amu ($C_{28}H_{30}Cu_2F_6SiN_4O_8$) for four formula weights per unit cell. The diffraction symmetry established the monoclinic crystal class and systematic absences ($\underline{h}$ $\underline{k}$ $\underline{l}$, $\underline{h}$ + $\underline{k}$ = 2n + 1 and $\underline{h}$ O $\underline{l}$, $\underline{l}$ = 2n + 1) indicated the space group to be C2/c or Cc; final analysis showed C2/c to be correct. A total of 1 871 reflections were collected using the ω/2θ scan technique (θ_{max} = 22.5°) with the $\underline{h}$ $\underline{k}$ $\underline{l}$ ranges: -14 → 13, 0 → 12, 0 → 20. Data were corrected for absorption using an empirical technique [126]. Tables 2.5.16 and 2.5.17 summarise the relevant crystal and data collection parameters.

2.5.6(d) Structure solution and refinement

The copper atom site was located by direct methods [159] and returned a residual of 0.40. Subsequent electron and difference electron density syntheses revealed all non-hydrogen atoms. These were included with isotropic temperature factors and yielded a residual of 0.07 for two full-matrix least-squares refinement cycles. Difference electron density maps revealed all hydrogen atom sites and these were included in the calculations; those in the phenyl rings and on N(2) in fixed positions with N-H and C-H distances of 1.08 Å. The values of R and R_w for the final refinement cycle were 0.0509 and 0.0451 respectively for the 210 parameters and 955 data for which $F^2 > 3\sigma(F^2)$. The function minimised was $\Sigma w(|F_o| - |F_c|)^2$ with the weight, w, being defined as $1.3997/(\sigma^2(F) + 0.0032\ F^2)$.

All non-hydrogen atoms were refined assuming anisotropic thermal motion with the two phenyl rings being treated as rigid groups (C-C 1.395 Å). The highest peak in the final difference electron density map was 0.47 $\bar{e}$ $Å^{-3}$ and the largest shift per e.s.d. was 0.07.

Final atomic parameters and the observed and calculated structure factors are presented on the microfiche inside the back cover packet of this thesis. The bond length and bond angle data are presented in Tables 2.5.3 and 2.5.4 respectively.

TABLE 2.5.16
$[(Cu(sbH)H_2O)_2SiF_6]\cdot 2H_2O$

CRYSTAL DATA

Compound:	μ-Hexafluorosilicato-bis[aqua(salicylaldehyde benzoylhydrazonato)copper(II)] Dihydrate
Colour:	Green
Formula:	$C_{28}H_{30}Cu_2F_6SiN_4O_8$
Formula weight:	819.8 g mol^{-1}
Space group:	C2/c
a:	13.677(5) Å
b:	11.876(3) Å
c:	20.336(7) Å
β:	105.92(3)°
V:	3 176.4 $Å^3$
Z:	4
ρ_c:	1.714 g cm^{-3}
Crystal faces:	{0 0 1}, {1 $\bar{1}$ 0}, {1 1 0}, {0 0 $\bar{1}$}, {$\bar{1}$ 1 0}, {$\bar{1}$ $\bar{1}$ 0}
Crystal dimensions:	0.040 x 0.044 x 0.060 cm
μ (M_o-K_α):	13.95 cm^{-1}
F(OOO):	1 668

TABLE 2.5.17
$[(Cu(sbH)H_2O)_2SiF_6]\cdot 2H_2O$

Parameters Associated with Data Collection

Radiation used:	$M_o(K_\alpha)$ (λ = 0.71069 Å)
Graphite monochromator used:	Yes
Scan type:	$\omega/2\theta$
Scan range:	2.0°
Scan speed:	7.32°/min
θ Range:	2.5 – 22.5°
Total number of reflections in data set:	1 871
Observed data criterion:	955 unique reflections with $F^2 > 3\sigma(F^2)$
Collection temperature:	153 K

2.5.6(e) Data collection procedure for Bisethanoldiperchloratobis-(μ-[salicylaldehyde benzoylhydrazonato (1–)]-μ-O, N, O′)dicopper(II)

The synthesis of the title complex is described in section 2.5.6(b). Faces of the forms {0 1 $\bar{1}$}, {1 0 $\bar{2}$}, {0 $\bar{1}$ $\bar{1}$}, {$\bar{1}$ 0 0}, {0 1 1}, {1 0 0}, {0 $\bar{1}$ 1}, {$\bar{1}$ 0 2} were displayed by a crystal of approximate dimensions 0.070 x 0.030 x 0.030 cm. Cell dimensions determined from a least-squares refinement of the setting angles of 25 reflections are: $\underline{a}$ = 11.2281(9), $\underline{b}$ = 7.9129(4), $\underline{c}$ = 21.0430(14) Å, β = 98.560(6)°. For a cell volume of 1848.8 Å^3 and a molecular weight of 896.7 amu ($C_{32}H_{34}Cl_2Cu_2N_4O_{14}$) the density was calculated to be 1.611 g cm^{-3} for two formula weights in the unit cell. Systematic absences ($\underline{h}$ 0 $\underline{l}$, $\underline{l}$ = 2n + 1 and 0 $\underline{k}$ 0, k = 2n + 1) established the space group as $P2_1/c$. A total of 1 540 reflections were collected on an Enraf-Nonius CAD-4 diffractometer with Cu-K_α radiation (μ(Cu-Kα) = 31.86 cm^{-1}) using the ω/2θ scan technique (θ_{max} = 40°). The $\underline{h}$ $\underline{k}$ $\underline{l}$ limits were: -10 → 10, 0 → 7, 0 → 19.

The intensities of three standard reflections were monitored at 2 hourly intervals during the data collection. The data were collected in shells depending on θ and for where θ ≤ 40° very little decomposition was observed (as indicated by the intensity loss of only 0.7%). However, for the shell with data greater than 40° there was a sudden and drastic intensity loss (69%) when only a few reflections had been measured. It was obvious the crystal had decomposed and the data had to be abandoned. No other crystals were available hence the data set was limited to this inner θ shell. Corrections for anisotropic decay were applied to the relatively unaffected data with the minimum and maximum corrections being 0.9923 and 1.0204 respectively.

Analytical absorption corrections were applied [124,125] with the minimum and maximum transmission coefficients being 0.3741 and 0.7689 respectively.

The relevant crystal and data collection parameters are summarised in Tables 2.5.18 and 2.5.19 respectively.

2.5.6(f) Structure solution and refinement

The copper atom site was located from the Patterson synthesis and returned an R factor of 0.53. Subsequent electron density and difference electron density maps revealed all non-hydrogen atoms and showed disorder to be present in both the perchlorato and ethanol moieties. The residual at this stage was 0.15. Inclusion of the disordered atoms, with their appropriate weights, and refinement of the copper and chlorine atoms assuming anisotropic thermal motion for the final refinement cycle yielded values for R and R_w of 0.123 and 0.163 respectively. The function minimised was $\Sigma w(|F_o| - |F_c|)^2$ with the weight, w, being defined as $1.000/(\sigma^2(F) + 0.0228\ F^2)$ for the 135 parameters and 1215 data for which $F^2 > 3\sigma(F^2)$. Further refinement was deemed unjustified as crystal decomposition meant that less than half the expected total data was collected and subsequent attempts to recrystallise the title complex were unsuccessful.

Final atomic parameters and the observed and calculated structure factors are given on the microfiche in the pocket inside the back cover of this thesis. The bond length and bond angle data are presented in Tables 2.5.3 and 2.5.4 respectively.

TABLE 2.5.18
$[Cu(sbH)ClO_4(EtOH)]_2$

CRYSTAL DATA

Compound:	Bisethanoldiperchloroatobis-(μ-[salicylaldehyde benzoylhydrazonato(1-)]-μ-O, N, O')dicopper(II)
Colour:	Green
Formula:	$C_{32}H_{34}Cl_2Cu_2N_4O_{14}$
Formula weight:	896.7 g mol^{-1}
Space group:	$P2_1/c$
a:	11.2281(8) Å
b:	7.9129(4) Å
c:	21.0430(14) Å
β:	98.560(6)°
V:	1 848.8 $Å^3$
Z:	2
ρ_c:	1.611 g cm^{-3}
Crystal faces:	{0 1 $\bar{1}$}, {1 0 $\bar{2}$}, {0 $\bar{1}$ $\bar{1}$}, {$\bar{1}$ 0 0}, {0 1 1}, {1 0 0}, {0 $\bar{1}$ 1}, {$\bar{1}$ 0 2}
Crystal dimensions:	0.070 x 0.030 x 0.030 cm
μ (M_o-K_α):	31.86 cm^{-1}
F(OOO):	908

TABLE 2.5.19
$[Cu(sbH)ClO_4(EtOH)]_2$

Parameters Associated with Data Collection

Radiation used:	Cu-Kα (λ = 1.5418 Å)
Graphite monochromator used:	No
Incident beam collimator (diameter):	1.2 mm
ω scan angle:	$(0.8 + 0.142 \tan \theta)^\circ$
Horizontal aperture width:	$(1.70 + 1.20 \tan \theta)$mm
Vertical aperture height:	4 mm
Scan type:	ω/2θ
Prescan speed:	(20/3)°/min
Prescan acceptance; relative $\sigma(F^2)/F^2$ required:	0.8
Final scan acceptance $\sigma(F^2)/F^2$:	0.018
Maximum time limit for final scan:	100 s
Intensity control frequency:	7 200 s
Orientation acceptance; maximum deviation of any scattering vector from its calculated position:	0.08°
θ Range:	1 – 40°
Total number of reflections in data set:	1 540
Observed data criterion:	1 215 unique reflections with $F^2 > 3\sigma(F^2)$
Collection temperature:	293 K

2.5.6(g) **Data collection procedure Aquachloro(salicylaldehyde acetylhydrazonato(1-))copper(II) Hydrate**

The procedure used to synthesise the title complex is described in section 2.5.6(b). A crystal of approximate dimensions 0.048 x 0.021 x 0.010 cm displaying faces of the form {0 0 $\bar{1}$ }, {1 $\bar{1}$ 0}, {$\bar{1}$ $\bar{1}$ 0}, {$\bar{1}$ 1 0}, {1 1 0}, {0 $\bar{1}$ 3) was selected. Cell dimensions determined from a least-squares refinement of the setting angles of 25 reflections are: $\underline{a}$ = 7.4877(4), $\underline{b}$ = 15.5806(7), $\underline{c}$ = 10.5208(3) Å and β = 103.563(4)°. For a molecular weight of 312.2 amu ($C_9H_{13}CuClN_2O_2$) and a cell volume of 1193.2 $Å^3$ the density was calculated to be 1.738 g cm^{-3} for four formula weights in the unit-cell. The space group was established as $P2_1/c$ from the systematic absences $\underline{h}$ 0 $\underline{l}$, l = 2n + 1; and 0 $\underline{k}$ 0, k = 2n + 1). A total of 2 392 reflections were collected on an Enraf-Nonious CAD-4 diffractometer with Cu–K_α radiation (μ(Cu-Kα) = 44.74 cm^{-1}) using the $\omega/2\theta$ scan technique (θ_{max} = 75°). The $\underline{h}$ $\underline{k}$ $\underline{l}$ limits were: -9 → 8, 0 → 19, 0 → 13.

During the data collection, the intensities of three standard reflections were monitored at 2 hourly intervals. As the total loss of intensity was 0.3% , corrections for anisotropic decay were not applied. Analytical absorption corrections were calculated [124,125], giving the minimum and maximum transmission coefficients of 0.3741 and 0.7689 respectively.

Tables 2.5.20 and 2.5.21 summarise the relevant crystal and data collection parameters respectively.

2.5.6(h) Structure solution and refinement

The site of the copper atom position was calculated from the Patterson synthesis and yielded a residual of 0.51 when included in a structure factor calculation. All non-hydrogen atoms were located in the subsequent electron density and difference electron density maps and returned a value 0.10 for R after two cycles of full-matrix least-squares refinement (assuming isotropic thermal motion). All hydrogen atoms were located from difference electron density syntheses and were included in calculated positions, those attached to the phenyl ring and on N(2) at 1.08 Å. The values of R and R_w for the final refinement cycle were 0.0634 and 0.0689 respectively for the 152 parameters and 2 046 data for which $F^2 > 3\sigma(F^2)$. The function minimised was $\Sigma w(|F_o| - |F_c|)^2$ with the weight, w, being defined as $1.0000/(\sigma^2(F) + 0.07415\ F^2)$.

Refinement of all non-hydrogen atoms was carried out assuming anisotropic thermal motion with the atoms in the phenyl ring being treated as a rigid group (C-C 1.395 Å). In the final refinement cycle the largest shift per e.s.d. was less than 0.3. The highest peak in the final difference electron density map of 0.73 $\bar{e}$ $Å^{-3}$ was associated with residual electron density around the copper atom.

Final atomic parameters and the observed and calculated structure factors are presented inside the back cover pocket on a microfiche. The bond length and bond angle data are listed in Tables 2.5.8 and 2.5.9 respectively.

TABLE 2.5.20
$[Cu(saH)Cl(H_2O)]H_2O$

CRYSTAL DATA

Compound:	Aquachloro(salicylaldehyde acetylhydrazonato)copper(II) Hydrate
Colour:	Green
Formula:	$C_9H_{13}CuClN_2O_2$
Formula weight:	312.2 g mol^{-1}
Space group:	$P2_1/c$
a:	7.4877(4) Å
b:	15.5806(7) Å
c:	10.5208(3) Å
β:	103.563(4)°
V:	1 193.2 $Å^3$
Z:	4
ρ_c:	1.738 g cm^{-3}
Crystal faces:	{0 0 $\bar{1}$}, {1 $\bar{1}$ 0}, {$\bar{1}$ $\bar{1}$ 0}, {$\bar{1}$ 1 0}, {1 1 0}, {0 $\bar{1}$ 3}
Crystal dimensions:	0.048 x 0.021 x 0.010 cm
μ (M_o-K_α):	44.74 cm^{-1}
F(OOO):	628

TABLE 2.5.21
$[Cu(saH)Cl(H_2O)]H_2O$

Parameters Associated with Data Collection

Radiation used:	Cu-Kα (λ = 1.5418 Å)
Graphite monochromator used:	No
Incident beam collimator (diameter):	0.8 mm
ω scan angle:	$(0.8 + 0.142 \tan \theta)^\circ$
Horizontal aperture width:	$(1.70 + 1.20 \tan \theta)$mm
Vertical aperture height:	4 mm
Scan type:	ω/2θ
Prescan speed:	(20/3)°/min
Prescan acceptance; relative $\sigma(F^2)/F^2$ required:	0.8
Final scan acceptance $\sigma(F^2)/F^2$:	0.018
Maximum time limit for final scan:	100 s
Intensity control frequency:	7 200 s
Orientation acceptance; maximum deviation of any scattering vector from its calculated position:	0.08°
θ Range:	1 – 75°
Total number of reflections in data set:	2 392
Observed data criterion:	2 046 unique reflections with $F^2 > 3\sigma(F^2)$
Collection temperature:	293 K

CHAPTER 6

CYTOTOXICITY RESULTS

2.6.1 INTRODUCTION

The mechanisms by which the ligands 2-formylpyridine thiosemicarbazone (LH) and salicylaldehyde benzoylhydrazone (sbH_2) and their transition metal complexes (and related systems) exert their biological activities are poorly understood.

For LH and its copper and iron complexes, possible antitumour mechanisms include the deactivation of the enzymes ribonucleoside diphosphate reductase (rdr) [59] or RNA dependant DNA polymerase [26]. However, several other DNA and RNA polymerases were deactivated by the related system, Cu(isatin-β-thiosemicarbazone), and its N-methyl analogue [25,26] (see Figure 1.3). As well, the marked difference in the activity between LH and its Cu and Fe complexes was suggested by Petering *et al.* [276] to indicate that three different cytotoxic species were being observed. A large variety of substituted compounds, based on the thiosemicarbazones of 2-formylpyridine, 1-formylisoquinoline, 2-formylpyrazine, 2-formylpyrrole and 2-formylindole (amongst others) have previously been prepared by several groups [57-59,81]. These same authors correlated the antitumour activity and inhibition of rdr for series of these compounds with Hammett substituent constants (σ), Hansch hydrophobicity constants (π), field constants (F) and molar refractivities (MR), in order to gain some insight into the factors governing their activities. In one of these reports [57], correlations between the basic Hammett substituent constants σ_m and σ_p of substituent groups and certain equilibrium properties (protonation constants, complex and adduct formation constants and reduction potentials) and cytotoxicities were determined for (where appropriate) a series of 5-substituted LH congeners and their Cu(II) complexes.

In this study, LH, 3 of its congeners and a selected range of their transition metal complexes have been synthesised and trends within the cytotoxicity data and between other reported data

discussed. In contrast to LH, salicylaldehyde benzoylhydrazone (sbH_2), its congeners and their complexes have received little attention. The mechanism of action for these compounds is not understood and studies, similar to those conducted on LH, appear not to have been performed. Related systems have demonstrated a variety of biological activities (including antitubercular, antiviral [277], antitumour [231,232] and growth modulation [17,18]) with an equally wide range of mechanisms being postulated (deactivation of RNA dependent DNA polymerase [277], superoxide dismutase like activity [207], involvement of the hosts immune system [248] and deactivation of pyridoxal kinase [278]).

Johnson *et al.* [246] suggested that as sbH_2 appeared to be able to cross cell membranes, intracellular inhibition of cell growth by such mechanisms as binding to proteins, direct binding to nucleic acids or disruption of metal transport may be possible. The lipid solubility of sbH_2 was therefore implicated as being important for cytotoxicity. However, from this and the preceding discussion it is apparent very little is known about the mechanistic action of these compounds.

In this study, sbH_2 and a selection of its transition metal complexes as well as a range of sbH_2 congeners and their Cu(II) complexes have been prepared and tested for their cytotoxicity on the cell line HCT-8. The importance of both lipid solubility (π) and electronic (σ) parameters upon the cytotoxicity have been investigated. As well, the statistical significance of the cytotoxicities for the copper(II) complexes compared with the corresponding free ligands is examined.

Antiviral activities for a selection of compounds were also determined but no significant activity was found.

2.6.2 CYTOTOXICITY RESULTS

Background

All cytotoxicity testing (Tables 2.6.1 and 2.6.2) were very generously determined by Drs Graeme Finlay and William Denny at the Cancer Research Laboratory, University of Auckland, School of Medicine. The cell line used in this study was HCT-8, a human colon adenocarcinoma [279 and refs. therein]. HCT-8 cells are generally resistant to intercalating drugs (relative to other cell lines) and fairly crude comparisons suggest it is also one of the more resistant lines to cisplatin [280]. The cell line is not in widespread use.

The cytotoxicity data are given as IC_{50} values; the concentration of compound required to inhibit the growth of the cells by 50% relative to a control. Included in Tables 2.6.1 and 2.6.2, for a comparison with a proven drug against this cell line, are the values for cisplatin. The difference between the two pairs of results for cisplatin (as noted in these tables), may reflect a genetic drift in the cells, as the values were obtained at different times. To be considered genuinely different, an approximate two-fold difference in values should be observed. Some idea of the variability of the results can be seen by examination of the data for compounds where several determinations have been made. Also included in the Tables are the IC_{50} values for dmso (1.9 and 3.7% (v/v)) as all compounds were initially dissolved in this solvent (due to their limited aqueous solubility) to give a final concentration of 1% (v/v). The effect of the dmso at this concentration is minimal as cultures containing compounds which were inactive ($IC_{50} > 20$ μM) showed no decrease in cell growth.

2.6.3 RESULTS AND DISCUSSION

2.6.3(a) LH Congeners and their Complexes

The most striking feature of the cytotoxicity data presented in Table 2.6.1 for LH analogues and their transition metal complexes is that, contrary to previous studies [26,74,84,276], CuL^+ is less active (IC_{50} ~14 μM) than the free ligand LH (IC_{50} ~4.7 μm). Petering *et al.* reported the IC_{50} values for the inhibition of ribonucleoside diphosphate reductase by LH and CuL^+ to be 0.90 and 0.75 μM respectively and the T/C* values for Ehrlich ascites tumour cells for the same ordered compounds to be 0.74 (1 mg/cm^3) and 0.29 (0.75 mg/cm^3) [276]. The observed reversal in this study is probably due to the cell line used (HCT -8).

As ethylenediaminetetraacetic acid (edta) can quantitatively remove the Cu(II) from CuL^+ (see Chapter 2 discussion) (and $Cu(sbH)^+$), the cytotoxicities of both LH and CuL^+ were re-evaluated with edta present (0.5 mM for the whole culture determination). This was to ensure the activity of LH was not due in part to the formation of cytotoxic metal chelates in the culture medium. The cytotoxicity of kethoxal-bisthiosemicarbazone ($KTSH_2$ -see Figure 1.3) was shown to be due to the formation *in vivo* of the complex CuKTS as $KTSH_2$ has no activity in animals maintained on a copper-deficient diet [281]. The IC_{50} value of 3.8 μM for LH + edta is not significantly changed from the average value of 4.7 μM for LH above, therefore the activity is due to the uncomplexed LH. This also demonstrates that edta, or any metal complexes which may form through sequestering of accessible metal ions in the assay medium do not change the activity of LH. The addition of edta to CuL^+ has however increased the cytotoxicity when compared with CuL^+ alone (IC_{50} values of 7.6 and ~14 μM respectively) again showing the uncomplexed ligand to be more active than its Cu(II) complex.

---

* change in weight per week of mice which have previously had tumour cells implanted after either being treated with the compound in question (T) at the stated dosage, or a control (C).

TABLE 2.6.1

Cytotoxicity Data for Section 1 Compounds

Compound[a]	IC_{50} (μM)[b]	Compound[a]	IC_{50} (μM)[b]
LH	3.9; 5.4; 4.8	$[CuL(CH_3COO)]_2$	13; 13; 14; 15
LH + edta[c]	3.8	$[CuL(CH_3COO)]_2$ + edta[c]	7.6
		$[Zn(LH)Cl_2]H_2O$	5.3
		$[Ag(LH)(NO_3)]$	4.1
		[Au(LH)Cl]	5.5
6LH	> 20	$[Cu(6L)(CH_3COO)]_2$	> 20
2′L	> 20	$[Cu(2'L)Cl_2]$	> 20
4′LH	3.7	$[Cu(4'L)(CH_3COO)]_2$	2.1
pbH	> 20	$[Cu(pb)(CH_3COO)]_2$	> 20
cisplatin[d]	3.9; 4.5: 1.7; 2.3	dmso	1.9%; 3.7% (v/v)[e]

a see Figure 4.1 for ligand abbreviations
b IC_{50} data are Inhibitory Concentrations to 50% of the cell count compared with a control (per metal atom where applicable)
all compounds are in 1% dmso
the cell line used was HCT-8
c determination carried out with 0.5 mM ethylenediaminetetraacetic acid (edta) added
d the first two values were obtained at a different time to the other two; the differences may reflect a genetic drift in the cells
e IC_{50} values for dmso (v/v) - see note b

The IC_{50} values for $Zn(LH)^{2+}$ (5.3 μM), $Ag(LH)^{+}$ (4.1 μM) and $Au(LH)^{+}$ (5.5 μM) are all approximately the same as the free ligand, LH (4.7 μM). Petering *et al.* [128] have determined the logarithm of the formation constant for ZnL^{+} to be 9.18 (compared with 16.90 for CuL^{+}). Although this is large for a zinc complex, stability is substantially reduced at pH 7.4 by the competition of hydrogen ions. The complex ZnKTS was thought to be an independent cytotoxic agent in animals; however, *in vitro*, under metal free conditions, this chelate is not effective [9 and refs. therein]. Petering proposed that ZnKTS served as a donor of the ligand, by dissociation, to form the active species CuKTS [75]. The cytotoxicities in this study of $Zn(LH)^{2+}$ and, by analogy $Ag(LH)^{+}$ and $Au(LH)^{+}$ (the formation constants of LH with Ag^{+} and Au^{+} have not been determined) may therefore be due to LH, released by the dissociation of the complexes at physiological pH.

The ligand 6-methyl-2-formylpyridine thiosemicarbazone (6LH) and its Cu(II) complex, $Cu(6L)^{+}$, are both inactive (IC_{50} > 20 μM). In a study by French *et al.* [58], 6LH caused little change in the therapeutic effect when compared with LH (on four cell lines) although the potency per unit weight was reduced over tenfold. The same substitution, changing 3-hydroxy-2-formylpyridine thiosemicarbazone (30H-LH) to the disubstituted congener (30H-6LH) however resulted in total loss of activity. A later study by the same author [59] upon three of the same cell lines as previously used, showed the same trend for these four compounds with the IC_{50} values for the inhibition of partially purified rdr being: LH 0.28; 6LH 7.76; 30H-LH 6.46; 30H-6LH ~190 μM.

The general decrease in activities for the 6-methylated ligands was thought to be a steric effect, due to interference with the ring N chelation, and partly electronic due to changes in the conjugated ligand system [58,59]. The single-crystal X-ray structure for the cation of the complex [Cu(6L)(bipy)]Cl [282] is shown in Figure 2.6.1 along with selected changes in bonding angles and distances compared with the unmethylated ligand complex

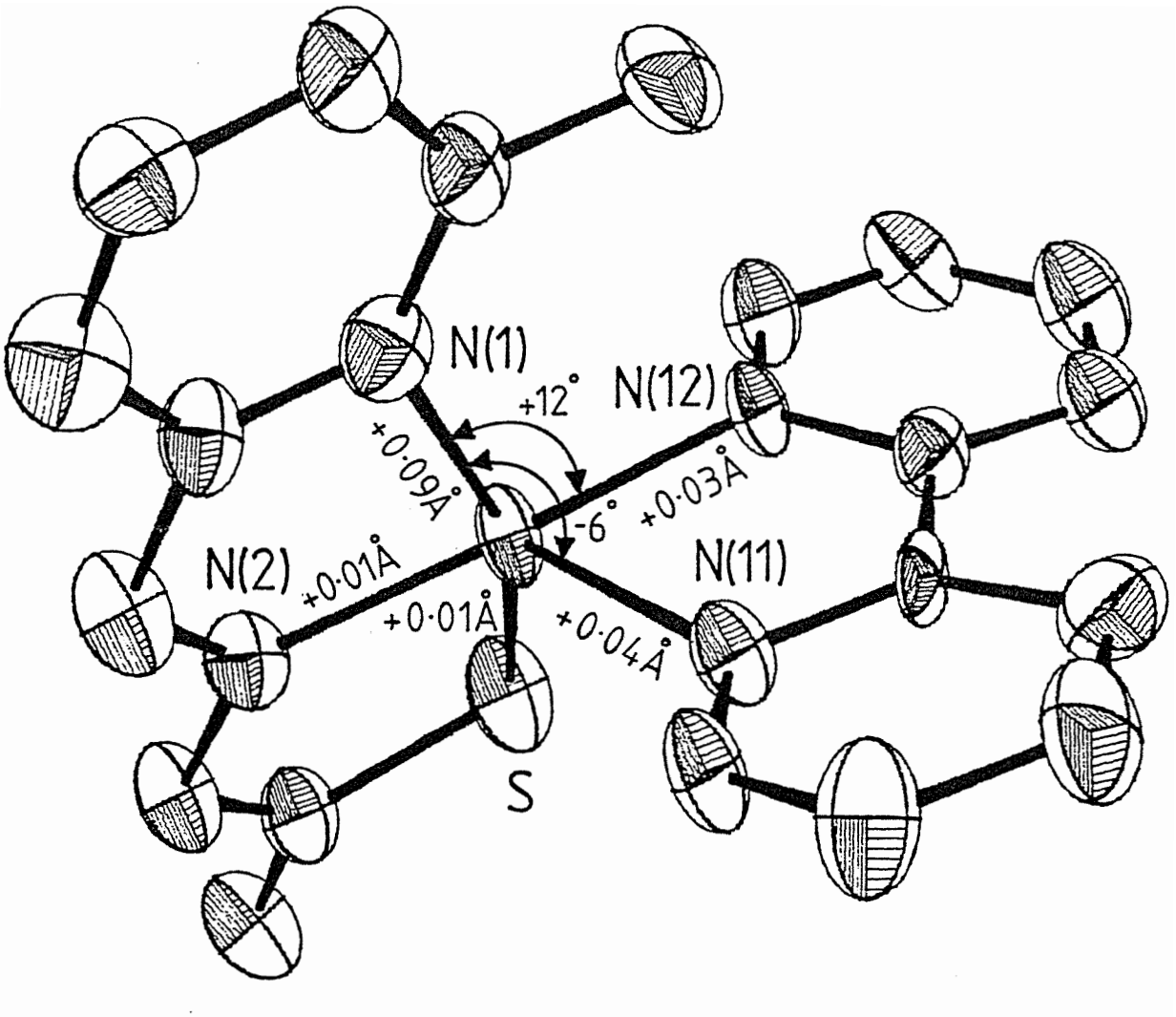

Figure 2.6.1: The monomeric cation for [Cu(6L)(bipy)]Cl (after [282]) showing selected atom numbering. The non-coordinated Cl^- ion and hydrogen atoms have been omitted for clarity. The difference in selected bond angles and bond distances between this structure and [CuL(bipy)]ClO_4 ([this work] see Figure 1.2.3) are given.

[CuL(bipy)]ClO_4 (Δ[Cu(6L)(bipy)$^+$ minus CuL(bipy)$^+$]). From this diagram it can be seen that the bond angle between the basal 6-methylpyridine N and the bipyridyl N about the Cu, N(1)-Cu-N(12), has increased by 12°, whereas the angle to the apical N, N(1)-Cu-N(11), has correspondingly decreased by 6°. Surprisingly, all five bonds to the copper atom have lengthened with the Cu-N(1) distance increasing by 0.09 Å. It is plausible that these changes are predominantly a result of the steric interaction of the (pyridine) methyl group with the chelated bipyridyl moiety, although electronic changes cannot be ignored. *In vivo* therefore, steric interactions such as these for 6LH may well destabilise or prevent the formation of critical adducts which confer activity upon LH.

The ligand 2′L and its Cu(II) complex Cu(2′L)$^{2+}$ are also both inactive as cytotoxic agents when tested on cell line. French *et al.* [59] also found for this compound that *in vitro* and *in vivo* activity of any significance was lost, as exemplified by the IC_{50} values for the inhibition of partially purified rdr being 0.28 μM for LH and > 5 000 μM for 2′LH. The addition of the 2′ methyl effectively traps the ligand in the thione form (see Figure 1.1(a)), rendering impossible the overall conjugation as observed in the crystal structures of the ligand 5-hydroxy-LH [91] and the Cu(II) complexes of LH and L$^-$ (see Chapter 1 of this work). The loss of activity for 2′L may therefore be due to the ligand being unable to have this delocalised form and/or its inability to coordinate as an anionic moiety. It is interesting to note however, that a range of 2-acetylpyridine thio- and selenosemicarbazones were generally less active as antimalarial agents in infected mice (*Plasmodium berghei*) than the corresponding 2-acetylpyridine thio- and selenosemicarbazides (imine reduced), although the latter are not conjugated in the side chain [283].

The ligand 4′LH shows activity comparable to that of LH with the respective IC_{50} values being 3.7 and 4.7 μM. The corresponding Cu(II) complexes do not however display equal cytoxicities with Cu(4′L)$^+$ requiring 6.5 times less compound (IC_{50} = 2.1 μM) than CuL$^+$ (IC_{50} ~14 μM) for an equal effect. The results for the ligand are in contrast to the findings of French *et al.* [58,59] where substitution on the terminal nitrogen N(4′) (methyl, ethyl, phenyl

or 2-pyridyl) resulted in each case in reduced or lost activity. It was postulated by the above group that replacement of hydrogens on N(4') would be adverse due to steric interference with the SH group. However, changes in the electronic distribution of the ligand via an alteration of the resonance forms, modified hydrogen-bonding ability of the $-NH_2$ group by substitution and changes in the ligand lipophilicity may also be important. It is difficult to reconcile the increased activity of 4'LH compared with the results of French *et al.* The difference is probably (as invoked previously) a property of the cell line used in testing and highlights the important point that compounds should be tested on as wide a spectrum of cell lines as practically possible to avoid overlooking any potential biological activity.

Although the ligand 2-formylpyridine benzoylhydrazone (pbH) chemically resembles LH in its complex and adduct forming ability (see Chapter 4), both pbH and $Cu(pb)^+$ have IC_{50} values > 20 μM showing them to be inactive. The structural differences between pbH and LH are in effect the substitution of the thioamide S and the terminal NH_2 group in LH for the respective amide O and phenyl ring in pbH (see Figure 4.1, Chapter 4 for diagrams). Replacement of the S in LH and related thiosemicarbazones to give the corresponding semicarbazones has been shown to result in loss of biological activity [81,283,284]. This was attributed to a reduction in the metal binding ability of these species. Although replacement of the NH_2 group by a phenyl ring in any thiosemicarbazone analogues of LH does not appear to have been carried out previously, as noted for 4'LH, substitution of one of the NH_2 hydrogens with a phenyl ring results in loss of activity, presumably due to unfavourable steric interactions [58,59].

In Chapter 4, the e.s.r. study of $Cu(pb)^+$ and $Cu(2'L)^{2+}$ showed the interactions of the complexes with human blood components to be very similar. However, there were several marked differences between the spectral properties of these complexes and those of the unsubstituted ligand complex CuL^+. Possibly paralleling these findings are the cytotoxicity results: whereas CuL^+ shows activity (IC_{50} = 14 μM) both $Cu(pb)^+$ and $Cu(2'L)^{2+}$ are inactive (IC_{50} > 20 μM). The differences observed between these complexes for the e.s.r. spectra may be a reflection of a mechanistic difference. As the first contact such drugs normally have is

with the blood, further insights into the mode of action for CuL^+ could possibly be gained by studying this reaction in more detail.

The activities for LH, 4'LH and $Cu(4'L)^+$ are comparable to that of cisplatin (see Table 2.6.1) for the HCT-8 cell line. However, further testing on animal models would be required to establish the antitumour properties of these compounds and hence their potential usefulness. Trials on the metal-free 5-hydroxy LH were conducted but side effects such as severe disruption of iron metabolism prevented clinical use [77]. However, by administering a preformed metal complex, sequestering of metal ions may be eliminated [74 and refs. therein].

Petering *et al.* [108] found for a series of 5-substituted LH congeners and their Cu(II) complexes that there was a trend in antitumour activity for both the Sarcoma 180 and Lewis Lung tumour systems with respect to Hammett σ constants, if only the active compounds were considered. The justification for using the active compounds was that there may be many unrelated reasons which result in inactivity, such as differences in solubility. Correlations between σ and

(i) the reduction potentials ($E_{½}$) of the Cu(II) complexes
(ii) the formation constants for the ligands with Cu(II) and the preformed complex with ethylenediamine and
(iii) the protonation constants of the ligands and their Cu(II) complexes

were also investigated. A positive correlation between σ_{para} and $E_{½}$ was found although variations in $E_{½}$ have little important effect upon the formation constants for these complexes. It was expected that all of the Cu(II) complexes would be sufficiently stable in biological systems so they could reach critical reaction sites undissociated. They would therefore be available to react with thiols, which is believed to be the first step in their catalytic oxidation [57] (hence the correlation with $E_{½}$). For the Cu(II) complexes of $KTSH_2$ congeners, the degree of cytotoxicity for the complexes correlates directly to their rate of reaction with thiols,

i.e. reduction [74]. Put simply; the more negative the reduction potential of the Cu(II) complex, the more stable it is in the presence of biological thiols and the less active it is (because it is more difficult to reduce the complex and subsequently release the ligand). As only four ligands based on LH and their Cu(II) complexes were prepared in this investigation, with only two of these being considered active, similar studies to those described above were not possible.

Two other investigations will briefly be mentioned here for completeness. Antholine *et al.* [74] studied the combined modality of CuL^+ and radiation and clearly established CuL^+ as the most effective derivative of LH (out of LH, CuL^+ and FeL_2^+) with respect to toxicity against Chinese Hamster Ovary (CHO) cells. The combined effect on CHO cell survival for both CuL^+ and X-radiation was significantly greater than the product of CuL^+ and X-rays individually. Although cells were most sensitive to CuL^+ at the G_1/S interphase, some whole cycle killing was observed. As this sensitivity mimics that of radiation, it was suggested an alternative or secondary mechanism similar to radical formation on the molecular level may be operating, as CuL^+ in the presence of thiols and O_2 is known to generate $O_2^{\cdot-}$ and ·OH [74 and refs. therein]. As tumour cells have reduced superoxide dismultase (sod) activity, if equal amounts of $O_2^{\cdot-}$ could be delivered to cancer and normal cells a favourable outcome may be possible.

The second investigation, carried out by Dunn and Hodnett [81], was a re-examination of data by French *et al.* [59] for the inhibition of rdr. A structure-activity relationship for the 3- and 5-substituted (pyridine ring) congeners of LH was established for 28 data giving R = 0.88:

$$pIC_{50} = 6.30 - 0.81\ \Sigma F_{3,5} + 0.29\ \Sigma\pi_{3,5} - 0.24\ MR_5$$

$\Sigma F_{3,5}$ is the sum of the field/inductive constants for the 3 and 5 positions (F is derived from σ_m and σ_p for a particular substituent [285]); $\Sigma\pi_{3,5}$ is the sum of the Hansch hydrophobicity π constants for the substituents in positions 3 and 5 and ; MR_5 is the molar refractivity (polarisability) of the group at carbon 5. Other independent variables had been explored but

these proved not to be statistically justified. The term in F for the above equation suggested that the substituents capable of the greatest electron withdrawal are less active. This supported previous proposals [283 and refs. therein] that these ligands may act by chelating at the site of action as electron withdrawal would destabilise complex formation. The π and MR terms were not as easily interpreted due to their small coefficients but were thought to indicate that lipid solubility and steric inhibition of binding at the site of action respectively were important. However, care must be taken in using both π and MR as they may be highly interrelated [286].

2.6.3(b) sbH_2 Congeners and their Complexes

The cytotoxicity data for the sbH_2 congeners, some related ligands and their transition metal complexes, along with the comparative values for cisplatin and dmso, are presented in Table 2.6.2.

The average IC_{50} value of 3.7 μM for sbH_2 is significantly reduced upon complexation with copper(II), giving a value of 1.6 μM for $Cu(sbH)^+$. The increase in potency of the Cu(II) complex compared with the free ligand has also been observed for human bladder carcinoma (T-24) with IC_{50} values (concentration which reduces DNA synthesis by 50%) of 0.05 and 0.5 $\mu g/cm^3$ respectively and for rat hepatoma (HTC_4) with IC_{50} values of 0.5 and 30 $\mu g/cm^3$ respectively [231]. The concentration of copper complex required for the cell lines T-24 and HTC_4 was, respectively 10 and 60 times less than for the free ligand (sbH_2), whereas in this study for HCT-8 it was 2.3. The difference between these values is possibly a reflection of the cell line used. When Mohan *et al.* [247] tested a selection of 3- and 5-substituted sbH_2 ligands, and several of their transition metal complexes (including Cu(II)) on the lymphocytic leukaemia (P388) cell line they surprisingly found no activity for any of the compounds.

Trials on sbH_2,$s2mbH_2$, $s4abH_2$ and their Cu(II) complexes were repeated in the presence of 0.5 mM edta. The average values for the ligands are not significantly changed when edta is added, showing (as for LH) that sequestering of trace amounts of metals by the ligands, and/or edta does not affect the activity. As edta can quantitatively remove the Cu(II) from $Cu(sbH)^+$, the ligands are less active than their copper chelates and from the cytotoxicity data for CuL^+ and edta (see previous discussion), it was expected that the addition of edta to the preformed Cu(II) complexes would result in activities comparable to the respective free ligands. However, if anything, the cytotoxicities slightly improved compared to the complexes, and in all three cases, the complex plus edta was significantly more active than the ligands alone. These results are puzzling and may suggest that edta and the Cu(II) complexes are acting synergistically.

TABLE 2.6.2

Cytotoxicity Data for Section 2 Compounds

Compound[a]	IC_{50} (μM)[b]	Compound[a]	IC_{50} (μM)[b]
sbH_2	2.5; 3.6; 3.6; 3.9; 4.9	$[Cu(sbH)Cl]_2$	1.6; 1.6; 1.5
sbH_2 + edta[c]	2.5	$[Cu(sbH)Cl]_2$ + edta[c]	0.96
		$[Ni(sbH)NO_3]\frac{1}{2}H_2O$	6.7; 3.6
		$[Co(sbH)NO_3]\frac{1}{2}H_2O$	19
		$[Fe(sbH)_2]NO_3 \cdot H_2O$	> 20
		$[Zn(sbH)_2]H_2O$	1.8
		[Cr(sbH)(sb)	> 10
$3msbH_2 \cdot H_2O$	2.6	$[Cu(3msbH)Cl]H_2O$	1.5
$3mosbH_2$	3.7	$[Cu(3mosbH)Cl] \cdot \frac{5}{2}H_2O$	1.5
$5msbH_2$	1.5; 2.8	$[Cu(5msbH)Cl]_2$	0.94
$5csbH_2$	< 3.1, 2.2	[Cu(5csbH)Cl]	1.0
$5nsbH_2$	12; 17	[Cu(5nsbH)Cl]	4.0
$s2mbH_2$	> 4.0; 7.2; 6.9; 6.3	$[Cu(s2mbH)Cl]_2$	2.5; 2.3; 1.5
$s2mbH_2$ + edta[c]	4.5	$[Cu(s2mbH)Cl]_2$ + edta[c]	1.6
$s3mbH_2$	1.9; 3.1	$[Cu(s3mbH)Cl]_2$	1.4
$s4mbH_2$	2.0; 3.4	$[Cu(s4mbH)Cl] \cdot \frac{1}{2}H_2O$	1.5
$s4fbH_2 \cdot H_2O$	2.1	[Cu(s4fbH)Cl]	1.6
$s4cbH_2 \cdot H_2O$	1.3; 1.5	[Cu(s4cbH)Cl]	1.3
$s4BbH_2 \cdot H_2O$	1.7	[Cu(s4BbH)Cl]	1.6
$s4abH_2$	12; 21; 16; 14	$[Cu(s4abH)Cl]_2 \cdot 3H_2O$	10; 12; 11
$s4abH_2$ + edta[c]	10	$[Cu(s4abH)Cl]_2 \cdot 3H_2O$ + edta[c]	7.2
$s4mobH_2$	3.8	$[Cu(s4mobH)Cl]H_2O$	2.3
$s2hbH_3$	1.8	$[Cu(s2hbH)]_2$	1.1
$s4hbH_3$	5.7; 8.6	$[Cu(s4hbH_2)Cl]H_2O$	9.7
$s4nbH_2$	1.7	[Cu(s4nbH)Cl]	1.5
$5ms4mbH_2$	2.3	[Cu(5ms4mbH)Cl]	1.1
$5ms4cbH_2$	1.8	[Cu(5ms4cbH)Cl]	0.98
$5ms4abH_2 \cdot H_2O$	6.9	$[Cu(5ms4abH)Cl]_2H_2O$	6.9
$5cs4mbH_2$	1.4	[Cu(5cs4mbH)Cl]	1.4
$3c5csbH_2 \cdot H_2O$	3.5	[Cu(3c5csbH)Cl]	1.2
$b5nbH_2$	14	[Cu(b5nbH)Cl]	3.4
psH_2	17	[Cu(psH)Cl]	18
saH_2	> 50	$[Cu(saH)Cl(H_2O)]$	> 20
bsH_2	> 20	$saaH_2$	> 20
salicylaldehyde	> 50	$[Cu(sal)_2]$	> 20
5-methylsalicylaldehyde	> 20	$[Cu(5msal)_2]$	> 20
benzoylhydrazide	> 20	4-chlorobenzoylhydrazide	> 20
cisplatin[d]	3.9; 4.5: 1.7; 2.2	dmso	1.9%; 3.7% (v/v)[e]

a see Figure 2.5.11 for ligand abbreviations
b IC_{50} data are Inhibitory Concentrations to 50% of the cell count compared with a control (per metal atom where applicable)
all compounds are in 1% dmso
the cell line used was HCT-8
c determination carried out with 0.5 mM ethylenediaminetetraacetic acid (edta) added
d the first two values were obtained at a different time to the other two; the differences may reflect a genetic drift in the cells
e IC_{50} values for dmso (v/v) - see note b

The effect of varying the transition metal was examined by determining the cytotoxicities for the complexes $Ni(sbH)^+$, $Co(sbH)^+$, $Fe(sbH)_2^+$, $Zn(sbH)_2$ and Cr(sbH)(sb). The Co(II), Fe(III) and Cr(III) complexes have IC_{50} values of 19, > 20 and > 10 μM respectively and are considered to be inactive. For $Ni(sbH)^+$, the average value of 5.2 μM has significantly increased relative to the $Cu(sbH)^+$ value of 1.6 μM and is not considered to enhance the activity of the free ligand (average IC_{50} value of 3.7 μM). The only complex tested to have cytotoxicity comparable to $Cu(sbH)^+$ is $[Zn(sbH)_2]H_2O$. The formation constants for these complexes have not been determined, but by analogy with CuL^+ and ZnL^+ [57,128] and many other systems [156], the binding of sbH^- to Zn(II) is expected to be many orders of magnitude lower than for Cu(II). It is possible that in the assay medium both ligands are displaced from $Zn(sbH)_2$ by biological chelators e.g.

$$Zn(sbH)_2 + 2(HL_{cell}) \rightleftarrows Zn(L_{cell})_2 + 2(sbH_2)$$

The cytotoxicity of $Zn(sbH)_2$ may therefore be due to the complex or, if the above displacement occurs, it may result from the 2 released ligands (2 x 1.8 μM for $Zn(sbH)_2$ = 3.6 μM compared with 3.7 μM for the average sbH_2 value).

In an attempt to investigate the contributions of the solubility and electronic properties of substituents to the cytotoxicities of the ligands and their copper complexes, statistical fits of activities against π (Hansch hydrophobicity parameter [287]) and σ (Hammett-Taft electronic parameter [288]) were carried out. The ligands with substituents in the benzoyl ring were chosen (except for the ortho position due to steric problems inherent with these) giving 10 compounds (including the unsubstituted sbH_2). The π constant was chosen as it gave a better fit than MR, and σ^+ (corrected for through-conjugation) was chosen over σ and R for similar reasons. A least-squares linear regression analysis (l.s.l.r.) with more than 2 variables for only 10 data is difficult to justify statistically, therefore only π and σ were used. As it is, with the choice of substituents, π and σ do show some correlation to each other (R = 0.82).

A two-variable l.s.l.r. analysis of π and σ versus $\log(1/IC_{50})$ for the ligands substituted into the benzoyl ring (excluding the ortho position) and their corresponding copper complexes resulted in the correlation coefficients (R) of 0.98 and 0.92 respectively. However, the one-variable plots showed σ was not statistically needed as π was more highly correlated to $\log(1/IC_{50})$. This can be seen from the l.s.l.r. R values of 0.97 and 0.91 for the free ligands and their copper complexes respectively and is shown graphically in Figure 2.6.2; the plot of π versus $\log(1/IC_{50})$. Figure 2.6.2 shows several important features of these compounds. Both the ligands and the complexes show a positive correlation with π i.e. the more lipid soluble they are (within the range of π values studied) the greater the cytotoxicity. Johnson *et al* [231] noted that of 8 active aroylhyrazones of pyridoxal and salicylaldehyde they tested, the most active was sbH_2, the derivative with the least number of hydrophilic sites. The results of this study tend to confirm Johnson's findings. The slopes of both l.s.l.r. lines are relatively small (~0.4) and show that large changes in lipophilicity are required to produce noticeable changes in the cytotoxicities. Consequently, the cytotoxicity data only show approximately a 20-fold difference in concentration for the active compounds. It is possible also that there exists an optimum value of π for the substituent/s on a ligand. Increasing the lipid solubility above this may reduce activity due to absorption problems. It should also be noted that the 'copper line' is approximately parallel to the 'ligand line' and is above it. This may suggest that the mechanism of action for the complexes is similar to the ligands, as the lines are parallel, and the increased activity of the complexes results from an increase in lipophilicity. A study of some salicylates found the most lipid soluble ligands resulted in the best activity and that complexation with Cu(II) was anticipated to increase the lipid solubility while the relative order of the active compounds would not change [210].

Previous evidence has shown that sbH_2 is able to cross cell membranes of reticulocytes *in vitro* [228]. Therefore, if $Cu(sbH)^+$ can cross the cell membrane, competing equilibria or e.g.

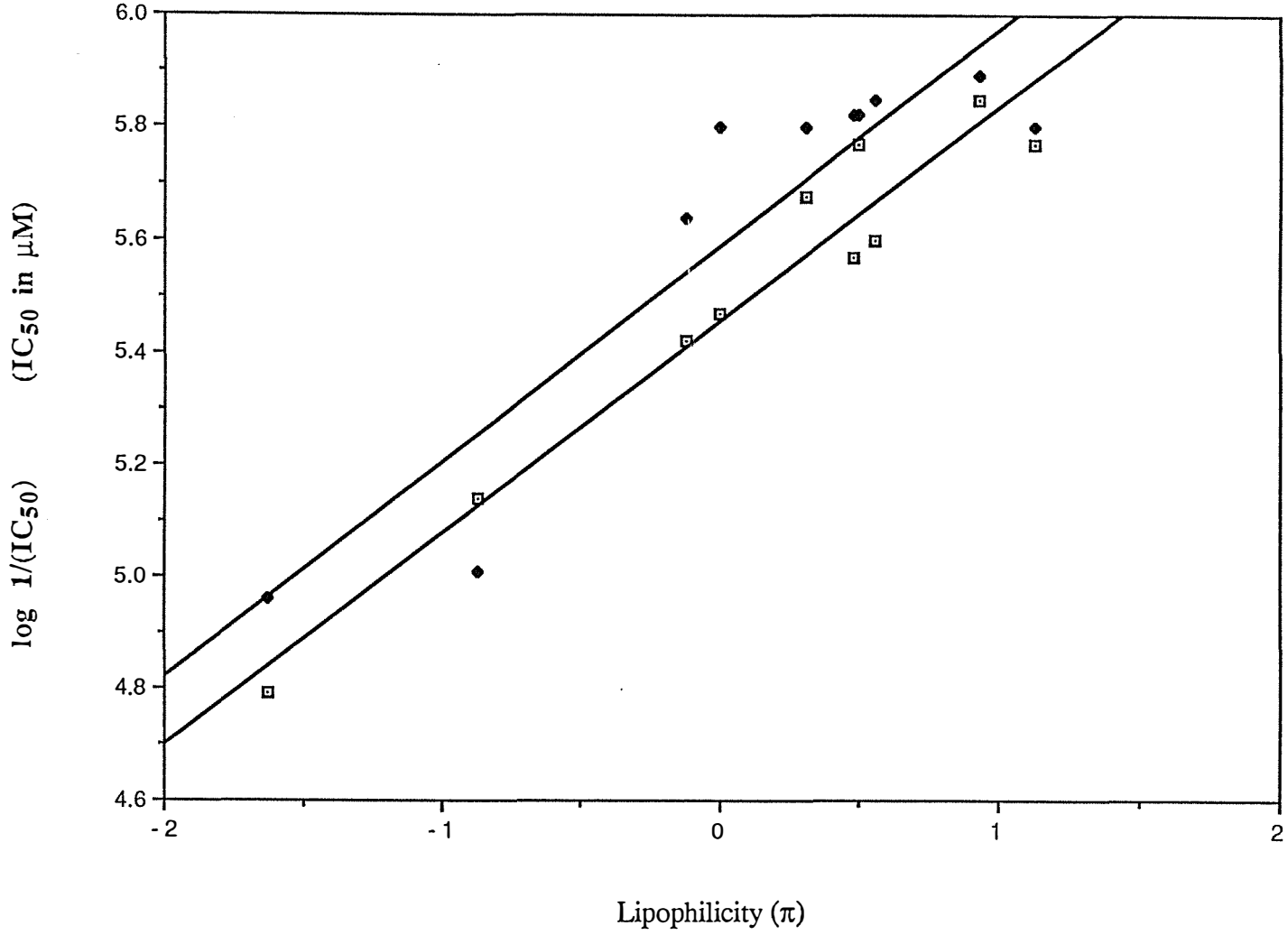

Figure 2.6.2: Plot of log $1/(IC_{50})$ vs. π for sbH_2 congeners (▫) substituted into the benzoyl ring (excluding ortho substituents) and their corresponding copper(II) complexes (◆).

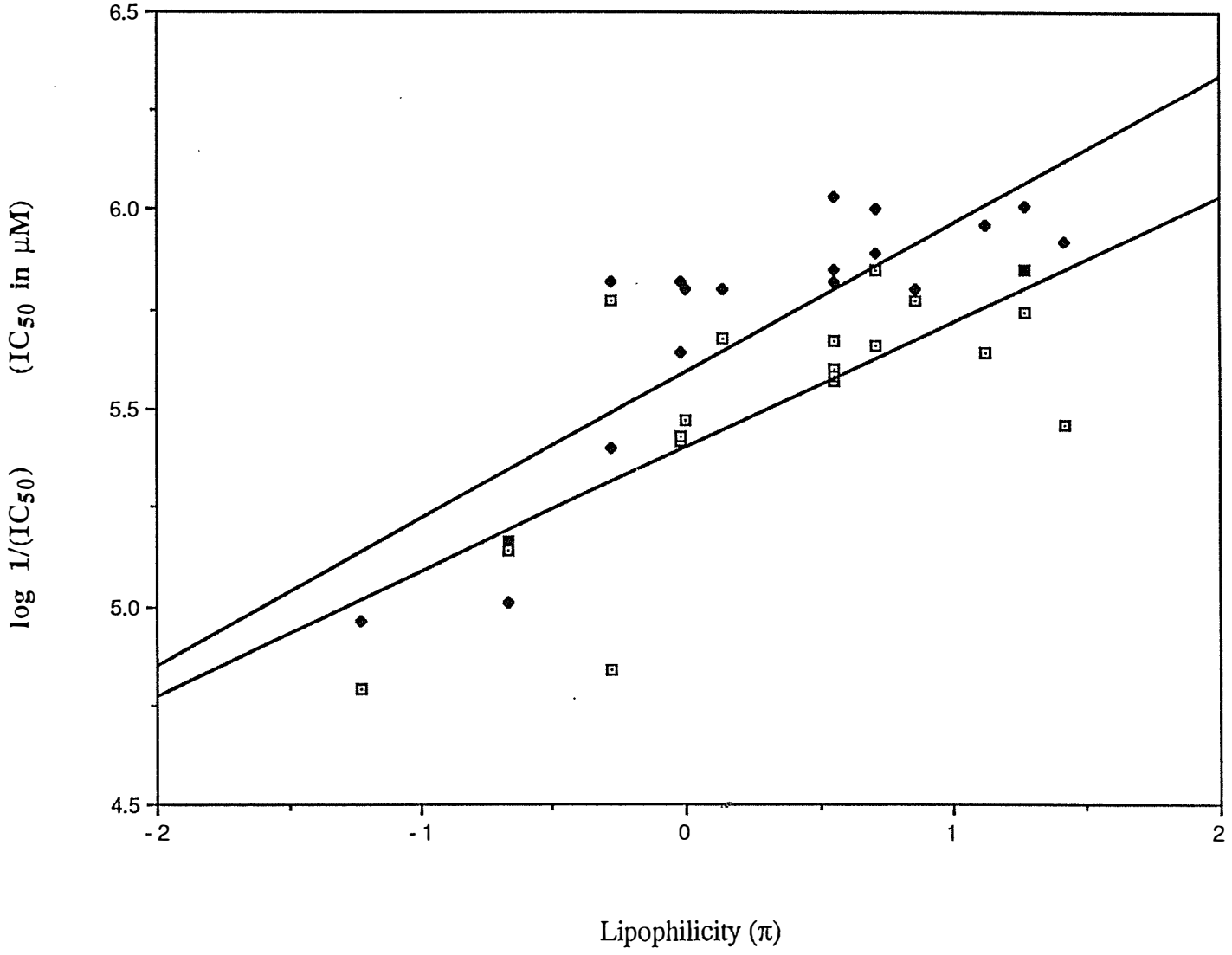

Figure 2.6.3: Plot of log $1/(IC_{50})$ vs. π for all sbH_2 congeners (▫) and their corresponding copper(II) complexes (•).

interaction with thiols to reduce the Cu(II) to Cu(I), may release the ligand, which is then free to exert its cytotoxic effect. Johnson *et al.* also determined the LD_{50}^{*} values of sbH_2 and Cu(sbH)Cl to be 1 900 and 60 mg/kg respectively and interpreted these values as showing that complexation with copper not only increased the cytotoxicity of the ligand but also the acute toxicity to the intact animal.

In Figure 2.6.3, a plot of log ($1/IC_{50}$) for all the sbH_2 congeners (both the ligands and their Cu(II) chelates) versus π is given. The π values used take no account of the position in the ring of the substituent and where more than one substituent is present, the individual π values for these are simply added. The validity in doing this can be seen by examining the IC_{50} values for $5msbH_2$, $s4abH_2$ and the ligand with both of these substituents $5ms4abH_2$. In $5msbH_2$, the methyl group confers some degree of lipid solubility (compared with sbH_2) and has an average IC_{50} value of 2.2 μM whereas the amino group in $s4abH_2$ is lipophobic as seen by the average IC_{50} value of ~16 μM. The value obtained for $5ms4abH_2$ of 6.9 μM is significantly different from both of the monosubstituted ligands and is close to the value of ~9 μM expected if the individual lipophilicities conferred by each group were independent and additive. The correlation for the data (R = 0.75 for the ligands and R = 0.83 for the complexes) has not unexpectedly decreased compared with the selected benzoyl substituted compounds (Figure 2.6.2). However, the general trends of increasing activity with increasing lipid solubility, slopes of ~0.4, and the copper complexes being more active than the free ligands are still present.

To test whether the copper chelates are significantly more active than the uncomplexed ligands, all 22 pairs of compounds which are substituted congeners of sbH_2 and $Cu(sbH)^+$ were analysed using a paired difference two-tailed t-test (21 d.o.f.). The calculated value for t_{21} of 2.96 indicates the increase in activity for the copper chelates is highly significant (99.7%).

* LD_{50} is the 50% lethal dose i.e. the single injected dose required to kill 50% of animals tested.

In order to test whether the cytotoxicities were related to the reduction potentials for the Cu(II) sbH_2 analogues (as for the Cu(KTS) and $Cu(5XL)^+$ congeners - see the previous discussion) the $E_{½}$ values were measured (in dmf - see Chapter 4 experimental for details). For the 22 complexes measured, the $E_{½}$ values ranged from 0.05 to 0.15 V with an average of 0.09 V (but the polarograms were non-ideal). No correlation between the reduction potentials and cytotoxicities were found however. The small variation found for the $E_{½}$ values suggests that there is little dependence upon these values from the substituents. This result and the lack of correlation with the IC_{50} values tends to reinforce the previous conclusion that the electronic properties conferred by a substituent are not the dominant factor for activity.

The previous findings can not however rule out the copper playing an integral role in the activity of these complexes (e.g. the delivery to, and activation of, copper dependent enzymes [17] or superoxide dismutase mimetic activity [207]) and only by further detailed investigation can this be resolved.

In an attempt to establish which properties sbH_2 required for activity, a number of different compounds were tested for their cytotoxicities. The aldehydes, salicylaldehyde (salH) and 5-methylsalicylaldehyde (5msalH), their respective Cu(II) complexes, $Cu(sal)_2$ and $Cu(5msal)_2$, and the hydrazides benzoylhydrazide and 4-chlorobenzoylhydrazide all had IC_{50} values > 20 μM and were considered inactive. The cytotoxicity is therefore a property of the intact, tridentate Schiff base ligand and not of its component or hydrolysis products.

The ligand $b5nbH_2$ is the imine reduced analogue of $5nsbH_2$ (see Figure 2.5.11). The IC_{50} values for $b5nbH_2$ and $5nsbH_2$ are 14 and 14.5 μM respectively whereas the respective activities of the complexes $Cu(b5nbH)^+$ and $Cu(5nsbH)^+$ are 3.4 and 4.0 μM. This demonstrates that there is no difference between the two sets of compounds and that the conjugation conferred upon the unsaturated, imine compound does not appear to be a necessary condition for activity. This is an important point, as the activity of the thiosemicarbazones (see

previous discussion) has been stated to be dependent upon the ligands retaining a conjugated trident configuration [58,59,283,289].

If, in sbH_2, the phenyl ring is replaced with a methyl group, the ligand is saH_2 and all activity is lost, both for the ligand (IC_{50} > 50 μM) and its copper complex, $Cu(saH)^+$ (IC_{50} > 20 μM). The π constants for a phenyl ring and a methyl group are 1.96 and 0.56 [285] respectively. The loss of cytotoxicity may therefore be the result of reduced lipid solubility rather than an electronic charge, as the equivalent bonding distances and angles in $[Cu(saH)Cl(H_2O)]H_2O$ and $[Cu(sbH)Cl]H_2O$ are very similar (see the crystal structure description of $[Cu(saH)Cl(H_2O)]H_2O$ in Chapter 5).

The ligands psH_2 and bsH_2 (see Figure 2.5.11) may be considered as structural variations on sbH_2 if, instead of salicylaldehyde, 2-formylpyridine (psH_2) or benzaldehyde (bsH_2) are used and an ortho-hydroxy group is added to the benzoyl ring. The cytotoxicities of psH_2 (17 μM) and $Cu(psH)^+$ (18 μM) have been reduced significantly compared with sbH_2 (3.7 μM) and $Cu(sbH)^+$ (1.6 μM) although the ligand is expected to be coordinating as a monoanionic tridentate moiety. In contrast, bsH_2 is thought to be a bidentate chelator and is inactive (IC_{50} > 20 μM). If the aldehyde used is salicylaldehyde, then the ligand is $s2hbH_3$, with its corresponding complex being $[Cu(s2hbH)]_2$ with the respective IC_{50} values of 1.8 and 1.1 μM. Both this ligand and its Cu(II) complex are amongst the most active in this series tested. Mohan *et al.* [227] tested this ligand and six of its substituted congeners as well as a range of their transition metal complexes for their antitumour activity on the lymphocytic leukaemia (P388) test system in mice, but found no significant activity at the dosages used. This again highlights the importance of using more than one test system to screen compounds.

The diprotic ligand $saaH_2$, (formed by the condensation of 2 moles of salicylaldehyde with 1 mole of hydrazine) is expected to coordinate as an ONO tridentate species (as does sbH_2) but is inactive (IC_{50} > 20 μM). The complex [Cu(saa)] was not tested due to its very low solubility in all solvents tried.

From the preceding results it is apparent that the ligand should be lipid soluble and a tridentate chelator. However, the actual donor set may also be critical to the activity, as substituting a phenol O for a pyridine N, or a carbonyl O for a phenol O can decrease or remove the cytotoxicity of the species.

A comparison of the data in Table 2.6.2 for the sbH_2 congeners with the average value for cisplatin of 3.1 μM shows a large number of the compounds to have comparable or better cytotoxicities than this proven drug (for the HCT-8 cell line). Similar findings were also reported for a comparison of sbH_2 and $Cu(sbH)^+$ against cisplatin, bleomycin and several other anticancer drugs for a range of human and mouse cell lines. At this level, at least, the system shows it has potential and warrants further investigation to determine the viability of obtaining beneficial anticancer drugs.

2.6.3(c) In the Future

Further studies upon the salicylaldehyde benzoylhydrazone systems and its copper(II) complexes are required to establish the 'optimum' congener for cytotoxicity. Several more single-substituent analogues which break the correlation between π and σ may help to definitely establish the critical factors for activity. If, as it appears, lipid solubility is the dominant factor, then there may be an optimum value for this. A l.s.l.r. fit of an extended range of substituted sbH_2 congers to the equation

$$\log 1/C = a(\log P)^2 + b \log P + c \log k + d$$

where C is a concentration - in this case IC_{50}

a, b, c and d are constants

P is the octanol/water partition coefficient ($\pi_X = \log P_X - \log P_H$ where P_X is the partition coefficient of a derivative and P_H is that of the parent compound)

$\log k = e\pi + f\sigma + gE_s + h$ (e, f, g and h are constants; σ is the Hammett parameter for a substituent and E_s is a steric parameter for a substituent)

may yield the optimum value of P for a derivative [286] (it is possible some of the terms in this equation may be superfluous and therefore not included, reducing the number of variables). From this value of P, a range of compounds could be designed and synthesised maximising any other properties found to be important and hopefully yielding the 'best' drug for the system.

2.6.3(d) Antiviral Results

The antiviral testing was very kindly carried out at Canterbury University by Dr J W Blunt. The viruses used were Herpes Simplex type I (HSV) and Polio Vaccine virus type I (PV1) on monkey kidney (BSC) cells. Ten compounds were tested: LH; $CuL(CH_3COO)$; $Cu(6L)(CH_3COO)$; $Cu(2'L)Cl_2$; $Cu(4'L)(CH_3COO)$; sbH_2; Cu(sbH)Cl; Cu(s4cbH)Cl; $Cu(sal)_2$; $Cu(asp)_2$ (see Abbreviations page x, Figure 4.1 and Table 2.5.11 for abbreviations; aspH = acetylsalicyclic acid). All compounds at concentrations of 0.1 and 0.2 mg/cm^3 were cytotoxic, making it impossible to tell if viral inhibition was occurring. On dilution to 0.01 mg/cm^3 the compounds were either inactive or cytotoxic. The most cytotoxic compounds appear to be $Cu(4'L)(CH_3COO)$ and Cu(sbH)Cl but 0.01 mg/cm^3 was not considered low enough to warrant further investigation.

2.6.3(e) Summary

For both 2-formylpyridine thiosemicarbazone (LH) and salicylaldehyde benzoylhydrazone (sbH_2), their congeners and their transition metal complexes, the cytotoxicity data have demonstrated the importance of testing compounds on a range of cell lines A number of compounds, previously tested on different cell lines, showed a change in the observed ordering of their activities. Several sbH_2 congeners which had been found by other workers to be inactive, all showed activity in this study on the cell line HCT-8.

Transition metal complexes generally had activities different to the corresponding free ligands. For LH congeners the complexes were no better than the ligands whereas for sbH_2 analogues the copper(II) complexes were statistically more cytotoxic than the ligands. Transition metals other than copper(II) did not improve the activity, possibly due to complex decomposition.

The addition of edta to several ligands resulted in no change of activity, demonstrating that sequestering of metal ions from the test medium was not responsible for the observed

cytotoxicity. However, when the Cu(II) chelates of these compounds were assayed with edta, the interpretation was not obvious.

For LH congeners, the changes in cytotoxicity could be related to changes in the electronic and steric properties of the ligand whereas for sbH_2 congeners, the lipophilicity conferred by a substituent appeared to be the dominant factor. The increased cytotoxicity for the Cu(II) complexes of these latter ligands may be the result of enhanced lipid solubility of the chelates compared with the metal free compounds.

In the future, it may be possible by examining derivatives and related systems, to determine the properties critical for activity and therefore design better and potentially beneficial drugs.

All of the compounds tested for their antiviral activity were either cytotoxic or inactive at the concentrations employed.

The problems of drug synthesis are outlined in this quote (after [286]):

> *"The ultimate problem in drug research is to account for the principal interactions of about 10^{20} molecules of drug injected into a mouse or human with an unknown but incredibly large number of macromolecules that make up the living organism. To make matters worse, one gets only a few highly integrated signals out of the black box (mouse); that is, there may be scores of different interactions with different macromolecular systems in the mouse (not the least of which is a complex pathogen) but the final visible response is often only the difference between a dead and a live mouse! From the chemical point of view, the cause of this relatively small but rather significant change in the mouse is in general too complicated to delineate at the molecular level. Despite the incredible odds, the undaunted medicinal chemists continue to develop better and better drugs."*

APPENDIX 1

GENERAL TECHNIQUES

Purification of Solvents

Unless otherwise specified, laboratory grade solvents were used. Dmso and D_6-dmso were dried over molecular sieves, type 4A.

Instrumentation

Electronic Spectra were recorded on a Shimadzu UV-160 spectrophotometer in the range 200 - 1 100 nm whereas for the range 900-1 300 nm a Shimadzu MPS 5000 spectrophotometer was used.

Electron Spin Resonance Spectra were recorded at 110 K on a Varian E-104A spectrometer, operating at X-band frequencies, equipped with a Varian E-257 variable temperature accessory. Spectral 'g' values were calibrated with diphenylpicrylhydrazyl (dpph) as a standard.

Infrared Spectra were recorded on a Pye Unicam SP-300 spectrophotometer using Nujol (paraffin oil) mulls with KBr discs and were calibrated against polystyrene.

Nuclear Magnetic Resonance Spectra were recorded on a JEOL GX270 spectrometer using the deuterated solvent or tetramethylsilane (TMS; $\delta = 0.0$ ppm) as the internal calibrant at 300 K.

Conductance Measurements were made on ~10^{-3} M solutions of the complexes using a Philips PW9509 digital conductivity meter and a PW9510/60 cell.

Mass Spectra were run on A.E.I. MS902 and MS30 mass spectrometers.

Room Temperature Magnetic Susceptibilities were measured using the Faraday method on a CAHN Model 7550 Millibalance with [$Hg(Co(CNS)_4)$] as the calibrant. The molar susceptibilities were corrected for diamagnetism using the appropriate Pascal constants [273].

pH Measurements were recorded using a Watson Victor PHM82 standard pH meter.

APPENDIX 2

REAGENTS

Solvents, metal salts and organic compounds were laboratory grade chemicals and used as supplied.

The following chemicals were supplied by the respective manufacturers:

BDH

1,10-phenanthroline

$FeCl_3 \cdot 6H_2O$

$CdCl_2$

$Cu(ClO_4)_2 \cdot 6H_2O$

$CuBr_2$

$Hg(NO_3)_2 \cdot H_2O$

$NaAuCl_4 \cdot 2H_2O$

p-nitrobenzoic acid

methyl benzoate

May and Baker

$Co(NO_3)_2 \cdot 6H_2O$

$Ni(NO_3)_2 \cdot 6H_2O$

$ZnCl_2$

$Cu(CH_3COO)_2 \cdot H_2O$

KSCN

Sigma

N,N-dimethylaminopyridine

acetylsalicylic acid

Hopkin and Williams

$CuCl_2 \cdot 2H_2O$

$AgNO_3$

sodium metal pellets

Fluka

2,2′-thiodiethanol

Ajax Chemicals Ltd

$Cu(NO_3)_2 \cdot 2\frac{1}{2}H_2O$

Anisaldehyde

HBr 50% solution

Frinton Laboratories

p-tritylphenol

G. Frederick Smith Chemical Company

tetraethylammonium perchlorate

Riedel-de Haën Ag Seelze

$Pb(CH_3COO)_2 \cdot 3H_2O$

$Fe(NO_3)_3 \cdot 9H_2O$

CuI was kindly prepared by Mr Andrew Trow according to literature methods [274].

Unless listed above, all other reagents were from Aldrich Chemical Company.

APPENDIX 3

MOLAR CONDUCTIVITIES AT 25° C (s mol^{-1} l)

Ion type	Water	dmso	Ethanol	Acetone	Nitromethane
1–1	100-130	50-70	60-80	100-130	70-90
2–1	210-250	100-130	120-160	230-250	150-170
3–1	340-380	150-180	200-240	350-370	230-250

APPENDIX 4

MISCELLANEOUS REACTIONS FOR SECTION 1

Several reactions were carried out in attempts to prepare Cu(I) complexes of the ligand 2-formylpyridine thiosemicarbazone (LH) but were deemed unsuitable to include in the main body of this text. Calculated analysis figures are given in parentheses.

$(CuL)_2(P(C_6H_5)_3)_3 \cdot 2H_2O$

To a solution of $[Cu(P(C_6H_5)_3)_2NO_3]$ (650 mg, 1.00 mmols) in methanol (80 cm^3) was added LH (190 mg, 1.05 mmols) in methanol (30 cm^3). The clear yellow/red solution which formed was refluxed for 2 hours then had the volume reduced (to 20 cm^3). This solution was placed in a fridge for 2 weeks and the orange globular compound which separated was filtered off and washed with ethanol and diethyl ether then vacuum dried. Yield 278 mg (42%). Anal. figures (5); C 62.6 (62.4); H 5.0 (4.9); N 8.2 (8.6); P 4.8 (4.7).

$LH \cdot HNO_3$

A solution of LH (190 mg, 1.05 mmols) in boiling methanol (30 cm^3) was added to a solution of $Cu(diphos)NO_3$ (522 mg, 1.00 mmols; diphos = 1,2-bis(diphenylphosphino)ethane) in hot methanol (80 cm^3) and the resulting orange solution was refluxed for 1 hour. The volume was then reduced (to 20 cm^3) and the orange solution put in a fridge overnight. The pale yellow crystalline material which separated was removed from solution and given a cursory wash with methanol then dried under vacuum. Yield 25 mg (10%). Anal.figures (%); C 35.1 (35.6); H 4.1 (3.7); N 28.6 (28.8).

$LH \cdot HClO_4 \cdot H_2O$

To a solution of $Cu(ClO_4)_2 \cdot 6H_2O$ (190 mg, 0.51 mmols) in ethanol (5 cm^3) was added 2,5-dithiahexane (5 cm^3, 42.5 mmols). To the resulting white compound in suspension was added LH (124 mg, 0.69 mmols) in ethanol (15 cm^3). This was refluxed for 1 day then the bright yellow solid was filtered off and washed with ethanol and diethyl ether and vacuum dried. Yield 76 mg (50%). Anal. figures (%); C 28.6 (28.2); H 3.1 (3.7); N 18.6 (18.8); Cl 11.8 (11.9).

$Cu(I)Cu(II)(L\text{-}H_2S)_2OH \cdot$ ½ dmso

A mixture of copper metal (0.62 g, 9.9 mmols) and LH (1.80 g, 10.0 mmols) was stirred in dmso (20 cm^3). After 4 hours with no heating, the solution had turned dark green. However, upon heating this suspension overnight, the colour changed to red/brown. As not all of the copper flitters had dissolved excess LH was added then the mixture was heated for 1 day. The red/brown powder which had separated was filtered and washed thoroughly with ethanol and diethyl ether then dried under vacuum. Yield 830 mg (35%). Anal. figures (%); C 37.7 (38.0); H 2.8 (3.0); N 23.2 (23.7); Cu ~24 (26.8). Mass spectral analysis shows dmso to be present and a peak at 146 a.m.u. corresponding to the desulphurised ligand (LH-H_2S), py-CH=N-NH-C≡N (or py-CH=N-N=C=NH) but no peak for LH. Desulphurisation of the ligand was also confirmed in the ir spectrum where a very strong band at 2 130 cm^{-1} was observed corresponding to a cyanide moiety (or diimide linkage). As well, 2 strong bands at 1 028 and 1 057 cm^{-1} corresponding to free or weakly sulphur coordinated dmso (ν(S=O) for dmso occurs at 1 045 cm^{-1} [107,275]) and a broad peak at ~3 400 cm^{-1} for ν(O-H), which were not present in the spectrum of $[CuL(CH_3COO)]_2$, were observed. The magnetic moment calculated for the title, mixed valent formulation is 1.71 B.M. for the Cu(II) ion.

REFERENCES

1. B. Rosenberg, L. Van Camp, J.E. Trosko, and V.H. Mansour, *Nature*, 1969, **222**, 385.
2. Memorandum, *Bull. World Health Org.*, 1985, **63**, 999.
3. M.P. Hacker, E.B. Douple, and I.H. Krakoff (eds.), *Platinum Coordination Complexes in Cancer Chemotherapy*, Martinus Nijhoff, Boston, 1984.
4. G.N. Schrauzer (ed.), *Inorganic and Nutritional Aspects of Cancer,* Ch. 10, Plenum Press, New York, 1978.
5. S.E. Sherman, and S.J. Lippard, *Chem. Rev.*, 1987, **87**, 1153.
6. C.F. Barnard, M.J. Cleare, and P.C. Hydes, *Chem. in Britain*, 1986, **Nov.**, 1001.
7. J.R. Sorenson, and W.M. Willingham, *Trace Elements in Medicine*, 1986, **3**, 139.
8. W.E. Antholine, D. Solaiman, L.A. Saryan, and D.H. Petering, *J. Inorg. Biochem.*, 1982, **17**, 75.
9. G.N. Scrauzer (ed.), *Inorganic and Nutritional Aspects of Cancer*, Ch. 12, Plenum Press, New York, 1978.
10. P. Köpf-Maier, and H. Köpf, *Chem. Rev.*, 1987, **87**, 1137.
11. J.H. Toney, and T.J. Marks, *J. Am. Chem. Soc.*, 1985, **107**, 947.
12. S.J. Berners-Price, and P.J. Sadler, *Chem. in Britain*, 1987, **June**, 541.
13. C.K. Mirabelli, R.K. Johnson, D.T. Hill, L.F. Faucette, G.R. Girard, G.Y. Kuo, C.M. Sung, and S.T. Crooke, *J. Med. Chem.*, 1986, **29**, 218.
14. S.J. Berners-Price, R.K. Johnson, C.K. Mirabelli, L.F. Faucette, F.L. McCabe, and P.J. Sadler, *Inorg. Chem.*, 1987, **26**, 3383.
15. K.D. Karlin, and J. Zubieta (eds.), *Biological and Inorganic Chemistry,* Adenine Press, 1985, 139.
16. A. Albert, *Selective Toxicity*, Ch. 10, Chapman and Hall, London, 1973.
17. L. Pickart, J.H. Freedman, W.J. Loker, J. Peisach, C.M. Perkins, R.E. Stenkamp, and B. Weinstein, *Nature*, 1980, **288**, 715.
18. L. Pickart, *Lymphokines*, 1983, **8**, 425.
19. L. Pickart, D. Downey, S. Lovejoy, and B. Weinstein, *Superoxide Dismutase Chem., Biol. Med., Proc. Int. Conf., 4th*, 1986, 555.
20. E.A. Rao, L.A. Saryan, W.E. Antholine, and D.H. Petering, *J. Med. Chem.*, 1980, **23**, 1310.
21. S. Okuyama, S. Hashimoto, H. Aihara, W.M. Willingham, and J.R. Sorenson, *Agents and Actions*, 1986, **19**, 1.
22. Y. Kamamoto, S. Makiura, S. Suigihara, Y. Hiasa, M. Arai, and N. Ito, *Cancer Research*, 1973, **33**, 1129.
23. J.R. Sorenson, *Chem. in Britain*, 1984, **Dec.**, 1110.
24. R.A. Sheldon, and J.K. Kochi, *Metal-Catalyzed Oxidations of Organic Compounds*, Academic Press, New York, 1981.
25. W.E. Levinson, *Antibiotics Chemother.*, 1980, **27**, 288.

25a. L. Thelander, and P. Reichard, *Ann. Rev. Biochem.*, 1979, **48**, 133.

26. W.C. Kaska, C. Carrano, J. Michalowski, J. Jackson, and W. Levinson, *Bioinorg. Chem.*, 1978, **8**, 225.

27. W. Rohde, R Shafer, J. Idriss, and W. Levinson, *J. Inorg. Biochem.*, 1979, **10**, 183.

28. P.A. Cerutti, *Science*, 1985, **227**, 375.

29. G.A. Reed, *Peroxide Scavenging by Cu(II) Sulfate and Cu(II)[3,5-Diisopropylsalicylate]2*, The Humana Press, (paper from a symposium), in Press.

30. P.A. Egner, B.G. Taffe, and T.W. Kensler, *Effects of Copper Complexes on Multistage Carcinogenesis*, The Humana Press, (paper from a symposium), in Press.

31. E. Kimoto, H. Tanaka, J. Gyotoku, F. Morishige, and L. Pauling, *Cancer Research*, 1983, **43**, 824.

32. F.P. Dwyer, and D.P. Mellor (eds.), *Chelating Agents and Metal Chelates*, Academic Press, New York, 1964.

33. V.M. Leovats, N.V. Gerbeleu, and M.D. Revenko, *Zh. Neorg. Khim.*, 1978, **23**, 1272, (C.A. 89:122058h).

34. M.A. Ali, S.E. Livingstone, and D.J. Phillips, *Inorg. Chim. Acta*, 1972, **6**, 11.

35. M.A. Ali, S.E. Livingstone, and D.J. Phillips, *Inorg. Chim. Acta*, 1972, **6**, 39.

36. J.F. Geldard, *Inorg. Chem.*, 1965, **4**, 417.

37. P. O'Brien, J.D. Pedrose de Jesus, and T.M. Santos, *Inorg. Chim. Acta*, 1987, **131**, 5.

38. M.A. Ali, and S.E. Livingstone, *Coord. Chem. Rev.*, 1974, **13**, 101.

39. P.S. Ciria, and S.E. Livingstone, *Aust. J. Chem.*, 1969, **22**, 1613.

40. K. Ison, and E. Kokot, *Aust. J. Chem.*, 1979, **23**, 661.

41. M.A. Ali, S.E. Livingstone, and D.J. Phillips, *J.Chem.Soc. Chem. Comm.*, 1972, 909.

42. F. Pavelcík, J. Krätsmár-Smogrovic, O. Svajlenová, and J. Majer, *Collection Czechoslavak Chem. Comm.*, 1981, **46**, 3186.

43. S.G. Murray, and F.R. Hartley, *Chem. Rev.*, 1981, **81**, 365.

44. A.W. Addison, T.N. Rao, and E. Sinn, *Inorg. Chem.*, 1984, **23**, 1957.

45. G. Domagk, R. Behnisch, F. Mietzsch, and H. Schmidt, *Naturwissenschaften*, 1946, **33**, 315.

46. M.J. Campbell, *Coord. Chem. Rev.*, 1975, **15**, 279.

47. B.A. Gringras, R.W. Hornal, and C.H. Bayley, *Can. J. Chem.*, 1960, **38**, 712.

48. K. Geetharani, and D.N. Sathyanarayana, *Aust. J. Chem.*, 1977, **30**, 1617.

49. M.J. Campbell, and R. Grzeskowiak, *J. Chem. Soc. (A)*, 1967, 396.

50. G.F. Gasparri, A. Mangia, A. Musatti, and M. Nardelli, *Acta Cryst.*, 1968, **B24**, 367.

51. L.C. Capacchi, G.F. Gasparri, M. Ferrari, and M. Nardelli, *Chem. Comm.*, 1968, 910.

52. S. Padhyé, and G.B. Kauffman, *Coord. Chem. Rev.*, 1985, **63**, 127.

53. N.V. Gerbeleu, M.D. Revenko, and V.M. Leovats, *Russ. J. Inorg. Chem.*, 1977, **22**, 1009.

54. V.M. Leovats, N.V. Gerbeleu, and V.D. Canic, *Russ. J. Inorg. Chem.*, 1982, **27**, 514.

55. N.V. Gerbeleu, and F.K. Zhovmir, *Russ. J. Inorg. Chem.*, 1982, **27**, 309.

56. D.A. Winkelmann, Y. Bermke, and D.H. Petering, *Bioinorg. Chem.*, 1974, **3**, 261.

57. J.M. Knight, H. Whelan, and D.H. Petering, *J. Inorg. Biochem.*, 1979, **11**, 327.
58. F.A. French, and E.J. Blanz, *J. Med. Chem.*, 1966, **9**, 585.
59. F.A. French, E.J. Blanz, S.C. Shaddix, and R.W. Brockman, *J. Med. Chem.*, 1974, **17**, 172.
60. K.N. Thimmaiah, W.D. Lloyd, and G.T. Chandrappa, *Inorg. Chim. Acta*, 1985, **106**, 81.
61. T.T. Bamgboye, and O.A. Bamgboye, *Inorg. Chim. Acta*, 1987, **133**, 247.
62. N. Mishra, B.B. Mohapatra, and S. Guru, *J. Inorg. Nucl. Chem.*, 1979, **41**, 408.
63. M. Mathew, and G.J. Palenik, *J. Am. Chem. Soc.*, 1969, **91**, 6310.
64. A.G. Bingham, H. Bögge, A. Müller, E.W. Ainscough, and A.M. Brodie, *J. Chem. Soc., Dalton Trans.*, 1987, 493.
65. C.F. Bell, and C.R. Theocharis, *Acta Cryst.*, 1987, C**43**, 26.
66. C.F. Bell, K.A. Lott, and N. Hearn, *Polyhedron*, 1987, **6**, 39.
67. M.F. Belicchi, G.F. Gasparri, E. Leporati, C. Pelizzi, P. Tarasconi, and G. Tosi, *J. Chem. Soc. Dalton Trans.*, 1986, 2455.
68. M.B. Ferrari, G.G. Fava, C. Pelizzi, P. Tarasconi, and G. Tosi, *J. Chem. Soc., Dalton Trans.*, 1987, 227.
69. P. Barz, and H.P. Fritz, *Z. Naturforsch*, 1970, **25**, 199.
70. D.X. West, R.M. Makeever, J.P. Scovill, and D.L. Klayman, *Polyhedron*, 1984, **3**, 947.
71. H. Sigel (ed.), *Metal Ions in Biological Systems*, Ch. 4, Marcel Dekker, New York, 1980.
72. W.E. Antholine, B. Kalyanaraman, and D.H. Petering, *Environ. Health Prospec.*, 1985, **64**, 19.
73. D.H. Petering, *Bicinorg. Chem.*, 1972, **1**, 255.
74. W.E. Antholine, P. Gunn, and L.E. Hopwood, *Int. J. Radiation Oncology Biol.. Phys.*, 1981, **7**, 491.
75. G.N. Schrauzer (ed.), *Inorganic and Nutritional Aspects of Cancer*, Ch. 13, Plenum Press, New York, 1978.
76. D.L. Banville, W.D. Wilson, and L.G. Marzilli, *Inorg. Chem.*, 1985, **24**, 2479.
77. R.C. DeConti, B.R. Toftness, K.C. Agrawal, R. Tomchick, J.A. Mead, J.R. Bertino, A.C. Sartorelli, and W.A. Creasey, *Cancer Research*, 1972, **32**, 1455.
78. H. Beraldo, and L. Tosi, *Inorg. Chim. Acta*, 1983, **75**, 249.
79. H. Beraldo, and L. Tosi, *Inorg. Chim. Acta*, 1986, **125**, 173.
80. W.A. Creasey, K.C. Agrawal, R.L. Capizzi, K.K. Stinton, and A.C. Sartorelli, *Cancer Research*, 1972, **32**, 565.
81. W.J. Dunn, and E.M. Hodnett, *Eur. J. Med. Chem. - Chimica Therapeutica*, 1977, **12**, 113.
82. R.W. Brockman, J.R. Thomason, M.J. Bell, and H.E. Skipper, *Cancer Research*, 1956, **16**, 167.
83. F.A. French, and B.L. Freedlander, *Cancer Research*, 1958, **18**, 1290.
84. L.A. Saryan, E. Ankel, C. Krishnamurti, and D.H. Petering, *J. Med. Chem.*, 1979, **22**, 1218.
85. W. Antholine, J. Knight, H. Whelan, and D.H. Petering, *Mol. Pharm.*, 1977, **13**, 89.
86. W. Antholine, and F. Taketa, *J. Inorg. Biochem.*, 1982, **16**, 145.
87. W. Antholine, and F. Taketa, *J. Inorg. Biochem.*, 1984, **20**, 69.
88. *International Tables for X-ray Crystallography*, Kynoch Press, Birmingham, England, 1974, **III**.

89. B. Morosin, *Acta Cryst.*, 1975, **B31**, 632.

90. L. Coghi, A.M. Lanfredi, and A. Tiripicchio, *J. Chem. Soc. Perkin Trans.* II, 1976, 1808.

91. G.J. Palenik, D.F. Rendle, and W.S. Carter, *Acta Cryst.*, 1974, **B30**, 2390.

92. M. Mathew, and G.J. Palenik, *Acta Cryst.*, 1971, **B27**, 59.

93. A.C. Villa, A.G. Manfredotti, and C. Guastini, *Cryst. Struct. Comm.*, 1972, **1**, 207.

94. G.R. Clark, and G.J. Palenik, *Cryst. Struct. Comm.*, 1980, **9**, 449.

95. D.D. Perrin, B. Dempsey, and E. Sergeant, *pKa Prediction for Organic Acids and Bases*, Chapman and Hall, London, 1981, 3.

96. R.C. Weast (ed.-in-chief), *CRC Handbook of Chemistry and Physics*, CRC Press, Florida, 1984.

97. L. Pauling, *The Nature of the Chemical Bond*, Cornell University Press, New York, 1960.

98. M.E. Noble, K. Folting, J.C. Huffman, and R.A. Wentworth, *Inorg. Chem.*, 1984, **23**, 631.

99. R. Österberg, and B. Sjöberg, *Chem. Comm.*, 1970, 1408.

100. R.J. Dudley, B.J. Hathaway, and P.G. Hodgson, *J. Chem.Soc. (A)*, 1971, 3355.

101. M.D. Glick, D.P. Gavel, L.L. Diaddario, and D.B. Rorabacher, *Inorg. Chem.*, 1976, **15**, 1190.

102. A. Bianchi, L. Bologni, P. Dapporto, M. Micheloni, and P. Paoletti, *Inorg. Chem.*, 1984, **23**, 1201.

103. P.A. Tasker, and L. Sklar, *J. Cryst. Mol. Struct.*, 1975, **5**, 329.

104. G.A. Lawrance, B.W. Skelton, A.H. White, and P. Comba, *Aust. J. Chem.*, 1986, **39**, 1101.

105. B.J. Hathaway, and D.E. Billing, *Coord. Chem. Rev.*, 1970, **5**, 143.

106. W. Kneen, M. Rogers, and P. Simpson, *Chemistry Facts, Patterns and Principles*, Addison-Wesley, London, 1972, 326.

107. K. Nakamoto, *Infrared and Raman Spectra*, Wiley-Interscience, New York, 1986.

108. M.C. Jain, A.K. Srivastava, and P.C. Jain, *Inorg. Chim. Acta*, 1977, **23**, 199.

109. L.T. Taylor, and W.M. Coleman, *Inorg. Chim. Acta*, 1982, **63**, 183.

110. S.K. Jain, B.S. Garg, and Y.K. Bhoon, *Spectrochimica Acta*, 1986, **42A**, 959.

111. M.J. Campbell, A.J. Collis, and R. Grzeskowiak, *J. Inorg. Nucl. Chem.*, 1976, **38**, 173.

112. A.B. Lever, *Inorganic Electronic Spectroscopy*, Elsevier, Amsterdam, 1984.

113. C.L. Jain, R.C. Saxena, B.S. Saxena, and L.R. Gupta, *Curr. Sci.*, 1978, **47**, 328.

114. M.A. Ali, S.E. Livingstone, and D.J. Phillips, *Inorg. Chim. Acta*, 1971, **5**, 493.

115. M. Mohan, P. Sharma, M. Kumar, and N.K. Jha, *Inorg. Chim. Acta*, 1986, **125**, 9.

116. M. Mohan, P. Sharma, and N.K. Jha, *Inorg. Chim. Acta*, 1985, **107**, 91.

117. G.B. Deacon, F. Huber, and R.J. Phillips, *Inorg. Chim. Acta*, 1985, **104**, 41.

118. A.M. Golub, H. Köhler, and V.V. Skopenko, *Chemistry of Pseudohalides*, Elsevier, Amsterdam, 1986.

119. K.D. Karlin, and J. Zubieta (eds.), *Biological and Inorganic Chemistry*, Adenine Press, 1985.

120. A.W. Addison, P.J. Burke, K. Henrick, T.N. Rao, and E. Sinn, *Inorg. Chem.*, 1983, **22**, 3645.

121. P.J. Barker, and S.R. Stobart, *J. Chem. Soc., Chem. Comm.*, 1980, 969.

122. C.G. Pierpont, L.C. Francesconi, and D.N. Hendrickson, *Inorg. Chem.*, 1978, **17**, 3470.

123. P. Hemmerich, B. Prys, and H. Erlenmeyer, *Helv. Chim. Acta*, 1958, **41**, 2058.

124. W.R. Busing, and H.A. Levy, *Acta Cryst.*, 1957, **10**, 180.

125. P. Coppens, J. de Meulenaer, and H. Tompa, *Acta Cryst.*, 1967, **22**, 601, and refs. therein.

126. A.C. North, D.C. Phillips, and F.S. Mathews, *Acta Cryst.*, 1968, **A24**, 351.

127. *International Tables for X-ray Crystallography*, Kynoch Press, Birmingham, England, 1974, IV.

128. W.E. Antholine, J.M. Knight, and D.H. Petering, *Inorg. Chem.*, 1977, **16**, 569.

129. S.Z. Haider, K.M. Malik, K.J. Ahmed, H. Hess, H. Riffel, and M.B. Hursthouse, *Inorg. Chim. Acta*, 1983, **72**, 21.

130. S.Z. Haider, K.M. Malik, S. Das, and M.B. Hursthouse, *Acta Cryst.*, 1984, C**40**, 1147.

131. F.A. Cotton, G.E. Lewis, C.A. Murillo, W. Schwotzer, and G. Valle, *Inorg. Chem.*, 1984, **23**, 4038.

132. F.A. Cotton, L.R. Falvello, R. Llusar, E. Libby, C.A. Murillo, and W. Schwotzer, *Inorg. Chem.*, 1986, **25**, 3423.

133. G. Jovanovski, B. Kamenar, and D. Grdenic, *Cryst. Struct. Comm.*, 1982, **11**, 263.

134. Y. Okaya, *Acta Cryst.*, 1969, **B25**, 2257.

135. M. Joesten, and L. Schaad, *Hydrogen Bonding*, Dekker, New York, 1974.

136. C.B. Castellani, G. Gatti, and R. Millini, *Inorg. Chem.*, 1984, **23**, 4004.

137. G. Druhan, and B. Hathaway, *Acta Cryst.*, 1979, **B35**, 344.

138. N.J. Ray, and B.J. Hathaway, *Acta Cryst.*, 1978, **B34**, 3224.

139. L. Antolini, G. Marcotrigiano, L. Menabue, and G.C. Pellacani, *Inorg. Chem.*, 1983, **22**, 141.

140. R.A. Nyquist, and R.O. Kagel, *Infrared Spectra of Inorganic Compounds*, Academic Press, New York, 1971.

141. E.W. Ainscough, A.G. Bingham, and A.M. Brodie, *Inorg. Chim. Acta*, 1987, **138**, 175.

142. D. Kivelson, and R. Neiman, *J. Chem. Phys.*, 1961, **35**, 149.

143. J. Becher, D.J. Brockway, K.S. Murray, P.J. Newman, and H. Toftland, *Inorg. Chem.*, 1982, **21**, 1791.

144. S. Siddi, and R.E. Shepherd, *Inorg. Chem.*, 1986, **25**, 3869.

145. S.J Barclay, and K.N. Raymond, *Inorg. Chem.*, 1986, **25**, 3561.

146. W.E. Antholine, F. Taketa, J.T. Wang, P.T. Manoharan, and J.M. Rifkind, *J. Inorg. Biochem.*, 1985, **25**, 95.

147. W.E. Antholine, R. Basosi, J.S. Hyde, and F. Taketa, *J. Inorg. Biochem.*, 1984, **21**, 125.

148. N. Aoi, G. Matsubayashi, and T. Tanaka, *Inorg. Chim. Acta*, 1986, **114**, 25.

149. J.L. Hughey, T.C. Fawcett, S.M. Rudich, R.A. Lalancette, J.A. Potenza, and H.J. Schugar, *J. Am. Chem. Soc.*, 1979, **101**, 2617.

150. E. John, P.K. Bharadwaj, J.A. Potenza, and H.J. Schugar, *Inorg. Chem.*, 1986, **25**, 3065.

151. O.P. Anderson, C.M. Perkins, and K.K. Brito, *Inorg. Chem.*, 1983, **22**, 1267.

152. N. Aoi, G. Matsubayashi, and T. Tanaka, *J. Chem. Soc., Dalton Trans.*, 1987, 241.

153. J. Buckingham (ed.), *Dicitonary of Organic Compounds*, Chapman and Hall, New York, 1982.

154. B.A. Gingras, R.L. Somarjai, and C.H. Bayley, *Can. J. Chem.*, 1961, **39**, 973.

155. B.A. Gingras, T. Suprunchuk, and C.H. Bayley, *Can. J. Chem.*, 1962, **40**, 1053.

156. see e.g. L.G. Sillén, and A.E. Martell, *Stability of Metal-Ion Complexes*, The Chemical Society, London, Special Publication 17, 1964.
D.D. Perrin, *Stability of Metal-Ion Complexes Part B Organic Ligands*, Pergamon Press, Oxford, 1979 (and Supplement No. 1 Special Publication 25, 1971).
157. A.V. Ablov, N.V. Gerbeleu, and B.T. Oloi, *Russ. J. Inorg. Chem.*, 1971, **16**, 99.
158. J.V. Dacie, and S.M. Lewis, *Pratical Haematology*, Churchill, London, 1968.
159. Program *Multan*, PDP package.
160. K. Aoki, and H. Yamazaki, *J. Am. Chem. Soc.*, 1980, **102**, 6878.
161. B.E. Fischer, and R. Bau, *Inorg. Chem.*,1978, **17**.
162. K. Aoki, *J. Am. Chem. Soc.*, 1978, **100**, 7106.
163. D.E. Corbridge, *Phosphorus - An Outline of its Chemistry, Biochemistry and Technology*, Elsevier, Amsterdam, 1985.
164. M.R. Taylor, J.P. Glusker, E.J. Gabe, and J.A. Minkin, *Bioinorg. Chem.*, 1974, **3**, 189.
165. L.E. Warren, and W.E. Hatfield, *Chem. Phys. Letters*, 1970, **7**, 371.
166. G.W. Bushnell, and A.Y Tsang, *Can. J. Chem.*, 1979, **57**, 603.
167. K.Y. Leung, and C. Calvo, *Can. J. Chem.*, 1972, **50**, 2520.
168. C. Calvo, *Acta Cryst.*, 1967, **23**, 289.
169. B.E. Robertson, and C. Calvo, *Acta Cryst.*, 1967, **22**, 665.
170. N. Krishnamachari, and C. Calvo, *Acta Cryst.*, 1972, **B28**, 2883.
171. B.E. Robertson, and C. Calvo, *Acta Cryst.*, 1967, **22**, 665.
172. H.N. Ng, and C. Calvo, *Can. J. Chem.*, 1973, **51**, 2613.
173. C. Calvo, and P.K. Au, *Can. J. Chem.*, 1969, **47**, 3409.
174. F.A. Cotton, and G. Wilkinson, *Advanced Inorganic Chemistry*, Wiley-Interscience, New York, 1966, 115.
175. K.R. Dunbar, D. Powell, and R.A. Walton, *Inorg. Chem.*, 1985, **24**, 2842.
176. E. Philipoot, and O. Lindquist, *Acta Chem. Scand.*, 1971, **25**, 512.
177. W.S. Sheldrick, *Angew. Chem., Int. Ed. Engl.*, 1981, **20**, 460.
178. G.R. Clark, J.D. Orbell, and J.M. Waters, *Biochim. Biophys. Acta*, 1979, **562**, 361.
179. K. Aoki, *J. Chem. Soc., Chem. Comm.*, 1977, 600.
180. J. Emsley, N.M. Reza, H.M. Dawes, M.B. Hursthouse, and R. Kuroda, *Phosphorus and Sulphur*, 1988, **35**, 141.
181. A.F. Wells, *Structural Inorganic Chemistry*, Clarendon Press, Oxford, 1984.
182. E.W. Ainscough, A.G. Bingham, A.M. Brodie, J.M. Husbands, and J.E. Plowman, *J. Chem. Soc., Dalton Trans.*, 1981, 1701.
183. S.F. Lincoln, and D.R. Stranks, *Aust. J. Chem.*, 1968, **21**, 37.
184. B. Bleaney, and K.D. Bowers, *Proc. R. Soc. London, Ser. A.*, 1952, **214**, 451.
185. F. Nepveu, F. Barmuth, and L. Walz, *J. Chem. Soc., Dalton Trans.*, 1986, 1213.
186. W.E. Blumberg, and J. Peisach, *J. Chem. Phys.*, 1968, **49**, 1793.

187. S.L. Lambert, T.R. Felthouse, and D.N. Hendrickson, *Inorg. Chim. Acta*, 1978, **29**, L223.

188. L.K. Thompson, and B.S. Ramaswamy, *Inorg. Chem.*, 1986, **25**, 2664.

189. D. Wiles and T. Supreunchuk, *J. Med. Chem*, 1971, **14**, 252.

190. E.W. Ainscough, A.G. BIngham, A.M. Brodie, D.R. Englebretsen, and J.M. Husbands, *J. Chem. Res.*, 1988, 60.

191. F. Calderazzo, F. Marchetti, G. Dell'Amico, G. Pelizzi, and A. Colligiani, *J. Chem. Soc., Dalton Trans.*, 1980, 1419.

192. F.A. Cotton, and G. Wilkinson, *Advanced Inroganic Chemistry*, Wiley-Interscience, New York, 1980.

193. R.E. Hagenbach, and H. Gysin, *Experientia*, 1952, **8**, 184.

194. P. Grammaticakis, *Bull. Soc. Chim. France*, 1956, 109.

195. S. Patai (series ed.), *The Chemistry of Amides*, Interscience Publishers, London, 1970.

196. A.J. Paulson, and D.R. Kester, *J. Soln. Chem.*, 1980, **9**, 269.

197. R.N. Sylva, and M.R. Davidson, *J. Chem. Soc., Dalton Trans.*, 1979, 232.

198. R. Waglman, *J. Phys. Chem.*, 1984, **84**, 3433.

199. D.T. Minkel, and D.H. Petering, *Cancer Research*, 1978, **38**, 117.

200. E. Breitmaier, and W. Voelter, *^{13}C NMR Spectroscopy*, Weinham, New York, 1978.

201. G. Martin, M. Martin, and J. Gouesnard, *NMR Basic Principles and Progress, 18 ^{15}N-NMR Spectroscopy*, Springer-Verlag, Berlin, 1981.

202. M.A. Brimble, M.T. Brimble, R. Hodges, and G.A. Lane, *Aust. J. Chem.*, in press.

203. *Varian NMR Spectra Catalog*, The National Press, 1963, see e.g. spectra numbers 234, 256 and 293.

204. A.K. Al-Sáady, K. Moss, C.A. McAuliffe, and R.V. Parish, *J. Chem. Soc., Dalton Trans.*, 1984, 1609.

205. F. Kurzer, *J. Chem. Soc.*, 1949, 3033.

206. D.R. Williams, *The Metals of Life*, Camelot Press, New York, 1971.

207. J.R. Sorenson, L.W. Oberley, R.K. Crouch, T.W. Kensler, V. Kishore, S.W. Leuthauser, T.D. Oberley, and A. Pezeshk, *Bio. Trace Element Res.*, 1983, **5**, 257.

208. J.R. Sorenson, *Med. Chem.*, 1976, **19**, 135.

209. H. Siegel (ed.), *Metal Ions in Biological Systems*, Marcel Dekker, New York, 1982, **14.**

210. J.R. Sorenson, L.W. Oberley, T.D. Oberley, S.W. Leuthauser, K. Ramakrishna, L. Vernino, and V. Kishore, *Environ. Health*, 1982, **XVI**, 362.

211. W.M. Willingham, and J. R Sorenson, *Trace Elem. Med.*, 1986, **3**, 139.

212. J.R. Sorenson, *Comprehensive Therapy*, 1985, **11**, 49.

213. J.R. Sorenson, L.W. Oberley, R.K. Crouch, and T.W. Kensler, *Oxygen Radicals Chem. Biol.*, 1984, 821.

214. S.W. Leuthauser, L.W. Oberley, T.D. Oberley, J.R. Sorenson, and K. Ramakrishna, *J. Natl. Can. Inst.*, 1981, **66**, 1077.

215. L.W. Oberley, K.L. Rogers, L. Schutt, T.D. Oberley, S.W. Leuthauser, and J.R. Sorenson, *J. Natl. Can. Inst.*, 1983, **71**, 1089.

216. H.R. Maghler, and E.H. Cordes, *Biological Chemistry*, Harper and Row, New York, 1971, 393.

217. M.R. Wagner, and F.A. Walker, *Inorg. Chem.*, 1983, **22**, 3021.

218. H.M. Dawes, J.M. Waters and T.N. Waters, *Inorg. Chim. Acta*, 1982, **66**, 29.

219. G. Plesch, C. Friebel, O. Svajlenová, and J. Krätsmár-Smogrovic, *Inorg. Chim. Acta*, 1987, **129**, 81.

220. R.D. Gillard, and R. Wootton, *J. Chem. Soc. (B)*, 1970, **5**, 364.

221. T. Ueki, T. Ashida, Y. Sasada, and M. Kakudo, *Acta Cryst.*, 1969, **B25**, 328.

222. *Chem. Eng. News*, 1979, **57**, 17.

223. D.K. Johnson, M.J. Pippard, T.B. Murphy, and N.J. Rose, *J. Pharm. Exp. Ther.*, 1982, **221**, 399.

224. T.B. Murphy, D.K. Johnson, N.J. ROse, A. Aruffo, and V. Schomaker, *Inorg. Chim. Acta*, 1982, **66**, L67.

225. T.B. Murphy, N.J. Rose, V. Schomaker, and A. Aruffo, *Inorg. Chim. Acta*, 1985, **108**, 183.

226. M. Mohan, N.S. Gupta, A. Kumar, and M. Kumar, *Inorg. Chim. Acta*, 1987, **135**, 167.

227. M. Mohan, N.S. Gupta, M.P. Gupta, A. Kumar, M. Kumar, and N.K. Jha, *Inorg. Chim. Acta*, 1988, **152**, 25.

228. P. Poňka, J. Borová, J. Neuwirt, O. Fuchs, and E. Nečas, *Biochim. Biophys. Acta*, 1979, **586**, 278.

229. C.M. Perkins, N.J. Rose, B. Weinstein, R.E. Stenkamp, L.H. Jensen, and L. Pickart, *Inorg. Chim. Acta*, 1984, **82**, 93.

230. H.A. Offe, W. Siefken, and G. Domagk, *Z. Naturforsch.*, 1952, **7b**, 446.

231. D.K. Johnson, T.B. Murphy, N.J. Rose, W.H. Goodwin, and L. Pickart, *Inorg. Chim. Acta*, 1982, **67**, 159.

232. L. Pickart, and T.B. Murphy, *Biochem. Pharm.*, 1983, **32**, 3868.

233. G.A. Barclay, C.M. Harris, B.F. Hoskins, and E. Kokot, *Proc. Chem. Soc.*, 1961, 264.

234. G.A. Barclay, B.F. Hoskins, *Proc. Chem. Soc.*, 1965, 1979.

235. N.S. Biradar, and B.R. Havinale, *Inorg. Chim. Acta*, 1976, **17**, 157.

236. T. Tokii, Y. Muto, M. Kato, K. Imai, and H.B. Jonassen, *J. Inorg. Nucl. Chem.*, 1973, **35**, 1539.

237. W.E. Hatfield, and F.L. Bunger, *Inorg. Chem.*, 1966, **5**, 1161.

238. M. Kato, Y. Muto, H.B. Jonassen, K. Imai, and A. Harano, *Bull. Chem. Soc. Japan*, 1968, **41**, 1864.

239. D.K. Rastogi, S.K. Dua, V.B. Rana, and S.K. Sahn, *J. Inorg. Nucl. Chem.*, 1978, **40**, 1323.

240. D.K. Rastogi, S.K. Dua, and S.K. Sahni, *J. Inorg. Nucl. Chem.*, 1980, **42**, 323.

241. D.R. Yarian, United States Patent, 1982, 4334015.

242. S.K. Dua, D.K. Rastogi, and S.K. Sahni, *J. Inorg. Nucl. Chem.*, 1980, **42**, 1711.

243. T. Ueki, T. Ashida, Y. Sasada, and M. Kakudo, *Acta Cryst.*, 1967, **22**, 870.

244. M.F. Iskander, A.M. El-Aggan, L.S. Refaat, and L. El Sayed, *Inorg. Chim. Acta*, 1975, **14**, 167.

245. A.A. Aruffo, T.B. Murphy, D.K. Johnson, N.J. Rose, and V. Schomaker, *Acta Cryst.*, 1984, C**40**, 1164.

246. A.A. Aruffo, T.B. Murphy, D.K. Johnson, N.J. Rose, and V. Schomaker, *Inorg. Chim. Acta*, 1982, **67**, L25.

247. M. Mohan, A. Kumar, M. Kumar, and N.K. Jha, *Inorg. Chim. Acta*, 1987, **136**, 65.

248. S. Agrawal, N.K. Singh, R.C. Aggarwal, A. Sodhi, and P. Tandon, *J. Med. Chem.*, 1986, **29**, 199.

249. J.R. Sorenson, *J. Med. Chem.*, 1984, **27**, 1747.

250. F.T. Greenaway, L.J. Norris, and J.R. Sorenson, *Inorg. Chim. Acta*, 1988, **145**, 279.

251. P. Domiano, A. Musatti, M. Nardelli, C. Pelizzi, and G. Predieri, *Transition Met. Chem.*, 1979, **4**, 351.

252. H. Lynton, and P.Y. Siew, *Can. J. Chem.*, 1973, **51**, 227.

253. S. Ray, A. Zalkin, and D.H. Templeton, *Acta Cryst.*, 1973, **B29**, 2741.

254. S. Ray, A. Zalkin, and D.H. Templeton, *Acta Cryst.*, 1973, **B29**, 2748.

255. A.G. Gash, E.H. Griffith, W.A. Spofford, and E.L. Amma, *J. Chem. Soc., Chem. Comm.*, 1973, 256.

256. G.W. Hunt, N.W. Terry, and E.L. Amma, *Acta Cryst.*, 1979, **B35**, 1235.

257. R.A. Driessen, F.B. Hulsbergen, W.J. Vermin, and J. Reedijk, *Inorg. Chem.*, 1982, **21**, 3594.

258. J. Demuynck, A. Veillard, and U. Wahlgren, *J. Am. Chem. Soc.*, 1973, **95**, 5563.

259. G. Marcotrigiano, L. Menabue, and G.C. Pellacani, *Inorg. Chem.*, 1976, **15**, 2333.

260. I.A. Tossidis, and C.A. Bolos, *Inorg. Chim. Acta*, 1986, **112**, 93.

260a. C.N. Rao, *Chemical Applications of Infrared Spectroscopy*, Academic Press, New York, 1963.

261. L. El-Sayed, and M.F. Iskander, *J. Inorg. Nucl. Chem.*, 1971, **33**, 435.

262. H.L. Schäfer, J.C. Morrow, and H.M. Smith, *J. Chem. Phys.*, 1965, **42**, 504.

263. J.F. Boas, R.H. Dunhill, J.R. Pilbrow, R.C. Srivastava, and T.D. Smith, *J. Chem. Soc. (A)*, 1969, 94.

264. U. Sakaguchi, and A.W. Addison, *J. Chem. Soc., Dalton Trans.*, 1979, 600.

265. E.W. Ainscough, A.M. Brodie, J.E. Plowman, K.L. Brown, A.W. Addison, and A.R. Gainsford, *Inorg. Chem.*, 1980, **19**, 3655.

266. D.C. Harris, *Biochem.*, 1977, **16**, 560.

267. L.M. Jackman, and S. Sternhall, *Applications of Nuclear Magnetic Resonance Spectroscopy in Organic Chemistry*, Pergamon Press, Oxford, 1969.

268. W. Kemp, *NMR in Chemistry*, Macmillan Education, London, 1986.

269. E. Breit-Maier, and W. Voelter, *^{13}C NMR Spectroscopy, Monographs in Modern Chemistry 5*, Weinheim, New York, 1978.

270. G. Palla, C. Pelizzi, G. Predieri, and C. Vignall, *Gaz. Chim. Ital.*, 1982, **112**, 339.

271. D.A. Denton, and H. Suschitzky, *J. Chem. Soc.*, 1963, 4741.

272. J.C. Duff, *J. Chem. Soc.*, 1941, 547.

273. A. Earnshaw, *Introduction to Magnetochemistry*, Academic Press, London, 1968, 48.

274. G.B. Kauffman, and R.P. Pinnell, *Inorg. Syn.*, 1960, **VI**, 3.

275. D. Meek, D. Straub, and R. Drago, *J. Am. Chem. Soc.*, 1960, **82**, 6015.

276. W.E. Antholine, J.M. Knight, and D.H. Petering, *J. Med. Chem.*, 1976, **19**, 339.

277. A. Anthony, T. Ramakrishnan, P. Mikelens, J. Jackson, and W. Levinson, *Bioinorg. Chem.*, 1978, **9**, 23.

278. P.O. Lumme, and H.O. Elo, *Inorg. Chim. Acta*, 1985, **107**, L15.

279. G.J. Finlay, B.C. Baguley, and W.R. Wilson, *Anal. Biochem.*, 1984, **139**, 272.

280. G.J. Finlay, personal communication.

281. H.G. Petering, H.H. Buskirk, and J.A. Crim, *Cancer Research*, 1967, **27**, 1115.

282. R. Cresswell, Honours Project, Massey University, 1988.

283. D.L. Klayman, J.P. Scovill, J.F. Bartosevich, and J. Bruce, *J. Med. Chem.*, 1983, **26**, 35.

284. E.C. Moore, M.S. Zedeck, K.C. Agrawal, and A.C. Sartorelli, *Biochem.*, 1970, **9**, 4492.

285. C.Hansch, A. Leo, S.H. Unger, K.H. Kim, D. Nikaitani, and E.J. Lien, *J. Med. Chem.*, 1973, **16**, 1207.

286. N.B. Chapman, and J. Shorter (eds.), *Correlation Analysis in Chemistry: Recent Advances*, Plenum Press, New York, 1978, 397.

287. T. Fujita, J. Iwasa, and C. Hansch, *J. Am. Chem. Soc.*, 1964, **86**, 5175.

288. C.G. Swain, E.C. Lupton, *J. Am. Chem. Soc.*, 1968, **90**, 4328.

289. E.J. Blanz, F.A. French, J.R. DoAmaral, and D.A. French, *J. Med. Chem.*, 1970, **13**, 1124.